ESCOLA POLITÉCNICA DA UNIVERSIDADE DE SÃO PAULO
PROGRAMA DE PÓS-GRADUAÇÃO EM ENGENHARIA MECÂNICA (PPGEM)

CRISLEY DE SOUZA PEIXOTO

Modeling, simulation and control of hybrid power systems for vessels

SÃO PAULO
2022

CRISLEY DE SOUZA PEIXOTO

Modeling, simulation and control of hybrid power systems for vessels

Corrected version

Dissertation submited to the Department of Mechanical Engineering in partial fulfillment of the requirements for the degree of Master of Science in Mechanical Engineering at the Escola Politécnica da Universidade de São Paulo.

Concentration area: Mechanical engineering of energy and fluids

Supervisor: Prof. Dr. Bruno Souza Carmo

SÃO PAULO

2022

Este exemplar foi revisado e corrigido em relação à versão original, sob responsabilidade única do autor e com a anuência de seu orientador.

São Paulo, 05 de Setembro de 2022

Assinatura do autor: Crisley de Souza Peixoto

Assinatura do orientador: Bruno Souza Carmo

Catalogação-na-publicação

Peixoto, Crisley de Souza
Modeling, simulation and control of hybrid power systems for vessels / C. S. Peixoto -- versão corr. -- São Paulo, 2022.
183 p.

Dissertação (Mestrado) - Escola Politécnica da Universidade de São Paulo. Departamento de Engenharia Mecânica.

1.Sistemas híbridos 2.Eficiência energética 3.Baterias elétricas 4.Combustiveis (Aspectos econômicos) 5.Propulsão naval I.Universidade de São Paulo. Escola Politécnica. Departamento de Engenharia Mecânica II.t.

ACKNOWLEDGEMENTS

I would like to express my deepest gratitude to God and to my family for their unconditional love and support. Also, I extend my deepest gratitude and thank my supervisor, Bruno Souza Carmo, for his patient guidance, constant support, and insightful advice throughout the research work.

I wish to especially thank the members of Project 7 of hybrid power systems for vessels, from different departments, for the collaboration, discussions, support, and sharing of ideas. Also, I will extend my gratitude to the industry partners that collaborate with Project 7, sharing real data from vessel operations.

I would like to gratefully acknowledge the support of the RCGI – Research Centre for Gas Innovation, sponsored by FAPESP – São Paulo Research Foundation (2014/50279-4) and Shell Brasil, the Foundation of Support to the University of São Paulo (FUSP), and the Brazilian National Council for Scientific and Technological Development (CNPq) for the financial support in the form of scholarship.

ABSTRACT

PEIXOTO, C.S . **Modeling, Simulation and Control of Hybrid Power Systems for Vessels**. 2022. 182 p. Dissertation (Master of Science in Mechanical Engineering) – Escola Politécnica da Universidade de São Paulo. São Paulo, 2022.

Climate concerns, regulations, and fuel costs are driving higher efficiency designs in the shipping industry. Research works suggest that hybrid power systems can be a viable option to reduce fuel consumption and emissions. However, more studies are required to analyze its net gains in different applications. In this work, we perform numerical simulations of powertrains for a diesel-electric Platform Supply Vessel (PSV) in a causal approach using MATLAB. To study such systems, we developed dynamical and static models for the power source representation and optimization, including models of diesel generator sets (gensets), a lithium-ion battery, and electric motors integrated with drivetrains and models that represent the vessel physics. All these models were combined using a static AC electrical network. The genset model was validated with errors below 2% for fuel consumption, and the engine speed results were kept within acceptable ranges, considering measured data from a project partner from the shipping industry. The battery cell model has shown errors below 1% for system states compared to literature results. We performed simulations considering hybrid and non-hybrid topologies, static models for optimization, and static and dynamical models for power source representation, comparing different energy management strategies. Also, we developed a representative response surface to model fuel consumption reductions using the software R to help in the hybrid power system design and selection of operation parameters. Through simulation experiments, it was possible to reduce fuel consumption, emissions, and genset running hours through strategic loading and hybridization using real operating profiles or a profile based on actual operations, considering different operational parameters. Through optimization, we observed the following reductions for the non-hybrid configuration: 5%-8% for fuel, 7%-8% for CO_2, 23%-30% for genset operating time, and 27%-32% for particulate matter (PM). The NO_x emissions varied, decreasing in 10% or increasing in 10%; however, an after-treatment system was not considered in any simulation. The genset redundancy had a negative and significant impact on all quantities of interest. The introduction of a battery brought additional benefits to the vessel's power system compared to the non-hybrid topology, except for the NO_x, which depended on the case. We compared the optimized non-hybrid operation with a hybrid configuration testing different energy management strategies, including ECMS formulations and a rule-based implementation. The comparisons indicate additional reductions that vary on the power profile but can be put into the ranges: 5%-10% for fuel, 5%-10% for CO_2, 23%-49% for genset operating time, 26%-47% for PM. The NO_x emissions decreased up to 11% and increased up to 9% depending on the simulation case. Most battery benefits were achieved in Dynamic Positioning (DP) or operating near the port. Energy efficiency increases above 3% were observed depending on the operating profile. Simulations that focused on the dynamic behaviour of the system showed that a 10% increase in the power system efficiency can be achieved by using a hybrid solution in a vessel typical acceleration ramp. The dynamic simulations also allowed the assessment of battery degradation, and the results indicated that a battery bank can last for around eight years of uninterrupted use, for a typical operating profile of a PSV.

Keywords: hybrid power systems. marine vessels. multi-level control. energy efficiency and emissions. lithium-ion batteries.

LIST OF ACRONYMS, ABBREVIATIONS, AND CHEMICAL COMPOUNDS

ABBREVIATIONS

Fig.	Figure
Tab.	Table
Eq.	Equation
AUX	Auxiliary
arg min	Argument of the minimum

ACRONYMS

AC	Alternating Current
AE	Algebraic Equation
AECMS	Adaptive Equivalent Fuel Consumption Minimization Strategy
AHTS	Anchor Handling Tug Supply vessel
AVR	Automatic Voltage Regulator
B&B	Branch & Bound
BSFC	Brake Specific Fuel Consumption
CCD	Central Composite Design
CNPq	Brazilian National Council for Scientific and Technological Development
COBEM	International Congress of Mechanical Engineering
CPP	controllable pitch propeller
CV	Control Volume
DC	Direct Current
DG	Diesel Generator
DOD	Depth of Discharge
DP	Dynamic Positioning
DPC	Dynamic Positioning Closed (bus-tie)
DPO	Dynamic Positioning Open (bus-tie)
DTC	Direct Torque Control
ECA	Emission Control Area
ECMS	Equivalent Fuel Consumption Minimization Strategy
EGR	Exhaust Gas Recirculation
EM	Electric Motor
EMF	electromotive force
EMS	Energy Management System
EMSA	European Maritime Safety Agency
EOL	End of Life
ESS	Energy Storage System

FAPESP	São Paulo Research Foundation
FLC	Fuzzy Logic Control
FO	First Order
FOC	Field Oriented Control
FPP	Fixed Pitch Propeller
FUSP	Foundation of Support to the University of São Paulo
GB	Gearbox
GHG	Greenhouse Gas
HC	Hydrocarbon
HEV	Hybrid Electric Vehicle
HSC	Hybrid Supervisory Control
HT	High Temperature
HV	High Voltage
HVAC	Heating, Ventilation, and Air Conditioning
ICE	Internal Combustion Engine
IM	Induction Motor
IMO	International Maritime Organization
IPCC	International Panel on Climate Change
IPOPT	Interior Point Optimizer
IPS	Integrated Propulsion System
LFP	Lithium Iron Phosphate
$LiFePO_4$	Lithium Iron Phosphate
LNG	Liquefied Natural Gas
LP	Loading in Port
LT	Low Temperature
LV	Low Voltage (electrical network) / Laden Voyage (mission profile)
MARPOL	International Convention for the Prevention of Pollution from Ships
MATLAB	Matrix Laboratory
MD	Motor Drive
MPC	Model Predictive Control
MT	Main Thruster
NLP	Non Linear Programming
NG	Natural Gas
OCV	Open Circuit Voltage
ODE	Ordinary Differential Equation
OSVs	Offshore support vessel
PDE	Partial Differential Equation
PI	Proportional Integral
PID	Proportional Integral Derivative

PEMFC	Proton Exchange Membrane Fuel Cell
PEMS	Power and Energy Management System
PLV	Partial Load Voyage
PM	Particulate Matter
PMP	Pontryagin's Minimum Principle
PMS	power management system (PMS)
PSV	Platform Supply Vessel
RCGI	Research Centre for Greenhouse Gas Innovation
RB	Rule Based
RC	Resistor and Capacitor
RL	Reinforcement Learning
RMF	Rotating Magnetic Field
RSM	Response Surface Methodology
SB	Standby
SCR	selective Catalytic Reduction
SFC	Specific Fuel Consumption
SMC	Sliding Mode Control
SO	Second Order
SOC	State of Charge
SOFC	Solid Oxide Fuel Cell
SOH	State of Health
SQP	Sequential Quadratic Programming
TB	Bow Thruster
TPN	Numeric Offshore Tank
TS	Stern Thruster
TWI	Two Way Interaction
UAC	Urban Assault Cycle
UPS	Uninterrupted Power Supply
VLSFO	Low-Sulfur Fuel Oil

CHEMICAL COMPOUNDS

H_2O	Water
CO_2	Carbon Dioxide
NO_x	Nitrogen Oxides
CO	Carbon Monoxide
SO_x	Sulphur Oxides
O_2	Oxygen Gas
N_2	Nitrogen Gas

LIST OF SYMBOLS

GREEK LETTERS

α	Coordinate in the $\alpha - \beta$ frame
β	Coordinate in the $\alpha - \beta$ frame
γ	Polynomial coefficient
δ	Polynomial coefficient
η	Efficiency
λ	Co-state vector in J
λ_α	Magnetic flux on the α axis in Wb
λ_β	Magnetic flux on the β axis in Wb
μ	Penalty function | index
ρ	Specific mass in kg/m^3
σ	Mean DOD
τ	Time in s
ϕ	Boundary layer thickness (sliding surface) | Power factor angle
ω	Angular velocity in rad/s

NOTATIONS

$\mathbf{A}$	State or system matrix
A_{tol}	Charge throughput in Ah
a	Polynomial coefficient (Genset) | Transformers ratio
$\mathbf{B}$	Input matrix
B	Damping in Ns/m | Exergy in J
b	Polynomial coefficient
$\mathbf{C}$	Output matrix
C	Capacitance in F
C_{bat}	Battery capacity in As
C_c	Core heat capacity in J/K
C_s	Surface heat capacity in J/K
c	C-rate in h^{-1}
c_f	Friction factor
D	Diameter in m
d	Disturbance or exogenous input
E	Energy in kWh
E_a	Activation energy in J/mol
e	Error
$\mathbf{F}$	Disturbance matrix
F	Force in N

f	Frequency in Hz | function
f_p	Parameter to customize upper power in RB strategy
G	Function
g	Function
H	Enthalpy in J | Hamiltonian
h	Specific enthalpy in J/kg
i or I	Current in A
it	Charge flowing through the battery in time in As
J	Cost function | Moment of inertia in Kgm^2
$J^{'}$	Bounded advance ratio
K	Constant
$K^{'}$	Coefficient
k	Gain
L	Inductance in H | Lagrangian
$\mathbf{M}$	Power allocation vector in kW
M	Pre-exponential factor in h$^{0.45}$ | Genset Torque in kNm
m	Mass in Kg
N	Number of generators RB | Number of cycles
NP	Number of cells in parallel
N_P	Polynomial order
N_r	Number of pole pairs
NS	Number of cells in series
P	Power in kW
P_{ebat}	Battery power after the converter in kW
P_{GT}	Total generator power in kW
P_{out}	Consumers power in kW
P_p	Number of poles
p_1	Thermal ICE efficiency polynomial
p_2	Genset efficiency polynomial
p_3	CO_2 mass flow rate polynomial in kg/s
p_4	CO mass flow rate polynomial in kg/s
p_5	NO_x mass flow rate polynomial in kg/s
p_6	HC mass flow rate polynomial in kg/s
p_7	PM mass flow rate polynomial in kg/s
p_8	Fuel mass flow rate polynomial in kg/s
pa	Power law factor
Q	Heat in J
Q_{hv}	Low heat value in kJ/kg
R	Ideal gas constant in Jmol $^{-1}$ K $^{-1}$ | Ohmic resistance in Ω

R_0	Series resistance (battery circuit) in Ω
R_1	Resistance (RC pair 1) in Ω | First rule used for the RB strategy
R_2	Resistance (RC pair 2) in Ω | Second rule used for the RB strategy
R_c	Conduction resistance in K/W
R_u	Convection resistance in K/W
r	Total vessel resistance coefficient in kg/m
r_{eq}	Equivalent electrical resistance in Ω
r_g	Generator electrical resistance in Ω
S	Entropy in J/K
SOC_a	Lower SOC limit
SOC_b	Upper SOC limit
s	Specific entropy in J/(kg K) | Equivalence factor
sgn	Signal function
T	Torque | Temperature
T_c	Core temperature in K
T_f	Ambient temperature in K
T_s	Surface temperature in K
t	Time | Reduction coefficient (Propeller model)
U	Voltage V
$\mathbf{u}$	input or control vector
u	input or control | voltage (DC motor and genset) in V
V	Voltage in V
V_t	Terminal voltage in V
v	Linear velocity in m/s
W	Work in J
w	Wake number | optimization weights
$\mathbf{x}$	state vector
x	state of variable
$\mathbf{y}$	output vector
z	Power law factor

SUBSCRIPTS

0	Reference state
A or a	Armature
b	Exergy
bat	Battery
bkW	Brake Power
cb	Combustion
cmax	Maximum charge
const	Constant
d	Demand
dest	Destroyed
dg	Diesel generator
dmax	Maximum discharge

e	Effective (shaft) | EMF
ekW	Electrical Power
el	Electric
eq or eqv	Equivalent
F	Field
f	Final | fuel
G	Generator
G1	Generator 1
G2	Generator 2
GB	Gearbox
g	Synchronous generator
HT	High temperature
h	Mutual
hs	High-speed
k	Counter
i	Index | Integral (gain)
im+fc	Induction machine and motor drive
in	Input
j	Index
k	Index
L	Load
LT	Low temperature
ls	Low speed
M or m	Motor
max	Maximum
min	Minimum
n	Nominal
oc	Open circuit
opt	Optimum
out	Output
P	Products
p	Propeller | Proportional (gain)
prop	Propeller
ps	Power system
Q	Torque
R	Reagents
r	Resistive / Rotor
rad	Radiation
red	Reduced

ref	Reference
rec	Converter
SOC	State of Charge
s	Stator (IM)
sh	Ship
T	Thrust
t	Thermal (ICE) | Torque (electrical motors)

SUPERSCRIPTS

0	Combination of vectors
T	Transpose

TABLE OF CONTENTS

1 INTRODUCTION

Concerns about the impacts of greenhouse gas (GHG) emissions on climate change have been rising in recent years, pressing governments and other institutions around the world to discuss and implement strategies to reduce atmospheric pollution. Hence, international agreements have taken place to prevent negative changes in the climate system by human action.

On the 4th of November 2016, the Paris Agreement entered into force with the central objective to endorse a stronger and comprehensive response to keep global temperature increase below 2 degrees Celsius, preferably 1.5 degrees Celsius, regarding pre-industrial levels [1]. Potential negative consequences of an increase of 1.5 degrees Celsius are presented in the 2018 report provided by the International Panel on Climate Change (IPCC) [2]. In addition to the global warming concerns, air pollutants such as NOx, SOx and PM represent a threat to human life and ecosystems in general.

The international shipping industry represents the carriage of 90% of the world trade, with a projected growth in the following years [3]. Vessel operation is responsible for an expressive amount of emissions, around 1.8% of the total 37.9 Gt of CO_2, being comparable the 8th nation on the ranking of top-emitting countries [4]. Vessels also emit approximately 12% and 13% of the global NOx and SOx, respectively. If no action takes place, the future projections indicate increases in emissions. A study published in 2014 estimated a CO_2 increase of 50-250% from 2012 to 2050 [5].

Diesel engines are still the main prime movers for most marine vessels, providing propulsion power or being a part of generator sets to produce electricity used for propulsion. Although the combustion process is responsible for the power generation, it is also the cause for emissions of GHG and other components, including carbon monoxide and dioxide (CO and CO_2), water vapour (H_2O), nitrogen and sulphur oxides (NOx and SOx), unburned hydrocarbons (HC), as well as particulate matter (PM) [6].

The International Maritime Organization (IMO) was addressed with the responsibility to regulate emissions from the shipping industry. To cover the pollution of the marine environment, the International Convention for the Prevention of Pollution from Ships (MARPOL) was adopted. Annex VI of the convention addresses air pollution from ocean-going vessels, specifying limits on NOx, SOx and PM, as well as measures to increase energy efficiency and reduce GHG

emissions. Besides, the IMO established the protection of sensitive regions through the definition of emission control areas (ECAs) [7].

The restrictions are becoming more stringent, and to be consistent with the Paris Agreement, the IMO's strategy to reduce GHG emissions from vessels include strengthen the energy efficiency design requirements; cut CO_2 emissions by at least 40% by 2030 and up to 70% by 2050 as well as reducing the total annual GHG by at least 50% by 2050, compared to 2008. Moreover, the long-term aim is to pursue efforts towards the eradication of emissions [8].

Besides climate concerns and regulations, fuel costs represent another driver for change in the shipping industry. Fuel costs can account for as much as 50% to 60% of total operating costs in maritime operations [9], depending on the type of vessel and service, and can fluctuate depending on the global context and regulations. With the recent IMO decision to limit the sulfur content of vessel fuel to 0.5% (from 3.5%) which entered into force in January 2020, the price of very low-sulfur fuel oil (VLSFO) is expected to rise, affecting more than 50,000 merchant vessels worldwide [10].

The importance of the shipping industry activities for the global economy, the fuel cost, and the necessity to substantially reduce GHG emissions and other air pollutants over the next decades require techno-economic and political efforts among all stakeholders in the shipbuilding industry. In this scenario, there is a demand for power system frameworks that can improve energy efficiency and reduce emissions.

In a short-term context, for existing vessels, reciprocating engines with improvements in emission attenuation and alternative low sulfur fuels are the main option to reduce emissions. In particular, Liquefied Natural Gas (LNG) is the most likely fuel in the short to medium term, due to the available engine and system technology, class regulations, operational experience, fuel cost, and availability of Natural Gas (NG) [9].

Recently, technology advancements in power electronics and power devices, including batteries, ultra-capacitors, and fuel cells have created possibilities for hybridization in maritime applications [11]. Specifically, the increase of energy and power density of lithium-ion batteries opened up new markets in recent years, with prices falling through the years [12].

In the medium-term time horizon, the option to include hybrid propulsion systems with conventional power modes offers the potential to cut emissions and cost, but the actual gain depends on the vessel size and operational power profile [9]. Hybrid technology allows the flexibility to combine different power modes meeting the operational demands strategically. The

automotive industry has already been exploring hybrid options through the use of fuel cells, ultra-capacitors, and batteries to improve performance, reduce emissions, and fuel consumption [13]. In the shipping industry, hybrid power systems also look promising. Research works suggest reductions in fuel consumption and emissions of up to 10-35%, with results that strongly depend on the vessel power profile, previous and later system configuration and operation. Besides that, it is possible to minimize noise and improve maintainability, maneuverability, and comfort [14].

Hybridization in vessels is characterized by a plant with (1) hybrid propulsion: comprising mechanical and electrical propulsion, and (2) hybrid power supply: a combination of different power modes, such as Diesel generators and batteries (mostly used with electric propulsion) [3, 14]. For vessels with significant power demand peaks, followed by long periods of low loading (compared to optimal loading), and highly dynamical loads, hybrid technology can reduce fuel consumption and emissions significantly [3]. However, to achieve the full potential of the hybridization, adequate sizing and advanced control strategies are required [14].

Offshore support vessels (OSVs) such as Platform Supply Vessels (PSVs) are among the options to receive power supply hybridization due to their operation profile, constraints, and importance to the offshore oil and gas industry. They require a highly dynamical response, including Dynamic Positioning (DP) with high levels of reliability and safety [15], which is generally associated with power source redundancy and operation in low loads (compared to optimal loads). Also, OSVs have large variations in their power demand, with different operational modes, making it hard to keep the engines operating within desired optimal ranges [6].

According to [16], in 2019, there were more than 300 hybrid vessels with batteries installed or on order. The current numbers from the Maritime Battery Forum are of more than 400 vessels with batteries installed or on order for 2021. Recently, in later 2020, the CBO Group, one of Brazil's main operators of offshore support vessels, and the Wärtsilä Group, a global leader in marine technology, signed an agreement to adapt a PSV with a battery system, leading to the first hybrid vessel in Latin America [17]. The literature results, cases of success, and industry trends show that hybridization is a promising technology framework for the near future of vessels.

Research projects have an essential role in producing knowledge to support decisions towards more efficient and greener designs. This work was developed within the scope of hybrid power systems for vessels as a part of Project 7, which is an initiative that started in the Research Centre for Greenhouse Gas Innovation (RCGI) to analyze hybrid power systems for vessels,

including risk assessment, dynamical modeling, simulation, and integration with maneuvering simulators (from the Offshore Numerical Tank Laboratory, TPN), electrical analysis and energy dispatch.

In Project 7, there are also partnerships with players from the maritime industry interested in powertrain solutions for vessels. This way, it is possible to reduce the gap between academia and industry, promoting innovation and positive transformation. In this work, we use sensitive data from companies to perform simulations. Therefore, some of the data and results will be omitted due to non-disclosure agreements.

1.1 OBJECTIVE

1.1.1 General objective

The objective of this project is to develop models of hybrid and non-hybrid power systems for Diesel-electric PSVs, perform simulations to predict the performance of these systems, and propose control strategies to improve the performance of the hybrid solutions. With this, we intend to contribute to the understanding of the hybridization of vessels, including the behavior of the powertrain components and improvements in energy efficiency, which can lead to fuel economy, and emission reduction.

1.1.2 Specific goals

- To improve the current vessel powertrain simulator of Project 7 through parameter identification, modeling and control;
- To develop models which can be integrated with the Numeric Offshore Tank (TPN) maneuvering simulator, allowing vessel dynamics evaluation in different environmental situations;
- To propose control strategies for hybrid power systems used in vessels to better exploit their potential and improve performance.
- To design optimal energy management strategies for hybrid and non-hybrid vessel systems to improve energy efficiency and reduce emissions;

- To define the load demand inputs for simulation based on the literature and real data from a vessel fleet operator;
- To propose a methodology to help in the hybrid power system design and parameter selection;
- To perform real-time numerical simulations of individual and associated components of powertrains;
- To compare hybrid and non-hybrid power system topologies, quantifying and analyzing important information for the understanding of the feasibility and benefits of the hybrid systems on vessels, such as energy efficiency, fuel savings, genset running hours, battery degradation, and emission reduction.

1.2 JUSTIFICATION

Despite its advantages, the implementation of hybrid power systems offers new challenges. The net gains of the hybrid solutions depend on several variables such as the type of vessel and its operational profile, energy and power density of the device (batteries, for example), the energy management strategy, reliability and safety risks, costs, as well as infrastructure [3, 14, 18].

The emerging technologies in power systems for vessels require substantial studies to evaluate their feasibility. Vessels are complex, expensive, and can have a large scale. Physical tests of various powertrain topologies and energy management strategies in different scenarios, mainly in the early stages of development, are not practical, therefore, model-based simulations are essential for research.

Different powertrain models are available in the literature. It is important to consider a balance between the complexity and accuracy of models to select the proper ones. A vessel power system comprehends a significant number of complex components, thus assumptions are necessary. Still, it is important to preserve the central aspects to be evaluated depending on the objectives of study. While the dynamic modeling approach is not strictly required for fuel consumption estimation, it is interesting because it allows the investigation of other aspects of performance [3], such as the loading of the generators and the synchronization, fuel injection, and engine speed control, battery electrical, thermal and degradation dynamics etc.

The hybridization of power systems allows the flexibility to combine different power modes to meet the operational demands. However, this increase in the number of power sources

and possibilities to dispatch power often increase the control complexity. Designing an energy management system (EMS) strategy capable of handling every combination of power dispatch, considering the restrictions of the devices and the different objectives, can be a very challenging task.

When the models are implemented using a causal approach, the system outputs depend only on past and current inputs, but not on future inputs. Such an approach allows real-time representation. However, the EMS cannot predict the future power demands, not always being able to manage the power modes to achieve the global optimum [3]. This is what happens in real power systems. Such modeling methodology is important to increase the accuracy of representation and to better understand the hybrid solution benefits.

An optimized EMS strategy is essential to improve energy efficiency. It allows better regulation of generation, distribution, storage, and power split between the power modes [14]. Combining the insights from island microgrids, hybrid vehicles and strategies in research for vessels, several EMS control approaches can be found, including heuristic, based on rules or fuzzy logic, optimal, predictive, intelligent, among others [14, 19].

According to [6], until recently, the majority of energy management control in the industry was based on rules/heuristic techniques. Rule-based techniques require the knowledge of the system and experience to exploit the potential of hybrid systems. Furthermore, the number and complexity of the rules increase considerably when more power sources are integrated into the vessel powertrain.

In [11], a hybrid topology for a tug, with two generators and a battery pack, required 12 sets of rules for the power split determination, with several parameters depending on the arbitrary choice of the strategy developer. Considering the same methodology for four generators and a battery pack, the number of rules could easily increase to 18 rules, or even more. Due to the complexity and number of rules, it becomes much harder to achieve optimality.

The energy management objectives depend on the vessel type, priorities, and load profiles, requiring specific control policies given the application. For example, navy vessels require a system able to supply power to balance short-pulsed loads related to weapons, ferries for passengers require low emissions and noise, while tugboats have multiple operational modes, with a requirement of full bollard pull during vessel assistance [6].

For a generic mission, PSVs require low power when the vessel is being loaded with goods in the port or in standby near the port, waiting for available space. When the vessel is

traveling to a platform loaded, or traveling back to the port half-loaded, there are high power requirements with small variations. When the vessel is keeping its position near the platform, in Dynamical Positioning (DP) mode, highly dynamical loads are expected, and a certain level of redundancy of power modes is required to assure reliability [15, 20]. The diversity of power profiles, even for one class of vessels, control objectives, and the number of power sources, makes it difficult to optimize power systems, especially hybrid ones.

In several works such as [3, 11, 18, 20], the main focus was to evaluate Diesel fuel consumption or CO_2 emissions. It seems implicit in some works that fuel savings are directly proportional to emission reductions in general. However, this is not true for all components. As mentioned in [6], the NOx emissions and fuel consumption can be conflicting goals. Some of the more efficient operation regions of engines also increase the emissions of NOx. Therefore, the energy management system has to be able to ensure fuel-efficient operation while assuring NOx limits.

Another issue is the determination of power profiles that represent real operational conditions. We could not find an equivalent to the standard driving cycles used in hybrid vehicles. Driving cycles consist of speed versus time points that can be used as input for vehicles models or experiments. These temporal series are produced by different institutions in the world to assess the vehicle performance, considering several aspects as fuel consumption and emissions [21]. For vessels, we generally, find generic power profiles or speed profiles. Since there are no standard inputs for vessels, having representative inputs for each case is fundamental to achieve more reliable results.

In the literature, all powertrain simulation approaches that integrate vessel physics, considering thruster models, vessel dynamics, and kinematics, for example, contemplate simplified models as in [3, 13, 22]. For powertrain performance evaluation under complex vessel operations, more accurate models can be required. The Project 7 framework integrates the power system simulator with the TPN accurate maritime simulator allowing vessel physics evaluation and propulsion load estimation if the propeller velocity inputs are given. From the TPN perspective, the powertrain models add value allowing fuel consumption and emission estimation for maneuvering simulators.

According to [14], advanced control strategies are required to tackle the challenges that hybrid power systems impose and to harvest all of their potential. Given the challenges, it is important to analyze hybrid solutions to justify the increase in cost and complexity. In this

context, representative model-based simulations are essential for research, decision making, and project design.

1.3 MATERIALS AND METHODS

A power system simulator was developed to model hybrid and non-hybrid architectures, predict the behavior, and propose control strategies to improve the performance of such systems. The power system simulator from Project 7 was used as the initial point to understand how the powertrains of vessels work, the modeling, simulation, and code implementation approach, including the main individual components, the integration of models, supervisory controllers, and the main inputs and outputs. Next, models and controllers were developed or changed to improve the power system simulator and to perform simulations that provide valuable information for understanding powertrain solutions and vessel hybridization. Moreover, a second-order hypersurface was developed through the response surface analysis to help in the hybrid power system design and parameter selection with a focus on fuel savings.

1.3.1 Project 7

The hybrid powertrain model from Project 7 was implemented using the MATLAB language and environment, similar to most of the simulators reported in the literature, such as [3,11,13,18,23], which use and develop models in MATLAB/Simulink. The Project 7 simulator considers discrete-time and causal approaches. It contains model parameters, algebraic equations (AE), and ordinary differential equations (ODEs) numerically integrated using MATLAB.

There is a graphical user interface, which provides real-time information about several components and overall control of the simulation. The software was built in a modular way, allowing flexibility to add functionalities, new models, and adaptation for new vessels and missions. Moreover, for the integration with the maneuvering simulators of TPN, an interface was already implemented. The powertrain simulator and the TPN vessel models are executed alongside with a run time actualization frequency of 10 Hz [24].

1.3.2 Modeling, simulation, control and optimization

Initially, a literature review was required to better understand hybrid power systems for vessels and comprehend the Project 7 framework and its dynamical systems. This study was essential to enable the further development and use of the existing tools. The contributions were produced following promising works in the literature, with a good balance between complexity and accuracy. The mathematical analysis, simulation, and algorithm implementations were performed using MATLAB and CasADi.

The algorithms and numerical strategies implemented in Project 7 were reviewed. The methods being used included curve fitting and interpolation, numerical differentiation, integration, numerical solution of ODEs using Runge-Kutta methods, etc. Besides, the manual in numerical methods for engineers and scientists using MATLAB [25], was used to aid the code implementation.

After reviewing the models from Project 7 and the scientific literature, some models were changed, and others were implemented in a modular way to allow individual simulation and integration for more comprehensive simulations. Some models were validated with measured data, literature results, or Simulink models. For the powertrain simulation, the global runtime frequency is 10 Hz, as in Project 7. This means that the individual models exchange information at the mentioned frequency, although they can be simulated at higher frequencies.

The individual component models were integrated to allow the electrical power system simulation. A multilevel power management strategy is proposed with energy management strategies to control the power generation and distribution for hybrid and non-hybrid systems to improve energy efficiency and reduce emissions. The gensets and batteries are connected through a static electrical network, which accounts only for power balance, considering electrical energy conservation.

The implemented models combine static and dynamic formulations, described by algebraic equations (AE) and ordinary differential equations (ODEs). The ODEs are solved using Runge-Kutta methods. The models and energy management strategies were implemented and simulated in MATLAB following the causal approach. For the numerical optimizations performed in this work, we used CasADi, an open-source tool for nonlinear optimization and algorithmic differentiation.

The complete dynamical system can be computationally expensive for real-time decisions regarding optimization techniques. For this purpose, model reductions were performed. As described in [3, 26], quasi-static efficiency maps of each power mode suffice for fuel economy estimation in some optimization formulations. The complete and transient model runs to provide global powertrain information, and an inner quasi-static loop runs with the reduced models for optimization of energy management.

Initially, we considered two approaches for nonlinear optimization, the interior-point method through the algorithm IPOPT and sequential quadratic programming (SQP) through the algorithm qpOASES. Due to better performance, SQP was selected as the standard approach for optimization. The optimizations follow the powertrain simulation frequency.

To produce information about the sensitivity of the hybrid power system fuel savings to the variation of different parameters and give us a tool for optimal sizing and operation, we considered the Response Surface Methodology (RSM) methodology. A second-order regression was performed using the rsm package of the R software to produce the hypersurface. Then, some analysis of parameter significance, parameter trade-offs and operational requirements were carried out.

We performed simulations using mission profiles from or based on real operations and compared hybrid and non-hybrid topologies for a PSV, quantifying and analyzing quantities of interest. In some analyses, we used real operating profiles from the maritime industry to produce and validate models and generate results that optimize the powertrain's operation through strategic loading and hybridization.

1.4 STRUCTURE OVERVIEW

The structure of the remainder of this text is as follows:

Chapter 2: presents a review on propulsion systems for vessels comprising mechanical propulsion and electrical propulsion. For electric propulsion systems, Diesel-electrical propulsion with a hybrid power supply is discussed, focusing on adding lithium-ion batteries to the power system, considering the energy storage functional roles, benefits, and main challenges. The different levels of control strategies are explained, and we overview the different energy management control approaches. More detailed explanations of rule-based and equivalent consumption minimization control strategies are also provided.

Chapter 3: describes Project 7 and discusses the main models used before this work to model Diesel-electric hybrid power systems with the addition of lithium-ion batteries, the powertrain model integration, information flux with inputs and outputs, and the integration with the TPN manouvering simulators. The component models explained are the engine generator sets (gensets), electric motors and drivetrain, battery pack, the electrical architecture, and a simplified vessel motion and propeller model. At the end of each model description, we bring to light some information about the state of the art in modeling powertrain components.

Chapter 4: presents the main contributions related to powertrain modeling for an Ulstein platform supply vessel (PSV). We present the description of the original powertrain and discuss about the battery integration for a hybrid solution. Then, we define the models required to model the propulsion system. A dynamic model for the engine-generator set oriented to fuel consumption and emissions is described and speed control is discussed. The model is tested in some simulations and is validated with data measured from real vessel operations. In sequence, through parameter identification, the efficiency of the DC motor, previously implemented in Project 7, is increased to more acceptable values based on the references. Additionally, a three-phase induction motor model integrated with a drivetrain and a simplified vessel physics is presented with a sliding mode control for speed and flux. Besides, we present a lithium iron phosphate cell model considering electro-thermal and aging effects. We discuss the models for the battery pack and the electrical architecture. Finally, we derive a global efficiency index to evaluate the overall energy efficiency of a hybrid power system, even if the battery state of charge is different from the initial.

Chapter 5: presents a multilevel power management framework for the modeling and control of the electrical power system of a vessel. The EMS supervisory control is discussed, considering its inputs and outputs. Various methods and models are considered. Subsequently, we present the model reduction methodology for gensets and the battery. Besides that, the energy management strategies are discussed, including a genset optimization using static models for the non-hybrid configuration and, for the hybrid topologies, a rule-based strategy and equivalent fuel consumption minimization strategies (ECMS).

Chapter 6: reports the simulation experiments performed combining different models to represent the power system of the Ulstein PSV and hybrid solutions to evaluate several powertrain aspects. The analyses carried out are based on operational data (power profiles) from a Platform Supply Vessel provided by the maritime industry. Through case studies, we discuss energy

efficiency, fuel consumption, emissions, genset running hours, battery capacity fading, and energy management strategies exploring the model set built in this work and different operational parameters for hybrid and non-hybrid configurations. Also, we provide a tool to help in the hybrid power system design and parameter choice.

Chapter 7: highlights the major contributions and results of this work and suggests paths for future works.

2 PROPULSION SYSTEMS FOR VESSELS

The operational profile of vessels has become diverse, with vessels being designed to perform a variety of tasks. Due to the different operating profiles and regulations, marine propulsion systems have to meet many performance criteria, including: fuel consumption, emissions, radiated noise, propulsion availability, maneuverability, comfort due to minimal noise, vibrations and smell, maintenance costs due to engine thermal and mechanical loading, and purchase cost [14, 15].

The number of performance criteria makes it difficult to optimize the power and propulsion systems of vessels. In addition, it can be noted that some objectives are conflicting, which adds to the complexity of the optimization problem [6]. This has been leading to a variety of power and propulsion architectures, including mechanical propulsion, electrical propulsion, or a hybrid combination; power generation by internal combustion engines, turbines, energy storage systems, fuel cells, or a hybrid configuration; with AC or DC electrical distribution [9, 14].

2.1 MECHANICAL PROPULSION

Due to high fuel efficiency, most vessels use Diesel engines as prime movers [14]. A typical Diesel-mechanical propulsion can be seen in Fig. 1. The plant comprises main engines (1) that can be coupled with propellers (3) directly or through a gearbox (2). Additionally, there are auxiliary engine generator sets (7) connected through an AC electrical network (6) to supply power to auxiliary systems (5) for lighting, heating, ventilation, and air conditioning (HVAC), variable-speed motors (4) etc.

The main advantage of mechanical propulsion is its high efficiency near the vessel's design speed. In this range, Diesel engines operate efficiently and the transmission losses are minimal. The main disadvantages include low fuel efficiency and high emissions at low loads, as well as the lack of redundancy, which leads to poor availability [14].

The power management control for a vessel with mechanical propulsion can be relatively simple or more complex, depending on the application. The main engines can operate simultaneously with fixed pitch propellers (FPP), regardless of the power load, while the auxiliary loads are supplied by generator sets [6]. However, more complex power management approaches

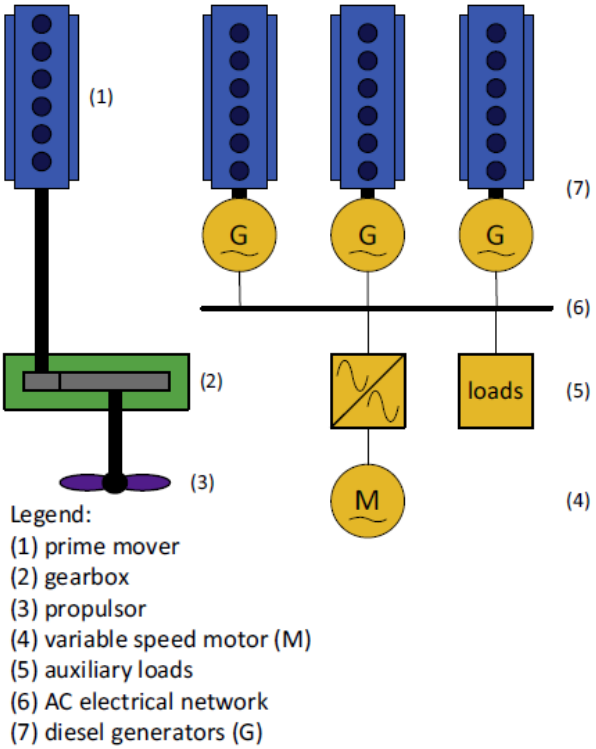

Figure 1 – Typical mechanical propulsion system [14].

are required when a controllable pitch propeller (CPP) is used to improve fuel efficiency, engine loading and cavitation, for example [14].

Mechanical propulsion can be a good option for vessels that sail at a single cruise speed most of the time, such as cargo ships. However, for tugs, which only use 20% of the maximum capacity during transit, and PSVs, which operate at very low power during DP due to safety requirements, mechanical propulsion would lead to low operational efficiency and high emissions. Therefore, electric or hybrid propulsion can be a good option to improve the performance of such vessels [14].

2.2 ELECTRIC PROPULSION

A proven solution to many mechanical propulsion challenges is the use of an electric propulsion system. Such a propulsion architecture has been used extensively in various marine applications, including cruise vessels, ferries, platform supply vessels (PSV), pipe-laying vessels, Dynamic Positioning (DP) drilling vessels, warships and more [6, 27].

Figure 2 shows a typical architecture of an electrical propulsion system. Multiple Diesel engine generator sets, or simply gensets (1), feed a high voltage electrical bus with a fixed frequency (2). The bus feeds the electric motors (5) for propulsion, as well as the auxiliary loads

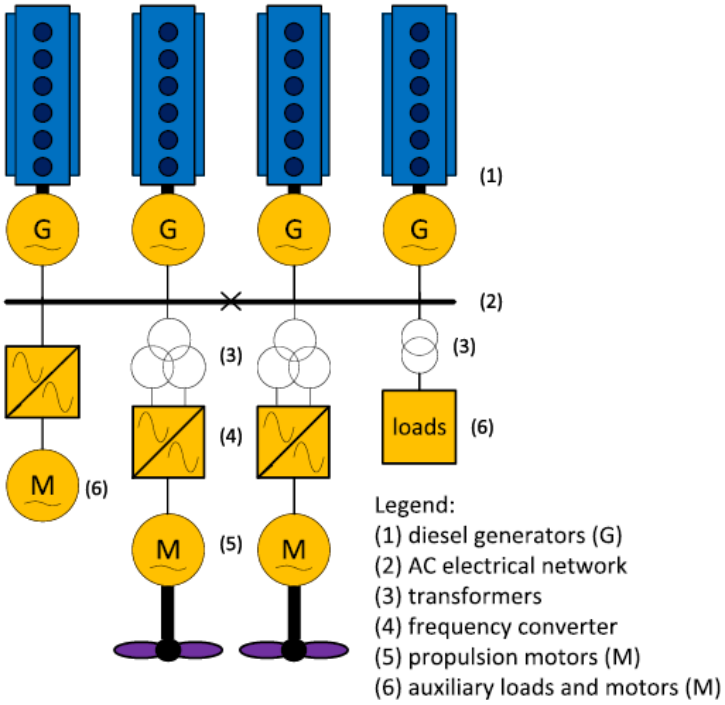

Figure 2 – Typical electric propulsion system [14].

(6), often using a transformer (3). The electric motors receive the power from a power electronic converter (4), which allows propeller speed control.

The arrangement of the electric propulsion system may vary, leading to three main classifications. When the gensets are separated, with one group of generators being used for propulsion loads and another for hotel and service loads, we have the separated electric propulsion system. Another option is having all generators supplying all the electrical loads. This arrangement is referred as the integrated propulsion system (IPS). Finally, when all hydraulic and pneumatic loads are converted to electric loads, we have the so-called all-electric vessels [27], as shown in Fig. 2. Considering the mechanical propulsion system as the base case, the advantages and disadvantages of electric propulsion can be listed as in Table 1.

To achieve fuel-efficient propulsion, the electrical architecture uses a power management system (PMS) that matches the number of generators to the power load. This power management is often described as the power station concept. The main control strategies for electric propulsion vessels consist of controlling the electrical network to assure robust power supply, guarantying voltage and frequency stability, load sharing among the power generation units, and protection, as well as controlling the propulsion system to allow vessel maneuvering [6, 14].

Table 1 – Advantages and disadvantages of the electric propulsion system [14, 27].

Advantages
With multiple available engines, it is possible to optimize power generation.
The generated power can be used for propulsion and to supply power for hotel and service loads. Especially when the hotel and service loads are a significant fraction of the propulsion power required, and the operating profile is diverse, electric propulsion is an efficient solution.
Reduced vulnerability and high reliability due to redundancy of power generation units.
Improved life cycle cost, consumption, emissions, and maintenance reduction [1], even when operating with low demand.
The use of lighter engines can reduce the weight and space necessary for the entire system [2].
Flexibility to position devices such as thrusters, gensets, and converters, since the energy is transmitted through cables. With this, the use of space can be improved.
Better maneuverability due to the use of azimuth thrusters or podded propulsion.
Despite the energy conversion losses due to the addition of devices to the powertrain, there are overall improvements in energy efficiency.
The use of electrical motors allows efficient vessel speed variation.
Disadvantages
Increased initial investment cost.
The addition of components to the power and propulsion plant increases the transmission losses at the full vessel speed.
Electronic converters produce harmonic distortion in the electrical power system.
When running generators with redundancy to achieve high availability for propulsion in DP operations, for example, the engines tend to run at low loads. This leads to an increase in fuel consumption and high emissions.

2.2.1 Voltage and frequency control

Electric AC networks used for electric propulsion usually operate at a fixed frequency controlled by the engine governor. The governor comes in the form of a hydro-mechanical or an electronic controller to adjust the engine speed via fuel injection. An automatic voltage regulator (AVR) is used to control the genset output voltage. The AVR is an electronic controller that adjusts the current supply to the field winding of the generator to regulate the voltage, considering, for example, a synchronous generator [6, 31].

The electrical network regulation is driven by the genset power generation control, given the load requirements. Figure 3 shows the isochronous control approach. In this control, the setpoints of engine speed and voltage are kept constant regardless of the power load. Although this method works well for a single generator, for multiple generators connected to the same

[1] If power generation is optimized, as mentioned in the table, we can decrease unnecessary machine use. However, with more components in electric propulsion, the overall cost of machinery maintenance may increase.

[2] With more components in electric propulsion, the overall weight may increase, as mentioned in [28]. However, the weight of mechanical equipment decreases due to less space between the Diesel engine and propeller shafts and rudders [29]. Also, in electric propulsion, engines are generally medium to high-speed, lighter than lower speed engines commonly used in mechanical propulsion [30].

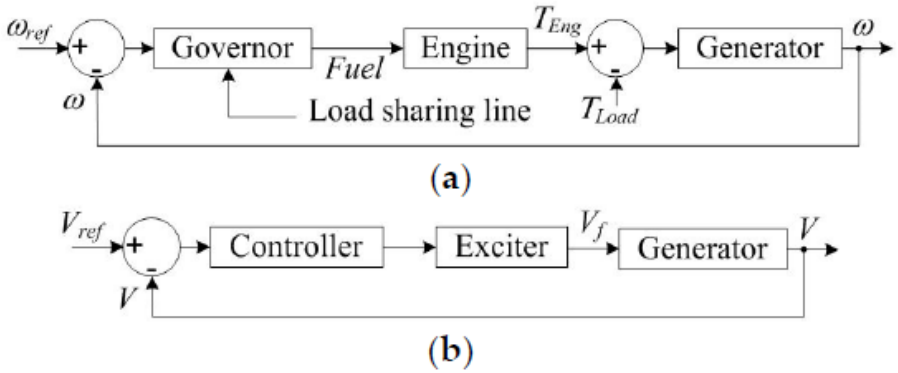

Figure 3 – Engine-generator control system: (a) Isochronous speed controller; (b) automatic voltage regulator [31].

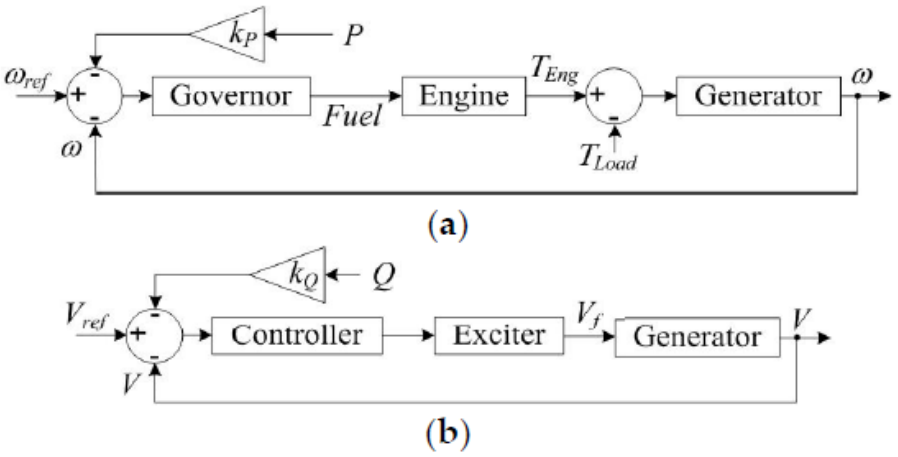

Figure 4 – Engine-generator control system: (a) speed droop; (b) voltage droop [31].

power bus, it can be a problem to share the loads. To solve this problem, communication between the governor controllers is usually required, and this brings technical challenges [31].

On the other hand, droop control is a popular choice for load sharing among multiple generators. It does not require communication among governor controllers and allows the frequency and voltage setpoints to change within narrow limits, in proportion to the active (P), and reactive power (Q) demands. Therefore, to control the load sharing of active power, it is necessary to define the speed droop setting of each engine. For reactive power, the voltage droop setting has to be determined. The amount of droop is a percentage variation of speed and voltage, considering these quantities at no load and full load [6, 31]. Figure 4 shows a simplified droop control diagram.

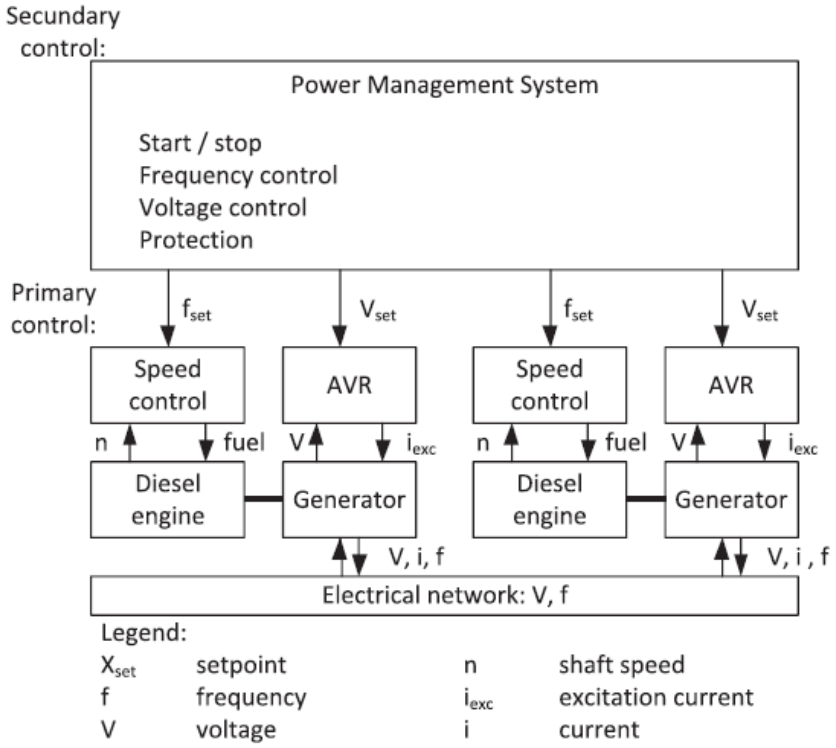

Figure 5 – Typical control strategy for fixed frequency AC networks [14].

2.2.2 Power management control

Figure 5 shows a power management system (PMS) control block diagram for a typical AC network equipped with droop control. The PMS is responsible for defining the voltage and frequency set-points and maintaining them within operating limits. Besides that, it manages the number of running gensets, synchronization, protection control, and blackout prevention. It can limit the propulsion drives and other loads to ensure the power demands are met. For vessels that execute sensitive operations such as DP, the PMS is also responsible to assure the spinning reserve [6, 14, 32].

2.2.3 Propulsion control

The propulsion control has to provide the necessary thrust to propel the vessel. Electrical motors are capable to work at every speed moving forward or backward, as well as delivering nominal torque at almost every speed. Therefore, most electric propulsion architectures use fixed pitch propellers. In general, the strategy is to control the speed of the electrical motor and the flux to assure constant torque switching signals of the electronic converter [14, 33, 34]. Other propulsion strategies can explore torque and power control directly, as mentioned in [14, 33].

2.3 DIESEL-ELECTRIC PROPULSION WITH HYBRID POWER SUPPLY

For vessels, propulsion hybridization typically refers to a plant with (1) hybrid propulsion and (2) hybrid power supply. The first case consists of a combination of mechanical and electrical propulsion. It can be an interesting solution for cases where the auxiliary loads are only a fraction of the required propulsion power. The second case is associated with vessels whose power generation uses a combination of different power sources, such as Diesel generators and batteries [3, 14], for example. For vessels with significant power demand peaks followed by long periods of low load, and highly dynamic loads, such as PSVs, hybrid technologies can reduce fuel consumption and emissions by 10% to 35%, according to [3].

A hybrid power supply system is a technological framework that combines the advantages of different power modes separately or in an integrated manner. Moreover, such hybridization can be used as a bridge to support the energy transition. The research in hybrid power sources can be truly comprehensive, from the use of primary power generation options, such as engines powered by Diesel, biofuels, or liquified natural gas (LNG), and gas turbines, to other propulsion technologies such as nuclear, batteries, fuel cells, renewable energy sources, among others [9]. In this work, we will focus on hybrid topologies that combine electric propulsion systems driven by Diesel engines (Diesel-electric propulsion) with lithium-ion batteries.

Figure 6 shows a scheme of an example of an electric propulsion system with a hybrid power supply. The system comprises the components that would be used in a typical electric propulsion system, with the addition of an energy storage system (ESS), which can be a battery, for example. The battery can be connected to the AC electrical system through a power inverter.

It is common to classify the hybrid vehicle architectures in the automotive field in series, parallel, and series-parallel or power-split. According to [14], this classification does not apply to vessel propulsion schemes because they can have multiple propulsion engines, electric motors, diesel generators, energy storage systems, and fuel cells. However, as in [35, 36], some authors combine the concepts of hybrid propulsion and hybrid power supply to classify vessel powertrains into series, parallel and series-parallel types.

According to [35], a serial configuration for a vessel consists of all power sources and consumers connected to a main electrical grid, as shown in Fig. 6. In the parallel configuration, there is also a direct mechanical connection between the internal combustion engines and the propellers, as shown in Fig. 7(a). Also, the mechanical propulsion can be assisted by an electric

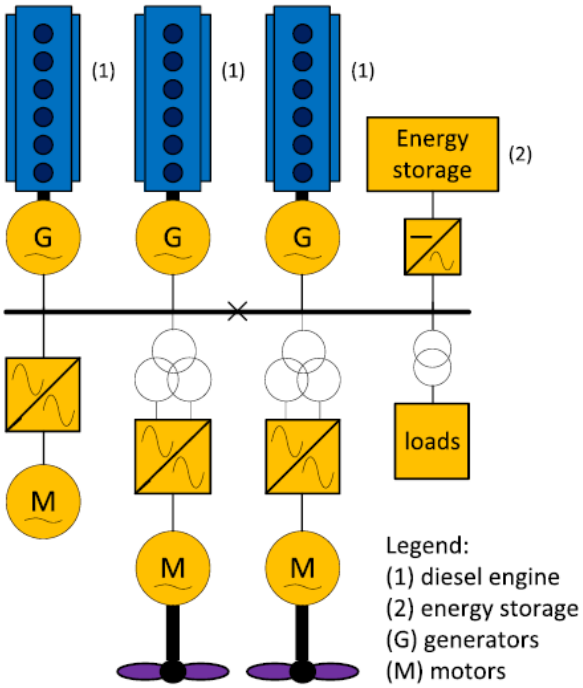

Figure 6 – Typical electrical propulsion system with hybrid power supply [14].

motor connected to the main electrical grid. The series-parallel configuration, shown in Fig. 7(b), combines both concepts. Having an engine that can generate electrical power for the main grid and run a propeller with a mechanical connection allows a variety of operational modes, e.g., directly mechanical, fully electric, series hybrid, only parallel hybrid, or both.

Hybrid power systems using batteries have recently become a feasible option for many maritime applications, thanks to advancements in power electronics and the development of high energy and power density batteries, which was driven mainly by the automotive industry. Hybrid power supply has been applied in various types of vessels, including tugs, yachts, ferries, and PSVs [3, 11].

2.3.1 Energy Storage System (ESS): lithium-ion batteries

A battery is not a power source like Diesel engines or gas turbines, but it is a device that can store and convert energy. As such, it enables a new approach to the design and operation of power systems. The battery can be used strategically to optimize the power systems based on different objectives, having a growing and promising impact on maritime applications [16].

Lithium-ion batteries, or simply Li-ion batteries, are energy storage systems (ESS) that use lithium ions as key components in the fundamental electrochemical reactions that enable the conversion of chemical energy to electrical energy and vice-versa [37]. Such batteries

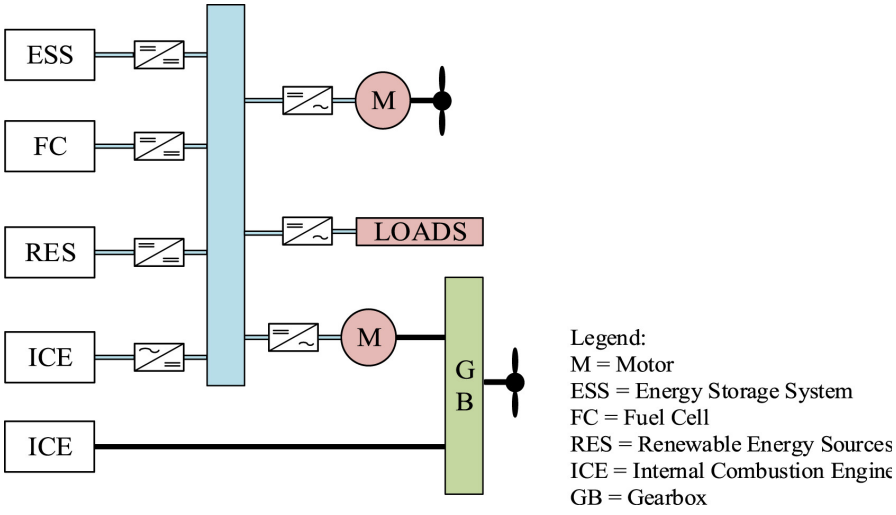

(a) Parallel hybrid power topology [35].

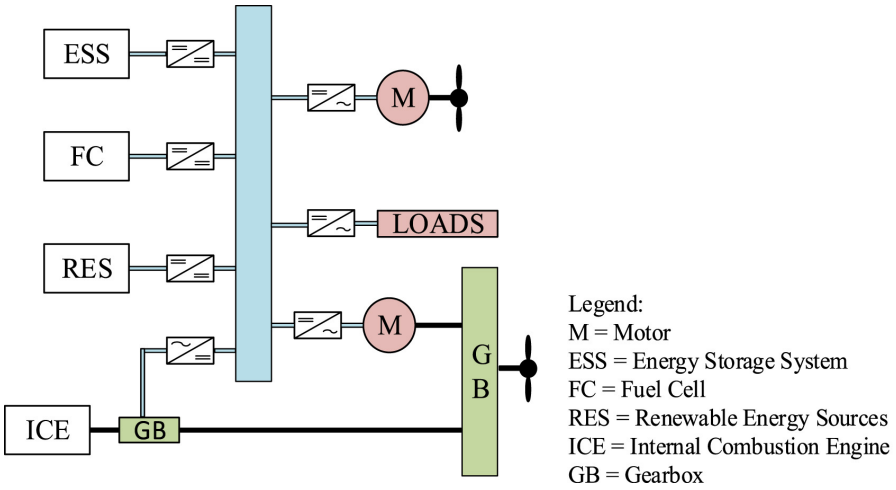

(b) Series-parallel hybrid power topology [35].

Figure 7 – Hybrid power propulsion topologies for vessels.

have the highest specific energy and energy density of commercially available batteries, with a relatively high life cycle. Disadvantages include cost, flammable electrolytes, and potential material shortages [16, 37].

In general, batteries have electrodes, the anode and the cathode, through which the electrons flow during operation. Most lithium-ion batteries use carbon graphite anodes with different cathode chemistry. The most suitable and commercially available battery technologies for marine applications are depicted in Fig. 8, considering several aspects, including power density, energy density, cost, and safety.

The application of lithium-ion batteries for hybrid-powered vessels can be diverse. The battery functional roles include spinning reserve, peak shaving, strategic loading (optimizing load sharing), enhanced dynamic support (immediate power delivery), harvesting energy, and

Battery technology	Specific energy [Wh/kg]	Advantages	Disadvantages	Applicable for maritime
Nickel manganese cobalt oxide (NMC)	150-220	Combination for High Specific Energy Adjustable power density, energy density cost and safety	Key properties equilibrium may be difficult to ensure for a stable life-span	Flexible design with respect to energy and power capabilities. The most used chemistry in marine applications at present
Lithium iron phosphate (LFP)	90-120	Higher Safety Characteristics Resilient to temperature fluctuations Cathode doping possible for higher power applications	Relatively low Specific Energy Lower Voltage Lower power capabilities	Used in marine applications because of its good safety features.
Nickel Cobalt Aluminium (NCA)	200-260	High specific energy and energy density Good calender life	Lower safety Higher cost	Suitable because of its high energy density
Lithium Titanate Oxide (LTO)	50-80	Higher safety characteristics Very high cycle life High power capability	Relatively low Specific Energy Initial cost is high, but total life time cost might be cheaper	Suitable for applications that requre fast charging, high power or very large amounts of cycling

Figure 8 – Promising commercially available batteries [16].

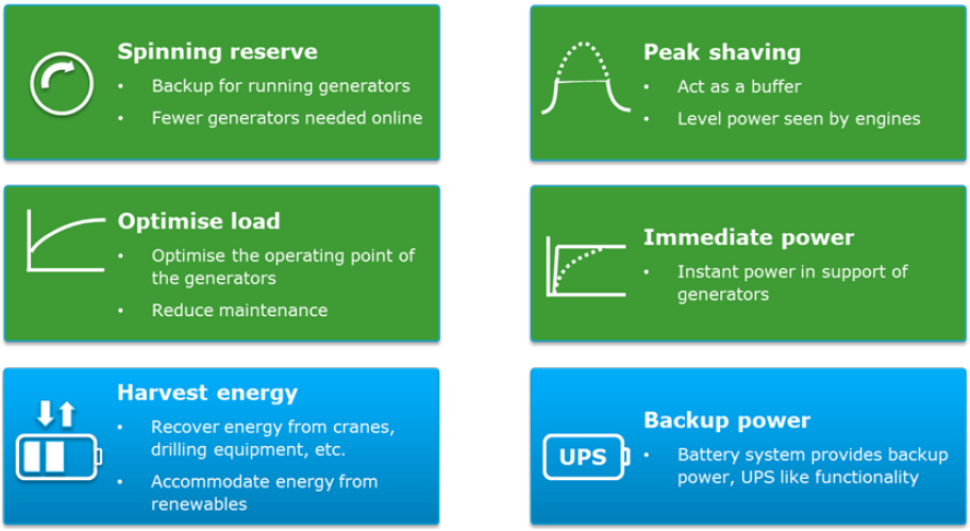

Figure 9 – Functional roles of battery systems onboard vessels [16].

providing backup power, as depicted in the Fig. 9. A list of functions and benefits of batteries for hybrid vessels is presented below, based on [6, 13, 14, 16, 38]:

- **Spinning reserve and backup power:** Recent developments in marine regulations allow the use of batteries as a spinning reserve. This function ensures the battery has sufficient energy to be used in case of a sudden loss of power generation capacity, such as a generator loss. Therefore, the battery can be used for redundancy, acting as a backup for running generators, requiring fewer engines online, reducing fuel consumption, emissions, and engine running hours.

- **Enhanced ride through and UPS:** similar to spinning reserve, but for a local sub-system like a thruster or other device. The battery can function as an uninterrupted power supply (UPS), ensuring the power system's availability.

- **Peak shaving:** the energy storage system can absorb the power load variations such that the engines operate with constant loads. In general, transient fuel consumption is higher than steady-state fuel consumption. With this, we can avoid the need to start engines to supply power for short periods or turn off engines and have the need to switch them on again. Hence, significant reductions in fuel consumption, CO_2, and NOx emissions can be achieved.

- **Enhanced dynamic support:** the battery absorbs sudden load changes such that the generator sees a gradual increase or decrease in load. Enhancing dynamic support allows instant power delivering, improving the system's response to fast load variations. This function is automatically included if the peak shaving function is enabled.

- **Strategic loading:** the battery charging and discharging can maintain the engines operating within the most fuel-efficient operating range. With this, it is possible to increase the overall energy efficiency of the power system, hence reducing fuel consumption and CO_2 emissions. In addition, by switching off generators, it can reduce noise, vibration and increase comfort.

- **Harvest energy:** batteries can store the energy regenerated in vessels when breaking the electric motors. Such power is generally dissipated through resistors. Vessels with heavy crane installations, offshore and drilling vessels, with heave compensation can regenerate a significant amount of energy.

- **Zero emissions operation:** batteries can provide zero-emissions operation under specific conditions. For example, near the port, while loading PSVs, or when the Vessels are on standby, the loads are relatively low. In such situations, a battery pack can completely power the vessel so the generators can be switched off.

Despite the benefits, the addition of a battery for hybrid power supply leads to the following challenges based on [6, 14, 16]:

- **System's and control complexity:** the increase in the number of power sources and power dispatch possibilities increases the control and system's complexity. The control needs to use the battery strategically to improve energy efficiency considerably.

- **Cost**: the battery addition implies a considerable investment that needs to be justified. In this context, the reduction of installed power from Diesel engines can be evaluated to minimize the cost of installing batteries.

- **Regulations**: there are specific requirements for using batteries for spinning reserve, especially in sensitive operations like dynamic positioning. Some regulations do not allow batteries for spinning reserve in retrofits unless significant changes in various systems are performed.

Some research works have shown performance improvements by adding lithium-ion batteries to vessels. However, more studies are required to understand the power supply hybridization feasibility better. A recent technical report from the European Maritime Safety Agency shows fuel savings potential for several vessels, as shown in Fig. 10. However, as clearly stated, the results vary depending on the vessel's type and operational profile.

In [13], the authors proposed a power system model to calculate the fuel savings and emission reduction potential of a generic vessel hybrid powertrain with a battery module. A fuel consumption reduction of approximately 45% and a NOx emission reduction of 85.6% were achieved. Nonetheless, neither the load demand nor the CO_2 were described. The work by [13] was extended in [23] to present an experimental validation of the mentioned hybrid power system models. However, the considered ranges of battery efficiency were not appropriate as pointed out in [20].

In [20], the authors analyzed the reduction of CO_2 emissions using a hybrid power system for a PSV and performed a sensitivity analysis. The energy dispatch was optimized, considering the cost of the energy sources. Reductions in CO_2 emissions of up to 8.7% were obtained with the addition of auxiliary Diesel engines and batteries. For a combination of generators and a battery, a reduction in emissions of 7.4% was achieved. The optimization methodology and the models were not discussed in detail. Besides, the global optimization requires the complete load profile, which is interesting for setting benchmarks. However, in a real situation, a causal approach is necessary.

Ship type	Fuel savings potential (%)	Payback time (years)	Main battery function considered	Factors which can maximize benefit
Ferry	Up to 100	Less than 5	All electric where feasible	Low electricity costs, high port time, low crossing distance
Offshore supply vessel	5 – 20	2 - 5	DP - Spinning reserve	Low power and energy needs for backup
Cruise	< 5	Highly variable	Hybrid operating in all electric, ticket to trade	Ability to operate in all electric mode for extended period
Offshore drilling unit	10 – 15	1 – 3	Spinning reserve and peak shaving	Closed bus, large battery size
Fishing vessel	3 - 30+	3 - 7	Hybrid load levelling and spinning reserve	Diesel sizing relative to loads
Fish farm vessel	5-15 %	3-7	Hybrid load levelling and spinning reserve	Diesel sizing relative to loads
Shuttle tanker	5 – 20	2 - 5	DP - spinning reserve	Low power and energy needs for backup
Short sea shipping	Highly variable	Highly variable	All electric or many hybrid uses	Vessel and duty cycle dependent
Deep sea vessels	0 – 14	Highly variable	PTO supplement	Highly variable, detailed duty cycle analysis
Bulk vessels with cranes	0 – 30*	0 - 3	Crane system hybridization	Integration with genset sizing
Tug boats	5 - 15 (100 if all electric)	2 - 8	All electric or many hybrid uses	Detailed duty cycle analysis
Yachts	5 – 10	Highly variable	Silent operation, spinning reserve	Detailed duty cycle analysis
High speed ferry	Up to 100	3 - 6	All electric or hybrid	Detailed duty cycle analysis
Wind farm support vessels	5 – 20	2 - 5	DP - Spinning reserve	Low power and energy needs for backup

Figure 10 – Summary table with typical values regarding application feasibility and benefit [16].

2.4 CONTROL STRATEGIES FOR ELECTRIC PROPULSION WITH HYBRID POWER SUPPLY

At sea, the vessel power system is often compared to island microgrids because both have to produce their energy to supply local demands and both are disconnected from a main and larger grid. However, significant differences associated with load characteristics and energy distribution exist. Despite the differences, terrestrial microgrid control strategies can provide important insights for hybrid power supply on vessels [14]. A typical control approach for hybrid systems in islands consists of three hierarchical levels. Such control can also be adopted for vessel microgrids [31].

The three-level hierarchical control framework can be seen in Fig. 11. The primary level is responsible for achieving the load sharing among the power sources, previously defined from upper control levels, and control voltage and frequency for stability, including generator speed and voltage control, battery converter voltage control, and electric motor speed control [14, 31].

The secondary control strategies, performed by the power management system (PMS), comprise the start/stop generator control and power quality management to correct fluctuations in voltage and frequency. Additionally, the PMS is responsible for guarantying the power demand supply. The tertiary control level manages dispatching and optimization, microgrid supervision, and generation plan [14, 31].

2.4.1 Energy Management control

An optimized Energy Management System (EMS) is essential to solve the power flow problem in tertiary control, improve energy efficiency, and harness the hybrid power supply potential. The EMS control allows to regulate the generation, distribution, storage, and power split between generators and the battery module to supply the necessary power, matching the loads with the existing constraints [3, 14, 31, 39].

It is important to mention that some authors in the scientific literature use the EMS and PMS terms interchangeably sometimes [3, 6, 14]. Such classification may happen because some control functions of the EMS can be available in a PMS, for example, or due to the relation between energy and power determination. Some works even use the term PEMS referring to the integration of an EMS and a PMS [39]. In this work, the term EMS will be used for tertiary control as explained, using Fig. 11 as reference.

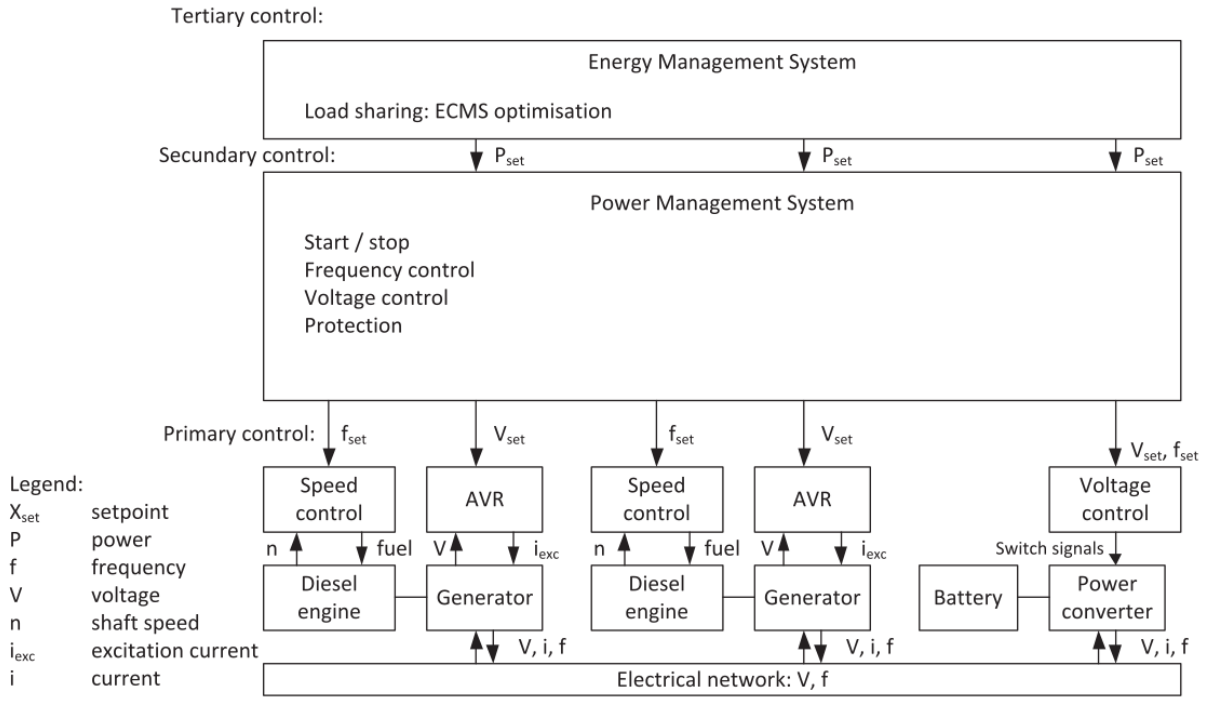

Figure 11 – Three-level hierarchical control framework.

There is an extensive research field driven by road vehicle applications concerning EMS control applied to hybrid power supply, as shown in Fig. 12. Combining the insights given by island microgrids, hybrid vehicles, and strategies in research for vessels, the EMS control can generally be classified into heuristic/rule-based (RB) or optimization-based [19, 31, 40, 41].

The heuristic strategies comprise several options, such as using simple rules or fuzzy logic control (FLC). Heuristic EMS strategies have been considered for vessels in [11, 42, 43]. Regarding optimization methods, there are offline optimization strategies, which can allow global optimization, and online or real-time optimization approaches. The last option includes strategies that can be used for causal systems, such as equivalent consumption minimization strategy (ECMS) and model predictive control (MPC). ECMS strategies are discussed for vessels in [3, 6, 11, 41], while MPC approaches are studied in works such as [18, 44, 45]. Besides, some works integrate the EMS strategy with a power demand estimation using optimization methods [46] or not [3,47]. Artificial intelligence approaches are also considered for hybrid vessel systems in the literature, including FLC, which is a heuristic method, and optimization-based methods such as reinforcement learning [19, 41].

In the following subsections, we will briefly describe and discuss rule-based and ECMS control strategies to be used as a foundation for the EMS approaches proposed in chapter 5. The

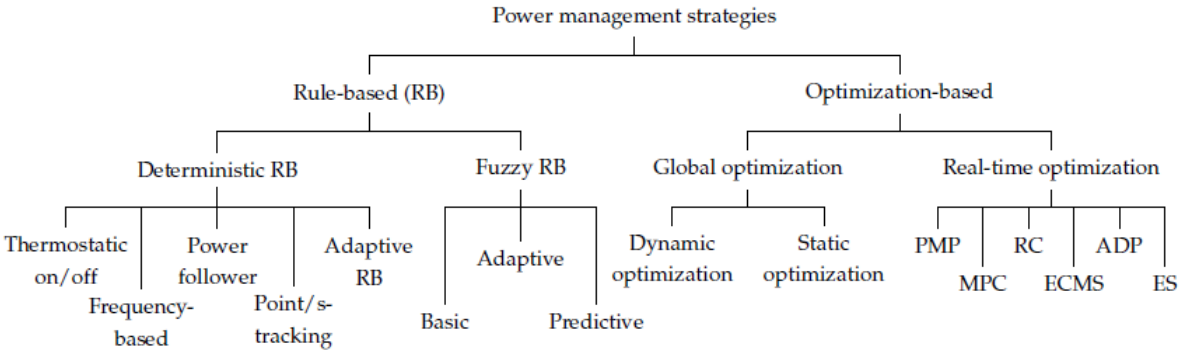

Figure 12 – Classification of energy management strategies [40].

EMS formulation review focuses on Diesel-electric propulsion systems with lithium-ion batteries that consider causal systems.

2.4.2 Rule-based (RB) strategy

Heuristic or rule-based (RB) control strategies consist of determining the plant power dispatch through logical rules. The rules can be implemented using if-then statements, for example, or more sophisticated methods, as mentioned above. The power follower approach is a common RB strategy that relies on the definition of different control cases taking into consideration the available power and the state of charge (SOC) of the battery [39].

The power follower control strategy has been implemented for vessels in [11, 42] to increase energy efficiency. Figure 13 shows the set of rules used in [11] to determine which power mode is selected based on the battery SOC and the magnitude of the power load P_{load}, with the main objective of avoiding the use of generators in low loads (less efficient regions).

The first line of the table in Fig. 13 considers the low load demands of the mission. If the SOC is below the limit SOC_{min}, one generator is switched on with optimal power $P_{G1} = P_{G1,opt}$. The excess of power can be used to charge the battery, considering the power limits of both battery and generator. If the battery is above the SOC_{min}, the battery takes the entire power load. If the battery power is not sufficient, a generator runs with the power difference.

In the second line of the table, the load demand is within the lower limit $P_{G1,on}$ to switch at least one generator and the optimum power reference $P_{G1,opt}$. In this regime, if the SOC is below the maximum, generator 1 is switched on at the optimal power set $P_{G1,opt}$, while genset 2 is kept off, $P_{G2=0}$. If there is any extra power from the generators, such energy is used to charge the battery. If the SOC is above the maximum limit SOC_{max}, genset 1 takes on all the load $P_{G1} = P_{load}$.

Power \ SOC	$SOC \leq SOC_{min}$	$SOC_{min} < SOC \leq SOC_{max}$	$SOC \geq SOC_{max}$
$P_{load} \leq P_{G1,on}$	$P_{G1} = P_{G1,opt}$, $P_{G2} = 0$ $P_{batt} = P_{load} - P_{G1}$ if $P_{batt} > P_{charge,max}$ $P_{batt} = P_{charge,max}$ $P_{G1} = P_{load} - P_{batt}$ end	$P_{G1} = 0$, $P_{G2} = 0$ $P_{batt} = P_{load}$ if $P_{batt} > P_{discharge,max}$ $P_{batt} = P_{discharge,max}$ $P_{G1} = P_{load} - P_{batt}$ end	$P_{G1} = 0$, $P_{G2} = 0$ $P_{batt} = P_{load}$ if $P_{batt} > P_{discharge,max}$ $P_{batt} = P_{discharge,max}$ $P_{G1} = P_{load} - P_{batt}$ end
$P_{G1,on} < P_{load} \leq P_{G1,opt}$	$P_{G1} = P_{G1,opt}$, $P_{G2} = 0$ $P_{batt} = P_{load} - P_{G1}$ if $P_{batt} > P_{charge,max}$ $P_{batt} = P_{charge,max}$ $P_{G1} = P_{load} - P_{batt}$ end	$P_{G1} = P_{G1,opt}$, $P_{G2} = 0$ $P_{batt} = P_{load} - P_{G1}$ if $P_{batt} > P_{charge,max}$ $P_{batt} = P_{charge,max}$ $P_{G1} = P_{load} - P_{batt}$ end	$P_{G1} = P_{load}$, $P_{G2} = 0$, $P_{batt} = 0$
$P_{G1,opt} < P_{load} < P_{G1,opt} + P_{G2,opt}$	$P_{G1} = P_{G1,opt}$, $P_{G2} = P_{G2,opt}$ $P_{batt} = P_{load} - P_{G1} - P_{G2}$ if $P_{batt} > P_{charge,max}$ $P_{batt} = P_{charge,max}$ $P_{G1} = P_{G1,opt}$ $P_{G2} = P_{load} - P_{G1} - P_{batt}$ end	$P_{G1} = P_{G1,opt}$, $P_{G2} = P_{G2,opt}$ $P_{batt} = P_{load} - P_{G1} - P_{G2}$ if $P_{batt} > P_{charge,max}$ $P_{batt} = P_{charge,max}$ $P_{G1} = P_{G1,opt}$ $P_{G2} = P_{load} - P_{G1} - P_{batt}$ end	$P_{G1} = \frac{P_{load}}{2}$, $P_{G2} = \frac{P_{load}}{2}$ $P_{batt} = 0$
$P_{load} \geq P_{G1,opt} + P_{G2,opt}$	$P_{G1} = \frac{P_{load}}{2}$, $P_{G2} = \frac{P_{load}}{2}$ $P_{batt} = 0$	$P_{G1} = P_{G1,opt}$, $P_{G2} = P_{G2,opt}$ $P_{batt} = P_{load} - P_{G1} - P_{G2}$ if $P_{batt} > P_{discharge,max}$ $P_{batt} = P_{discharge,max}$ end	$P_{G1} = P_{G1,opt}$, $P_{G2} = P_{G2,opt}$ $P_{batt} = P_{load} - P_{G1} - P_{G2}$ if $P_{batt} > P_{discharge,max}$ $P_{batt} = P_{discharge,max}$ end

Figure 13 – Rule based strategy for a case of all-electric hybrid power system consisting of two gensets and a battery. The variables are described as P_{G1}: Power reference of genset 1 from supervisory level (kW), P_{G2} Power reference of genset 2 from supervisory level (kW), $P_{G1,on}$: Power setpoint to switch on genset 1 (kW), $P_{G1,opt}$: Optimal operating power setpoint for genset 1 (kW), $P_{G2,opt}$: Optimal operating power setpoint for genset 2 (kW), P_{load}: Load demand (kW), $P_{charge,max}$: Maximum battery charging limit (kW), $P_{discharge,max}$: Maximum battery discharging limit (KW) [11].

In the third line, the situation is similar to the second one, but with a higher power load, although within the optimal power reference of the first generator, $P_{G1,opt}$, and the optimal power combination of both generators, $P_{G1,opt} + P_{G2,opt}$. The generators run with optimal load, and the battery is below the maximum SOC. The power split is readjusted, if necessary, to consider the power limits of the gensets and the battery. If the battery SOC reaches its maximum value, both generators share the load equally.

The fourth line considers the case in which the power load is above the optimal combination of both generators. The load is shared equally for a battery SOC below the minimum limit. The battery is used to shave peaks higher than the optimal power combination of the gensets, being discharged if its SOC is above the minimum limit.

The power follower rule-based strategies are a common control approach applied in hybrid power systems because they are easier to design and implement. However, the complexity can increase with a higher number of power sources. For the mentioned case, in Fig. 13, 12 rules were required. Following the same approach for a PSV with four generators and a battery pack, the number of rules could easily increase to 18 rules, or even more. RB approaches generally

rely on human expertise and intuition. Therefore, it can be hard to optimize the power dispatch, particularly if there is a high number of rules [11, 39].

Fuzzy logic control (FLC) is another option for managing power modes using a heuristic approach. The FLC is a branch of intelligent control based on fuzzy logic and on an inference system [43, 48]. The logical variables in a fuzzy system can take continuous values between 0 and 1, not strictly 0 or 1. The FLC is based on fuzzy sets which are groups of objects with intersections, a transition from a membership of one set to another. Through an inference process is possible to estimate values of interest based on rules and produce decisions, or control inputs [48].

This strategy allows smoother transition regions between the different operating modes and control robustness. For automotive applications, research works show promising results that outperform the basic rule-based strategies [39]. In [42], fuel economy was achieved by comparing a basic RB strategy and a fuzzy logic control (FLC) approach for a generic vessel power system topology. Good performance has been achieved for the management of multiple power sources in [43], including photovoltaic panels, a wind turbine, a battery pack, and a proton exchange membrane fuel cell (PEMFC).

2.4.3 Equivalent consumption minimization strategy (ECMS)

EMS optimization strategies rely on the minimization or maximization of some performance index to determine the power dispatch. Although global optimization control strategies are essential for determining benchmarks, they require the knowledge of the complete mission. Therefore, real-time strategies are necessary for representation accuracy and the development of an EMS that can actually be implemented in real systems.

The equivalent consumption minimization strategy (ECMS) concept was first introduced in automotive applications but has also been applied for hybrid power systems in vessels. This approach is an optimal control strategy, in which a cost function is defined for the fuel consumption of each power mode. The arguments that minimize the cost function are the control inputs. Regarding all electric hybrid power systems such as Diesel-electric systems with a battery, the cost associated with the battery is determined through the equivalent fuel that would be used to recharge the device, using the engines [3, 11, 26].

The most well-known ECMS formulations are derived from Pontryagin's Minimum Principle (PMP) [21, 49]. To describe the minimum principle for a general optimal control

problem, we can consider the system dynamics

$$\dot{\mathbf{x}} = f(\mathbf{x},\mathbf{u},t), \tag{1}$$

where $\mathbf{x}$ is the state vector, $\mathbf{u}$ the control vector, and t the time. The control problem consists of finding the sequence of control inputs $\mathbf{u}^0(t)$ that minimize the cost function:

$$J = \int_0^{t_f} L(\mathbf{x},\mathbf{u},t)dt, \tag{2}$$

given the constraints in control inputs and states [50]. For this problem, we can define the Hamiltonian function

$$H(\mathbf{x},\mathbf{u},t) = L(\mathbf{x},\mathbf{u},t) + \lambda^T(t) \cdot f(\mathbf{x},\mathbf{u},t), \tag{3}$$

with λ being the problem co-state vector. Assuming the optimal control $\mathbf{u}^0(t)$ exists and is unique, the control problem solution is

$$\mathbf{u}^0(t) = \arg\min_{\mathbf{u}} H(\mathbf{x},\mathbf{u},t) \tag{4}$$

and the co-state vector is determined through

$$\dot{\boldsymbol{\lambda}}(t) = -\frac{\partial H}{\partial \mathbf{x}}. \tag{5}$$

The standard and simpler ECMS formulation considers static models for the powertrain [26, 49], with the dynamics being governed by the battery state of charge as

$$\dot{SOC} = g_{SOC}(SOC,\mathbf{u},t), \tag{6}$$

where g_{SOC} can be a function of the SOC, control inputs $\mathbf{u}$, and time. According to [49], for the hybrid electric vehicle (HEV) case, in which only one engine is considered, the cost function can be defined in the following manner:

$$L = P_{fuel}(\mathbf{u},t) = Q_{lhv}\dot{m}_f(\mathbf{u},t), \tag{7}$$

where $P_{fuel}(\mathbf{u},t)$ is a measure of the power generated by the engine, Q_{lhv} is the low heat value of the fuel, and $\dot{m}_f$ is the fuel consumption, while $\mathbf{u}$ is the power allocation vector, which includes the engine and the battery power, $\mathbf{u} = [P_{fuel}, P_{bat}]^T$. The Hamiltonian,

$$H(\mathrm{SOC},\mathbf{u},t) = P_{fuel}(\mathbf{u},t) - \lambda(t) \cdot g_{\mathrm{SOC}}(\mathrm{SOC},\mathbf{u},t), \tag{8}$$

can be rewritten as

$$H(\mathrm{SOC},u,t) = P_{fuel}(\mathbf{u},t) + s(t) \cdot P_{bat}(\mathrm{SOC},\mathbf{u},t), \tag{9}$$

with $s(t)$ being the equivalence factor.

In Eq. (9), the Hamiltonian represents an equivalent fuel power. Dividing Eq. (9) by Q_{lhv}, the Hamiltonian can account for an equivalent fuel consumption. The variable $s(t)$ can be interpreted as a weighting factor of the battery power delivery [21, 26, 49]. The power allocation vector that minimizes the equivalent power/fuel in Eq. (9) defines the optimal control inputs, and the equivalence factor can be determined through

$$\dot{s}(t) = \frac{\partial H(\mathrm{SOC},\mathbf{u},t)}{\partial \mathrm{SOC}}. \tag{10}$$

Under the assumption that the battery power does not depend on the battery SOC, the equivalence factor s can be considered constant, and this allows to prove the existence and uniqueness of an optimal solution defined by the ECMS, as mentioned in [49]. Then, the problem becomes finding the optimal s value to get closer to the global optimum solution. The ECMS with the appropriate tuning can be identical or very close to the global optimum, with errors within 1%-2%, for vehicle applications. For vessels, in [3] ECMS formulations also achieved small errors in comparison with the optimal global approaches.

The equivalence factor is a critical control parameter for the ECMS, dictating its performance. For non-causal systems, offline optimization methods can be used to find the best s for specific operational conditions, as in [47]. For online or real-time approaches, various strategies can be used, including the definition of s through trial and error or some physical interpretation of the meaning of the equivalence factor, a PID controller for regulating s to achieve battery charge sustaining, mission estimation to predict load demands, pattern recognition using neural networks, among others [3, 11, 21, 26, 41, 49]. When the value of s is constantly adapted, the authors often refer to the control strategy as adaptive ECMS (A-ECMS).

The ECMS is a flexible approach because other effects can be added by changing the cost function. In [49], different objectives were added to the Hamiltonian, allowing multiobjective optimization for a HEV. The authors consider the minimization of cost functions that combine fuel consumption and emissions such as CO, HC, NOx, or battery aging, battery temperature, engine temperature, using static maps or lumped dynamics in the modeling process. The work shows good results; however, makes it clear that controller robustness and adding state constraints can be an issue. In [51], the authors also consider multiple objectives for a HEV, including fuel consumption minimization and limitation of NOx emissions, as well as avoiding too many engine starts and stops.

In the automotive field, comparative studies have demonstrated that for EMS, ECMS can outperform several heuristic strategies [26]. However, works like [49] explain that rules can be added using a hybrid approach to handle numerical issues caused by state constraints in ECMS. Furthermore, effective rules can be derived from offline ECMS optimizations.

The power system of vessels often has multiple generators, which increases the ECMS formulation complexity. The standard formulations found in the literature for vessels deal directly with the fuel consumption minimization as in [11]. A case study involving a tug with two generators and a battery was considered in the mentioned work and the optimization problem is defined as

$$\mathbf{u}^0(t) = \arg\min_{\mathbf{u}} \dot{m}_{f,eqv}(\mathbf{u},\mathbf{w}). \tag{11}$$

The vector $\mathbf{u}$ represents the control inputs, while $\mathbf{w}$ are the exogenous inputs. The cost function is expressed as

$$\dot{m}_{f,eqv}(t) = \sum_{i=1}^{N} \dot{m}_{f,dgi} + \dot{m}_{bat,eqv}. \tag{12}$$

In this equation, the expression $\sum_{i=1}^{N} \dot{m}_{f,dgi}$ is the combination of the fuel consumption rate of each genset i, of the total N generators, and $\dot{m}_{bat,eqv}$ is the equivalent fuel consumption of the battery. In [3], another tugboat was studied comprising hybrid propulsion and a hybrid power supply system. A cost function similar to Eq. (12) was build, but it considered the system's architecture, which comprised two main Diesel engines, one Diesel generator, and a battery pack. ECMS approaches considering fuel cell, batteries, and super-capacitors for vessels have been studied in [41], as well as other objectives such as battery and fuel cell degradation. In [6], a multi-objective ECMS includes the trade-off between fuel consumption minimization and NOx emissions.

To respect the limits of the power sources, the mentioned ECMS approaches for EMS control generally consider the upper and lower limits for the battery state of charge and the power limits of the energy sources. The latter includes the operating power of Diesel generators, fuel-cells, super-capacitors, engine torque, and the power balance constraint, which guarantees that the load demands are met by combining the power sources. Various formulations are described in the literature, but we could not find either causal EMS strategies or ECMS approaches specifically for PSVs.

The ECMS resulting optimization problems are usually nonlinear and are generally solved numerically, with the formulations involving only continuous variables or both continuous and integer variables. The last cases are classified as mixed-integer nonlinear optimizations.

Various numerical methods can be applied for solving such nonlinear problems through different algorithms, including the interior-point method, sequential quadratic programming (SQP), the augmented Lagrange multiplier method, Branch & Bound (B&B) methods for dealing with integers, among others [3, 11, 41].

For vessels, ECMS approaches look promising. In [11], an ECMS and a rule-based strategy were compared for a Diesel-electric hybrid tugboat. The simulation and the experimental results have demonstrated that the ECMS achieved higher savings, up to 24.4%, compared to the rule-based strategy, considering shore charging. In [3], simulation results for a tugboat have shown that, with an unknown load profile, 6% of additional fuel economy can be achieved by ECMS in comparison with rule-based strategies. [41] also compared heuristic strategies and ECMS, an obtained an increase of up to 6.47% in energy efficiency with the latter.

Different EMS options, considering ECMS for vessel power systems, were compared in some of the mentioned works [3, 6, 11, 41]. However, non-hybrid cases were not considered. Such cases can help us to understand the benefits of hybridization. In addition, the authors did not study the combination of rule-based strategies and the optimization of generators. The latter approach could improve the energy efficiency gains of rule-based strategies for hybrid power systems.

To overcome the limitations of an EMS strategy applied in real-time (ECMS, for example), predictive approaches can be considered. In [3], an adaptative ECMS, statistically predicting the load demand based on past missions is presented. However, the mean performance was similar to a regular ECMS, depending on the load and time horizon. [18] also studied a tugboat and presented a comparison between an ECMS strategy and a Model Predictive Control (MPC) for a specific powertrain and power profile. The last controller has shown a fuel saving increase of 2.36% in comparison with ECMS. In addition, intelligent controllers which employ techniques such as Reinforcement Learning (RL) have also been reported [19], showing good results and dealing with the sensitivity of EMS to different load profiles.

The hybrid powertrain and EMS design research field is extensive and is still in development. The ECMS has been showing a good balance between complexity and performance, based on the literature. The majority of works found in the literature define EMS to improve the power dispatch of tugs and ferries [3, 11, 18, 41]. In general, PSVs have more power sources and demand more power than tugs and ferries, increasing the EMS design complexity. Therefore,

studies are required to evaluate the performance and robustness of such energy management strategies in PSVs, with different load profiles and configurations.

3 REVIEW OF HYBRID PROPULSION SYSTEM MODELS

Project 7 is advancing due to the contributions of this work and efforts from other members, with improvements in models and control strategies. In this chapter, some of the main developments of Project 7 on the dynamical modeling of power systems will be presented, focusing on how the models were previous to this work. Also, we will discuss the modeling process of each component, taking into account the state of the art, important effects to be considered depending on the target analysis, and the balance between complexity and accuracy.

The set of dynamical models in Project 7 include two generator sets (gensets) with two different engines, Diesel and dual-fuel (Diesel and LNG). The ESS model represents a lithium-ion battery module. The propulsion system contains electric motors and drivetrains (gearboxes and propellers). To distribute the power, a static electrical architecture is considered. In addition, models of Solid Oxide Fuel Cell (SOFC) and Proton-Exchange Membrane Fuel Cell (PEMFC), with a steam methane reformer for hydrogen production are implemented, but still require integration to the main system.

In Fig. 14, a block diagram shows the information flux and interaction between the hybrid power system components mentioned above and the vessel. The TPN maritime simulator is responsible for providing valuable information about the physics of the vessel motion (dynamics and kinematics) and interaction with the sea, such as propulsion forces, propeller torques, current velocity and position. Besides the TPN model, a simplified vessel physics model is implemented in the Project 7 model set for fast solution prototyping.

The user defines a required shaft velocity on the thrusters (main, tunnel bow or tunnel stern). Then, the velocity controllers of the propellers set voltages U_M, which also induce currents I_M, in the electric motors, providing power in terms of angular speed ω_e and torque T_{red}. The gearboxes provide velocity and torque conversion, ω_{red} and T_{prop}/T_{red}, respectively. The load torques T_{prop} arise from propellers operation. The TPN simulator receives ω_{red} and calculates the resultant load torques, the propulsion forces and the current vessel velocity v_{sh}.

To achieve the required angular speeds of the propellers, the controllers set adequate voltages to the motors U_M, draining power from the grid. Two transformers are responsible to regulate the voltage and current and to connect the battery to the grid, as well as the service loads to the battery module. In Fig. 14, the mentioned fluxes of information in terms of current and

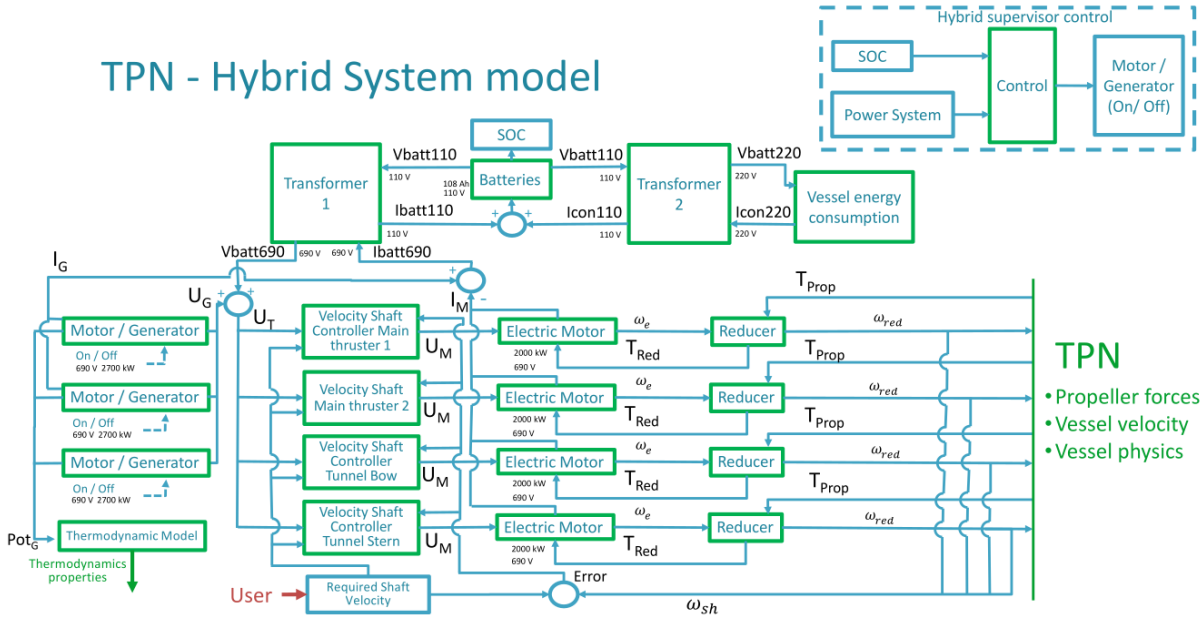

Figure 14 – Hybrid power system block diagram [24].

voltage can be seen. The electrical demand of power is shared among the generators connected to the AC power grid which runs at a constant voltage U_G, with current I_G.

The power demand is transferred to the combustion engines. Thermodynamic models account for the mass, energy and exergy balances and produce output information such as fuel consumption, CO_2 emissions, thermal efficiency, exergy efficiency etc. For the EMS, a rule-based algorithm is implemented for the Hybrid Supervisory Control (HSC). The HSC objective is to reduce CO_2 emissions operating the internal combustion engines close to maximum efficiency regions and managing the state of charge (SOC) of the battery.

3.1 ENGINE GENERATOR SETS (GENSETS)

Constant voltage and frequency are assumed for the generator, with the internal combustion engine (ICE) shaft running at nominal speed. The bus voltage is considered constant, and given the required power in the electrical network, the genset current is determined. The power demand of the generator is transferred to the ICE.

The models for a dual-fuel (Diesel/LNG) Wärtsilä 6L34DF and a Diesel CAT 3512C generator consist of two parts [24]. First, the start-up time and load ramps are considered from technical catalogs. In a second part of the ICE model, conservation equations are applied to a control volume (CV) considering a steady operation, and the thermodynamics is evaluated [52].

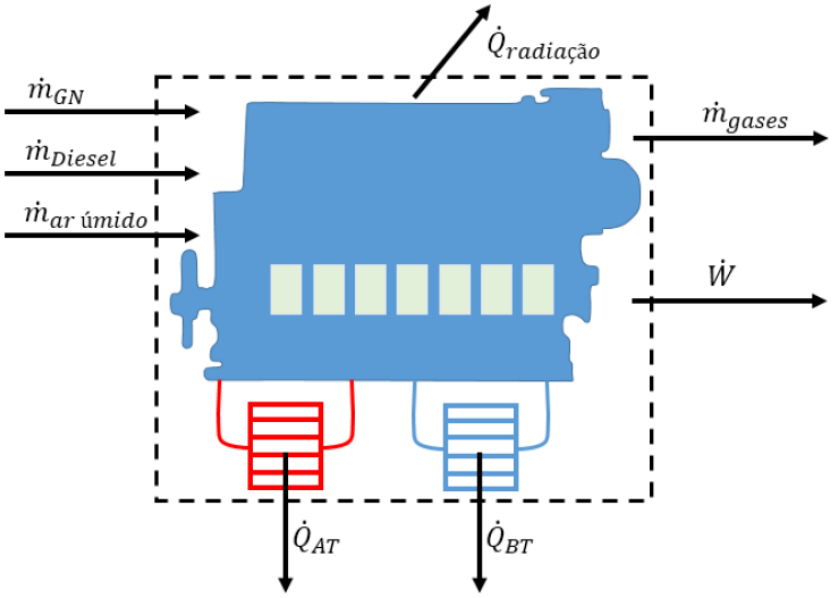

Figure 15 – Control volume considered for the ICE analysis [52].

The CV in which the analysis is performed comprehends the engine, the turbocharger, and the water cooling system (comprising the heat exchangers). The cooling system is divided into a high temperature (HT) and a low temperature (LT) circuit. An illustration of the CV for the dual-fuel Wärtsilä 6L34DF can be seen in Fig. 15.

The mass and energy conservation equations over the control volume are

$$\dot{m}_{gases} = \dot{m}_{wet\ air} + \dot{m}_{fuel}, \tag{13}$$

$$\sum_i \dot{Q}_i = \dot{W} + \dot{H}_P - \dot{H}_R. \tag{14}$$

In Eq. (13), the mass flow rate of the exhaust gases $\dot{m}_{gases}$ is equal to the mass flow rate of components entering the CV, which are the wet air $\dot{m}_{wet\ air}$ and the fuel (Diesel or Natural Gas) $\dot{m}_{fuel}$. It is important to note that the same mass flow rates that enter the CV through the heat exchangers in the HT and LT circuits leave the device, thus such rates are not represented in Eq. (13).

The energy conservation is considered in Eq. (14). The reagents (wet air and fuel) enter the CV with an enthalpy $\dot{H}_R$, while the products (the exhaust gases) leave the CV with an enthalpy $\dot{H}_P$. The engine produces mechanical power $\dot{W}$ and heat $\sum_i \dot{Q}_i$ is lost to the exchangers at high temperature, at low temperature, and to the environment, with heat fluxes of $\dot{Q}_{HT}$, $\dot{Q}_{LT}$, and $\dot{Q}_{rad}$, respectively.

The exergy balance in the CV, from Fig. 15, is given by

$$\dot{B}_R + \sum_i \dot{Q}_i \left(1 - \frac{T_0}{T_i}\right) = \dot{W} + \dot{B}_P + \dot{B}_{dest}. \tag{15}$$

In Eq. (15), the symbols $\dot{B}_R$ and $\dot{B}_P$ represent the inlet and outlet exergy fluxes, respectively. The term $\dot{W}$ represents pure exergy, while $\dot{B}_{dest}$ accounts for the destroyed exergy, and the remaining term is associated to the exergy change rate by heat transfer. The reference state considered is ambient temperature T_0 and pressure P_0, while T_i represents the temperature of the heat sources. The exergy fluxes of the reagents and the products, necessary in Eq. (15), are determined by

$$\dot{B}_R = \dot{H}_R - \dot{H}_{R0} - T_0(\dot{S}_R - \dot{S}_{R0}), \tag{16}$$

$$\dot{B}_P = \dot{H}_P - \dot{H}_{P0} - T_0(\dot{S}_P - \dot{S}_{P0}). \tag{17}$$

The variables $\dot{H}_R$, $\dot{S}_R$,$\dot{H}_{R0}$, $\dot{S}_{R0}$ and $\dot{H}_P$, $\dot{S}_P$,$\dot{H}_{P0}$, $\dot{S}_{P0}$ are the enthalpy and entropy fluxes considered in the exergy calculation, with $\dot{S}$ being the rate of entropy generation. The subscripts R, P, and 0 are associated with reagents, products, and the reference state, respectively. The enthalpy and entropy fluxes, required in Eq. (16) and Eq. (17), are evaluated using the specific quantities (in the lower case) of the reagents and products

$$\dot{H}_R = \sum_R \dot{m}_R h_R, \tag{18}$$

$$\dot{H}_P = \sum_P \dot{m}_P h_P, \tag{19}$$

$$\dot{S}_R = \sum_R \dot{m}_R S_R, \tag{20}$$

$$\dot{S}_P = \sum_P \dot{m}_P S_P. \tag{21}$$

With an averaged chemical composition of the fuel, setting a standard value for relative humidity, and considering complete combustion, it is possible to determine the composition of the reaction products. The performance curves of the engines provide information about the efficiency of the engine, the temperature of the exhaust gases, and other variables in terms of the supplied power. Considering the thermodynamic balance and the technical information, the engine model can be completed.

The combustion reactions with stoichiometric air for natural gas (NG) and Diesel with averaged compositions are described in Eq. (22) and Eq. (23), below:

$$1\,\text{kg NG} + 3.90\,\text{kg } O_2 + 12.84\,\text{kg } N_2 \rightarrow 2.77\,\text{kg } CO_2 + 2.12\,\text{kg } H_2O + 12.84\,\text{kg } N_2, \tag{22}$$

$$1\,\text{kg Diesel} + 3.46\,\text{kg } O_2 + 11.39\,\text{kg } N_2 \rightarrow 3.11\,\text{kg } CO_2 + 1.35\,\text{kg } H_2O + 11.39\,\text{kg } N_2. \tag{23}$$

From the technical catalog, the fuel consumption, the exhaust temperature of the gases, and the mass flow rate of the products were determined given the power input. With this information

together with the mass balance in Eq. (13), as well as the stoichiometric coefficients from the combustion reactions in Eq. (22) and Eq. (23), we can calculate the mass flow rates of all components.

Considering that the only useful effect is the mechanical power produced, the thermal and exergy efficiencies can be defined, respectively, as

$$\eta_t = \frac{\dot{W}}{\dot{m}_R h_R - \dot{m}_P h_p}, \tag{24}$$

$$\eta_b = \frac{\dot{W}}{\dot{B}_R}. \tag{25}$$

Thermodynamic proprieties, compositions and other data were extracted from the libraries Coolprop [53] and HOT [54]. To improve runtime efficiency, maps of variables of interest were produced with mechanical power as input. The model comprises: thermal and exergy efficiencies, heat balance, temperature of exhaust gases, mass flow rates of the water at HT and LT, fuel, CO_2, vapor, O_2 and N_2. The final model is described by

$$variable_k = G_k(\dot{W}) \tag{26}$$

for $k = 1, 2, \ldots, 14$, where G_k are polynomials.

The thermodynamic modeling for the engines, presented above is essential for exergy analyses and to allow the determination of important quantities such as thermal and exergetic efficiencies. However, the engine and generator models are completely static, hence the dynamics of the system is not considered, making some analyses inaccessible. Once the start-up time of the generator is reached, electrical power can be delivered instantaneously. Voltage and frequency are assumed to be constant throughout the simulation.

In general, the power generation plant in a Diesel-electric marine system comprises a generator set, which is a synchronous generator powered by a Diesel engine. In such systems, two fundamental controllers are the speed governor, which regulates the engine speed, and the automatic voltage regulator (AVR), which controls the terminal voltage. The engine speed and the genset voltage are directly related to the vessel microgrid operation, adjusting quantities such as the frequency, voltage, active and reactive power [55].

Models of different complexity and objectives are described in the literature [3, 55, 56]. For simulations including engine speed and torque dynamics, with assumptions regarding the combustion, and a two-axis-dq-model for the synchronous generator, the model can be as complex

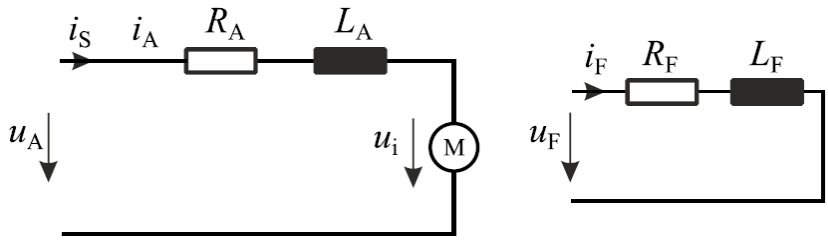

Figure 16 – Electric motor circuit diagram [57].

as a 7th order nonlinear dynamical system. With stronger assumptions, a 3rd order nonlinear control model can be developed, as pointed out in [55].

For studies focusing on fuel consumption and emissions, equivalent and static circuits are considered in some works to reduce the complexity of the models [3,56]. In such approaches, first-order dynamics can be assumed for the engine dynamics and for the exciter system, which is responsible for feeding the field voltage input for the synchronous generator voltage control. One advantage of simpler models, which still preserve important core dynamics of the genset, is the reduced amount of parameters to be estimated.

If measured data regarding the engine performance is available, static models with polynomial maps, for example, can be built to evaluate fuel consumption and emissions based on the requested electrical or mechanical power without considering the thermodynamics modeling and specific dynamic restrictions. However, these models cannot produce information such as grid frequency and voltage.

3.2 ELECTRIC MOTORS AND DRIVETRAINS

In Project 7, a linear, separately excited DC motor is modeled [24]. As depicted in Fig. 16, this machine is composed of two equivalent circuits: the armature circuit (on the left) and the field circuit (on the right). The armature circuit contains a total ohmic resistance R_A and an inductance L_A. The field circuit is a winding with inductance L_F and ohmic resistance R_F.

When a voltage u_A is applied to the armature, a current i_S flows through the circuit and the motor (M) starts to rotate. As a consequence, a counter-induced voltage (or back emf) arises due to the rotating rotor field [57]. Considering only voltage control, the flux can be maintained constant, thus only the dynamics of the right-hand side of Fig. 16 will be considered. Applying Kirchhoff's voltage law on the armature circuit in Fig. 16, and considering that the back emf is

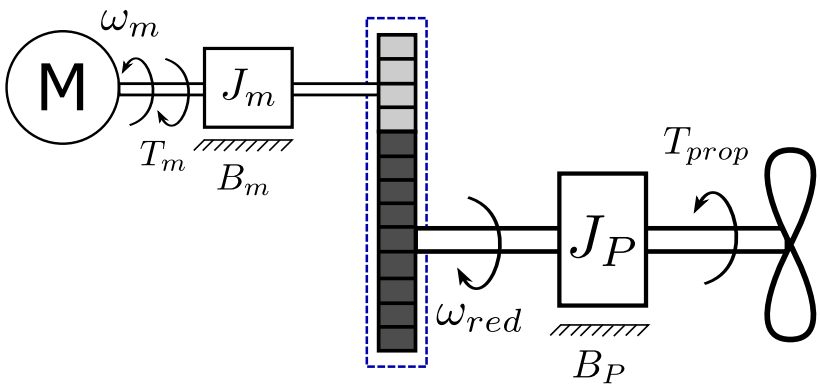

Figure 17 – Drivetrain scheme.

proportional to the angular velocity of the motor, it is possible to obtain the following equation:

$$L_A \frac{di_A(t)}{dt} + R_A i_A(t) + K_e \omega_m(t) = u_A(t). \tag{27}$$

The constant K_e is the back emf constant, which is considered equal to the motor torque constant K_t. The motor torque is considered linear with respect to the current ($T_m = K_t i_A(t)$). The DC electrical motor contains a stator (fixed) and the rotor, which can rotate and produce torque. The model of the mechanical part consists of the rotor and the drivetrain (gearbox and propeller) dynamics. In Fig. 17, a schematic view of the drivetrain coupled with the motor is shown.

When a voltage is applied to the armature of the electrical motor, an electrical current runs through the circuit. The electrical power is converted to mechanical power (in terms of motor angular velocity ω_m and torque T_m). However, due to devices such as bearings and brushes, a mechanical damping B_m is present in the motor. The rotor, with the moment of inertia J_m, is connected to the gearbox, in which only a single reduction red is available.

The shaft linked to the propeller develops velocity ω_{red}. Damping also arises in the shaft/propeller, being described by B_P. The torque applied to the shaft has to be able to overcome the mechanical losses and to move its equivalent inertia J_p, mainly determined by the propeller. The term T_{prop} is the resistance applied to the thruster due to hydrodynamic interaction.

Assuming an ideal gearbox, the torque and speed relations are defined as:

$$\frac{T_{ls}}{T_{hs}} = \frac{\omega_m}{\omega_{red}} = red.$$

In the equation above, T_{hs} and T_{ls} are the torques between the high-speed side and the low-speed side of the gearbox, respectively. Applying Newton's second law and considering an ideal gearbox, the mechanical motor drivetrain model can be defined as

$$J_{eq} \frac{d\omega_m(t)}{dt} + B_{eq} \omega_m(t) - K_t i_a(t) = -\frac{T_{prop}(t)}{red}. \tag{28}$$

The equivalent moment of inertia and damping of the mechanical model are given by

$$J_{eq} = J_m + \frac{J_p}{red^2} + J_{GB} \tag{29}$$

and

$$B_{eq} = B_m + \frac{B_p}{red^2} + B_{GB} \tag{30}$$

respectively. The constants J_{GB} and B_{GB} refer to the moment of inertia and damping related to the gearbox.

The complete electrical motor model can be written in the state-space form as:

$$\begin{aligned} \dot{\mathbf{x}}(t) &= \mathbf{A}\mathbf{x}(t) + \mathbf{B}\mathbf{u}(t) + \mathbf{F}\mathbf{d}(t), \\ \mathbf{y}(t) &= \mathbf{C}\mathbf{x}(t). \end{aligned} \tag{31}$$

The state vector is defined as $\mathbf{x} = [i_A,\ \omega_m]^T$, while the controlled input is $\mathbf{u}$. The propeller torque enters as an exogenous input $\mathbf{d} = T_{prop}$. The output and controlled variable is the angular speed of the motor $\mathbf{y} = \omega_m$. The current i_A is also observed, since it is an important quantity for the calculation of the electrical energy consumption. The matrices $\mathbf{A}$, $\mathbf{B}$, $\mathbf{C}$ and $\mathbf{F}$ are:

$$\mathbf{A} = \begin{bmatrix} -\frac{R_A}{L_A} & -\frac{K_e}{L_A} \\ \frac{K_t}{J_{eq}} & -\frac{B_{eq}}{J_{eq}} \end{bmatrix};\ \mathbf{B} = \begin{bmatrix} \frac{1}{L_A} \\ 0 \end{bmatrix};\ \mathbf{C} = \begin{bmatrix} 1 & 0 \end{bmatrix};\ \mathbf{F} = \begin{bmatrix} 0 \\ -\frac{1}{J_{eq} red} \end{bmatrix}. \tag{32}$$

An armature voltage PID control is implemented to control the velocity of the electric motor and to balance the torque demands. A reference angular velocity is set to the motor. After the measurement of the current velocity, the error is evaluated as ($e = \omega_{m\ ref} - \omega_m$). Then, the voltage input is calculated as:

$$u_A = k_p e(t) + k_i \int_0^t e(\tau) d\tau + k_d \frac{de(t)}{dt}. \tag{33}$$

In equation (33), k_p, k_i and k_d are the controller gains. Test simulations have shown that better results can be achieved using a PI controller (with $k_d = 0$). The voltage u_A is equal to U_M, which is the notation used for the voltage of the electrical motors in Fig. 14.

The electrical motor model above have been evaluated. In the simulations, the model was showing a low maximum efficiency, up to 75-80%, while an electric motor of that kind would run at efficiencies around 80-90%, with higher efficiencies for more powerful motors. Additionally, the electric motors generally used for vessel propulsion are of the alternating current (AC) type, being more efficient [58].

DC motors can be used in marine propulsion, examples include icebreaker vessels. They are especially interesting for their use in a DC distribution system. A DC machine architecture, similar to the one currently implemented in project 7, is presented in [59]. Nevertheless, for real applications, DC motors have some disadvantages, such as being quite large for the same rated power, and requiring more maintenance compared with AC machines.

The propulsion loads on vessels follow the propeller's law, with the propeller torque being approximately proportional to the square of the rotational speed of the propeller [60]. For this type of load, the technical specifications in [61] recommend the use of DC motors working with armature control; this includes the separately excited DC motor currently implemented in Project 7. Also, DC motor equivalent circuits are used in the literature to model core aspects of AC motors [56].

The model in the Project 7 framework represents a separately excited machine controlled by the armature. Therefore, according to the technical specifications and examples described in the literature review, the DC motor in use is suitable for electromechanical conversion in vessels, and its model is appropriate for carrying out simulations.

3.2.1 Three-phase induction motor

As already mentioned, the most used electric motors for propulsion are of AC type, including the most found during the literature review: the three-phase induction motor (IM), as can be seen in [3, 58, 62]. Therefore, the IM is an important model to be added to the model set for powertrain simulation, increasing the accuracy of component representation. Such machine is widely applied in practical systems due to simple mechanical construction, low maintenance, robustness, high efficiency, compactness, and low cost [34, 63].

From a modeling and control perspective, induction motors are considerably more complex, being nonlinear, high-order dynamical systems. Different models are mentioned in the literature [34, 64]. However, the most complete models are based on the study of equivalent circuits of the reference systems dq and $\alpha - \beta$. The most widely used approaches to control induction machines consist of v/f scalar control, field-oriented control (FOC), and direct torque control (DTC). The last two are the most sophisticated ones. Thus, they have been extensively explored for vessel electric propulsion [33].

The FOC strategy, also known as vector control, is a cascaded control based on rotor, stator or main flux oriented models. The individual controllers can be of the PID type, usually

with gain scheduling to account for non-linearities. It offers the advantage of constant switching frequencies and enables simple current limiting. However, it is necessary to determine, with accuracy, the flux angle and to have precise knowledge of the induction machine parameters. Otherwise, the control performance is reduced [34].

On the other hand, DTC is a very robust and precise cascade control with quick torque response, besides being simpler than FOC. The main controller can also be decoupled into individual PID controllers. However, in steady-state operation, consistent torque pulsation and current ripples can appear. In addition, the DTC requires fast sampling frequencies, performing worse than the FOC if the same average switching frequencies are used [34].

The control of induction machines is a current field of research, including a variety of strategies and algorithms. One efficient option to control complex high-order systems and increase robustness in terms of both disturbances and plant parametric deviations is to apply the sliding mode control (SMC). This strategy has been presented with excellent performance for three-phase induction motors in [34, 63]. Two disadvantages of SMC include full state measurement and the appearance of chattering.

3.3 BATTERY MODULE

The battery module model considers operation with a constant voltage. Coulomb counting is used to evaluate the amount of energy remaining in the energy storage system, i.e., the state of charge (SOC) [24]. This estimate is performed integrating the current over time,

$$\frac{dSOC}{dt} = \frac{i(t)}{C_{bat}}. \tag{34}$$

The charge flowing through the battery in time is given by

$$it = \int_0^t i(\tau)d\tau. \tag{35}$$

The model of lithium-ion battery above consists of the state of charge (SOC) counting, a constant voltage in the terminals of the device, and power delivery, without considering some other important dynamical behavior of the battery which includes electrical, thermal and chemical degradation (aging) effects. The benefits of the storage system in the hybrid topology, its management strategy, and safety depend on such information. Therefore, a more complete model was required.

Two fundamentally different types of battery cell models are common in the scientific literature. One is based on the governing physics of the cell, including how internal physical

chemistry dynamics produce macroscopic effects. These models provide more detailed information, being generally based on complex phenomena and modeled by partial differential equations (PDEs) [65].

On the other side, empirical equivalent circuit models are defined by ordinary differential equations (ODEs), which are simpler and computationally less expensive. Moreover, these last class of models can be tuned through parameter identification to evaluate electrical, thermal and aging effects accurately, being easily incorporated in control and state estimation analysis, as in [66]. The equivalent circuit model does not describe the construction of the cell, rather, it represents the battery macroscopic effects with electrical components such as resistors, sources and capacitors, whose behavior fits the actual dynamics.

It is important to understand the required accuracy and aspects that need to be taken into consideration to produce an appropriate simulation model. Regarding equivalent circuit models, the most trivial one has only a constant voltage source that represents the open-circuit voltage (OCV) of the battery cell. This model is quite limited, failing when a load is applied to the battery and when its remaining charge changes. The OCV is not constant even when the battery is at rest, being a function of the state of charge (SOC), which is a charge status (in percentage), a description of the remaining energy in the battery concerning its nominal capacity [65].

To improve the model, one may introduce an equivalent internal resistance to the circuit, which will make the terminal voltage drop below the OCV when the battery is discharging and will give a higher terminal voltage than the OCV while charging. The model containing a voltage source to represent the OCV and internal resistance is known as the internal resistance model. By decomposing the internal resistance in two parallel resistances for charge and discharge, and adding diodes to limit the current flow in required directions, the simpler modified Thévenin model is produced [67].

Another important aspect of a lithium-ion battery cell is the voltage polarization. This phenomenon is identified by a slow change in voltage when a cell is subjected to a discharge pulse followed by a rest, for example. This effect can be approximated by adding a resistor and a capacitor in parallel to the internal resistance model [65].

Several other effects such as hysteresis, for example, can be added by changing the topology of the equivalent circuit as described in [65, 67]. Impedance-based models are also an option. However, they also require a characterization of the frequency response of the cell. Moreover, some generic battery models including equivalent circuits and mathematical

transformations such as low pass filters, such as the Shepherd modified battery model, are described in other works, for instance [67, 68].

The Thévenin models can be accurate, simple, and have a considerable amount of experimental data available. Such models consist of a variable voltage source, which is a function of the SOC with a small dependence on the temperature of the cell, an internal resistance, and pairs of resistors and capacitors in parallel (RC pairs), which depend on the temperature and SOC. The number of RC pairs defines the so-called order of the system. The Thévenin models can be coupled with thermal balance equations and empirical electrochemical models to fit data and handle heat transfer and dissipation, as well as cell degradation [65–67].

3.4 ELECTRICAL ARCHITECTURE

The power flow is accounted by taking into consideration a steady-state electric system, see Fig. 14. Besides tracking the power flow, the transformers contain a static model [24]. We assume electrical power conservation without loss. The relation between currents I_{in}, I_{out} and voltages V_{in}, V_{out} are described by the transformers ratio a, as in

$$a = \frac{V_{in}}{V_{out}} = \frac{I_{out}}{I_{in}}. \tag{36}$$

According to [3], static electrical networks suffice for fuel consumption evaluation, which is one of the main focuses of this work along with emission analyses. However, it is important to consider at least the efficiencies of the equipment used in the electrical system, such as converters, for example. In works such as [69], the authors use a more complete equivalent static AC network model which accounts for the frequency, active and reactive power of the grid.

3.5 VESSEL AND PROPELLERS

The vessel propeller model in Project 7 [24], used when the powertrain is not integrated with the TPN simulator, consists of a thrust estimation for the marine propellers in four-quadrant and vessel velocity evaluation based mainly on the work by [70]. The model allows the determination of simplified vessel dynamics to study maneuverability. The parameters used for model fitting are validated with experimental data. A block diagram that represents the model scheme is depicted in Fig. 18.

The parameters screw pitch ratio, propeller diameter D, density of water ρ, total resistance coefficient of the vessel r, mass of the vessel m and added mass Δm are required as inputs. The model takes the angular velocity ω_{red} and the advance speed of the propeller relative to water v_p to calculate the bounded advance ratio J'. With ω_{red} and J', the thrust K'_T and torque K'_Q coefficients can be evaluated through the following polynomial equations:

$$K'_T = b_{0T} + b_{1T}J' + ... + b_{\mu T}(J')^{\mu}, \tag{37}$$

$$K'_Q = b_{0Q} + b_{1Q}J' + ... + b_{\mu Q}(J')^{\mu}. \tag{38}$$

It is important to mention that the coefficients b of the polynomials above depend on the sign of the angular speed ω_{red}. With the knowledge of J', K'_T, K'_Q, v_p, the wake fraction number w, and the reduction coefficient t, it is possible to calculate the torque on the propeller T_{prop} and the thrust F_{prop}. To obtain the velocity of the vessel, v_{sh}, the acceleration of the vessel is integrated over time, where F_r is the total resistive force. With the vessel velocity, the value of v_p can be determined and fed back to the model again through the time steps of the simulation.

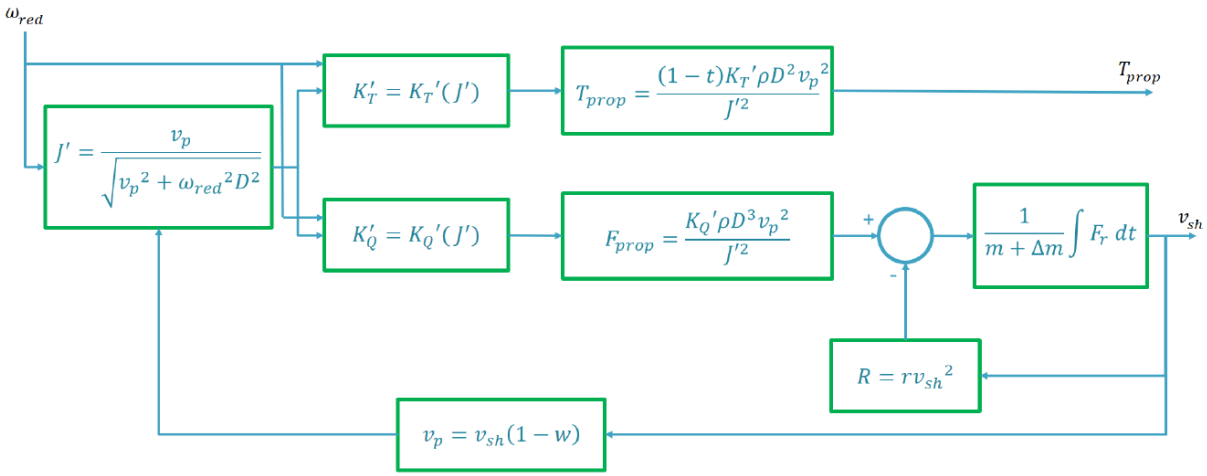

Figure 18 – Block diagram Vessel-Propeller model [24].

4 MODELING OF A DIESEL-ELECTRIC HYBRID VESSEL

In this work, we will study the propulsion system of an Ulstein Platform Supply Vessel (PSV), proposing the hybridization of the mentioned vessel and improvements in the operation of the original power system to increase energy efficiency and reduce emissions. A PSV example is depicted in Fig. 21. Also, two main power system topologies are considered for the mentioned PSV: a base case, which is the original design (non-hybrid), and a hybrid power system, which is characterized by the addition of a Li-ion battery to the base case.

Figure 19 shows a diagram of the main components of the original propulsion system of the Ulstein, with some information about the capacity of the power sources and consumers, and Fig. 20 shows the main hybrid configuration proposed in this work. The propulsion topology in Fig. 20 can be classified as a series configuration, according to the discussion presented in section 2.3.

Regarding Fig. 19 and Fig. 20, the terms ICE represent the Diesel internal combustion engines and G represents electrical generators. The energy storage system (ESS) comprising battery and converter are described by ESS. The propulsion system comprises frequency converters or motor drives, MD, electric motors, EM, gearboxes, GB, main thrusters, MT, and the tunnel thrusters T, with B for bow and S for stern. The electrical network includes a high voltage (HV) and low voltage bus (LV), transformers T1 and T2. The auxiliary systems are described by the term AUX. The ellipse in pink is the main bus tie breaker, which is a circuit breaker connecting the two sections of the electrical bus serving different power sources and consumers.

A Tie Breaker is a type of circuit breaker that connects two sections of electrical bus serving different power sources.

The power system of the base case comprises four equal Diesel generator sets (gensets), with 1700 kW of electrical power each, resulting in 6800 kW of combined power. For the hybrid case, the same number of gensets was considered, and we included an ESS with a battery pack of Lithium Iron Phosphate ($LiFePO_4$ or simply LFP). The rated power and energy of the battery will defined in the following chapters.

In the following sections, the models required for the PSV propulsion system simulation will be presented, with discussions about the modeling process and the performance of models, including comparisons using data from real operations and data from the literature and a MATLAB/Simulink model.

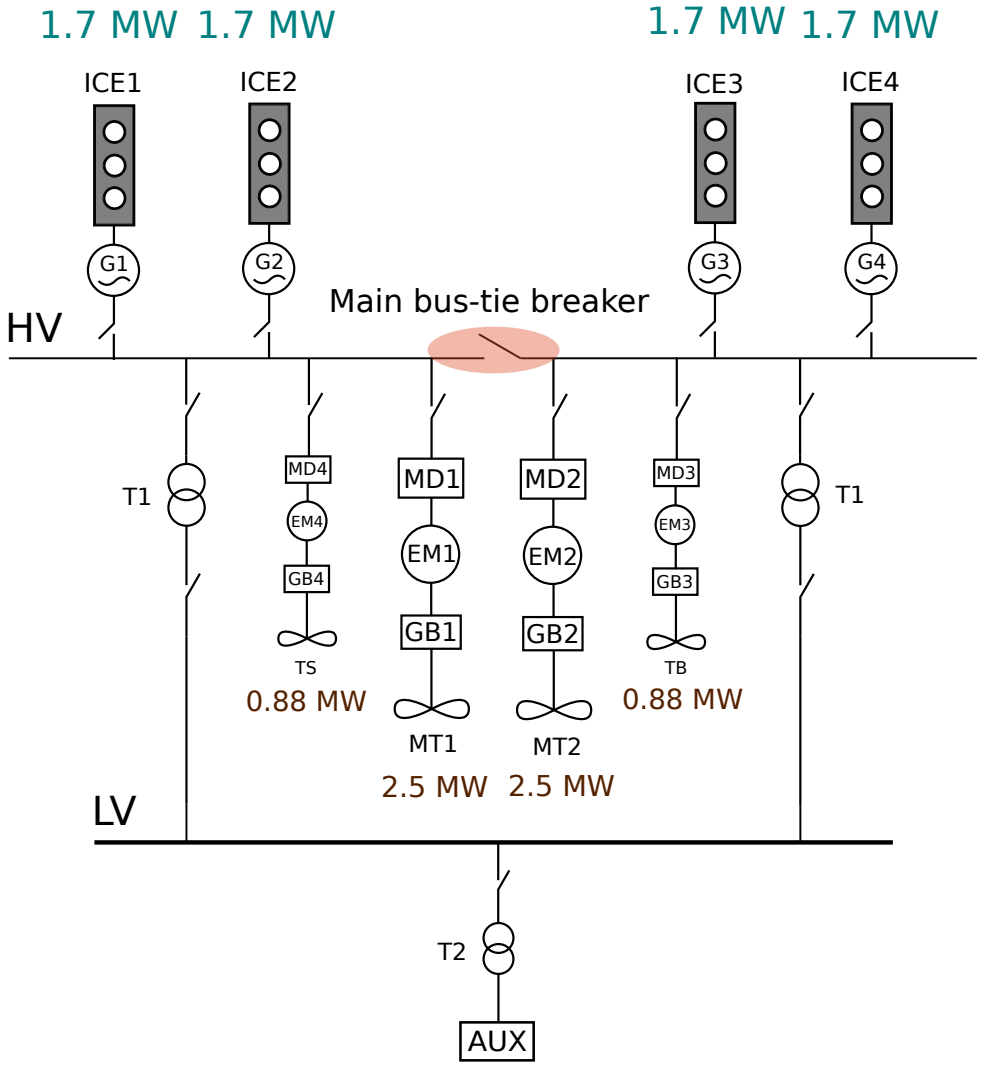

Figure 19 – Ulstein project propulsion system: original configuration (base case).

4.1 ENGINE GENERATOR SET (GENSET) MODEL

A Diesel genset dynamical model oriented to fuel consumption and GHG emissions has been developed, adapting the methodology presented in the work of [3]. A steady-state electrical model based on a simplified per-phase circuit, shown in figure (22), was considered for the synchronous generator, omitting the Automatic Voltage Generator (AVR) feedback control, but preserving the engine speed dynamics, for frequency and active power control. As shown in the mentioned work, simplified electrical models are suited for analyzing quantities such as fuel consumption and emissions.

The generator per-phase voltage u_g was defined as proportional to the engine speed ω_{dg},

$$u_g(t) = u_{g,nom}\frac{\omega_{dg}(t)}{\omega_{dg,nom}(t)}, \tag{39}$$

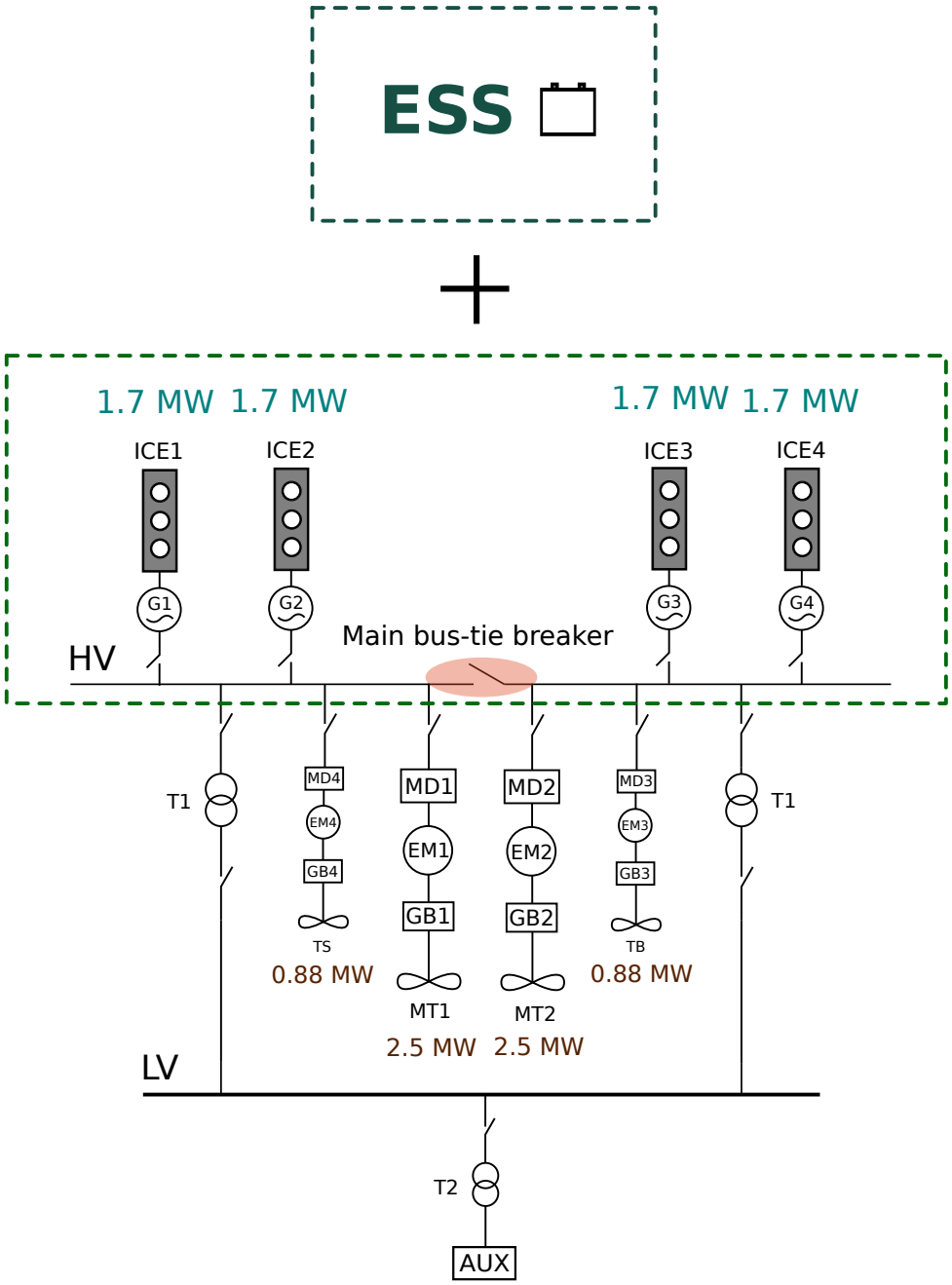

Figure 20 – Ulstein project propulsion system: hybrid configuration.

Figure 21 – Platform Supply Vessel (PSV) [71]

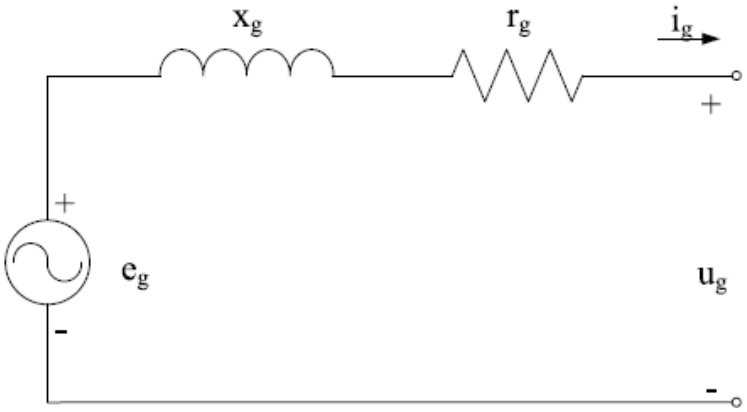

Figure 22 – Synchronous generator per-phase equivalent circuit [3].

using the nominal per-phase voltage $u_{g,nom}$ and the nominal engine speed $\omega_{dg,nom}$. Equation 39 considers the approach described in [3]; however, the same authors mention that another way to define u_g, omitting the AVR, would be considering $u_g = u_{g,nom}$. The electrical frequency f is determined through the relation between the engine speed and the number of poles of the electrical motor P_p,

$$f = \omega_{dg} \frac{Pp}{4\pi}. \tag{40}$$

The electrical power demand $P_{g,el}$ is translated into a current demand in the terminals of the generator i_g. The active power is defined as

$$P_{g,el} = 3u_g(t)i_g(t)\cos(\phi_p), \tag{41}$$

in which $\cos(\phi_p)$ is the power factor. Considering only friction and copper losses, the generator losses can be written as

$$P_{g,loss}(t) = P_{g,nom}c_f + i_g(t)^2 r_g, \tag{42}$$

where c_f is the friction rate and r_g is the resistance of the electrical motor per-phase. The mechanical load P_g due to the electrical demand can be defined as

$$P_g(t) = P_{g,el}(t) + P_{g,loss}(t), \tag{43}$$

while the torque load is determined through the power and rotational speed of the engine, as in

$$Mg(t) = \frac{P_g(t)}{\omega_{dg}(t)}. \tag{44}$$

A governor is required for the generator to regulate the fuel injection and control its angular speed. The rotation dynamics is described by

$$\frac{d\omega_{dg}}{dt} = \frac{M_{dg} - M_g}{J_{dg}}. \tag{45}$$

The variable M_{dg} is the engine torque obtained through the fuel combustion, and J_{dg} represents the generator moment of inertia. A polynomial fit was produced to represent the relation between the fuel consumption of the generator and the torque,

$$M_{dg} = a_0 + a_1\dot{m}_{f,dg} + a_2\dot{m}^2_{f,dg} + a_3\dot{m}^3_{f,dg} + a_4\dot{m}^4_{f,dg}, \tag{46}$$

in which the values a_i, with $i = 1, \ldots, 4$, are polynomial coefficients. To control the engine speed, a clamping anti-windup PI control was implemented. The fuel to be injected was determined through

$$\dot{m}_{f,dg} = k_p(\omega_{dg,ref} - \omega_{dg}(t)) + k_i \int_0^t (\omega_{dg,ref} - \omega_{dg}(t))dt, \tag{47}$$

where the proportional and integral gains of the controller are k_p and k_i, respectively, and $\omega_{dg,ref}$ is the reference velocity.

When a torque load M_g is applied to the engine, an unbalance occurs in the engine speed, according to Eq. (45). Then, the PI controller adjusts the amount of fuel to be injected into the combustion chamber. Due to the speed dynamics, neither mechanical nor electrical power can be delivered instantaneously. The engine output mechanical power is characterized by the product between the engine torque and its speed as

$$P_{bkW}(t) = M_{dg}\omega_{dg}. \tag{48}$$

After synchronization, the electrical output power can be defined as the combination of the power loss effects and the engine mechanical power as

$$P_{ekW}(t) = P_{bkW} - P_{g,loss}(t). \tag{49}$$

The model was produced using data provided by industry partners for the CAT 3512C generator set. To account for thermal and global genset efficiencies, a different approach from that in chapter 3 was considered, since data such as the specific fuel consumption (SFC) curve, mechanical and electrical output power were available for the rated engine speed. Applying the formulation described in [72], the thermal efficiency can be defined for the power rate as

$$\eta_t = \frac{P_m}{\eta_{cb}\dot{m}_f Q_{lhv}}. \tag{50}$$

Such an approach could also be used for defining a global genset efficiency,

$$\eta_{genset} = \frac{P_e}{\eta_{cb}\dot{m}_f Q_{lhv}}. \tag{51}$$

The symbols P_e, P_m, η_{cb}, $\dot{m}_f$ and Q_{lhv} represent electrical and mechanical power delivered, the combustion efficiency, the fuel consumption and the low heat value of the Diesel, respectively. According to [72], for Diesel engines operating lean, the combustion efficiency is about 98%. Considering the mentioned η_{cb}, and the data available, two 6$^{\text{th}}$ order polynomials (p) were produced for the evaluation of the efficiencies in equations (52) and (53):

$$\eta_t = p_1(P_{bkW}), \tag{52}$$

$$\eta_{genset} = p_2(P_{ekW}). \tag{53}$$

To consider emissions, static models were developed through polynomial fits, using tables of the mass flow rates of the substances and the mechanical power delivered by the engine. The equations below are used to calculate the emissions of carbon dioxide (CO_2), carbon monoxide (CO), nitrogen oxides (NOx as NO_2), unburned hydrocarbons (HC) and particulate matter (PM):

$$\dot{m}_{\mathrm{CO_2}} = p_3(P_{bkW}), \tag{54}$$

$$\dot{m}_{\mathrm{CO}} = p_4(P_{bkW}), \tag{55}$$

$$\dot{m}_{\mathrm{NOx}} = p_5(P_{bkW}), \tag{56}$$

$$\dot{m}_{\mathrm{HC}} = p_6(P_{bkW}), \tag{57}$$

$$\dot{m}_{\mathrm{PM}} = p_7(P_{bkW}), \tag{58}$$

with p_3, p_4, p_5, p_6, p_7, being polynomials of orders 4, 2, 4, 3, 4, respectively.

The emission models receive the mechanical output of the engine P_{bkW} as input and give as output the mass flow of the pollutants. It is important to mention that the models assume nominal speed and consider only the power as input. In this work, variable speed gensets are not being considered, so it is necessary to keep the engine speed within certain limits for grid frequency control.

The grid frequency is set at 60 Hz, hence the engine speed reference is set to be 1800 rpm or roughly this value if a droop control is considered, for example. Either way, the engine speed will be regulated through the governor to seek the speed reference. Therefore, a constant engine speed is a reasonable assumption.

In Fig. 23, a block diagram of the genset model is presented. In the diagram, it is possible to see the information flux and coupling of the different variables. The letter e represents the error ($e = \omega_{dg,ref} - \omega_{dg}$), and PI represents the anti-windup PI control. The engine block is defined by the engine speed dynamics from Eq. (45) and the torque from Eq. (46).

4.1.1 Comparison with operational data

The proposed model was validated for fuel consumption and engine speed using field data measured by an industry partner of Project 7. The engine speed was obtained directly through measurements. The electrical power demand of each generator was estimated based on fuel consumption rate measurements and fuel-to-power maps. The four generators were simulated separately considering nominal speed.

In Fig. 24, the engine speeds of the four generator sets are depicted throughout approximately 740 hours for a PSV in mission. It can be seen that the model matches the generator behavior, being turned on and off in accordance with the measured data. In addition, the lines and dots seem to be almost overlapping for the simulations in the four cases considered.

The reference engine speed, $\omega_{dg,ref}$, was set to 1800 RPM, following a 15 s ramp if the genset is on, for synchronization. If the genset is disconnected, the speed reference is set to 0. In Fig. 25, a closer look at the engine speed of genset 1 is available. In this image, it is possible to evaluate with more precision the results when the generator is connected to the grid, keeping its speed closer to the nominal value.

The observed differences were below 5%, comparing the speed results from the model with the measured data for all cases. The model has shown good performance given the number of

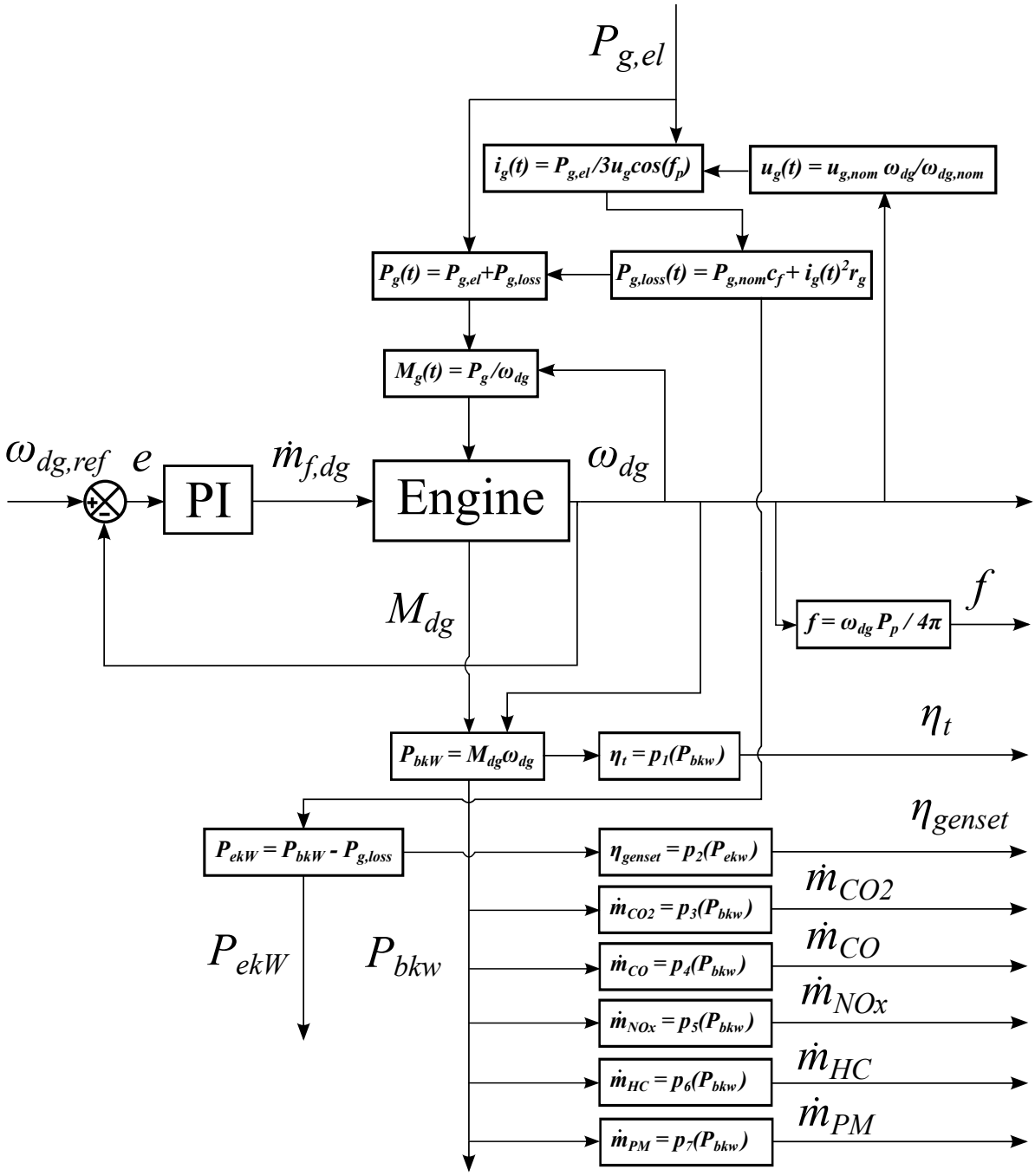

Figure 23 – Block diagram of the genset model.

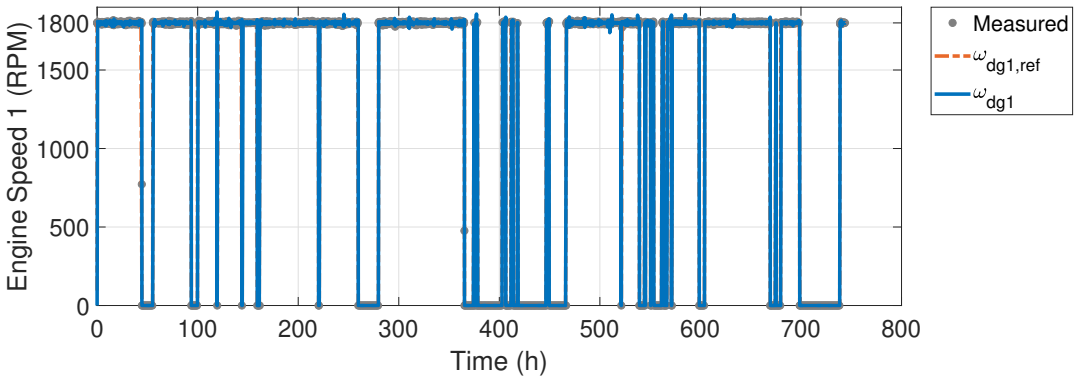

(a) Genset 1 engine speed.

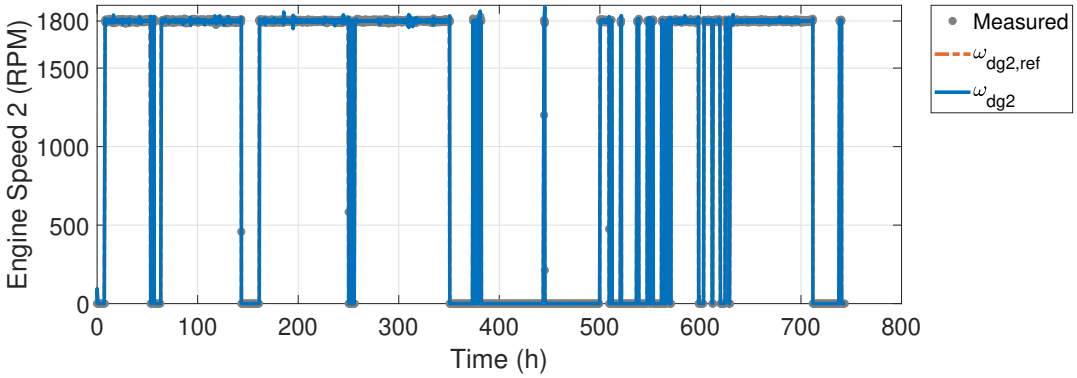

(b) Genset 2 engine speed.

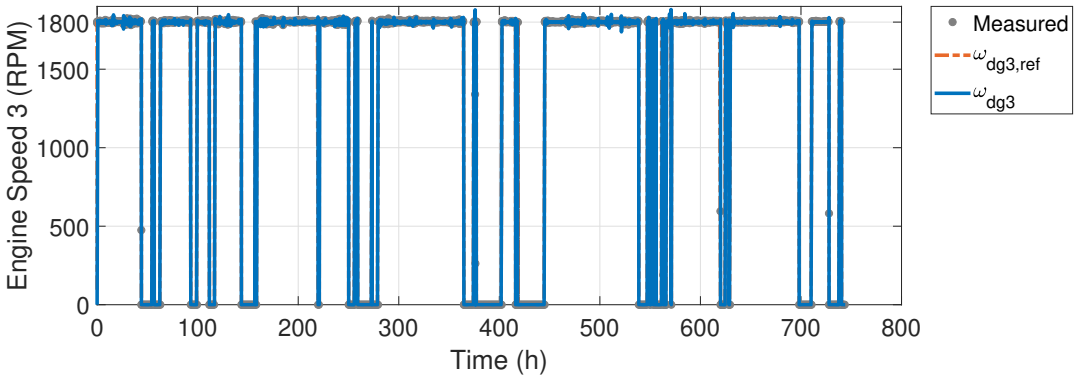

(c) Genset 3 engine speed.

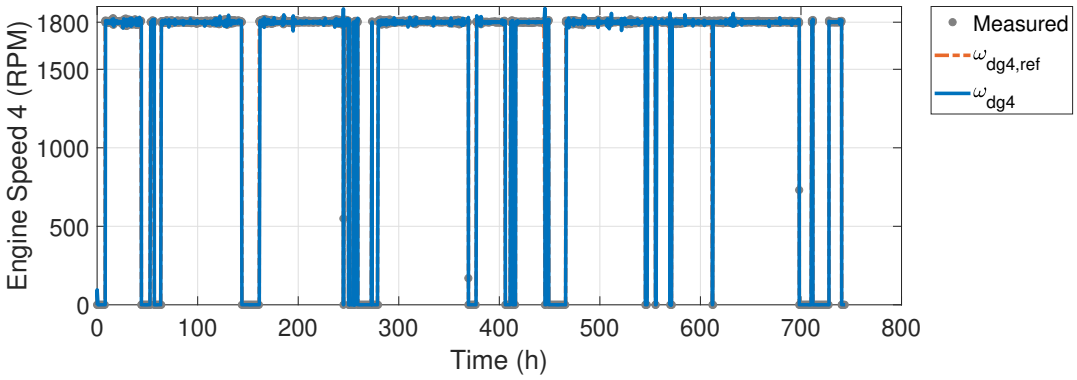

(d) Genset 4 engine speed.

Figure 24 – Engine speed validation for four generator sets with measurements from an industry partner.

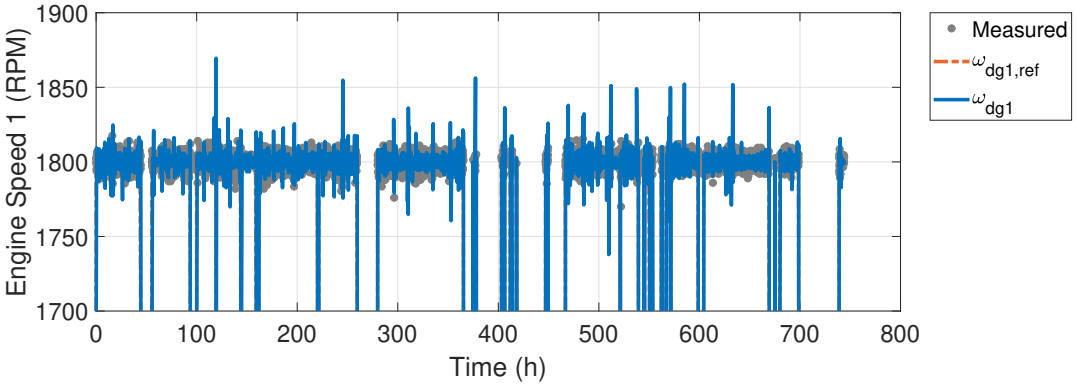

Figure 25 – Genset 1 engine speed in a closer view.

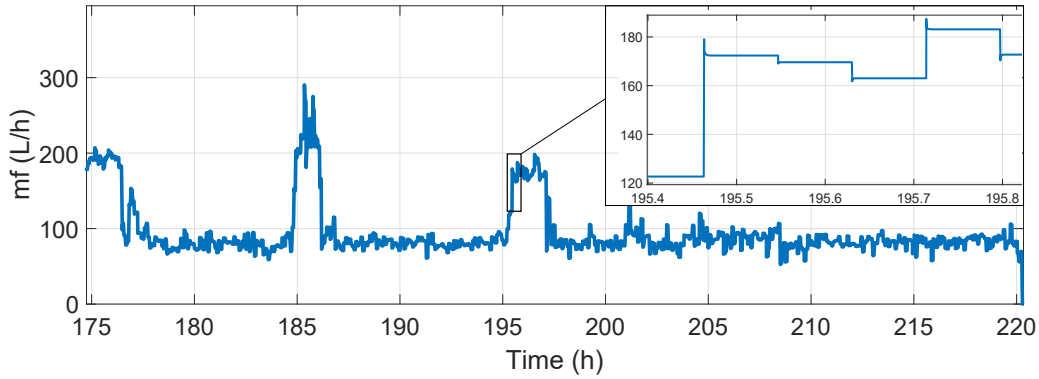

Figure 26 – Fragment of fuel consumption rate for the genset 1.

uncertainties in modeling and data measurements. Also, in this simulation, the engine speeds were set to the nominal value, thus frequency settings such as in droop control were not considered. The droop frequency control alone can account for up to 3% or 5% of difference in frequency [6].

It is important to mention that the data had to be interpolated for the simulation. The model receives power inputs at every 0.1 s, while the measured data was a mean of samples whose period was of the order of minutes. The nearest neighbor interpolation was performed, to maintain the same energy required in the mission. Therefore, the power inputs exhibited a step-like behavior, followed by a constant behavior. Such power steps change the instantaneous speed considerably. The higher peaks were within acceptable limits, according to most technical standards in [73], which allow up to 10% of deviation in grid frequency for the transient state.

The complete curves cannot be shown due to a non-disclosure agreement. However, a fragment of the fuel consumption rate in L/h for the genset 1 is depicted in Fig. 26. Due to the amount of time, the bigger picture seems to have a complete transient behavior, but it can be seen by zooming in that the transient behavior occurs in a small fraction of the simulation time, while the steady state dominates most of the time.

Table 2 – Coefficients of the polynomial fuel consumption map

Parameter	Symbol	Value	Unit	Reference
Coefficients for the polynomial fuel consumption map ($\dot{m}_{f,dg}$) $\star$	δ_0	2.23×10^{-3}	kNm	E
	δ_1	7.65×10^{-5}	kNm/kg	E
	δ_2	-1.95×10^{-8}	kNms^2/kg^2	E
	δ_3	1.03×10^{12}	kNms^3/kg^3	E
	δ_4	2.32×10^{-15}	kNms^4/kg^4	E

$\star$ - We consider the standard polynomial form $\sum_{j=0}^{N_P} \delta_j x^j$, where N_P represents the polynomial order, x is the input variable and δ_j are generic coefficients
E - estimated

For the fuel consumption simulations, the observed differences were smaller than 2% for each of the four generators. It is a small error given all uncertainties and the complexity of the machine. This result can be explained since the model has been constructed to fit the data provided by the industry partner. Besides, the steady behavior dominates the simulation most of the time, due to the mentioned interpolation. The parameters that have the greatest associated uncertainties are those related to the transient behavior.

As mentioned in section 3.1, in general, for the purpose of estimating the fuel consumption of the generators, quasi-static maps suffice. Mainly for low-frequency simulations, we will define the following polynomial fit that returns the fuel consumption given electrical power demands,

$$\dot{m}_{f,dg} = p_8(P_{ekW}),. \tag{59}$$

This model shows a very similar steady-state response to the dynamic model described above, and runs particularly faster. The coefficients are described in Tab. 2.

4.1.2 Dynamic performance

In this subsection, the genset model will be tested in some situations to have its dynamic performance analyzed. Initially, an electrical power load $P_{g,el}$ was considered. This load consists of several steps, with power changes varying from 20% to 50% of the generator rated power (1700 kW). The power demand was smoothed using a first-order pre-filter with a time constant of 1 s. The power tracking performance of the genset model can be seen in Fig. 27. Despite fast load variations, the results have shown good agreement between the power demand and the electrical power delivered.

In Fig. 28, the engine speed is depicted. Small overshoots and undershoots can be seen in the image. To be precise, the maximum variation observed was of 2.6% in the maximum smoothed power step. In general, when the load increased, the speed dropped, and the governor

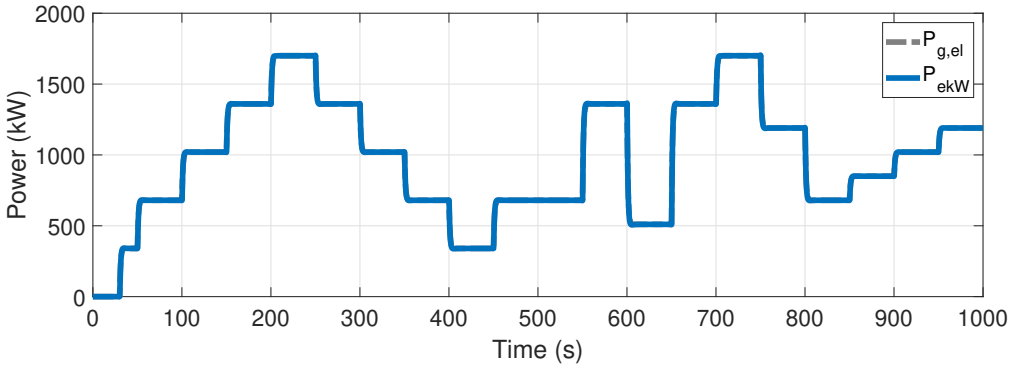

Figure 27 – Genset power tracking.

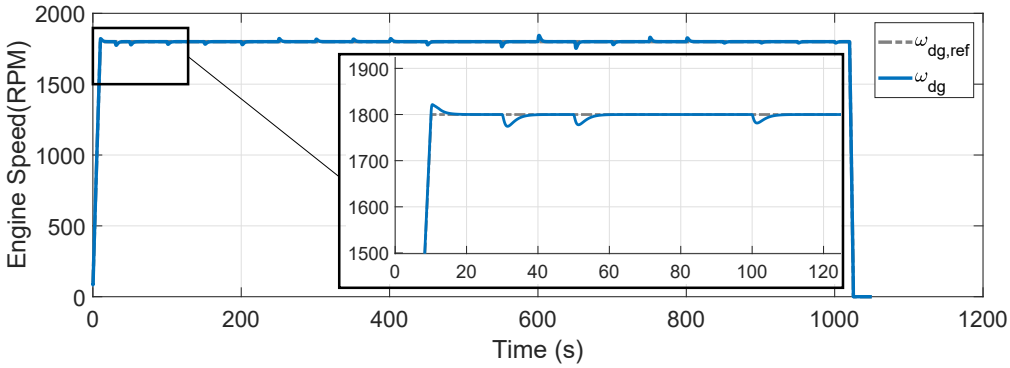

Figure 28 – Engine speed control.

was responsible for regulating the speed to the reference. The inverse happens if the load decreases. Larger and faster power changes produced larger variations in the engine speed.

The power management system (PMS) defines the genset loading. In general, there are loading ramps for the generators, as well as maximum instant load steps the machine needs to operate with. For the dual-fuel engine in [74], the maximum instant load step is about 33% of the rated power of that of the Diesel engine, depending on the available power.

In Fig. 29, an instantaneous load step of 40% of the rated power is applied. A 2.8% overshoot and a 3.5% undershoot were observed in the power delivery, considering the rated power. Specifically, the undershoot happens due to the abrupt and large power variation, causing a drop in engine speed of almost 4%, considering the rated speed.

When the smoothed step load with a time constant of 1 s is applied, the engine has more time to deliver power in a smoother way, as shown in Fig. 30. The differences in power were smaller than 1%, considering the rated power. No considerable undershoot in the power response was observed. In addition, the speed drop was smaller, about 2%, concerning the rated speed.

To analyze the robustness of the model, a noisy power demand profile with larger smoothed steps, with a first-order pre-filter and a time constant of 40 s was produced. The results

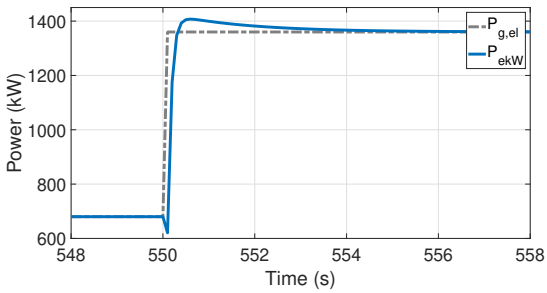

(a) Genset electrical power response.

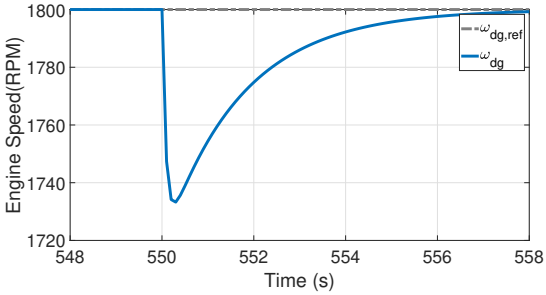

(b) Engine speed response.

Figure 29 – Genset dynamic response to step load.

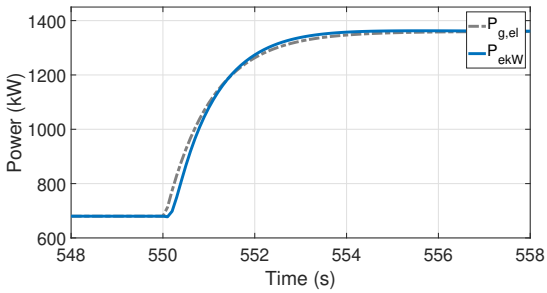

(a) Genset electrical power response.

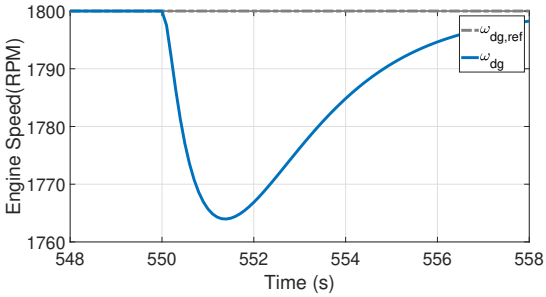

(b) Engine speed response.

Figure 30 – Genset dynamic response to smoothed step load.

for several variables of interest are shown in Fig. 31. It can be seen that, even for the noisy signal, the speed and power response is adequate, with small overshoots and undershoots, as well as the voltage and frequency of grid.

The parameters used for the genset models, shown in Tab. 3, and for some of the other models throughout this work, were found in the literature, estimated based on the literature results (E), were directly obtained (D) or estimated (E) using data shared with Project 7 through communication with the naval industry.

4.2 DC MOTOR

Although the AC motor is generally used in vessel propulsion, the DC motor model presented in chapter 3 has been considered adequate for simulation based on the literature review analysis in section 3.2. However, the efficiency of the DC motor is below the acceptable ranges found in the literature. Therefore, identification of parameters took place to increase the efficiency of the motor model.

Considering the difficulties to find the electrical motor parameters in the literature, a sizing approach was adopted for parameter identification to improve the efficiency of the machine.

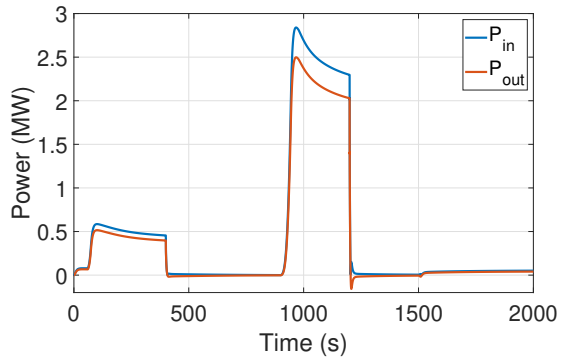

(a) Generator electrical power.

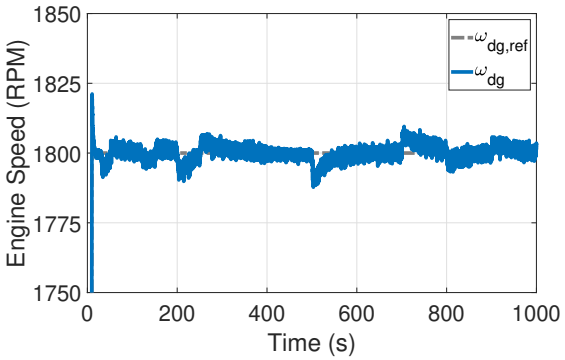

(b) Engine speed.

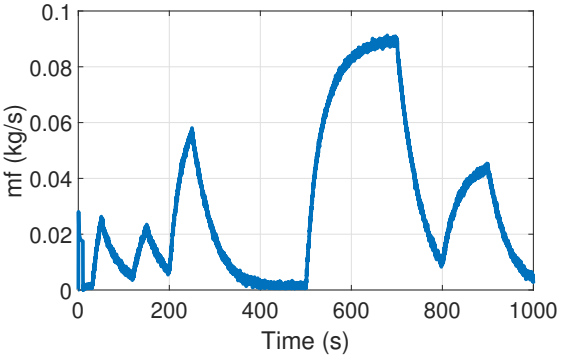

(c) Fuel consumption rate.

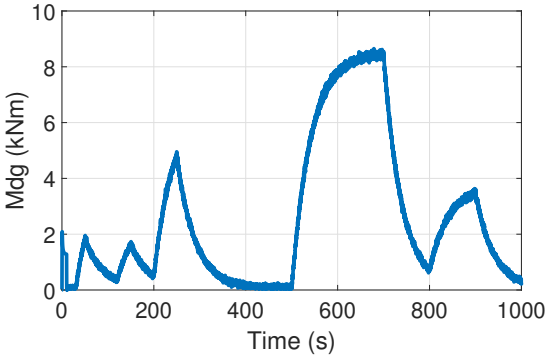

(d) Engine torque.

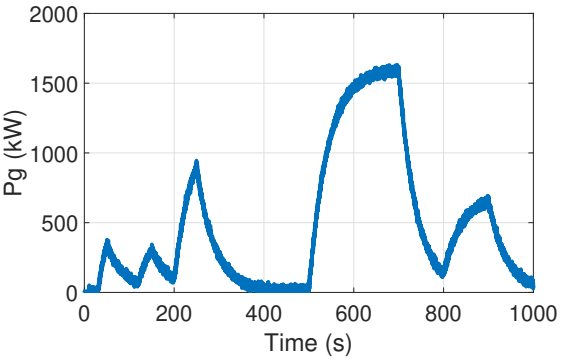

(e) Engine power.

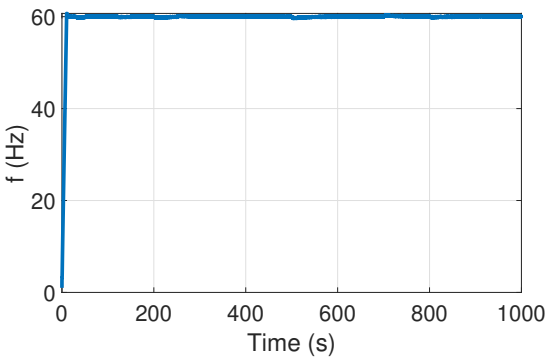

(f) Generator frequency.

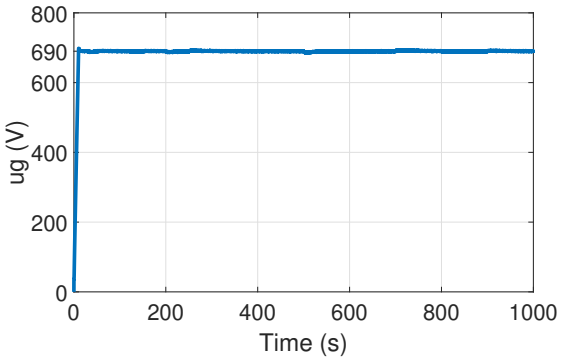

(g) Generator voltage.

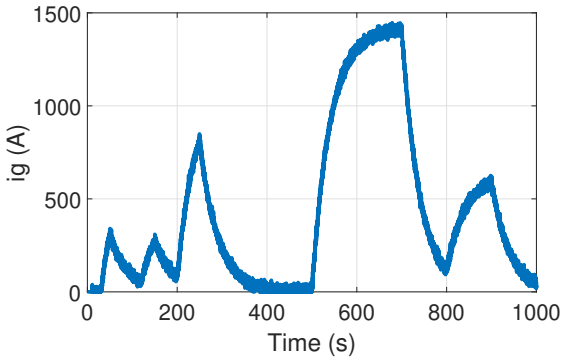

(h) Generator current.

Figure 31 – Important genset operating variables responding to noisy power demand profile.

Table 3 – Parameters of the genset model.

Parameter	Symbol	Value	Unit	Reference
Number of poles	P_p	4	-	D
Nominal frequency	f	60	hz	D
Power factor	$cos(f_p)$	0.9	-	E
Nominal electrical power	P_{nom}	1700	kW	D
Friction rate	c_f	0.005	-	E
Generator internal resistance	r_g	0.032	Ω	E
Moment of inertia	J_g	69.21	kgm^2	[75]
Nominal grid voltage	$u_{g,nom}$	690	V	D
Diesel low heat value	Q_{lhv}	42780	kJ/kg	D
Coefficients for the engine torque fit (M_{dg}) $\star$	δ_0	-6.7×10^{-2}	kNm	E
	δ_1	6.58×10	kNm/kg	E
	δ_2	3.22×10^2	kNms^2/kg^2	E
	δ_3	2.56×10^3	kNms^3/kg^3	E
	δ_4	-2.84×10^4	kNms^4/kg^4	E
Nominal grid voltage	$u_{g,nom}$	690	V	D
Coefficients for the thermal efficiency fit (η_t) $\star$	δ_0	3.18×10^{-4}	kg/s	E
	δ_1	2.2×10^{-3}	kg/(skW)	E
	δ_2	-6.18×10^{-6}	kg/(skW^2)	E
	δ_3	8.54×10^{-9}	kg/(skW^3)	E
	δ_4	-6.28×10^{-12}	kg/(skW^4)	E
	δ_5	2.35×10^{-15}	kg/(skW^5)	E
	δ_6	-3.54×10^{-19}	kg/(skW^6)	E
Coefficients the for genset efficiency fit (η_{genset}) $\star$	δ_0	4.08×10^{-4}	kg/s	E
	δ_1	2.28×10^{-3}	kg/(skW)	E
	δ_2	-6.45×10^{-6}	kg/(skW^2)	E
	δ_3	9.52×10^{-9}	kg/(skW^3)	E
	δ_4	-7.48×10^{-12}	kg/(skW^4)	E
	δ_5	2.99×10^{-15}	kg/(skW^5)	E
	δ_6	-4.79×10^{-19}	kg/(skW^6)	E
Coefficients for the CO_2 fit ($\dot{m}_{\mathrm{CO_2}}$) $\star$	δ_0	1.63×10^{-3}	kg/s	E
	δ_1	2.77×10^{-4}	kg/(skW)	E
	δ_2	-1.60×10^{-7}	kg/(skW^2)	E
	δ_3	8.62×10^{-11}	kg/(skW^3)	E
	δ_4	-1.46×10^{-14}	kg/(skW^4)	E
Coefficients for the CO fit ($\dot{m}_{\mathrm{CO}}$) $\star$	δ_0	2.16×10^{-4}	kg/s	E
	δ_1	-1.36×10^{-7}	kg/(skW)	E
	δ_2	-1.235×10^{-10}	kg/(skW^2)	E
	δ_3	1.38×10^{-13}	kg/(skW^3)	E
Coefficients for the PM fit ($\dot{m}_{\mathrm{PM}}$) $\star$	δ_0	1.53×10^{-5}	kg/s	E
	δ_1	4.89×10^{-8}	kg/(skW)	E
	δ_2	-8.76×10^{-11}	kg/(skW^2)	E
	δ_3	4.63×10^{-14}	kg/(skW^3)	E
	δ_4	-4.45×10^{-18}	kg/(skW^4)	E
Coefficients for the HC fit ($\dot{m}_{\mathrm{HC}}$) $\star$	δ_0	6.36×10^{-5}	kg/s	E
	δ_1	-9.84×10^{-8}	kg/(skW)	E
	δ_2	-2.94×10^{-10}	kg/(skW^2)	E
	δ_3	-2.53×10^{-13}	kg/(skW^3)	E
	δ_4	6.93×10^{-17}	kg/(skW^4)	E
Coefficients for the NO_x fit ($\dot{m}_{\mathrm{NOx}}$) $\star$	δ_0	3.01×10^{-6}	kg/s	E
	δ_1	5.04×10^{-6}	kg/(skW)	E
	δ_2	-1.17×10^{-8}	kg/(skW^2)	E
	δ_3	1.11×10^{-11}	kg/(skW^3)	E
	δ_4	-3.07×10^{-15}	kg/(skW^4)	E

$\star$ - We consider the standard polynomial form $\sum_{j=0}^{N_P} \delta_j x^j$

E - estimated / D - directly obtained

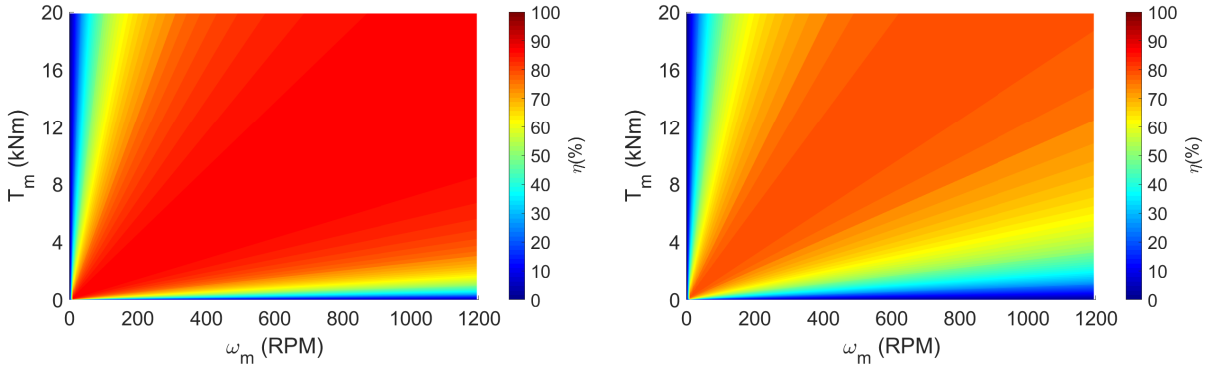

(a) Efficiency map after modifications. **(b) Efficiency map before modifications.**

Figure 32 – Efficiency maps of a DC motor connected to the drivetrain.

The work by [61] presents a method for parameter identification for different electric motor types based on desired operation conditions. Given information about the desired operation, all the other electrical parameters of the motor can be determined by an algorithm.

Following the mentioned work and giving operational parameters such as nominal armature voltage, speed, mechanical power, efficiency, mechanical and electrical time constants, all other required parameters could be found through a simple algorithm, with the main ones in Tab. 4. Some parameters as the mechanical and electrical time constants had to be estimated based on the expected motor response.

In Fig. 32, a comparison between the efficiency maps of the DC motor connected to the drivetrain before and after the modifications is presented. It is clear that the efficiency is higher after the modification of the parameters, in Fig. 32(a), in comparison with 32(b). The maximum value increased by approximately 10% (from 80% to 90%). Besides, there was a general increase in efficiency.

No changes in the PID controller were necessary. In terms of the motor drive, it was considered that a DC buck and boost converter is capable of providing the required voltage input signal. This way, both lower and higher voltage than that supplied from the line is possible. The parameters were changed to reduce the current to acceptable values according to technical advice provided by industry partners.

Regarding the dynamical behavior, the methodology used has shown consistent results. The DC motor model was decoupled from the hybrid power system simulator, described in chapter 3. Then, simulations of the DC motor were performed considering the drivetrain and the vessel-propeller model, also discussed in chapter 3.

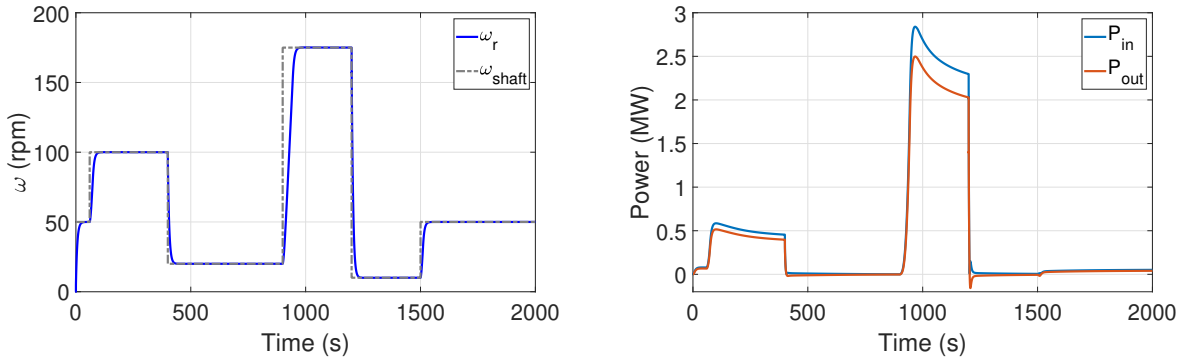

(a) Shaft angular velocity: ω_r, ω_{shaft} – shaft speed. **(b) Mechanical (P_{out}) and electrical (P_{in}) power.**

Figure 33 – Dynamic behavior of the DC motor.

Table 4 – Parameters of the DC motor: before and after changes.

Parameter	Symbol	Value	Unit	Reference
Nominal output power	P_{out}	2.5	MW	D
Nominal voltage	$u_{A,nom}$	690/3300	V	D
Nominal motor speed	ω_m	1200	RPM	D
Armature resistance	R_A	0.0127/0.2990	Ω	E
Armature inductance	L_A	8.98×10^{-4}/0.002	H	E
Torque constant	K_t	4.82/24.21	Nm/A	E
Equivalent inertia	J_{eq}	39.1/59.1	kgm^2	E
Equivalent damping	B_{eq}	24.74/7.56	kgm^2/s	E
Gearbox reduction	red	6.86	-	E

/ - separates values before (first ones) and after (second ones) changes
E - estimated
D - directly obtained

In Fig. 33(a) and 33(b), the shaft speed and the power input and output are shown. The nominal motor speed was considered to be 1200 RPM and the rated mechanical power delivered was 2.5 MW, with a gear ratio of 6.85. Results show consistency between the nominal operation point and the expected behavior; the shaft velocity of 175 RPM was achieved with the nominal power of approximately 2.5 MW in transient operation. Moreover, the velocity controller was adequate, reaching the desired references according to the control objectives

4.3 THREE-PHASE INDUCTION MOTOR

The induction motor (IM) model described in [34, 63] was implemented here, considering the equivalent circuit dynamics in the orthogonal stator coordinate frame, $\alpha - \beta$ coordinates, with stator current components i_α and i_β, and rotor flux components λ_α and λ_β as state variables, as well as the angular speed of the rotor ω_m. The power electronics of the inverter are assumed to be able to supply the required inputs to the IM.

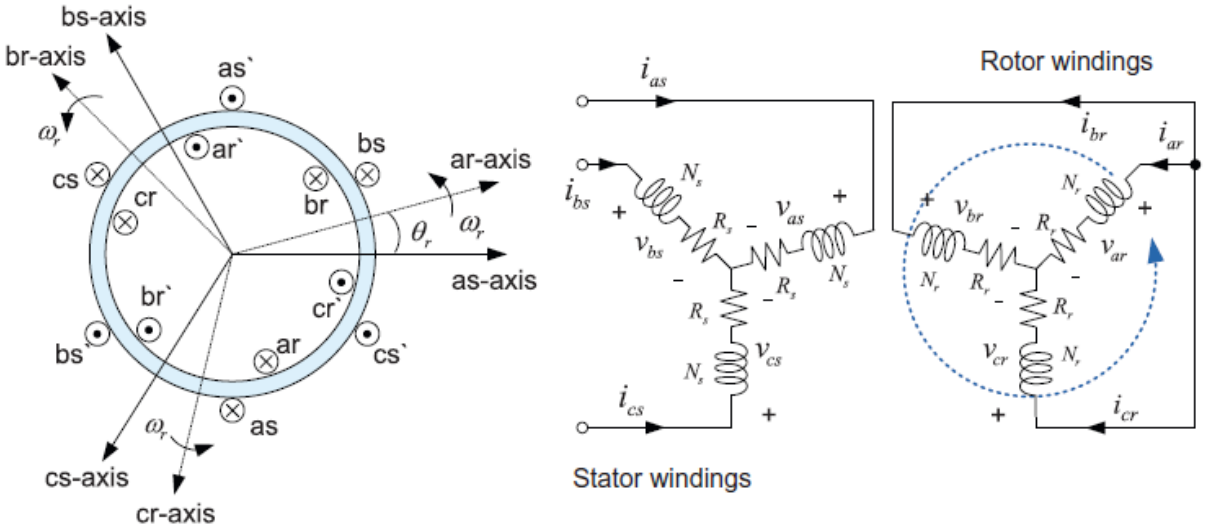

Figure 34 – Two-pole, three-phase, wye-connected symmetrical induction motor [76].

In Fig. 34, the stator and rotor windings for a two-pole, three-phase, wye-connected symmetrical induction motor are shown for illustration. The stator consists of three inductors, wye connected, oriented by $120°$. Each inductor is fed with an AC current, which generates a rotating magnetic field (RMF). The RMF induces a current in the rotor, producing itself a magnetic field that interacts with the RMF. As a result, torque is generated according to the Lenz law [34]. The dynamical equations are:

$$\frac{di_\alpha}{dt} = \underbrace{\beta\eta\lambda_\alpha + \beta N_r\omega_m\lambda_\beta - \gamma i_\alpha}_{f_1} + \frac{1}{\sigma L_s}u_\alpha, \tag{60}$$

$$\frac{di_\beta}{dt} = \underbrace{\beta\eta\lambda_\beta - \beta N_r\omega_m\lambda_\alpha - \gamma i_\beta}_{f_2} + \frac{1}{\sigma L_s}u_\beta, \tag{61}$$

$$\frac{d\lambda_\alpha}{dt} = \underbrace{-\eta\lambda_\alpha - N_r\omega_m\lambda_\beta + \eta L_h i_\alpha}_{f_3}, \tag{62}$$

$$\frac{d\lambda_\beta}{dt} = \underbrace{-\eta\lambda_\beta + N_r\omega_m\lambda_\alpha + \eta L_h i_\beta}_{f_4}, \tag{63}$$

$$\frac{d\omega_m}{dt} = \underbrace{\frac{1}{J}(T - B\omega_m - T_L)}_{f_5}, \tag{64}$$

with

$$\eta = \frac{R_r}{L_r}, \quad \sigma = 1 - \frac{L_h^2}{L_s L_r}, \quad \beta = \frac{L_h}{\sigma L_s L_r}, \quad \gamma = \frac{1}{\sigma L_s}\left(R_s + \frac{L_h^2}{L_r^2}R_r\right). \tag{65}$$

The state-space vector is $\mathbf{x} = [i_\alpha, i_\beta, \lambda_\alpha, \lambda_\beta, \omega_m]^T$, and the control inputs are the voltages $\mathbf{u} = [u_\alpha, u_\beta]$. The parameters L_r, L_s and L_h represent rotor, stator, and mutual inductance, respectively, while R_r and R_s represent the rotor and stator resistances. The number of pole pairs

is defined by N_r. The moment of inertia of the motor is described by J, and the damping is B. The load torque is defined as T_L. The electromagnetic torque can be written as

$$T = \mu(i_\beta \lambda_\alpha - i_\alpha \lambda_\beta), \tag{66}$$

where

$$\mu = \frac{3}{2} N_r \frac{L_h}{L_r}. \tag{67}$$

To integrate the electromechamical model described above to the drivetrain (with gearbox and propeller) described in section 3.2, we can change the equation responsible for the mechanical behavior of the motor, Eq. (64). The moment of inertia J and the damping B are replaced by the equivalent quantities J_{eq} and B_{eq}, following the approach mentioned in section 3.2, and the load torque T_L is equal to the reduced propeller torque T_{prop}/red. This way, Eq. (64) becomes Eq. (68), as below

$$\frac{d\omega_m}{dt} = \underbrace{\frac{1}{J_{eq}} \left(T - B_{eq}\omega_m - \frac{T_{prop}}{red} \right)}_{f_5}. \tag{68}$$

The sliding mode control (SMC) technique has been applied to control the IM, following the methodology described in Appendix A. In summary, the voltages u_α and u_β are changed to regulate the angular velocity of the motor ω_m and consequently the propeller velocity to produce thrust. For torque control, the flux is also regulated.

Some simulations were executed to analyze electric propulsion performance with the induction motor and drivetrain models, considering data from an AC motor of 2.5 MW, in Tab. 5 and the vessel-propeller model from section 3.5. Therefore, for the following simulations, we considered the simplified ship dynamics and the propulsion components from the propeller to the electric motors focusing on the operation of the two main thrusters.

The results in Fig. 36 show excellent tracking performance for the propeller angular velocity, Fig. 36(a), and square flux, Fig. 36(b). The voltage inputs in the (α, β) frame are shown in Fig. 36(c) and 36(d), respectively. The rotor fluxes and stator currents are depicted in Fig. 36(e) and 36(f), and Fig. 36(g) and 36(h). The three-phase currents, voltages, and fluxes can be easily found through Clarke matrix transformations.

The electromagnetic torque is shown in Fig. 37(a), while the input and the output power are illustrated in Fig. 37(b). From the numerical data, it was possible to verify an efficiency of 92.5% in the nominal operating point considering the AC motor coupled with the drivetrain,

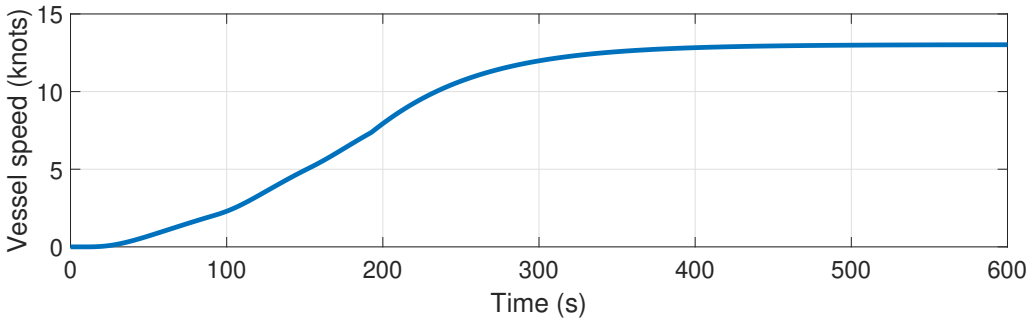

Figure 35 – Vessel velocity.

with a propeller speed of 175 RPM and a motor torque below the maximum of $20\,\mathrm{kN}\cdot\mathrm{m}$. The velocity of the vessel is shown in Fig. 35. It can be seen that the cruise velocity is about 13 knots, which is identical to the real cruise velocity of the Ulstein PSV.

4.3.1 Comparison with model from MATLAB/Simulink library

The presented IM model has gone through experimental validation, as reported in the literature [34]. Therefore, it is considered suited for application given the right parameters. Additionally, the implementation of the model in this work was compared with the asynchronous squirrel-cage model from the MATLAB/Simulink library, with the parameters in Tab. 5.

The results, shown in Fig. 38, were produced for the input load torque depicted in Fig. 38(a), with a line voltage of 690 V, a frequency of 50 Hz, and not considering the control of angular speed and flux. The angular velocity of the rotor is shown in Fig. 38(b), while the electrical power input and the electromagnetic torque are shown in Fig. 38(c) and in Fig. 38(d), respectively. In general, good agreement was achieved between the models in comparison. Some differences appeared in the electrical power in the first seconds of operation, but this difference faded quickly.

4.4 BATTERY MODEL FOR A LITHIUM IRON PHOSPHATE CELL

The lithium iron phosphate ($LiFePO_4$/LFP) ANR26650M1 cell model was chosen for implementation due to the LFP battery applications in both automotive and maritime applications [3] and by the availability of experimental data and models described in the literature. A complete second-order Thévenin equivalent circuit, validated with experimental results from the literature, was developed.

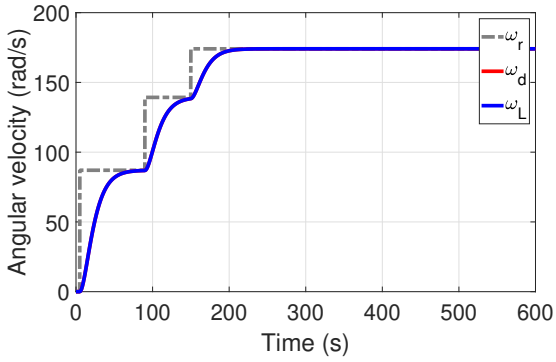

(a) Angular velocity: ω_r - step reference, ω_d - pre-filtered desired trajectory, ω - propeller speed.

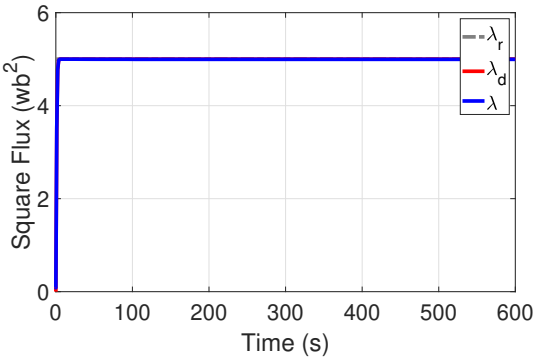

(b) Square flux: λ_r - step reference, λ_d - pre-filtered desired trajectory, λ - square flux.

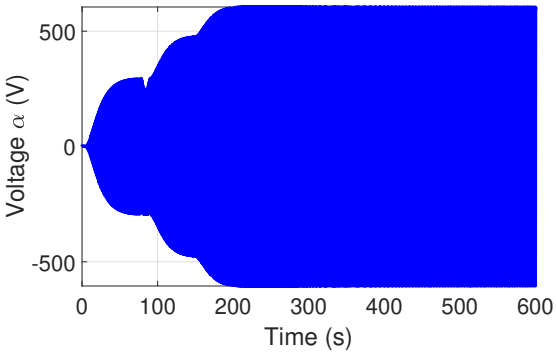

(c) Stator voltage in α axis.

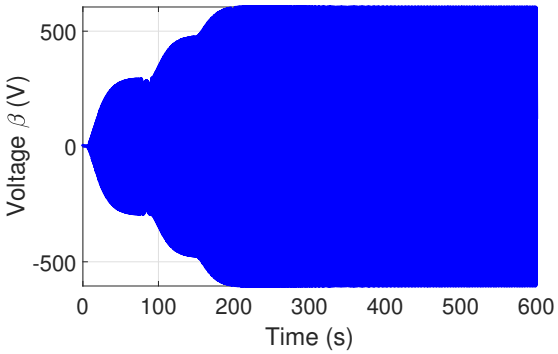

(d) Stator voltage in β axis.

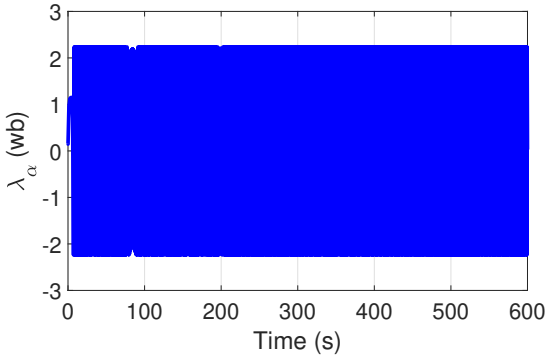

(e) Rotor flux in α axis.

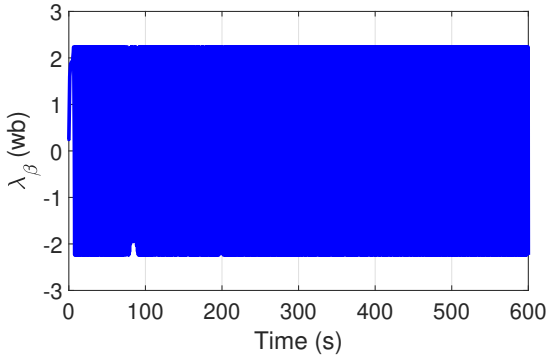

(f) Rotor flux in β axis.

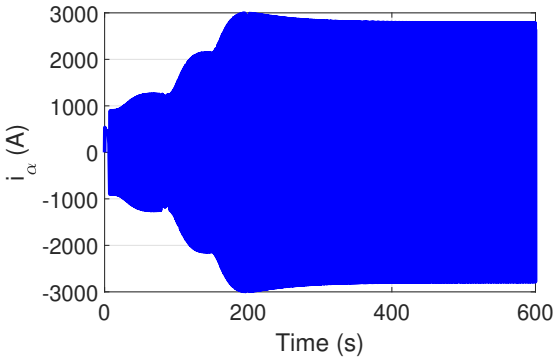

(g) Stator current in α axis.

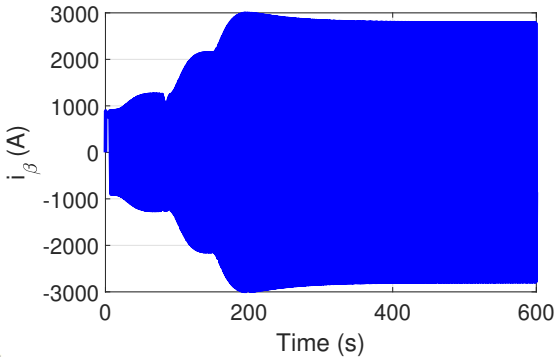

(h) Stator current in β axis.

Figure 36 – Sliding mode control of three-phase induction machine with $k_1 = 24$, $k_2 = 13.3$, $\tau_1 = \tau_2 = 5$, $\phi_1 = 0.08$, $\phi_2 = 0.03$.

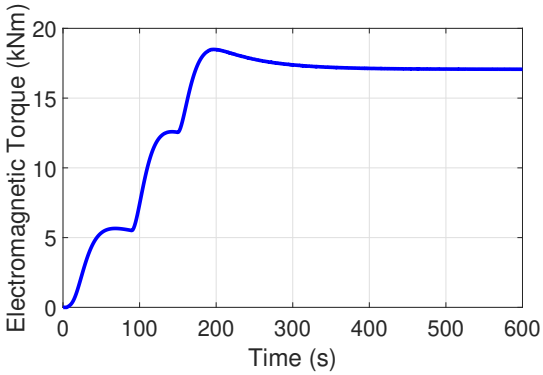

(a) Electromagnetic torque.

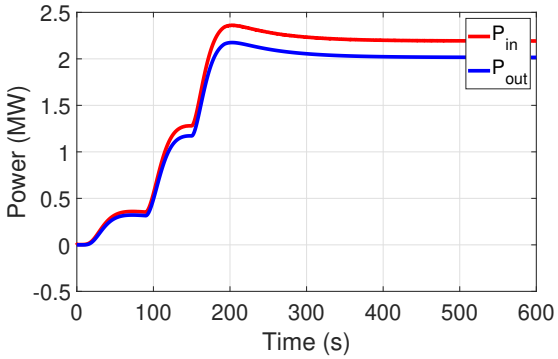

(b) Mechanical (P_{out}) and electrical (P_{in}) power.

Figure 37 – Sliding mode control of three-phase induction machine with $k_1 = 24$, $k_2 = 13.3$, $\tau_1 = \tau_2 = 5$, $\phi_1 = 0.08$, $\phi_2 = 0.03$.

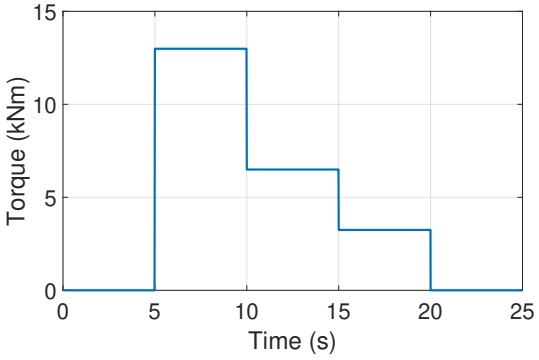

(a) Load torque input.

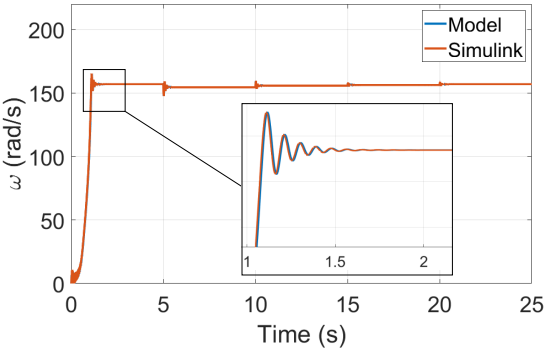

(b) Rotor speed.

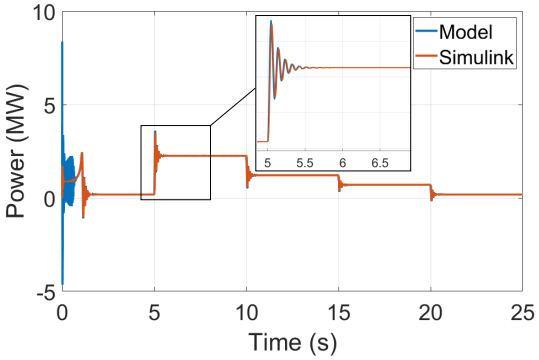

(c) Electrical power input.

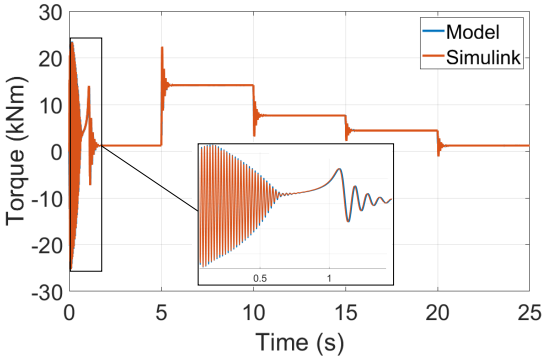

(d) Electromagnetic torque.

Figure 38 – Comparison: implemented IM model and Simulink model for the same parameters.

Table 5 – Parameters used for the induction machine model [77].

	Actual value		per unit (p.u.) value
Rated mechanical power (P_m)	2.5	MW	1.0
Grid frequency	50	Hz	
Rated stator voltage	690	V	1.0
Rated stator power	2.0	MW	0.8
Stator resistance (R_s)	2.6×10^{-3}	Ω	1.365×10^{-2}
Stator leakage inductance ($L_{\sigma s}$)	0.087×10^{-3}	H	0.144
Rotor resistance (R_r)	2.9×10^{-3}	Ω	1.523×10^{-2}
Rotor leakage inductance ($L_{\sigma r}$)	0.087×10^{-3}	H	0.144
Mutual inductance (L_m)	2.5×10^{-3}	H	4.124
Rated stator current ($I_s^{\max}$)	1760	A	0.841
Rated rotor current ($I_r^{\max}$)	1893	A	0.904

The structure of the developed model was mainly based on [66], in which the authors built a complete LFP battery cell model to evaluate the optimal charging, including minimum-time, aging and balanced charge scenarios. The works of [78] and [79] were used as references, besides their measurements, to extract experimental data including electrical, thermal, and degradation effects. In this work, the thermal and electrical parameters were taken from [78], due to easier parameter extraction from the graphics. The aging parameters were taken from [66].

4.4.1 Electrical Model

The electrical model was represented by the second-order Thévenin equivalent circuit model in Fig. 39(a). The circuit comprises an OCV source, V_{oc}, which is a function of the SOC, a series ohmic resistor R_0, and two RC pairs, (R_1, C_1) and (R_2, C_2), which are functions of the SOC and the temperature. The variable $I(t)$ defines the current running through the battery (positive for discharging and negative for charging) and C_{bat} is the nominal capacity. The voltages across the two RC pairs are V_1 and V_2.

The V_{oc} and C_{bat} values were obtained in [78] through the $C/20$ CC-CV test with high and low voltage limits of $3.6\,\mathrm{V}$ and $2\,\mathrm{V}$, and cutoff current of $50\,\mathrm{mA}$. To parametrize the RC pairs, a pulse relaxation test was executed, varying temperatures from 5 °C to 45 °C with a 10 °C interval. The set of differential equations below evaluates the voltage dynamics and the state of

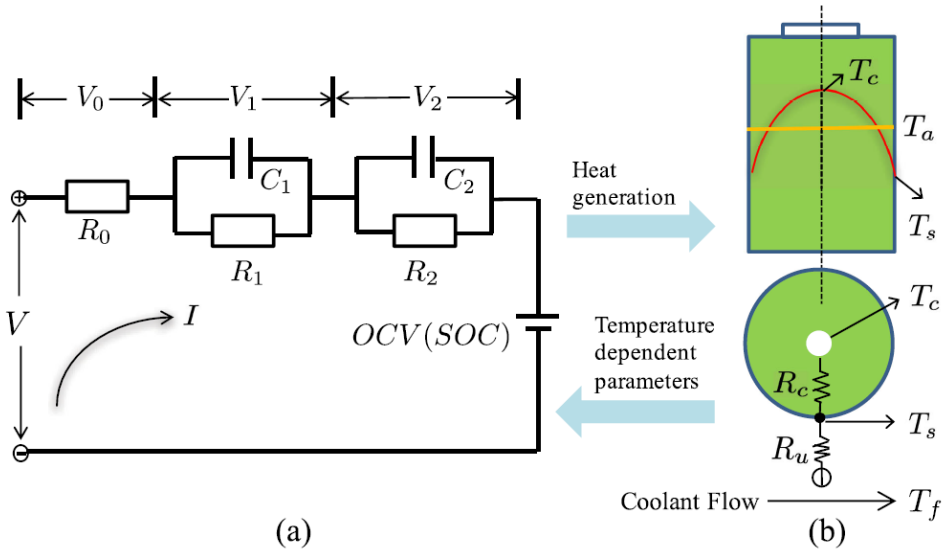

Figure 39 – Schematic of the thermo-electric model [80].

charge variation of the cell:

$$\frac{d\text{SOC}(t)}{dt} = -\frac{I}{C_{bat}}, \tag{69}$$

$$\frac{dV_1(t)}{dt} = \frac{-V_1(t)}{R_1C_1} + \frac{I(t)}{C_1}, \tag{70}$$

$$\frac{dV_2(t)}{dt} = \frac{-V_2(t)}{R_2C_2} + \frac{I(t)}{C_2}. \tag{71}$$

The voltage observed in the terminals of the battery cell is

$$V_t(t) = V_{oc}(\text{SOC}) - V_1(t) - V_2(t) - R_0I(t). \tag{72}$$

4.4.2 Thermal Model

The thermal model, depicted in Fig. 39(b), describes the heat transfer of a cylindrical battery considering as the state an array with the temperatures at the core T_c and at the surface T_s. The dynamics is expressed as

$$\frac{dT_c(t)}{dt} = \frac{T_s(t) - T_c(t)}{R_cC_s} + \frac{Q(t)}{C_c}, \tag{73}$$

$$\frac{dT_s(t)}{dt} = \frac{T_f(t) - T_s(t)}{R_uC_s} - \frac{T_s(t) - T_c(t)}{R_cC_s}, \tag{74}$$

where $Q(t) = \left|I(V_{oc} - V_t)\right|$ is a heat generation product of the joule effect and the energy dissipated in the electrode over-potentials. The constants R_c, R_u, C_c, C_s represent the heat conduction resistance, convection resistance, core heat capacity, and surface heat capacity respectively. Two assumptions are made: the ambient temperature T_f is considered constant,

although it can be set for different conditions; and the battery cell is cooled with constant air flow rate. The scaled urban assault cycle (UAC) was used used to generate a battery current profile, and the battery was tested in a flow chamber, as described in [78].

4.4.3 Aging Model

The aging model presented in [66] was based on the studies of [79]. The data used to produce the empirical model was obtained from a matrix of cycling tests ranging from different C-rates (discharge normalized currents), varying from $C/2$ to $10C$, and temperatures from $-30\,^{\circ}\mathrm{C}$ to $+60\,^{\circ}\mathrm{C}$, and depths of discharge (DOD), which are defined as $1-\mathrm{SOC}$, in the span of 10% to 90%. The experimental results of [79] have demonstrated for the ANR26650M1 that the capacity fade is strongly dependent on C-rate and temperature, while the DOD effect is less important.

The following semi-empirical model describes the capacity fading of the battery cell:

$$\frac{d\mathrm{SOH}(t)}{dt} = -\frac{\left|I(t)\right|}{2N(c,T_c)C_{bat}}. \tag{75}$$

The symbol SOH defines the state of health of the cell, a $\mathrm{SOH}=1$ defines a fresh battery, while a $\mathrm{SOH}=0$, represents the end of life (EOL). The symbol N represents the number of cycles of the battery, defined as

$$N(c,T_c) = \frac{3600A_{tol}(c,T_c)}{C_{bat}}, \tag{76}$$

where each cycle corresponds to the complete charge and discharge or $2C_{bat}$ of charge throughput. The term A_{tol} is the discharged Ah throughput used, defined as

$$A_{tol}(c,T_c) = \left[\frac{20}{M(c)exp\left(-\frac{E_a(c)}{RT_c}\right)}\right]^{\frac{1}{z}}. \tag{77}$$

A_{tol} should be doubled due to the charge and discharge in a cycle. In Eq. (77), the term $M(c)$ is the pre-exponential factor, a function of the C-rate. The Arrhenius correlation accounts for the core temperature T_c effect in the reaction kinematics. The activation energy E_a, is a function of the C-rate, as below,

$$E_a(c) = 31700 - 370.3c, \tag{78}$$

while R is the ideal gas constant and z is the power-law factor.

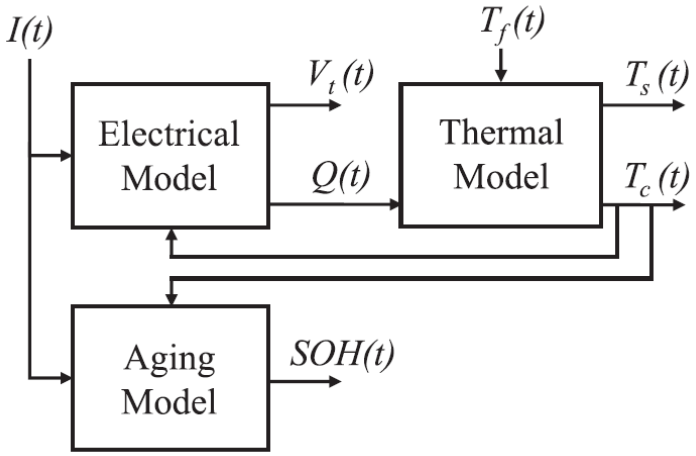

Figure 40 – Electro-thermal-aging model coupling [66].

Table 6 – Battery cell constant parameters.

Parameter	Symbol	Value	Unit	Reference
Conduction resistance	R_c	1.94	kW^{-1}	[66, 78]
Convection resistance	R_u	3.08	kW^{-1}	[66]
Core heat capacity	C_c	62.7	JK^{-1}	[66, 78]
Surface heat capacity	C_s	4.5	JK^{-1}	[66, 78]
Cell capacity	C_{bat}	2.2	Ah	[66]
Ambient temperature	T_f	298.15	K	A
Power law factor	z	0.55	kgm^2	[66]

A - assumption

4.4.4 Coupled electro-thermal-aging model and validation

In Fig. 40, a block diagram summarizes the coupling of the models described in the sections above. The complete model receives an input current $I(t)$, which enters directly into the electrical and aging models. Based on $I(t)$ and the core temperature $T_c(t)$, the electrical model outputs the terminal voltage $V_t(t)$ and the generation of heat $Q(t)$.

The term $Q(t)$ is an input to the thermal model, which also takes into consideration the ambient temperature $T_f(t)$. The outputs of the thermal model are the core and surface temperatures, $T_c(t)$ and $T_s(t)$ respectively. The core temperature affects the parameters of the Thévenin electrical circuit and the aging model. The core temperature and the current influence the aging model, whose output represents the chemical degradation of the battery over the simulation through the SOH.

The parametric data used to implement the model was taken from [66, 78, 79]. Besides the constant values, in Tab. 6, a total of 12 polynomial fits with small regression errors were produced, including surfaces and curves to account for the required parameters for charge and discharge. The graphics with data points and model fits are depicted in Fig. 41 and 42.

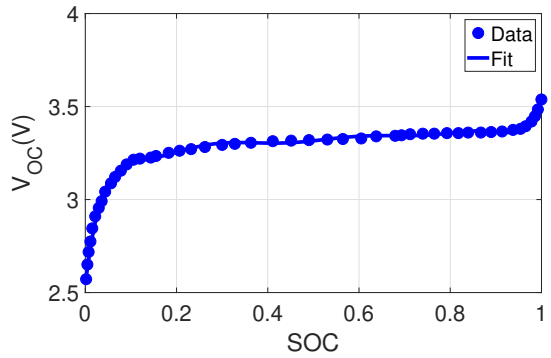

(a) Open Circuit Voltage.

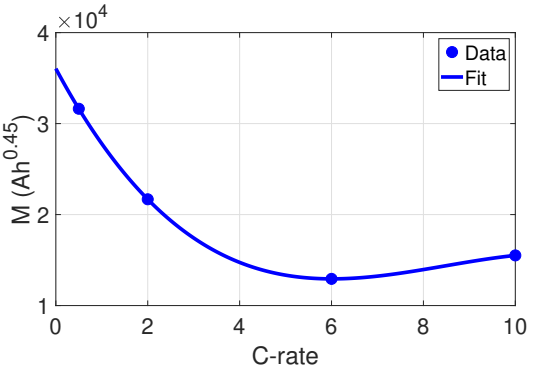

(b) Pre-exponential factor.

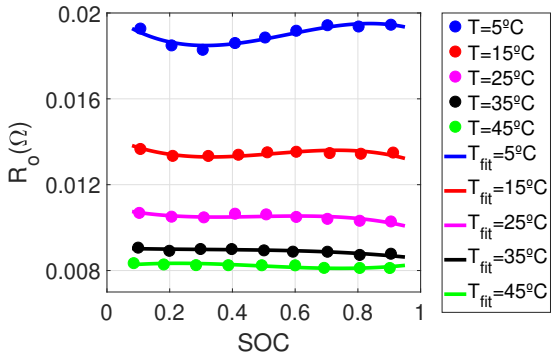

(c) Series resistance – discharge.

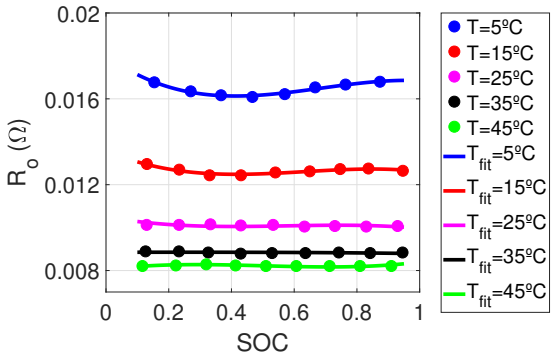

(d) Series resistance – charge.

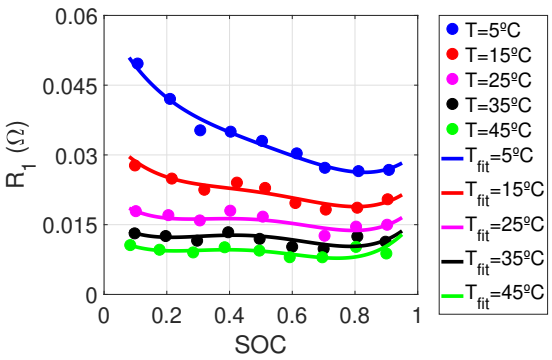

(e) First RC pair resistance – discharge.

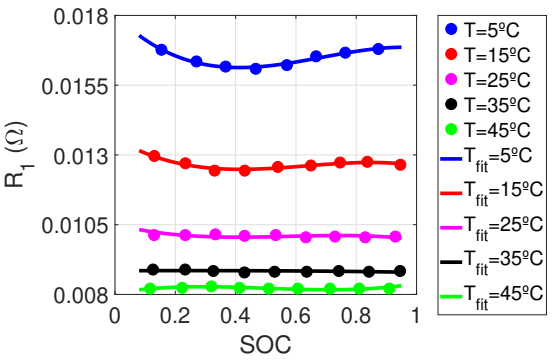

(f) First RC pair resistance – charge.

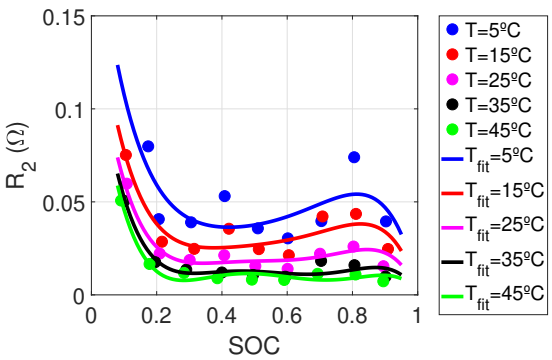

(g) Second RC pair resistance – discharge.

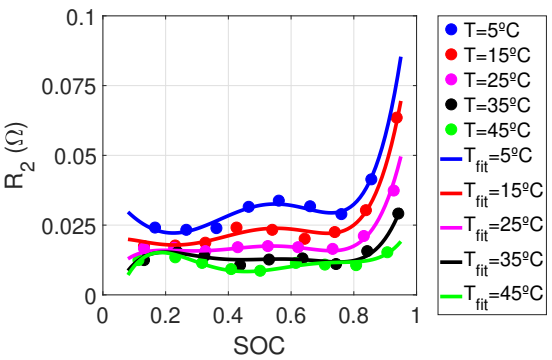

(h) Second RC pair resistance – charge.

Figure 41 – Battery cell parameters: OCV, pre-exponential factor; and resistance.

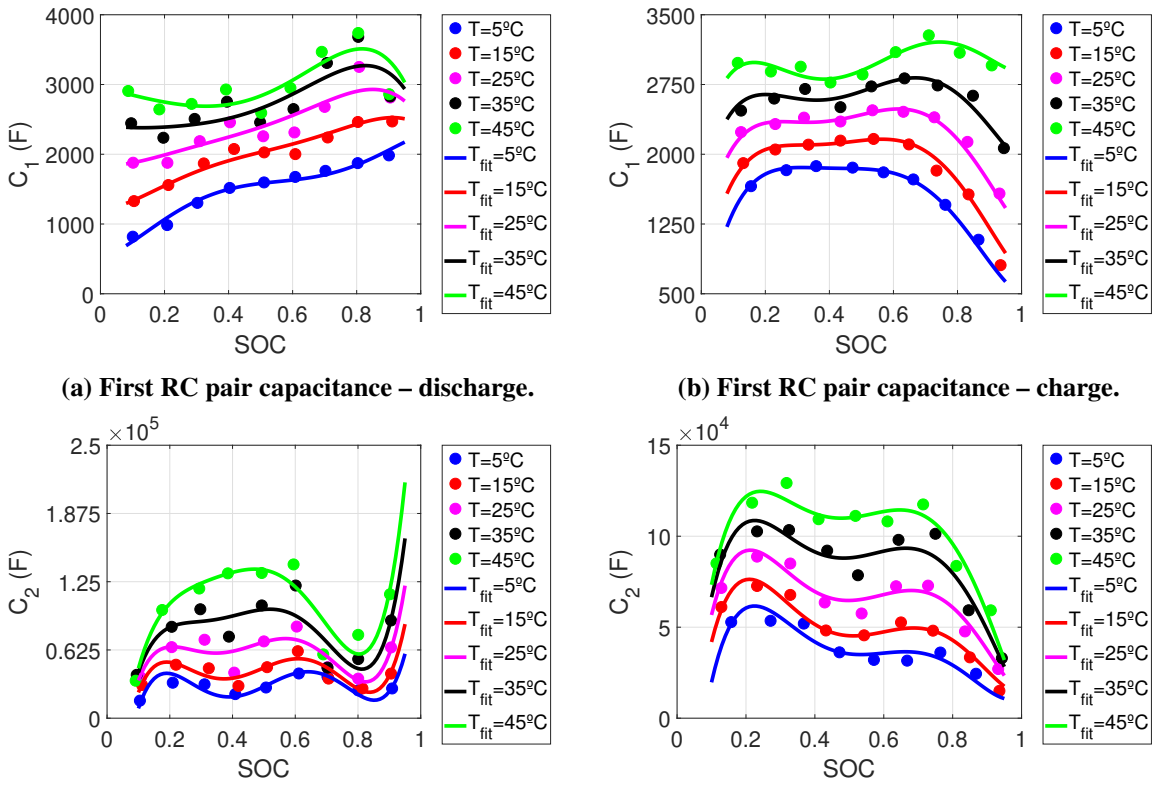

(a) First RC pair capacitance – discharge.

(b) First RC pair capacitance – charge.

(c) Second RC pair capacitance – discharge.

(d) Second RC pair capacitance – charge.

Figure 42 – Battery cell parameters: capacitance.

Figure 43 shows the relation of the EOL cycle and SOH decay rate with the C-rate for different core temperatures. The results obtained with the implemented model are also compared to data found in the literature. The SOH decay rate increases with increments in C-rate. It is interesting to note that more EOL cycles can be reached by this battery at medium C-rates (2-5C) than at lower C-rates. According to 66, the aging model also includes calendar-life effects, when there is a current applied, as the Ah throughput calculation is directly proportional to time in [79]. One cycle at a very low C-rate has a long duration, therefore, producing considerable degradation. Generally, it can be seen that the results are in accordance. It was possible to verify numerically that the maximum differences for the EOL and SOH decay rate were limited to 8% and 10%, respectively.

The implemented model was also compared with other literature data, including simulation and experiments. The input current of the cell, Fig. 44(a), was extracted from [66]. The terminal voltages are compared in Fig. 44(b). The temperatures of the core (T_c) and the surface (T_s) are compared in Fig. 44(c), as well as the SOC and SOH, in Fig. 44(d). Despite the visual discrepancies, the results have shown errors below 1% for all comparisons in Fig. 44.

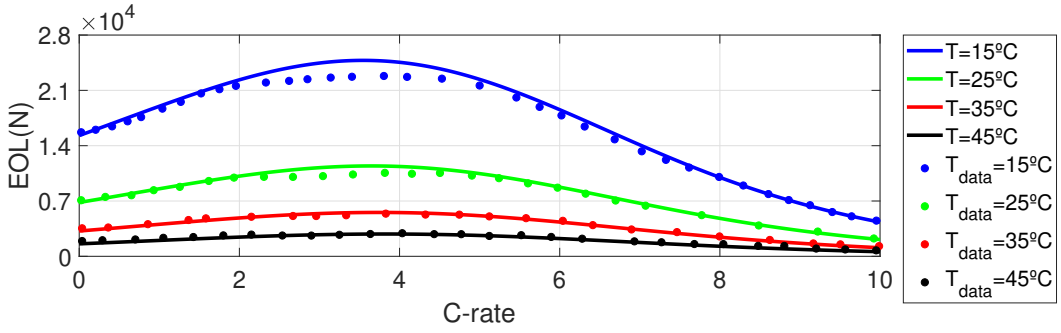

(a) EOL number of cycles defined in Eq. (76).

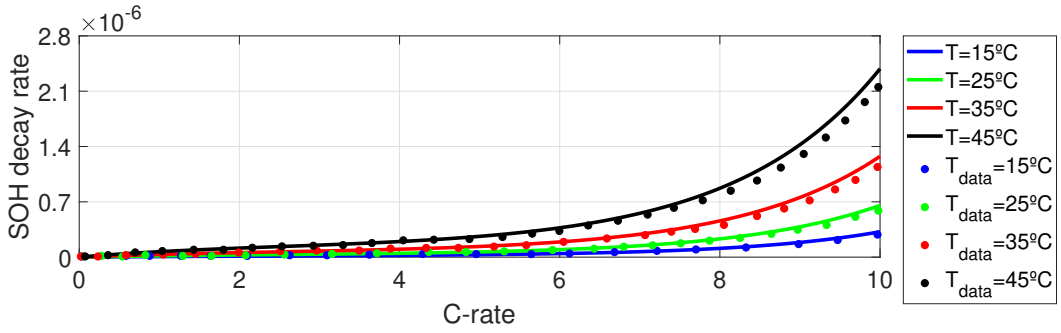

(b) SOH decay rate defined in Eq. (75).

Figure 43 – Cell degradation comparison with literature results [66].

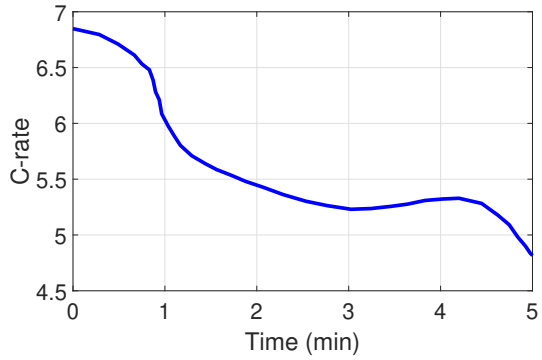

(a) Input current.

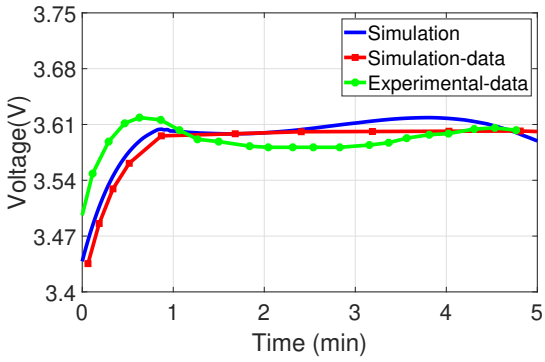

(b) Terminal voltage: simulation of implemented model, literature simulation and experimental data.

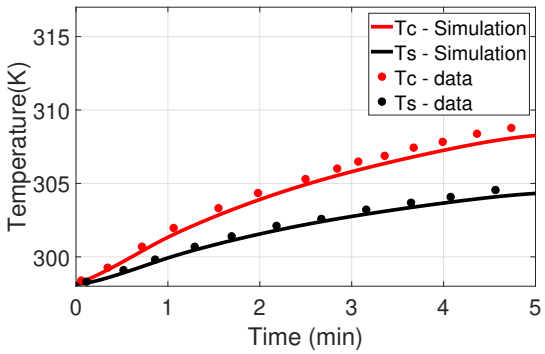

(c) Core and surface temperatures.

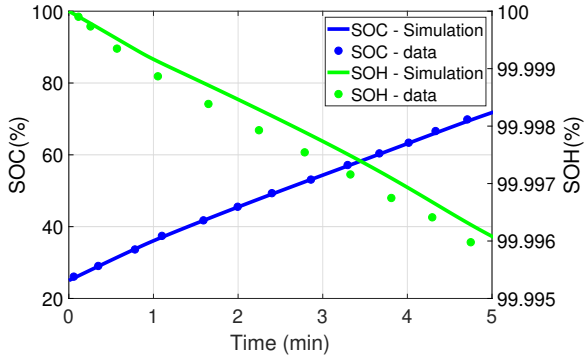

(d) SOC and SOH.

Figure 44 – Comparison of the implemented model and results from the literature [66].

4.5 BATTERY PACK MODEL

The battery pack model considers several cell circuits combined in series and parallel, all with uniform behavior, in a way that the variable states are considered the same among all cells. With the mentioned hypothesis, the total capacity C_{pack}, resultant voltage V_{pack}, current I_{pack}, stored energy E_{pack}, and power in the terminals P_{pack} of the battery become

$$C_{pack} = NP \times C_{bat}, \tag{79}$$

$$V_{pack} = NS \times V_t, \tag{80}$$

$$I_{pack} = NP \times I, \tag{81}$$

$$E_{pack} = C_{pack} \times V_{pack}, \tag{82}$$

$$P_{pack} = V_{pack} \times I_{pack}. \tag{83}$$

The number of cells in parallel and series are NP and NS, respectively. The values of NP and NS can be determined considering the total energy, nominal power of the battery, and C-rate, for example, as well as other constraints.

4.6 ELECTRICAL ARCHITECTURE

The power sources, consisting of gensets and batteries, are connected through a static electrical network which accounts only for power balance, considering the conservation of energy. The battery converter model considers only a constant efficiency, whose symbol is η_c. Furthermore, constant auxiliary loads are considered in this work. Regarding the electrical motors, static models account for converter efficiencies.

4.7 EFFICIENCY INDEX

A global efficiency index η_{ps} is proposed in this work to study how the hybrid power system can increase the overall efficiency of the vessel. In addition, it can help in comparisons to avoid false interpretations of results. In some situations, mainly when the mission simulation time is small, a fuel consumption reduction can be achieved along with a decrease in the SOC. Looking only at the fuel savings, the energy spent by the battery is not considered.

To consider the power modes in the same base, the methodology is based on the total energy input and output. In the base case, the input energy is given by the energy stored in the

fuel, $E_{in} = m_f Q_{lhv}$, where m_f considers the total mass of fuel consumed during the mission and Q_{lhv} is the low heat value of the Diesel. Since a power balance is achieved, the output energy along the mission is determined as $E_{out} = \int_0^{t_f} P_d \, dt$, where P_d is the power demand. For the base case, the efficiency is given by

$$\eta_{ps} = \frac{\int_0^{t_f} P_d \, dt}{m_f Q_{lhv}}. \tag{84}$$

For the hybrid case, the energy input of the gensets are the same as well as the output due to the power demand. However, it is necessary to consider the energy flow associated with the battery SOC. In general, the final state of charge of the battery can be different from the initial. Therefore, we consider the amount of energy that would be required to restore the initial SOC, defined as $E_{bat} = \int_{t_f}^{t_b} V_{pack} I_{pack} \, dt$. The integration goes from the final time t_f until the time t_b in which the battery restores its SOC_i. If the SOC_f is greater than the initial, the excess of energy could be used to supply some demand of the vessel. Thus, the efficiency is:

$$\eta_{ps} = \frac{\int_0^{t_f} P_d \, dt + |\int_{t_f}^{t_b} V_{pack} I_{pack} \, dt|}{m_f Q_{lhv}}. \tag{85}$$

When the SOC_f is smaller than SOC_i, it means that energy would be required for recharging the battery to its initial state. In that case, an input of energy would be necessary, so the efficiency becomes:

$$\eta_{ps} = \frac{\int_0^{t_f} P_d \, dt}{m_f Q_{lhv} + |\int_{t_f}^{t_b} V_{pack} I_{pack} \, dt|}. \tag{86}$$

5 ENERGY AND POWER MANAGEMENT STRATEGIES

In chapter 2, we have discussed electric propulsion topologies and controls, and in chapter 3, we have described the hybrid power system modeling and the integration of individual component models in Project 7, using Fig. 14. In chapter 4 we presented the modeling of the powertrain components used for the Ulstein PSV (original system and the hybrid solution). With the information from these chapters, the modeling approach can be divided into the electrical power system, propulsion system, auxiliary and service loads, and vessel physics.

5.1 MULTILEVEL POWER MANAGEMENT FRAMEWORK

Figure 45 summarises the model division structure. Reference speeds ω_{ref} are given to the propulsion system to propel the vessel, considering fixed pitch propellers. The shafts develop effective speeds ω_e, and due to the vessel physics, effective torques τ_e are required. The electrical power system supplies the power P_{ekW} necessary for the propulsion system and the auxiliary systems.

This work will focus on the electrical power system, which comprises the power sources connected through the electrical network, the energy, and power management strategies, as shown in Fig. 45. To simulate the electrical power system of a vessel for hybrid and non-hybrid configurations, we will consider a multilevel power management framework inspired by the three-level hierarchical control mentioned in [14], which has been discussed in chapter 2, and the multilevel control approaches described in [3, 6].

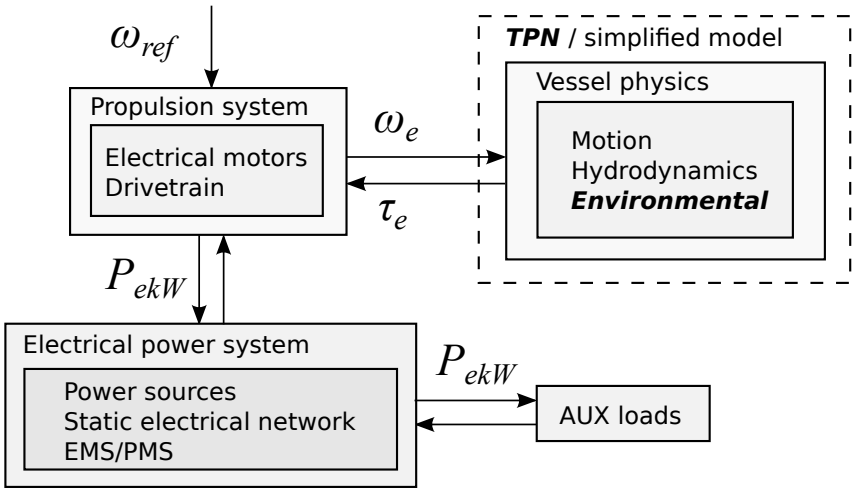

Figure 45 – Powertrain modeling block diagram for an electric propulsion vessel.

In Fig. 46, the Diesel-electric multilevel power system control is considered, and a block diagram shows the system topology, some control, and physical signals. The framework consists of three levels, namely, the tertiary, secondary, and primary control illustrated with numbers. The electricity consumers require the power P_L. With the power load demand and the measurements of the battery and generator states, $\mathbf{M}$, the tertiary control, through an EMS, decides the best way to use the power sources, defining power references for the gensets $P_{1,ref}; P_{2,ref}; ...; P_{n,ref}$, and for the battery $P_{bat,ref}$.

The secondary control, defined by the PMS control block, receives the power references set by the EMS, the power demand, and the states of the battery and generators. In this work, the modeling considered that the secondary control (PMS) controls the genset start/stop, and defines the speed references for the generators $\omega_{1,ref};\ \omega_{2,ref};\ \ldots;\ \omega_{n,ref}$. When we start or stop the generators, speed ramps can take the speed from zero to the nominal value and vice versa. The generator can be synchronized when the engine speeds achieve at least 95% of the rated speed. The power allocation vector $\mathbf{P_{alloc}}$ delivers the resulting active power references to the sources.

The governors in Fig. 46 are a part of the primary control and are responsible for regulating the engine speeds through the fuel injections $\dot{m}_{f1}, \dot{m}_{f2}, \ldots, \dot{m}_{fn}$. The engine speeds achieved are $\omega_{dg1}, \omega_{dg2}, \ldots, \omega_{dgn}$. The power converter model is static, and only a constant efficiency (η_{rec}) is considered. Therefore, the battery power P_{bat} is different from the actual power delivered or absorbed from the electrical network $P_{ebat} = \eta_{rec} P_{bat}$. Given the three-level control strategy, the sources can deliver or absorb, in the case of the battery, active power through a static electrical network that considers constant frequency and voltage, as well as the electrical energy conservation. Therefore, $\sum_{j=1}^{n} P_{j,ekW} + P_{ebat} = P_{out}$, where P_{out} represents the consumers' power, and n the number or gensets with $j = 1, 2, \ldots, n$.

In Fig. 47, we can have a closer view of the EMS supervisory control system. The measurement vector $\mathbf{M}$, which contains the battery converter and gensets output power, the SOC of the battery, and the battery voltage, are input to the EMS controller. Besides $\mathbf{M}$, the EMS also receives the power load demand P_L. With those inputs, the control decides the power references based on an optimizer or a rule set. The optimizer uses the measurements, system constraints, and reduced-order models to make decisions, while the rule set is model-free.

The advantage of implementing the EMS control at the supervisory level instead of directly at the primary level is the possibility to integrate the solution to an existent industrial power system topology and management control system without changing lower-level controllers

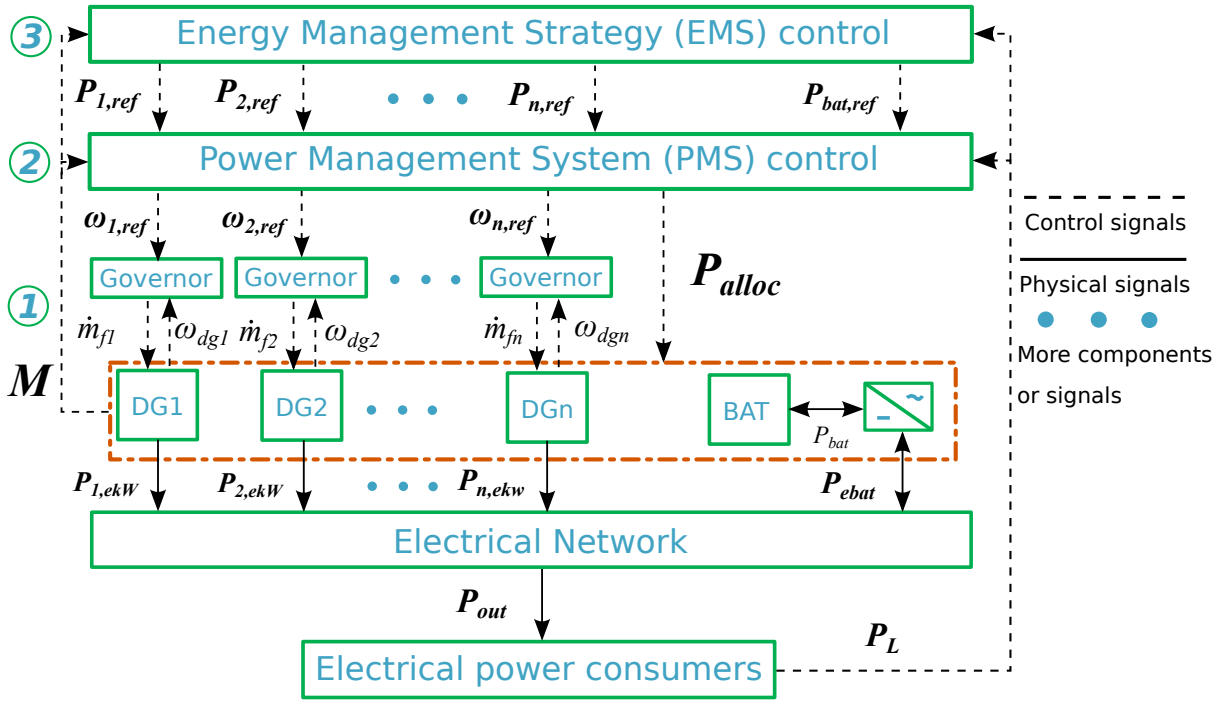

Figure 46 – Multilevel control strategy for hybrid power supply.

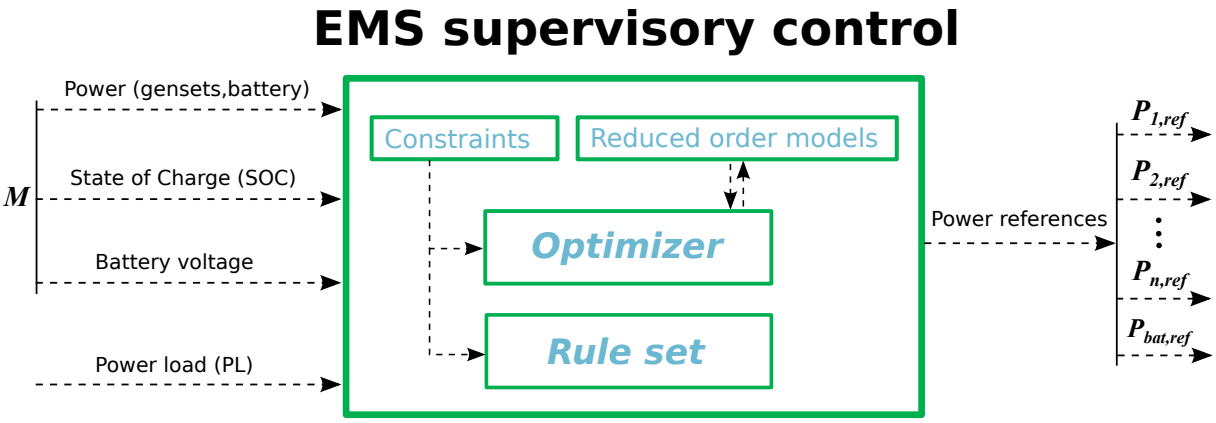

Figure 47 – Energy management system supervisory control.

and systems, as pointed out in [6]. Thus the power references can be generated considering the PMS functionality, and the power allocation reaches the primary level.

5.2 MODEL REDUCTION

As mentioned in [3,26], quasi-static maps for the power sources suffice for fuel economy estimation in an optimization process, allowing computationally fast optimization with acceptable accuracy. In some specific cases, such as engine cold-start operation, this hypothesis may not hold, and the solutions provided can be sub-optimal [49].

To build such maps, model reduction or experimental measurements are required. If the maps consist of functions, it is important to look for expressions that result in a convex

Table 7 – Parameters used for the genset reduced-order model.

Parameter	Symbol	Value	Unit
Coefficients for fuel power relation	b_0	4×10^{-3}	kg/s
	b_1	6.4×10^{-5}	kg/(skW)
	b_2	-5.1×10^{-9}	kg/(skW^2)

optimization problem to simplify the solving process. The complete and transient model runs to provide global powertrain information, and an inner quasi-static loop runs with the reduced models for optimization, as described in Fig. 47.

5.2.1 Gensets

For the genset optimization, a quadratic relation between the fuel consumption $\dot{m}_{f,dg}$, and the electrical power output P_{ekW} is established,

$$\dot{m}_{f,dg} = b_0 + b_1 P_{ekW} + b_2 P_{ekW}^2, \tag{87}$$

where b_0, b_1, b_2 are the polynomial coefficients, defined in Tab. 7

In general, the fuel consumption of Diesel generator sets is a quadratic relationship comprehending rotational speed and power output. As we considered a fixed frequency AC network, only small deviations of engine speed are allowed. Therefore, the second-order polynomial can be a good approximation for fuel consumption [3] in optimization formulations. However, to model the genset fuel consumption in long periods, we found through simulations that the fourth-order model from Eq. (59) is more indicated for the considered engine due to better precision.

Figure 48 shows a comparison between the reduced-order model using the polynomial fit from Eq. (87), and the complete model presented in chapter 4. The power inputs, defined in Fig. 27, consider several operational points in the generator power envelope, from 0 to 1700 kW. In Fig. 48(a), we can see the fuel consumption comparison, while Fig. 48(b) shows the fuel consumption percentage error.

At the beginning of the simulation, the genset is not synchronized with the electrical grid and needs to achieve the rated speed. The engine speed is controlled to follow a velocity ramp, as shown in Fig. 28, and this causes the initial fuel consumption. Then the machine waits for the signal to supply power to the grid. The reduced-order generator model considers some fuel consumption for small and zero power output to penalize the system operation at low loads.

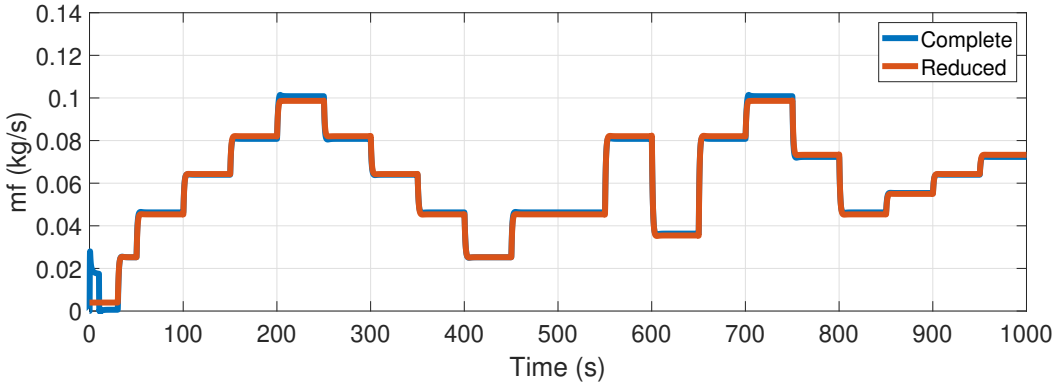

(a) Fuel consumption comparison.

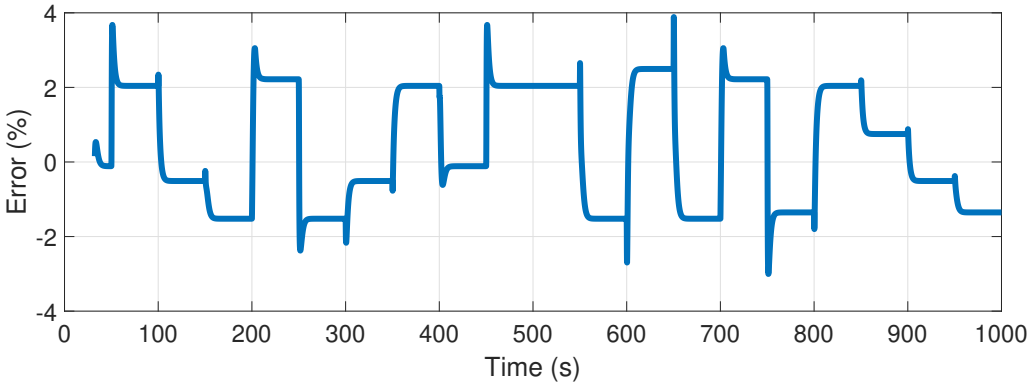

(b) Fuel consumption error in operation: $(m_{reduced} - m_{complete})/m_{complete} \times 100$**.**

Figure 48 – Comparison between the reduced-order model from Eq. (87) and the complete model presented in chapter 4.

When the genset is in operation supplying power to the grid, we can see that the fit is accurate, with differences below 4% considering the transient behavior and below 2.5% for steady-state.

5.2.2 Battery

Following the methodology presented in [3], we will reduce the second-order Thévenin circuit model presented in chapter 4 to an internal resistance model, as in Fig. 49. To be consistent with chapter 4, we will use V_t for the terminal voltage, V_{oc} for the open-circuit voltage, and I for the battery current.

For the reduced model we can determine the terminal voltage as

$$V_t(t) = V_{oc}(\mathrm{SOC}(t)) - r_{eq} I(t). \tag{88}$$

where r_{eq} is the equivalent internal resistance. The battery power for both the complete and the reduced model is defined by

$$P_{bat} = V_t(t) \times I(t). \tag{89}$$

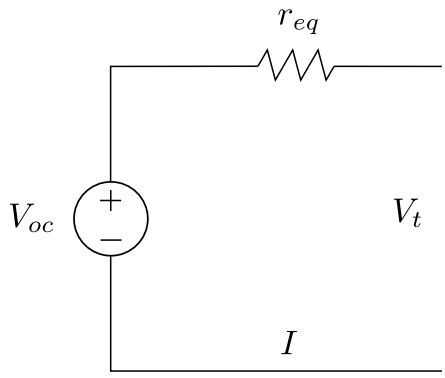

Figure 49 – Battery internal resistance equivalent circuit representation.

The same approach described in chapter 4 can be applied to extend the internal resistance model from cells to a pack, with the pack resistance defined as

$$r_{pack} = r_{eq}\frac{NS}{NP}. \tag{90}$$

Rearranging Eq. (88), we have a r_{eq} that depends on the battery's terminal voltage, current, and open-circuit voltage. Thus, it is possible to calculate a mean value for the equivalent resistance, given current inputs, and a variable battery state of charge, considering the complete battery model from chapter 4.

Figure 50 shows results of a simulation considering a square wave input with 5 A of amplitude, and a period of 40 min, which is enough for a battery depth of discharge (DOD) of 80%, with an initial state of charge of 90%. The results show that the differences are small when the current is constant, with errors smaller than 2%. However, when there are fast load variations, the differences can increase to 8%. Looking at the data, the results for power have shown smaller percentage errors, but with similar behavior.

Tests with different currents have shown that, with smaller current amplitudes, the results are better, but the quality of the results decreases with the increase of the current. The results, of course, depend on how the internal resistance was determined, including the current used to determine the value of r_{eq}, and the operational ranges considered. Despite the errors, the internal resistance models have been successfully used for EMS control strategies in [3, 26, 49]. If the optimization is performed with high frequency, measurements of the complete model can be used to avoid the modeling errors from the reduced-order battery model.

Considering the battery SOC between 20% and 80%, or in smaller sub-intervals, the open-circuit voltage is approximately constant, and a current expression as a function of the

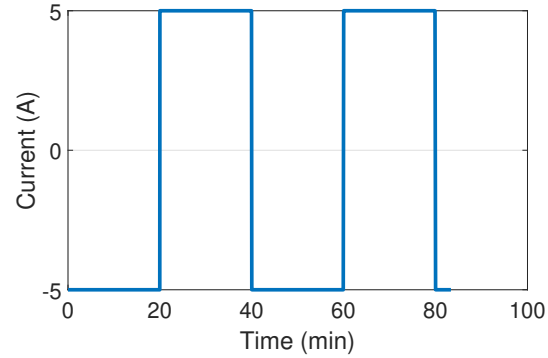

(a) Battery cell current.

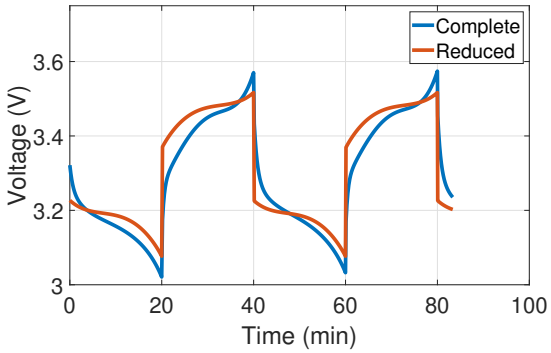

(b) Terminal voltage.

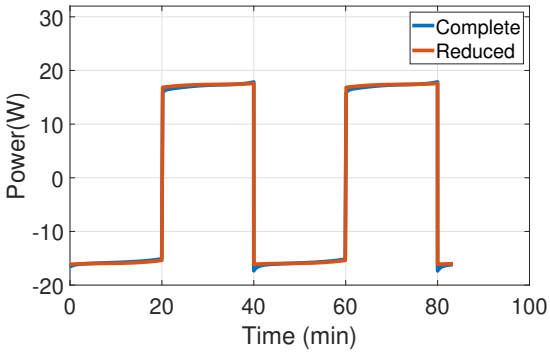

(c) Battery cell power.

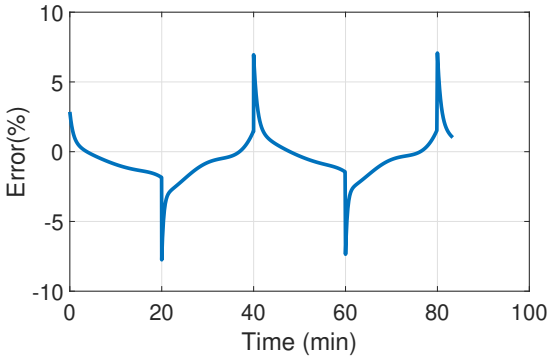

(d) Battery cell power error: $(P_{reduced} - P_{complete})/P_{complete} \times 100$.

Figure 50 – Battery cell model comparison.

battery power can be established as in

$$I = \frac{V_{oc}}{2r_{eq}} - \sqrt{\frac{V_{oc}^2 - 4r_{eq}P_{bat}}{4r_{eq}^2}}. \tag{91}$$

Such expression can be important for the EMS to determine the currents for each battery power and keep the current under pre-defined limits.

The Ragone power-efficiency plots are important for determining the battery efficiency given the power input or outputs. If the currents are too high, the battery dissipates a considerable amount of energy as heat, making the operation inefficient. Considering the methodology described in [81] and the internal resistance model, a second-order polynomial fit has been produced to model the Ragone power-efficiency relation, as below,

$$\eta_{bat} = 1 + \gamma_1 P_{bat}(t) + \gamma_2 P_{bat}^2(t). \tag{92}$$

5.3 STATIC OPTIMIZATION FOR GENSETS

To achieve fuel savings, we can define the operation of the generators based on optimization methods. For this, a cost function is assigned to the system, considering the total fuel

Table 8 – Parameters used for the battery reduced-order model.

Parameter	Symbol	Value	Unit
Approximate cell OCV (20%-80% SOC)	OCV	3.3	V
Internal resistance	r_{eq}	0.027	Ω
Coefficients for battery power-efficiency	γ_1	-4.19×10^{-5}	kW^{-1}
	γ_2	-1.99×10^{-5}	kW^{-2}

consumption for N generators, $\dot{m}_{f,opt}$,

$$\dot{m}_{f,opt}(t) = \sum_{i}^{N} w_i \dot{m}_{f,dgi}(t). \tag{93}$$

Index i represents each of the N generators, and their instantaneous fuel consumption rate are $\dot{m}_{f,dgi}(t)$. The genset fuel consumption is determined using the reduced-order model described in subsection 5.2.1. The variable w_i is a weight greater than or equal to zero, defined for each generator to allow customizing the cost function with rules, if necessary. Some constraints are imposed to the optimization formulation, such as the power balance equality,

$$\sum_{i}^{N} P_i = P_L. \tag{94}$$

In this constraint, the load assigned to the gensets P_L must be supplied, considering each of the power output of the individual generators, P_i. Moreover, the power operation envelope must be satisfied as well,

$$0 \leq P_i \leq P_{G,max}, \tag{95}$$

where $P_{G,max}$ is the genset loading limit used for the generators (assumed equal). The resulting optimization problem consists in finding the power assigned to each generator $\mathbf{u}^0$, minimizing the fuel consumption, and satisfying the mentioned constraints. That is,

$$\mathbf{u}^0(t) = \arg\min_{\mathbf{u}} \dot{m}_{f,opt}(P_i, P_L). \tag{96}$$

It is important to explain that there are two fundamental problem formulations for the optimization in a real operation: the economic dispatch and the unit commitment. The economic dispatch assumes that k generators are already connected to the grid, then the optimization consists in finding the best power allocation vector. The generators require some time to be connected and disconnected from the electrical network due to start and stop procedures and machine limitations. Therefore, it is essential to plan how many generators are required online, given the load demands, and considering the availability of the system. This latter problem refers to the short-term unit commitment optimization [32]. The fuel consumption optimization

proposed in this work, described in the equations above, does not consider the unit commitment problem, only the power split between the generators, assuming they can be used at anytime, without turning on/off delay.

5.4 RULE-BASED ENERGY MANAGEMENT STRATEGY

For the non-hybrid case, rule-based strategies can be simple. We can turn one generator up to some predefined power limit and then switch another on to supply the extra power required, for example, or share equal loads. For equally rated generators, sharing equal loads at high power demands can produce nearly minimum fuel consumption operation [32]. However, more complex rules can also be implemented, considering several operational constraints such as spinning reserve, power ramps, and efficiency ranges.

For hybrid cases, the complexity of the heuristic control increases, and the power split has to account for the battery, including its limitations and functional role. In works such as [11], the authors consider power-follower rule-based strategies, and the methods tend to perform considerably worse than optimization methods like ECMS, for example. However, the performance of such heuristic EMS methods can be increased if the optimization of generators is included, with the rules defining only the power share between the groups of generators and the battery.

In [11], the simulation time was relatively short; therefore, the SOC limits of the battery were not achieved. After performing different simulations, it was possible to observe that, for longer times, such rule-based strategies generate undesirable fast power dispatch oscillations (switching on and off generators and the battery system), depending on the power load, the SOC, and how long the vessel is operating under such power demand.

In this section, we will define a rule-based EMS for the hybrid power system, considering a combination of rule-based strategies that define the power split between the gensets and the battery and an optimization process for power dispatch of the generators. The set of rules are based on the work of [11], where a rule-based strategy was presented for two generators and a battery, as described in chapter 2. However, we implement a hysteresis approach over the rules to avoid the fast power dispatch oscillations and undesirable switching of power sources.

Figure 51 describes the implemented heuristic control considered for managing the power modes. The SOC of the battery and the load demand P_L are taken as inputs and, through

Power \ SOC	$SOC \leq SOC_{min}$	$SOC_{min} < SOC < SOC_{max}$	$SOC \geq SOC_{max}$
$P_L \leq P_{G,on}$	$P_{GT} = P_{opt}$ $P_{bat} = P_L - P_{GT}$ if($P_{bat} < P_{cmax}$) $P_{bat} = P_{cmax}$ $P_{GT} = P_L - P_{bat}$ end	hysteresis	$P_{GT} = 0$ $P_{bat} = P_L$ if($P_{bat} > P_{dmax}$) $P_{bat} = P_{dmax}$ $P_{GT} = P_L - P_{bat}$ end
$P_{G,on} < P_L \leq N \times P_{opt} \times f_p$	$P_{GT} = n_g \times P_{opt} \times f_p$ $P_{bat} = P_L - P_{GT}$ if($P_{bat} < P_{cmax}$) $P_{bat} = P_{cmax}$ $P_{GT} = P_L - P_{bat}$ end	hysteresis	$P_{bat} = 0$ $P_{GT} = P_L$ if($P_{dmax} \geq P_L - (n_g - 1) \times P_{opt} \times f_p$) $P_{bat} = P_L - (n_g - 1) \times P_{opt} \times f_p$ $P_{GT} = P_L - P_{bat}$ end
$P_L > N \times P_{opt} \times f_p$	$P_{GT} = N \times P_{opt}$ $P_{bat} = 0$	hysteresis	$P_{GT} = N \times P_{opt} \times f_p$ $P_{bat} = P_L - P_{GT}$ if($P_{bat} > P_{dmax}$) $P_{bat} = P_{dmax}$ $P_{GT} = P_L - P_{bat}$ $P_{GT} = \min(P_{GT}, N \times P_{opt})$ end

Figure 51 – Table with rule-Based strategy for an all-electric hybrid power system with N gensets and a battery.

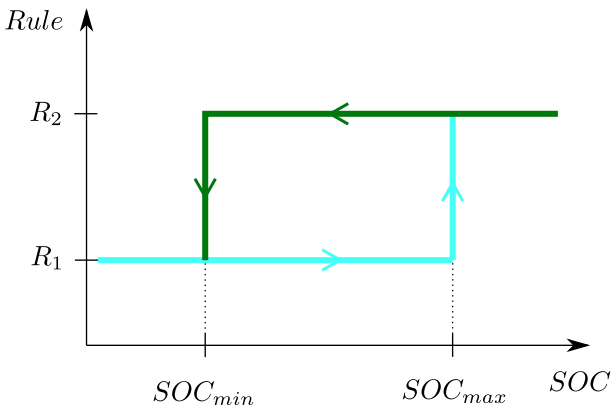

Figure 52 – Hysteresis approach over the rule-based strategy.

the decision table, the power references for the N generators and battery are determined. Then, the optimization occurs, according to section 5.3, to assign the power dispatch of each generator.

Between the SOC_{min} and SOC_{max}, in the second column of the table of rules in Fig. 51, we see the regions where the hysteresis occurs. The hysteresis approach adopted can be illustrated using Fig. 52. The rules R_1 are defined in the first column of the table of rules, while R_2 represents the rules in the third column. Thus, if the system starts with the battery fully charged (SOC_{max}), the set of rules R_2 is applied (green line). When SOC_{min} is achieved, the rules R_1 are used (blue line), and the system keeps operating in this loop. This helps to avoid switching fast and repeatedly between rules, which can lead to the mentioned power dispatch oscillations.

It is important to avoid the use of the generators in the less efficient regions, which are, in general, when the generators are working with low loads. The first line of Fig. 51 considers the

low load demands of the mission. For R_1, one generator is switched on with the optimal power $P_{GT} = P_{opt}$. The excess of power is used to charge the battery, given the maximum charging power of the battery P_{cmax}. If necessary, the generator power reference can be readjusted in a way that only the demand is supplied. For R_2, the battery will supply the power, limited to its maximum discharging power P_{dmax}, while the generator is kept off.

In the second line of Fig. 51, the load demand is above a lower limit to switch at least one generator on and below an upper bound. The value of f_p, which is between 0 and 1, can be used to customize the mentioned upper power bound. In the R_1 regime, the power set to the generators is optimal, given the power range and the least number of generators n_g required to balance the load. The excess power assigned to the generators is used to charge the battery. If necessary, the power of the gensets can be readjusted to supply the required power. When the battery reaches the maximum SOC, the operational condition switches to R_2. In R_2, we evaluate if the battery can be used to generate power, so the least number of generators are used near optimum operational points. If the required power from the battery is too much, the generators take all the load.

In the third line of Fig. 51, the generators take all the load or all power systems are used to supply the high power demands, depending on R_1 and R_2. If necessary, the function min is applied to keep the power set to the generators within nominal bounds. Like the other lines, the operation of the generators is optimized following the methodology described in section 5.3.

5.5 EQUIVALENT CONSUMPTION MINIMIZATION STRATEGY

The standard ECMS objective is to increase the overall energy efficiency, which is not different from the rule-based strategy presented in section 5.4. However, the process relies on equivalent consumption concepts and optimization techniques. The ECMS adds an equivalent fuel cost to the use of the battery, considering its average fuel consumption along the energy path between the storage system, the generators, and electrical consumers [3, 11, 26].

By charging or discharging, the battery allows generator load optimization. In the discharging mode, the battery delivers power, which allows the generators to be disconnected, avoiding their use at low loads. Regarding the charging mode, the generators running at low loads can increase their load and hence its efficiency, and the extra energy can be supplied to the battery, as mentioned in chapter 2. Besides, for energy storage systems, real-time decisions have future implications. If we use the battery effectively, charging the device means that energy

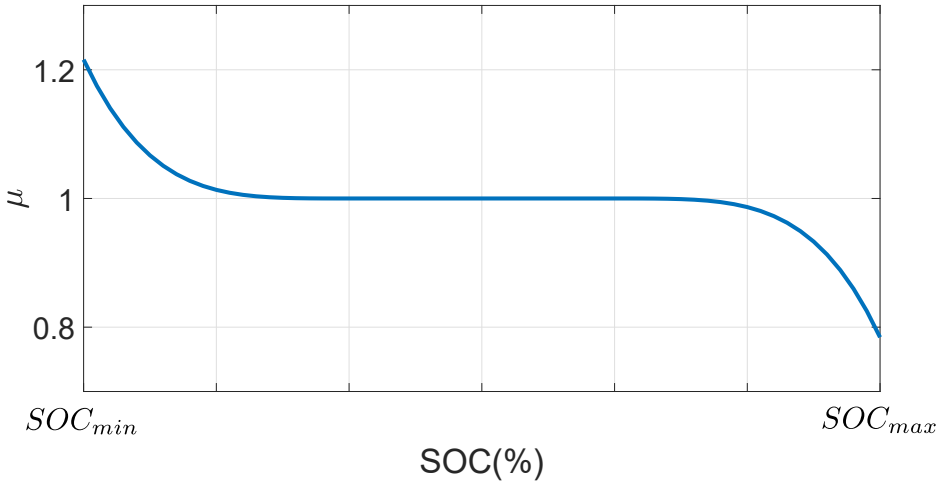

Figure 53 – Penalty function on the SOC.

can be saved for future use in situations where the power system would run inefficiently, and discharging the battery can ensure the storage device will be recharged at a more efficient state.

The causal ECMS strategy formulation considered for PSVs in this work follows the fuel consumption minimization methodologies applied for tugs in [3, 11]. We start by defining a cost function for the equivalent fuel consumption, as described in chapter 2,

$$\dot{m}_{f,eqv}(t) = \sum_{i=1}^{N} \dot{m}_{f,dgi} + \dot{m}_{bat,eqv}, \tag{97}$$

where $\sum_{i=1}^{N} \dot{m}_{f,dgi}$ is the combination of the fuel consumption rate of each genset i, of the total N generators. Equation 97 extends the formulation presented in section 5.3, with the genset fuel consumption being determined the same way, but with the addition of the equivalent fuel consumption of the battery $\dot{m}_{bat,eqv}$, following the approach in [3],

$$\dot{m}_{bat,eqv} = \frac{\mu s(t)}{\eta_{bat}(P_{bat}(t))^{sgn(P_{bat(t)})}} \frac{P_{bat}(t)}{Q_{lhv}}. \tag{98}$$

The equivalence factor, battery efficiency-power relation, Diesel low heat value, and battery power are $s(t)$, η_{bat}, Q_{lhv} and P_{bat}, respectively, with constant s or not. In Eq. (98), the artificial battery consumption is proportional to the equivalence factor, considering the Ragone power-efficiency relation from section 5.2.2, and whether the battery is charging or discharging, through the signal function sgn. The symbol μ represents a penalty function, illustrated in Fig. 53, used to keep the SOC within admissible limits. Near the SOC_{min}, the penalty function increases equivalent fuel consumption of the battery, favoring battery charging. The opposite occurs approaching the SOC_{max}.

The equations that describe the penalty function are below:

$$\mu(SOC) = \begin{cases} 1 + \left(\frac{SOC_a - SOC(t)}{\sigma}\right)^a & \text{for} \quad SOC(t) \leq SOC_a, \\ 1 & \text{for} \quad SOC_a \leq SOC(t) \leq SOC_b, \\ 1 - \left(\frac{SOC(t) - SOC_b}{\sigma}\right)^a & \text{for} \quad SOC(t) \geq SOC_b, \end{cases} \tag{99}$$

with

$$\sigma = \frac{SOC_{max} - SOC_{min}}{2} \tag{100}$$

and

$$SOC_{min} \leq SOC_a \leq SOC_b \leq SOC_{max}. \tag{101}$$

Here the symbol a is a power factor, while SOC_a and SOC_b represent, respectively, the lower and upper limits from which the power relations in Eq. (99) have an effect.

In [3], using the Pontryagin's Minimum Principle (PMP), the authors have demonstrated, for a tug with hybrid propulsion and power supply, that a constant equivalence factor leads to a nearly global optimum solution, regardless of the state of charge of the battery. Therefore, one of the approaches used in this work assumes a constant equivalence factor (named ECMS_const), determined to reflect the battery as a system that operates at the minimum specific fuel consumption (SFC) of the gensets, corrected by the efficiency along the path the energy takes from the battery to the propulsion system,

$$s = SFC_{min}\, \eta_{rec}\, \eta_{im+fc}\, Q_{lhv}. \tag{102}$$

Considering equally rated gensets, the SFC_{min} is the minimum SFC of the Diesel generators. According to [11], using the minimum SFC to determine the equivalence factor can help to ensure the operation of the engines around the optimal region. The term η_{rec} represents the battery power converter efficiency, and η_{im+fc} is an average induction machine and motor drive efficiency combination used for the propulsion system.

A proportional controller will be explored to add a charge sustaining capability to the ECMS strategy, or at least to help to keep the SOC within the predefined ranges without using the penalty function μ,

$$s_a = s + k_p(\text{SOC}_{ref} - SOC), \tag{103}$$

where s is the equivalence factor as defined in Eq. (102), k_p is the proportional gain, SOC_{ref} is the reference state of charge, SOC is the measured state of charge, and s_a is the adapted

equivalence factor. Such an adaptation of s is often called adaptative ECMS, or A-ECMS, as already mentioned in chapter 2. Another strategy considered in this work is the optimization of s within some pre-defined range (named ECMS_{opt}).

The resulting optimization problem can be expressed by

$$\mathbf{u}^0(t) = \arg\min_{\mathbf{u}} \dot{m}_{f,eqv}(\mathbf{u},\mathbf{w}), \tag{104}$$

with the cost function defined in Eq. (97). The vector $\mathbf{u}^0 = [P_1,\, P_2,\, \ldots,\, P_n,\, P_{bat}]^T$ represents the control inputs, which are also the power references set by the EMS in Fig. 46. The power load P_L, the state of charge SOC and the battery voltage are exogenous inputs that compose the vector $\mathbf{w} = [P_L,\, \mathrm{SOC},\, V_t]^T$.

For the EMS control, it is essential to consider the power source limitations. The gensets and batteries have to operate within the power limits. Also, it is not interesting to operate the storage system at SOC extremes or with too high absolute currents to reduce battery degradation. Such currents directly impact LFP battery temperature and capacity fading, as shown in Fig. 40.

In this work, the constraints used for the optimization problem are

$$\sum_{i=1}^{N} P_i + P_{bat} = P_L, \tag{105}$$

$$0 \leq P_i \leq P_{G,max}, \tag{106}$$

$$SOC_{min} \leq SOC \leq SOC_{max}, \tag{107}$$

$$I_{min} \leq I \leq I_{max}, \tag{108}$$

$$s_{min} \leq s \leq s_{max}. \tag{109}$$

They include the power balance equality, in Eq. (105), and the inequalities that keep the power of the gensets, the SOC, and the battery current of each cell within the predefined minimum (min) and maximum (max) limits, in Eq. (106), Eq. (107), and Eq. (108), respectively. When the equivalence factor is optimized, the inequalities also include the value of s, as in Eq (109). The battery pack power limits can vary with the state of charge, as can be seen in the expressions derived in [3]. With proper sizing and current limitation, the power will be kept within acceptable ranges.

The state of charge follows the dynamics in Eq. (69), which can be discretized, for optimization purposes as

$$\mathrm{SOC}(k) = \mathrm{SOC}(k-1) - \frac{I(k)\Delta t}{C_{bat}}, \tag{110}$$

where Δt represents the optimization time step, k represents the current step, and $k-1$ the previous one (measured by the sensor). The states of the battery cells are considered uniform for the pack, so SOC in Eq. (110) is determined using the cell current I, and the nominal cell capacity C_{bat}. The cell current can be calculated as

$$I(k) = \frac{1}{\eta_{rec}^{sgn(P_{bat}(k))}} \frac{P_{bat}(k)}{V_t(k-1)\ NS\ NP}, \tag{111}$$

considering measures of the terminal voltage V_t given by the complete model, the battery converter efficiency η_{rec}, the number of cells in series and in parallel NS and NP, as well as the battery pack power P_{bat}. In this work we will follow the mentioned approach to determine the current, unless stated otherwise. For offline optimizations, for example, it can be interesting to use Eq. (91) to calculate the current, adding the converter efficiency. The latter method can reduce computational costs.

5.6 OPTIMIZATION PROBLEM

Once the optimization problems are formulated, it is important to analyze how to solve them. In general, to achieve the best results, we look for global minima or maxima. In our case, we want to minimize fuel consumption. When the optimization problem is convex, the solution becomes easier because any local minimum is also the global one [82]. However, the problem is often non-convex, making this search more difficult.

We evaluate the objective function of the gensets optimization defined in Eq. (93) and the equivalent fuel consumption defined in the ECMS approach in Eq. (97). First, it can be noted that the mentioned objective functions are non-linear, and there are no integer variables. Therefore, the optimization problem can be classified as a non-linear programming (NLP) problem. Taking the Hessian of Eq. (93) with weights $w_i = 1$ (without loss of generality due to the problem formulation and because $w_i \geq 0$), we have the following matrix:

$$H = \begin{bmatrix} -1.02 \times 10^{-8} & 0 & 0 & 0 \\ 0 & -1.02 \times 10^{-8} & 0 & 0 \\ 0 & 0 & -1.02 \times 10^{-8} & 0 \\ 0 & 0 & 0 & -1.02 \times 10^{-8} \end{bmatrix}, \tag{112}$$

which is clearly negative definite for the entire domain of the objective function. According to [82], a function of n variables $f(x_1,x_2,...,x_n)$ defined on a convex set S is convex *if and only*

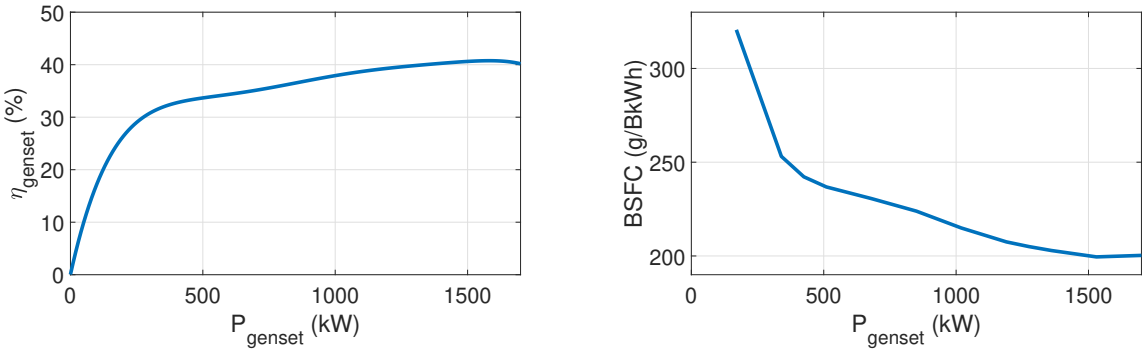

(a) Genset efficiency, η_{genset} as a function of the power load.

(b) Genset Brake Specific Fuel Consumption (BSFC) as a function of the power load.

Figure 54 – Efficiency and specific fuel consumption of genset based on the power load.

if the Hessian matrix of f is positive semidefinite or positive definite at all points in the set S. Consequently, the objective functions used for the genset optimization and for the ECMS approach are non-convex. The ECMS formulation consists of a sum of the genset and the equivalent battery fuel consumption, so its objective function is non-convex, according to the convexity preservation theorem in [3].

To solve the non-convex NLP, we will consider some methods used in similar applications, as mentioned in section 2.4.3. The interior-point method and sequential quadratic programming (SQP) will be evaluated to solve the optimization problem. For the first method, we use the algorithm IPOPT, and for SQP, we apply qpOASES.

5.6.1 Genset optimization: the interior-point method and Sequential Quadratic Programming (SQP)

The PX 105 has four equally rated generators with 1700 kW of power each. To understand how the engine load affects the generator efficiency and fuel consumption, we can look at the genset efficiency and the Brake Specific Fuel Consumption (BSFC), in Fig. 54(a) and Fig 54(b), respectively. The efficiency was determined through Eq. (53) and the BSFC curve was extracted from the engine performance data obtained through communication with the shipping industry. In these figures, we can see that the engine efficiency drastically decreases for power loads under 500 kW, which increases the fuel consumption per energy generated in the BSFC curve. The most efficient region, having the smallest BSFC, is between 1500 kW and 1700 kW. Therefore, it is important to keep the generator sets running at high loads, preferably in the most efficient regions, to minimize fuel consumption and maximize energy efficiency.

Applying the optimization formulation from section 5.3, the most frequent IPOPT solutions generated an equal load sharing among the generators at all loads. As mentioned before, according to [32], in high loads, equal load sharing can be nearly optimal. However, an inefficient operation is achieved by such power split at low loads, as it will be shown later.

To try to find better results for the IPOPT algorithm, we set the power of the fourth generator as

$$P_4 = P_L - \sum_{i}^{3} P_i, \tag{113}$$

using the power balance equality, in Eq. (94), to remove one optimization variable. The IPOPT method has shown sensitivity to this change of formulation and to the change of initial conditions. In our tests, the qpOASES algorithm has not shown considerable fuel consumption differences with different initial conditions, nor comparing the standard optimization formulation defined in section 5.3 with that in Eq. (113). Also, the qpOASES method was faster than IPOPT.

For the following simulations, we considered a power load demand increasing from zero to 6800 kW, which is the total genset combined capacity. Figures 55(a) and 55(b) show the best power dispatch achieved for the generators considering both algorithms, IPOPT and SQP. The IPOPT lets the genset (DG4) assume the entire load if the demand is below 1700 kW. Above this value, DG4 is loaded with the rated power, while the other gensets share equal loads. The SQP algorithm uses the same strategy for loads under 1700 kW. However, it always tries to run with the minimum number of generators, increasing the load of each genset until it reaches the rated power. When the nominal value is achieved, another generator is switched on to supply the extra required power.

According to the static optimization studies in [83], for lower power demands, the optimal solution to the fuel minimization problem for equally rated diesel generators is to run as many units at their maximum, while one unit takes the extra load. For some load demand points, the optimal solution is equal load sharing. In [32], the same results were mentioned for small loads. These solutions and the meaning of low load demands depend on the generators.

In Fig. 56 we compare the total instantaneous fuel consumption of the cost function for the power demands in Fig. 56(a), considering the interior-point method (IPOPT), sequential quadratic programming (SQP), and equal load sharing (Equal). For loads bellow 1700 kW, the IPOPT and SPQ have very similar performances, and for high loads, near the maximum genset combined capacity, the three cases show very similar results. However, for medium loads, the SQP approach outperforms the other methods, reducing the fuel consumed. In Fig. 56(b) the

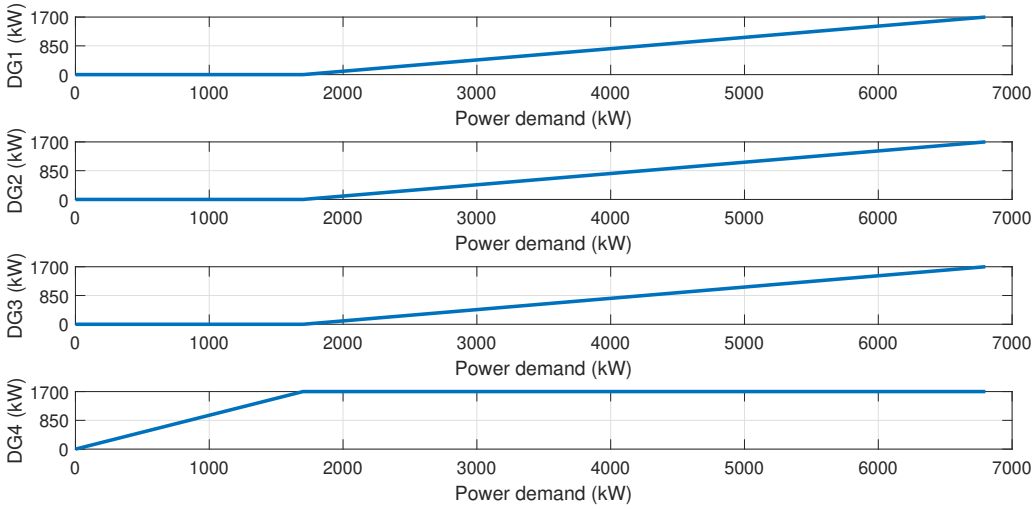

(a) Genset optimization using the interior-point method through IPOPT, with $w_i = 1$.

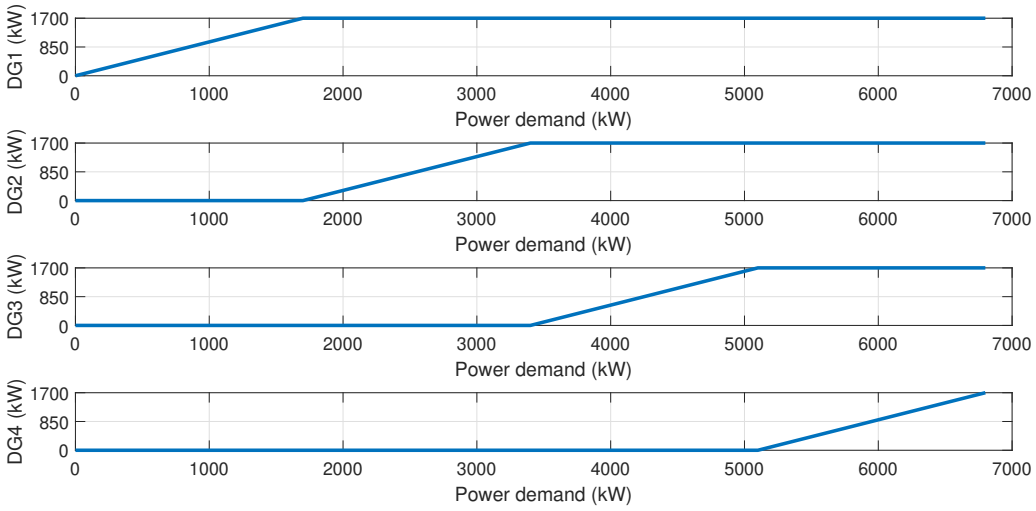

(b) Genset optimization using sequential quadratic programming (SQP) through qpOASES, with $w_i = 1$.

Figure 55 – Genset optimization: comparing algorithms IPOPT and qpOASES.

percentage errors show that the best results are obtained for the SQP algorithm, with less fuel consumption for all loads. Therefore, this method will be used as standard in the next analysis and in the fuel consumption optimizations for hybrid power systems.

5.6.2 Hybrid power system optimization using ECMS

For the optimization with the ECMS approach, we have applied the SQP algorithm qpOASES due to the better performance shown in the genset optimization problem. As mentioned before in section 2.4.3, the equivalence factor (s) is a critical control parameter for the ECMS.

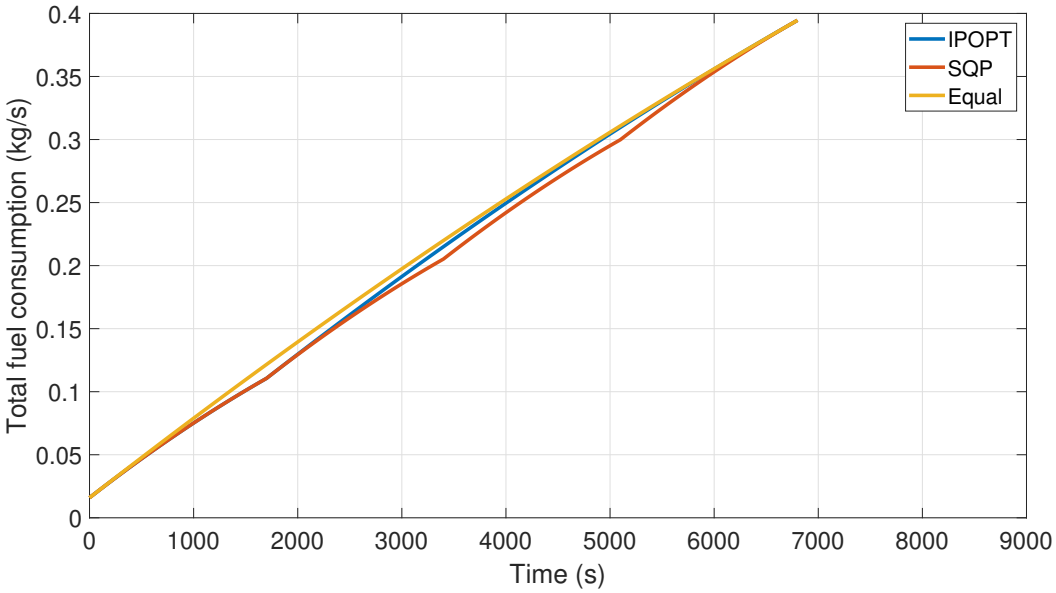

(a) Instantaneous fuel consumption calculated by cost function in Eq. (93), with $w_i = 1$, for different load sharing strategies.

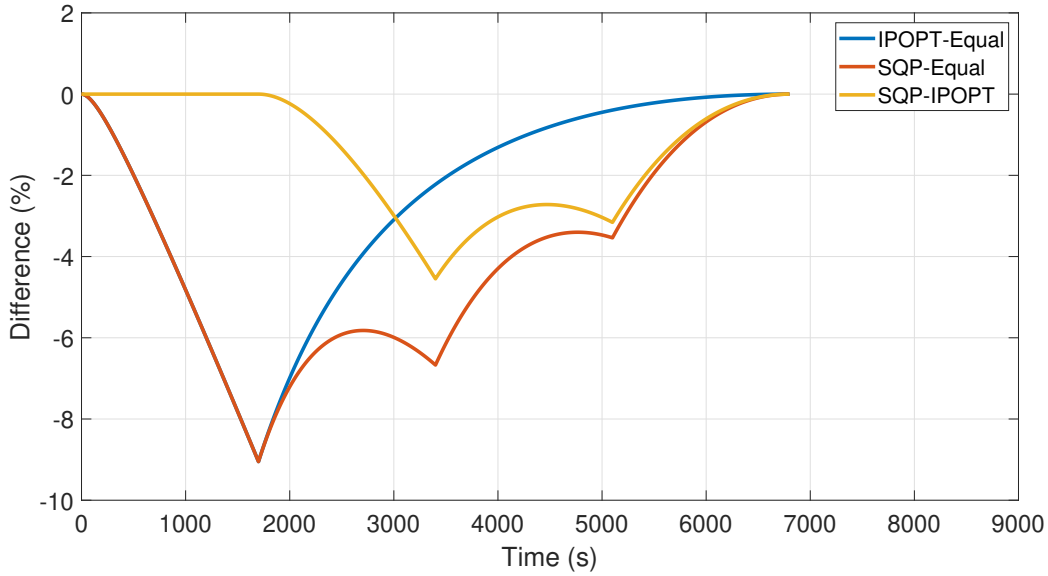

(b) Fuel consumption differences for different load sharing strategies: IPOPT-Equal $= \frac{IPOPT-Equal}{Equal} \times 100$**; SQP-Equal** $= \frac{SQP-Equal}{Equal} \times 100$**; SQP-IPOPT** $= \frac{SQP-IPOPT}{IPOPT} \times 100$**.**

Figure 56 – Genset optimization comparing IPOPT, SQP and equal load sharing.

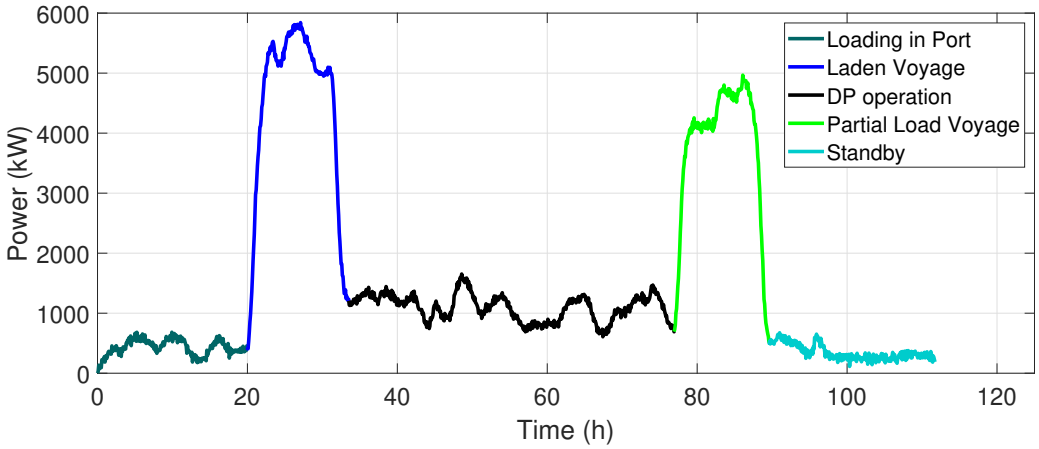

Figure 57 – Power demand profile used in the simulations.

Therefore, it is important to understand the effect of this parameter in the optimization solution to improve results. Due to the capacity of the battery to store energy for future use, just looking into the instantaneous fuel consumption for different power loads in a causal simulation, as in section 5.6.1, may not be the best way to analyze the optimization performance. We will evaluate how the equivalence factor affects the optimization performance considering the total fuel consumption of the power system on a standard mission based on the literature, and using data provided by the maritime industry from a vessel in operation.

The standard mission profile is illustrated in Fig. 57. To obtain this curve, we adapted the power demand in [20], normalizing the load demand based on the nominal installed power of the four equal gensets used by the authors (total of 7400 kW) and then multiplied by 94% of the nominal power installed of the four gensets studied in this work (total of 6800 kW). Next, white noise with a small amplitude was added to represent fast oscillations of the load demand.

The mission in Fig. 57 is divided into five parts, starting with the loading in port, where the ship is loaded with goods. In the laden voyage, the ship travels fully loaded heading to the platform. When it stops, given appropriate conditions, the ship starts the dynamical positioning (DP) operation, in which the forces acting on the vessel are counterbalanced by the thrusters to keep the ship at a defined position. After the DP, the ship travels back to the port with only part of the load, defining the partial load voyage. When the ship arrives near the port area, it must wait for a docking space to be available (standby).

Also, we considered a power profile with around 120 hours of operational data from the Ulstein PSV. As power demands can change considerably depending on vessel operation and environmental conditions, variations of the missions were produced to account for uncertainty. Besides two basic power profiles, the standard mission in Fig. 57 and a real mission, more

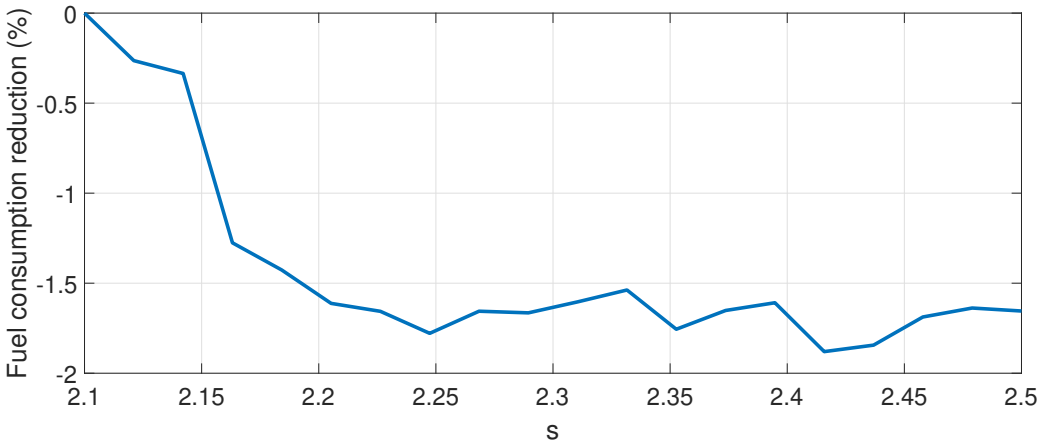

Figure 58 – ECMS performance dependence on the equivalence factor.

profiles were generated, varying the power demand of the missions by $\pm 10\%$ and $\pm 5\%$, totaling ten profiles.

For the simulations, we considered the power system configuration in Fig. 20, with the multilevel control strategy for hybrid power supply in Fig. 46. However, we considered only static models for the entire system, the EMS optimizer, in Fig. 47, the generators, and the battery system, to perform faster simulations. The battery parameters were the same used in the following sections, described in Tab. 11. To define the equivalence factor (s) range, we used Eq. (102), with a low heat value of 42.78 MJ/kg, the minimum specific fuel consumption from the curve in Fig. 54(b), a battery converter efficiency of 97 % and a combined efficiency of the electric motors and its drive system of 93 %. With this information, we found an s of 2.14. Then, results varying the value of s from 2.1 to 2.5, divided into 20 units, were produced.

The percentage results of fuel consumption reduction for different values of s compared to an s of 2.1 are presented in Fig.58. The comparison was made to put the reductions of the ten mission profiles in the same base. In general, there is a tendency of reducing fuel consumption when the value of the equivalence factor is increased, but with some peaks and valleys in the path. However, based on our simulations, it is important not to increase the value of s too much because that favors battery charging, and at a certain point it can increase the battery usage considerably or generate oscillations in the power dispatch. Due to the good performance, equivalence factor values around 2.25, 2.35 and 2.43 will be considered for further simulations.

6 SIMULATION EXPERIMENTS FOR A PLATFORM SUPPLY VESSEL

Now that we have the tools for modeling the complete propulsion system of the Ulstein PSV, developed in chapters 4 and 5, we will perform several simulation experiments, combining different models to represent the vessel's power system and hybrid solutions to evaluate several powertrain aspects. The analyses carried out are based on operational data (power profiles) from a Platform Supply Vessel provided by the maritime industry. Through case studies, we discuss energy efficiency, fuel consumption, emissions, genset running hours, battery capacity fading, and energy management strategies exploring the model set built in this work and different operational parameters for hybrid and non-hybrid configurations. Also, we provide a tool to help in the hybrid power system design and parameter choice.

6.1 STRATEGIC LOADING AND HYBRIDIZATION TO INCREASE VESSEL ENERGY EFFICIENCY USING REAL POWER DEMAND PROFILES AND STATIC MODELS

This section will describe some simulations performed with actual power demand profiles provided by the maritime industry. The objective of the simulations is to show how we could reduce the total fuel consumption, improving the vessel energy efficiency with strategic loading, i.e., optimizing the power dispatch, the amount of power that each power source component delivers to the powertrain, considering the original topology of the Ulstein PSV, and using the hybridization concept through the addition of Li-ion batteries. In addition, we will analyze the effects of changing different operational parameters and understand how these changes impact not only fuel consumption but also the number of genset running hours and pollutant emissions.

The data comprehends time series with the power load on each generator, which combined represent the total demand on the power system. The load demands were measured over five months, including around 2900 h of data with the vessel operating in conditions such as transit, Dynamic Positioning (DP), activities at the port, and standby. The DP condition accounts for around 20% of the total operation time. Figure 59 shows the complete power demand profile used for the simulations, with some information omitted due to a confidentiality agreement.

Due to the number of vessel's running hours and the low sampling rate (around 5 minutes), it is adequate to apply static models for such simulations due to the high computational

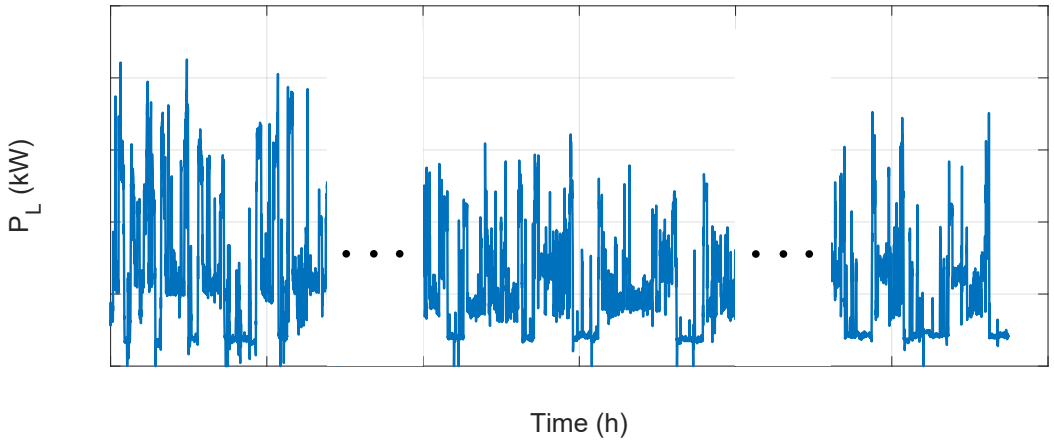

Figure 59 – Power demand data

cost of dynamic models and the inability to represent the transient behavior with the low-frequency inputs. Therefore, we applied the models defined in sections 5.2.1 and 5.2.2, with the power and energy management structure presented in Fig. 46 and Fig. 47, modeling the electrical power system, i.e., the power sources (generators and battery), electrical network, converter, and the EMS/PMS, of the Ulstein PSV topologies in Fig. 19 and Fig. 20. For the original topology (non-hybrid), we considered the dispatch optimization presented in section 5.3. For the hybrid configuration, we applied the ECMS with a constant equivalence factor ($ECMS_{const}$) described in section 5.5, due to a better performance shown in our tests. For the power system fuel consumption, we applied the static genset model from Eq. (59), and for the emissions, we considered the polynomial fits defined in Eq. (54), Eq. (56) and Eq. (58). The models and the optimizations ran on a time step of 5 minutes.

To represent real conditions, we considered some technical constraints in vessel operations. Spinning reserve is often necessary due to safety requirements and diesel engine generators' start/stop procedures, which take time to be executed. Generally, the generator loading is restricted to run below rated power under normal conditions. To consider the loading limits, we limited the generator power in Eq. (95) to a fraction of the nominal power. Also, it is essential to understand the Dynamic Positioning requirements for station keeping, to maintain position and heading under fault conditions because safety requirements on DP often have considerable impacts on fuel consumption and emissions.

6.1.1 Static optimization of gensets with constraints on genset loading limit and Dynamic Positioning (DP).

Before the hybridization, we will evaluate if it is possible to optimize the operation of the original system, topology described in Fig. 19. The base case (non-hybrid) used for comparison represents the measured data in the real vessel operation, with a genset loading limit of around 60%. Besides changing the genset load limit, we will consider the Dynamic Positioning (DP) restrictions to generate the results.

Different aspects can be used to measure the benefits of modifications in a vessel's power topology or operation. It is essential to analyze fuel consumption savings and CO_2 emissions to achieve a more cost-effective and cleaner operation. A more comprehensive emissions analysis also includes the quantification of other pollutant emissions under regulations, not only CO_2. The MARPOL Annex VI for vessel emission defines limits for NOx, SOx, particulate matter (PM), and other substances [7].

The Ulstein PSV is a vessel with DPS-2 notation. This notation requires the power system to be sized and arranged for Worst Case Failure of any bus section. The vessel must be designed to supply sufficient power to the thrusters to maintain position and heading within the operation envelope, supplying the service loads. In the case of a single fault in any active component or system, there must be enough power to maintain essential vessel functions, as defined in the IMO MSC/Circ. 645 [84]. However, it is worth noting that no specific operation is required, such as with closed or open bus-tie breakers (main bus tie-breaker). The IMO allows the vessel owner, client, and coastal authorities to assess which level of equipment redundancy achieves the reliability given the operation [85].

We performed simulations with the main bus-tie closed for the non-DP parts of the mission and considered two DP operation modes. In the first case (DPC), a closed bus-tie operation is assumed in DP, as shown in Fig. 60, with no redundancy as safety requirement. This means that the least number of generators must be online to supply the power demand. In case of a generator fault, for example, no power would be available for the essential systems until the connection of a generator. For the second case (DPO), which comprises the current DP operation mode of the PSV under analysis (the base case), we assumed an open bus tie operation in DP, illustrated in Fig. 61, with all gensets running at equal loads, which assures plenty of spinning reserve to guarantee redundancy and, therefore, high availability for the DPO case. However,

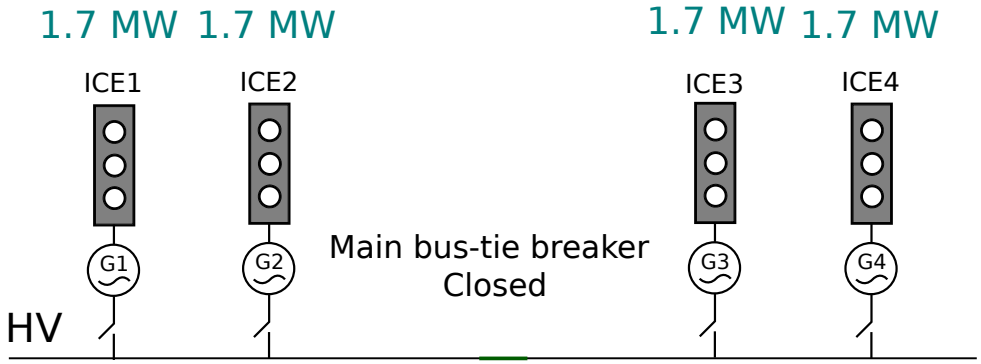

Figure 60 – Illustration of the power generation set with a closed main bus-tie breaker in DP (DPC)

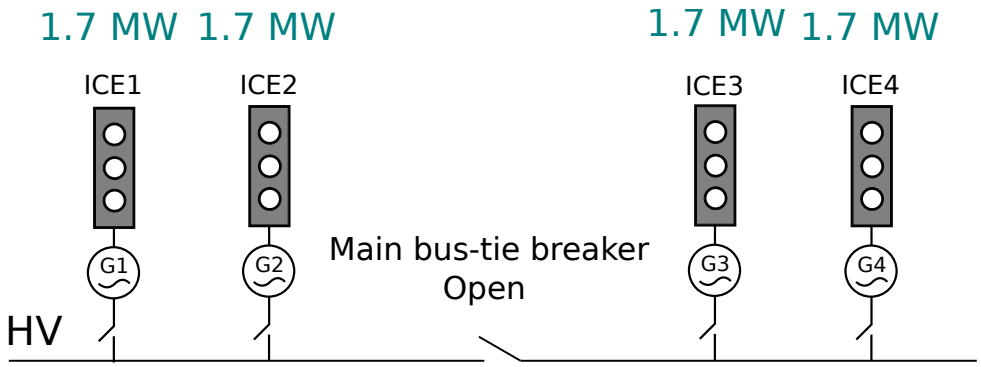

Figure 61 – Illustration of the power generation set with an open main bus-tie breaker in DP (DPO)

having a high impact on fuel consumption. Given the often required reliability and availability of power systems under DP operation, we consider the DPC more in the light of a benchmark condition and a measure of the impact of safety requirements on the vessel's performance, and not precisely as a viable solution.

With the simulations, we can analyze the effect of the genset optimization on fuel consumption, running hours, and pollutant emissions, looking at the percentage reduction or increase of quantities compared to the base case. The percentage quantities were calculated using the equation below

$$\text{Percentage quantity} = \frac{\text{(quantity (optimization) - quantity (base case))}}{\text{quantity (base case)}} \times 100. \tag{114}$$

The graphics from Fig. 62 to Fig. 67 follow the pattern: percentage quantity reduction on the Y-axis and genset loading limits on the X-axis, with two bars for each genset load, one in blue, representing the DPO case, and one in orange, for the DPC case. The mean value reductions for the five months of data are depicted over the bars, close to a symbol representing the standard deviation (when applicable). The mean values and standard deviations for the DPO and DPC cases are also arranged in tables 9, and 10, respectively.

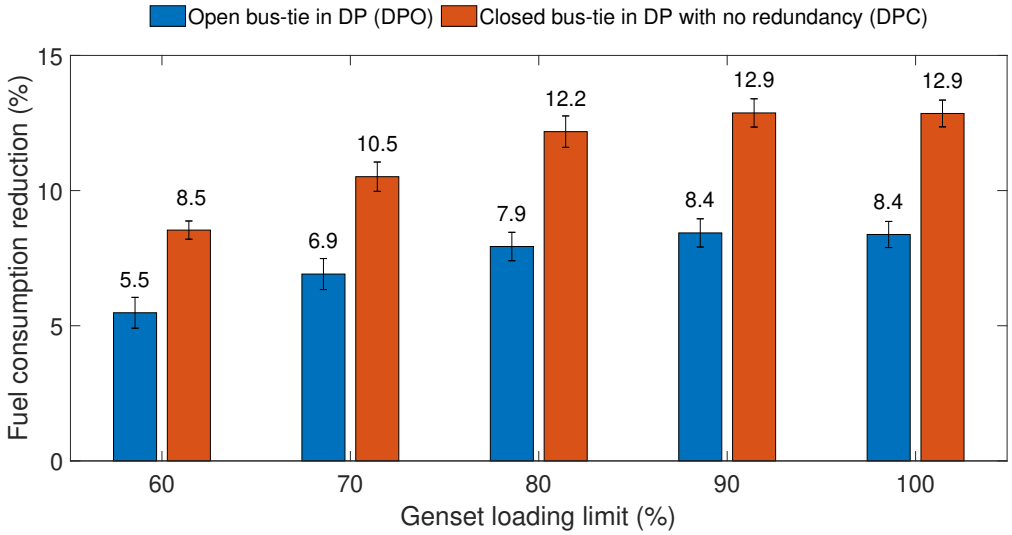

Figure 62 – Fuel consumption reductions for the base case (non-hybrid) with genset loading limits and DP constraints.

Figure 62 shows the fuel savings percentage considering the DPC and DPO cases with genset loading limits from 60% to 100%. Even at a genset loading limit of 60%, equal to the base case, there are fuel savings of 5.5% in the DPO case. The reductions increase proportionally to the loading limits reaching a plateau at 90%, with a decrease of 8.4%, which is reasonable since the minimum BSFC of the generator sets occurs at a 90% load, as shown in Fig. 54(b), and does not change much at 100% load. However, it needs to be mentioned that a more viable solution would consider genset loading limits in the range of 60%-80%, given the spinning reserve necessity and the start/stop generator procedures. In this scenario, the maximum and viable fuel savings would be close to 8% for the DPO case with the 80% limit.

The same consumption pattern happens with the DPC case; however, the reductions are 3.0%-4.5% larger than those in the DPO case (60%-100% load range), with maximum savings of 12.9% (90% load). The latter result illustrates how the genset redundancy significantly impacts the fuel consumption on DP. In a scenario where it is not possible to increase the genset loading limit from 60% due to safety requirements, the addition of a battery for backup power, being used solely in fault cases, could allow the gensets to run on higher loads. A change from 60% to 90% would lead to approximately 3% of additional fuel savings in the DPO case.

The CO_2 emission reductions, in Fig. 63, follow the fuel savings behavior, being proportional and almost equal to the fuel reductions in percentage, mainly in higher loads from 80% to 100%. The CO_2 emissions could be decreased from 6.6% to 8.3% for the DPO case in the genset power limit range from 60% to 80%; Then, in a more viable solution, with the genset

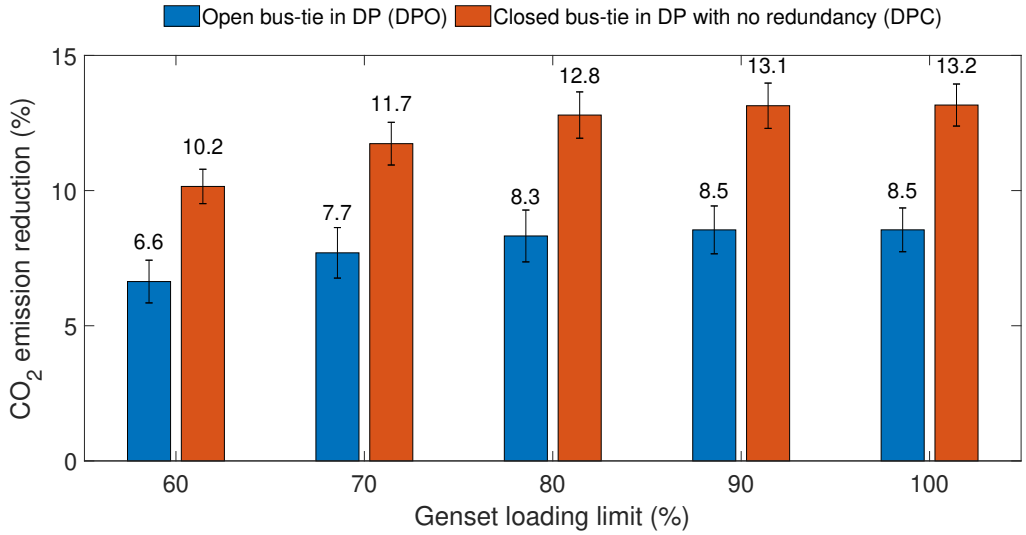

Figure 63 – CO_2 emission reductions for the base case (non-hybrid) with genset loading limits and DP constraints.

optimization and a genset loading limit of 80%, we could decrease the PSV CO_2 emissions in approximately 8%, against the maximum CO_2 decrease of 8.5% in 90% of genset load. The DPC results show that additional 3.6% to 4.6% (60% to 100% load range) reductions could be achieved, with a maximum of 13.1% (90% load), without the safety restrictions on DP.

The genset running hours were calculated as a sum of the operating hours of each generator. As mentioned in section 5.6.1, the optimization formulation for the gensets tends to switch on the least possible number of engines, which has a significant effect on the genset running hours, as shown in Fig. 64. The running hours decreased proportionally with the increase of loading limits, achieving the maximum reductions under 100% loads because, in this case, allowing the engines to run at higher loads reduced the necessity to switch on another genset. For the DPO case, the decrease in running hours went from 23% to 30% (60% to 80% load range), with a maximum of 33.6% (100% load). An additional reduction in the operating time of 14%-19% would be achievable considering the DPC case in the 60%-100% limits.

The PM reductions, in Fig. 65, were significant, going from 27.3% to 32.5% considering all the genset loading limits for the DPO case, with the maximum value of 32.5% at 80% and 90% loads. After reaching a maximum value, the reductions decrease at the 100% load limit. The same reduction behavior can be noted for the DPC case; but with a 16% to 20% additional decrement and a maximum PM decrease of 52.4% at a 90% load. Considering the standard deviation in the DPC, there is no significant difference between the means at loads of 80% and 90%. The same happens in the DPO case.

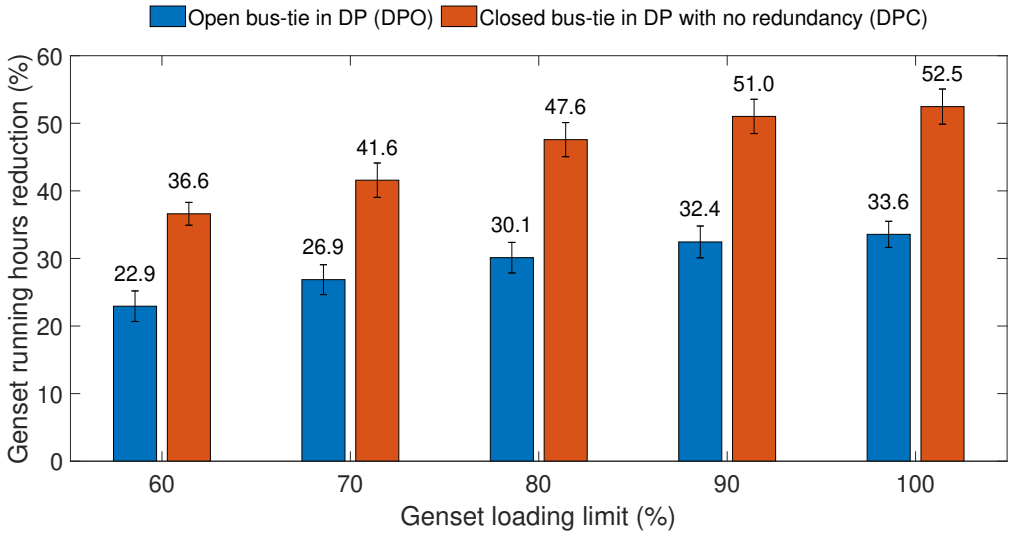

Figure 64 – Genset running hours reductions for the base case (non-hybrid) with genset loading limits and DP constraints.

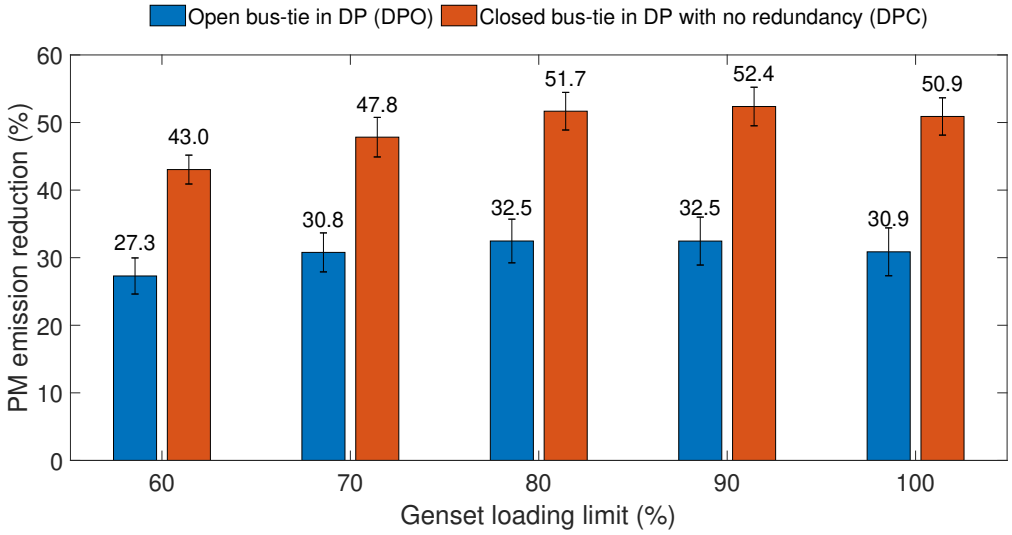

Figure 65 – PM emission reductions for the base case (non-hybrid) with genset loading limits and DP constraints.

The NO_x emissions were separated into the first month(month 1), Fig. 66, and the rest(months 2-5), Fig. 67, given significant differences. The general behavior of the NO_x is similar for both charts. The major reductions occur at lower loads such as 60% and 70% and the reductions tend to decrease until the emissions increase. Here, we did not consider the after-treatment modeling. An exhaust gas recirculation (EGR) or a selective catalytic reduction (SCR) system, for example, could be used to deal with the NO_x emission increase. However, it must be noted that the after-treatment system can have an impact on the engine operation, and involve implementation and operational costs with consumables [86].

The maximum reductions for DPO and DPC happened at 60% loads for month 1, Fig. 66, with 3% and 11% means, respectively. At the 80% load limit, where the highest viable reductions in fuel consumption, genset running hours, CO_2 and PM emissions occur, the NO_x increases approximately 10% for the DPO case, and around 2% for the DPC, reaching the maximum values of 16% and 9% for the DPO and DPC cases (100% load), respectively. The NO_x emissions could be around 7% to 8% smaller, with the DPC operation instead of DPO, if redundancy were not necessary.

For months 2-5, the results are depicted in Fig. 67. The mean NO_x reductions were positive from 60% to 80% of load for DPO and DPC. Although the means at 80% load are 0.8% and 5.4%, for the DPO and DPC, respectively, the DPO reductions could be negative due to the standard deviation, representing a slight increase. The maximum decreases were observed for a 60% loading limit, with 10% for the DPO case and 17% for the DPC case, reaching a maximum increase of 4% for DPO and around zero for DPC (100% load). The DPC case would allow 4% to 7% of extra reductions.

The results in this section show that reductions in fuel consumption, genset running hours, and emissions of CO_2, PM, and NO_x can be achieved through strategic loading in comparison with the base case even keeping the current genset load limit of 60%. In general, increasing the genset loading limits brought benefits with maximum reductions for different loads, with some exceptions to NO_x emissions. With strategic loading, for the DPO case, increasing the generator load limit from 60% to 80% lead to a 2.5% fuel-saving, for example. Significant differences were observed in the DPO and DPC cases, with the DPC case being more beneficial in the quantities under analysis, highlighting the impacts of dealing with the safety operation requirements with genset redundancy.

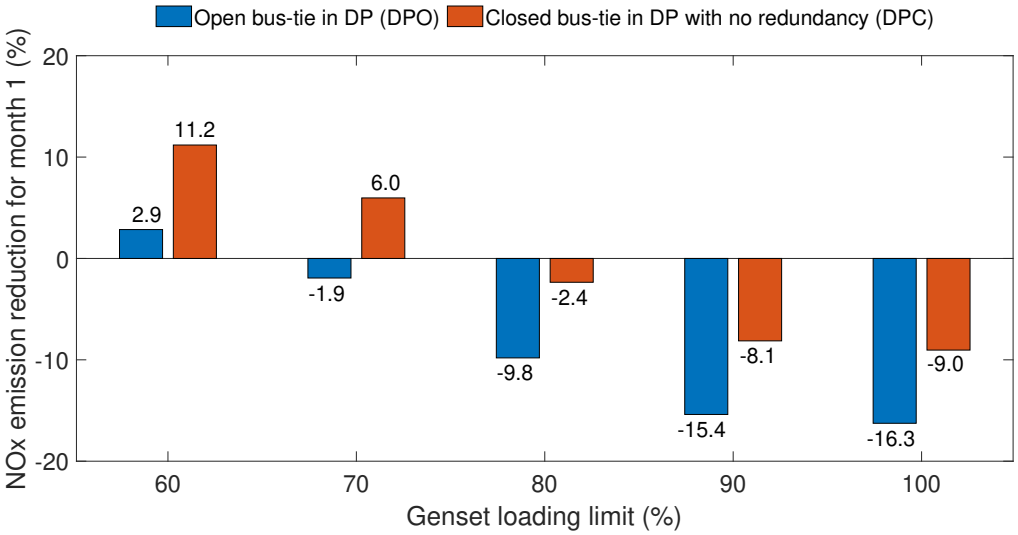

Figure 66 – NO_x emission reductions for the base case (non-hybrid) with genset loading limits and DP constraints for month 1.

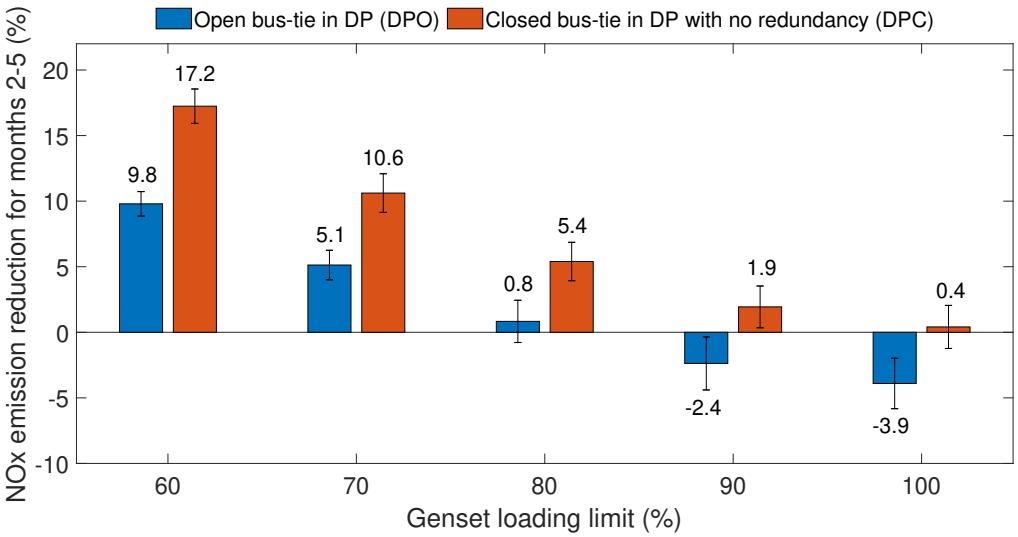

Figure 67 – NO_x emission reductions for the base case (non-hybrid) with genset loading limits and DP constraints for months 2-5.

Table 9 – Compilation of percentage reductions comparing the optimized (non-hybrid DPO) and original operation with mean and standard deviation

Reductions non-hybrid case DPO (%)					
Quantity	Genset loading (%)				
	60	70	80	90	100
Fuel consumption	5.48 ± 0.57	6.91 ± 0.57	7.93 ± 0.53	8.43 ± 0.52	8.38 ± 0.48
Genset running hours	22.93 ± 2.26	26.86 ± 2.21	30.12 ± 2.26	32.44 ± 2.36	33.57 ± 1.93
CO_2 emission	6.63 ± 0.79	7.7 ± 0.93	8.32 ± 0.96	8.55 ± 0.89	8.55 ± 0.81
PM emission	27.29 ± 2.67	30.78 ± 2.89	32.47 ± 3.23	32.46 ± 3.55	30.87 ± 3.54
NO_x emission month 1	2.85	-1.93	-9.81	-15.39	-16.26
NO_x emission months 2-5	9.79 ± 0.93	5.13 ± 1.12	0.83 ± 1.61	-2.37 ± 2.02	-3.90 ± 1.93

Table 10 – Compilation of percentage reductions comparing the optimized (non-hybrid DPC) and original operation with mean and standard deviation

Reductions non-hybrid case DPC (%)					
Quantity	Genset loading (%)				
	60	70	80	90	100
Fuel consumption	8.54 ± 0.34	10.51 ± 0.54	12.18 ± 0.58	12.87 ± 0.52	12.85 ± 0.5
Genset running hours	36.61 ± 1.69	41.58 ± 2.54	47.58 ± 2.52	51.02 ± 2.54	52.47 ± 2.6
CO_2 emission	10.15 ± 0.64	11.74 ± 0.79	12.79 ± 0.86	13.14 ± 0.84	13.16 ± 0.78
PM emission	43.04 ± 2.14	47.83 ± 2.93	51.68 ± 2.78	52.37 ± 2.85	50.9 ± 2.76
NO_x emission month 1	11.19	5.97	-2.35	-8.13	-9.04
NO_x emission months 2-5	17.24 ± 1.31	10.62 ± 1.47	5.4 ± 1.46	1.94 ± 1.59	0.41 ± 1.64

The highest viable fuel savings, reductions in generator operating time, emissions of CO_2 and PM occur at higher load limits such as 80%; however, at this setting, the NO_x emissions increase for the DPO. We can indicate two main competing effects influencing the NO_x yield: running the gensets at higher and more efficient loads, in general, requires the engines to operate at higher temperatures emitting more NO_x [72]; the strategic loading procedure reduces the number of gensets running unnecessarily, which reduce the NO_x emissions. An after-treatment system could be used to approach the NO_x emission increase. For a more comprehensive optimization, it would be necessary to consider the after-treatment model and establish an energy efficiency and NO_x emission increase trade-off.

6.1.2 Static optimization of a hybrid power system with constraints on genset loading limit and Dynamic Positioning (DP)

In the last section, we showed how to optimize the operation of the original system through optimal scheduling of the Diesel generators. This section will evaluate the impacts of the power system hybridization by adding a Li-ion battery (ESS) and performing power dispatch optimization, varying the genset loading limits and considering DP restrictions. The battery will have two main functions: strategic loading and spinning reserve.

Table 11 – Parameters used for the hybrid power system simulation considering static models.

Parameter	Symbol	Value	Unit
Max discharging power	P_{dmax}	1700	kW
Max charging power	P_{cmax}	-1700	kW
Min state of charge	SOC_{min}	20%	-
Max state of charge	SOC_{max}	80%	-
Battery DOD	DOD	60%	-
Number of cells in parallel	NP	703	-
Number of cells in series	NS	333	-
Battery converter efficiency	η_{rec}	97%	-
Equivalence factor	s	2.2	-
Min cell current	I_{min}	-2.2 (1C)	A
Max cell current	I_{max}	2.2 (1C)	A
Capacity of each cell	C_{bat}	1.129	Ah
Battery rated energy	E	870	kWh
Battery rated power	P	1700	kW
Time step	Δt	5	minutes

In non-DP parts of the missions, the battery will allow the gensets to run at the most fuel-efficient operating ranges, enabling a more strategic loading of the generators. The battery response time is short, providing almost instantaneous power. Therefore, it can be used as a spinning reserve without fuel consumption, which is impossible for generators. In the DP operations, we consider the open bus-tie operation already being used in the original system (base case), represented as DPO in the last section, and we turn off two generators. So the power system will run with two generators sharing equal loads, one on each side of the main bus tie and a battery system that can supply power on each side of the main bus tie, as shown in Fig. 68, keeping safety and improving energy efficiency.

The parameters used for the simulations can be found in Tab. 11. The battery sizing considered the power profile, cell efficiency, and safety requirements. The rated current was considered low to allow higher cell efficiency. The battery rated power is equivalent to one generator and the rated energy was calculated so the battery can supply power for enough time to connect other gensets to the grid in case of a power system single fault.

The same quantities analyzed on section 6.1.1 will be evaluated in this section, calculating the percentages using Eq. (114), but the information will be presented in a format that indicates additional benefits of the ESS and the strategic loading. The hybrid power system results are compared with the base case (the original operation) and the genset optimization results with the DPO case.

The graphics from Fig. 69 to Fig. 72 follow the pattern: percentage quantity reduction on the Y-axis and genset loading limits on the X-axis, with two stacked bars, a blue bar representing

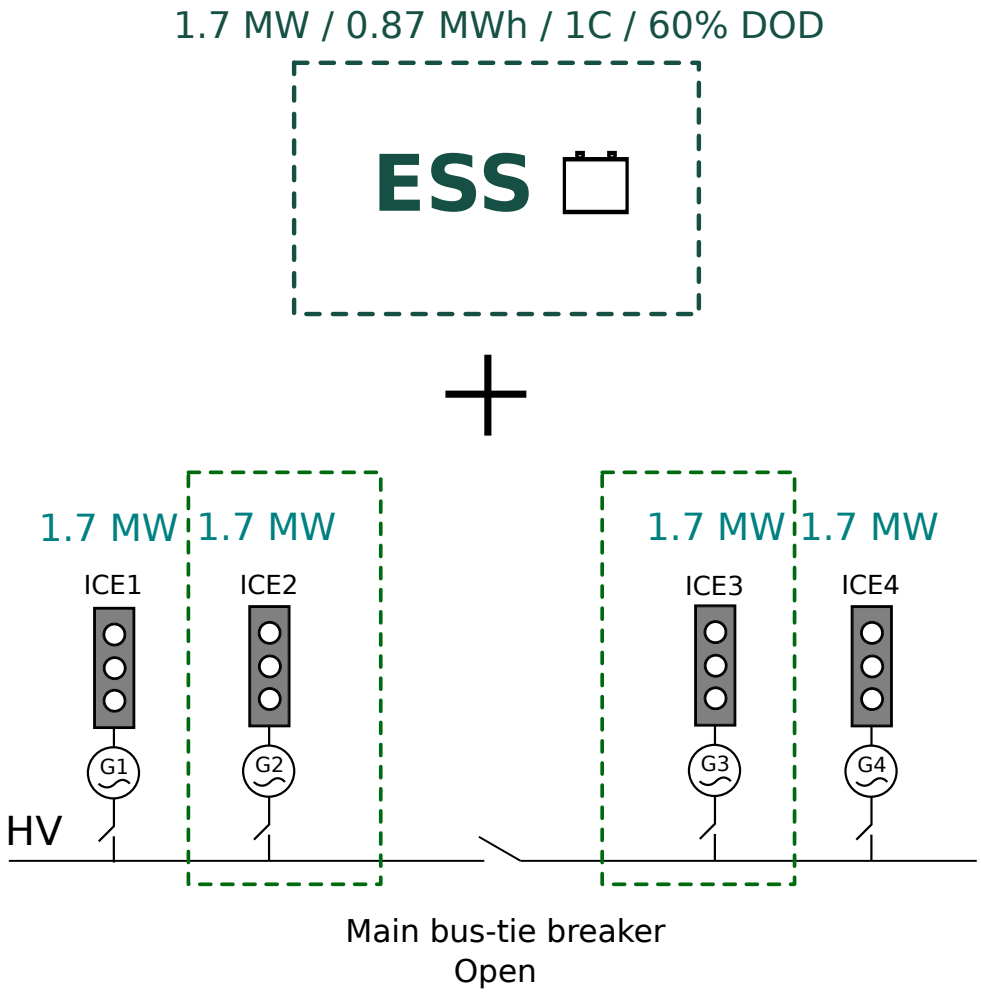

Figure 68 – Illustration of the power generation set with an open main bus-tie breaker representing the DPO case.

the reduction achieved with the optimization for the DPO case (from section 6.1.1), and an orange bar showing the additional reductions with optimization and an ESS for the hybrid topology. Figures 73 and 74 were plotted using grouped bars instead of stacked because the signal changes can make stacked bars confusing. The mean values are over the top of the bars and inside bars on the charts. The absolute reductions for the hybrid power system are illustrated over the bars in the charts. All the mean reduction values and standard deviations for the hybrid topology are arranged in Tab. 12.

Figure 69 shows the fuel savings percentage for the non-hybrid and hybrid cases with optimization and genset loading limits from 60% to 100%. Even at a genset loading limit of 60%, equal to the base case, there are fuel savings of 10% for the hybrid topology, representing additional savings of 4.7%. The reduction behavior follows a similar pattern recognized in section 6.1.1, increasing with the load, with a maximum value at the 90% limit, but decreasing for a 100% load. Keeping more viable solutions in mind, we can consider the 60%-80% load

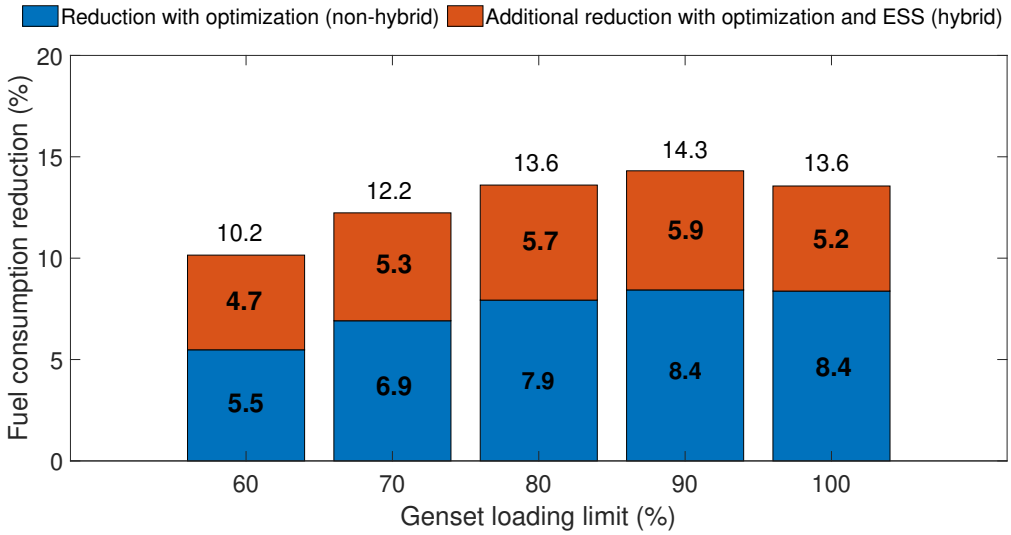

Figure 69 – Fuel consumption reductions for the hybrid case with genset loading limits and DP constraints, including the additional reductions provided by the battery (ESS) and system optimization compared to the genset optimization in the non-hybrid configuration.

limit range or even stretch it to 60%-90%, having in mind that with the battery onboard more spinning reserve would be available for the vessel even at non-DP operations. Then, the hybrid system could enable 14% fuel reductions, which represents additional savings of around 6% compared to the non-hybrid case.

For the hybrid configuration, in Fig. 70 the CO_2 emission reductions follow the fuel savings pattern, mainly in higher loads from 80% to 100%, as previously noted in section 6.1.1. The CO_2 emissions could be decreased from 12% to 14% using the battery system, with an additional decrease of around 5% in comparison with the non-hybrid case.

The performance of the power system is substantially affected by the new operational modes enabled by the ESS. The battery is used to perform the strategic loading in the non-DP parts of the missions, avoiding unnecessary genset connections. In DP operations, having the battery system ready to maintain essential services allows the operation with two generators instead of four simultaneously. In Fig. 71, we can see the genset running hours reductions. In the load limit of 60%-100%, the operating time is reduced from 46% to 62%, decreasing proportionally with the load limits. As in section 6.1.1, the higher the limit, the higher the reductions in genset running hours. In a limit of 90%, the reductions achieve 60%, with an additional decrease of 27.4% for the hybrid system. In general, the battery almost doubled the reductions in generator operating time for all loading limits.

The particulate matter (PM) reductions, in Fig. 72 were significant, going from 53.4% to 59.5% considering all the genset loading limits for the hybrid case, with the maximum at the

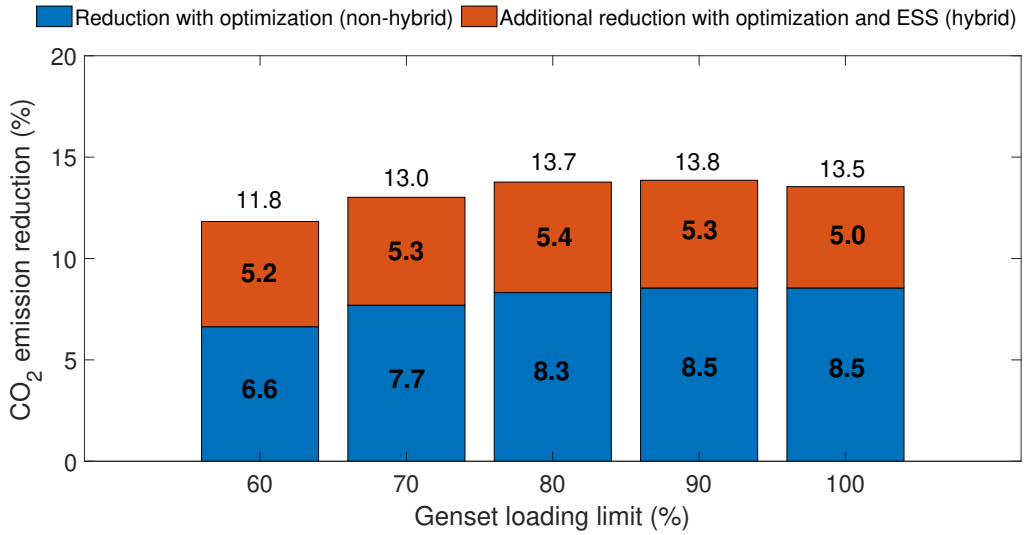

Figure 70 – CO_2 emission reductions for the hybrid case with genset loading limits and DP constraints, including the additional reductions provided by the battery (ESS) and system optimization compared to the genset optimization in the non-hybrid configuration.

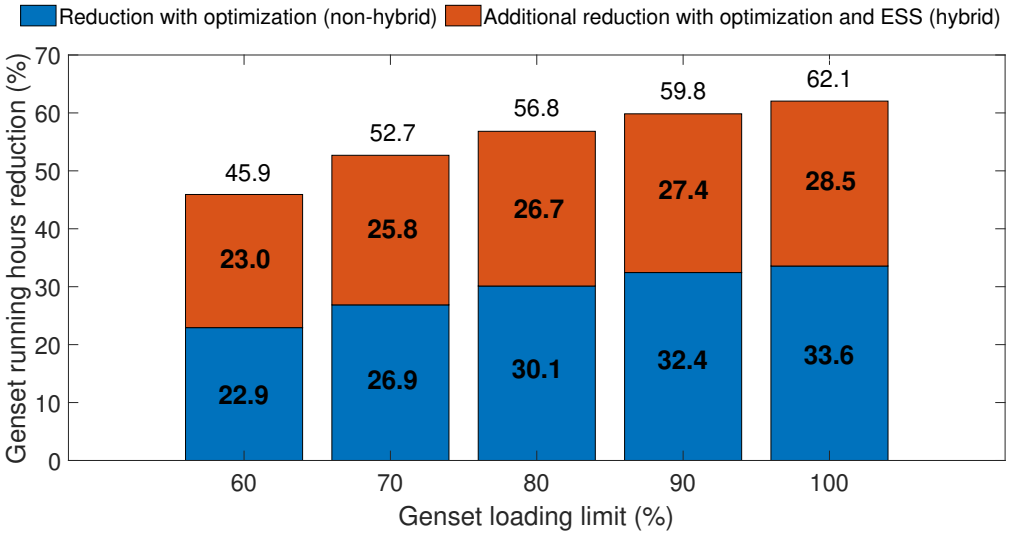

Figure 71 – Genset running hours reductions for the hybrid case with genset loading limits and DP constraints, including the additional reductions provided by the battery (ESS) and system optimization compared to the genset optimization in the non-hybrid configuration.

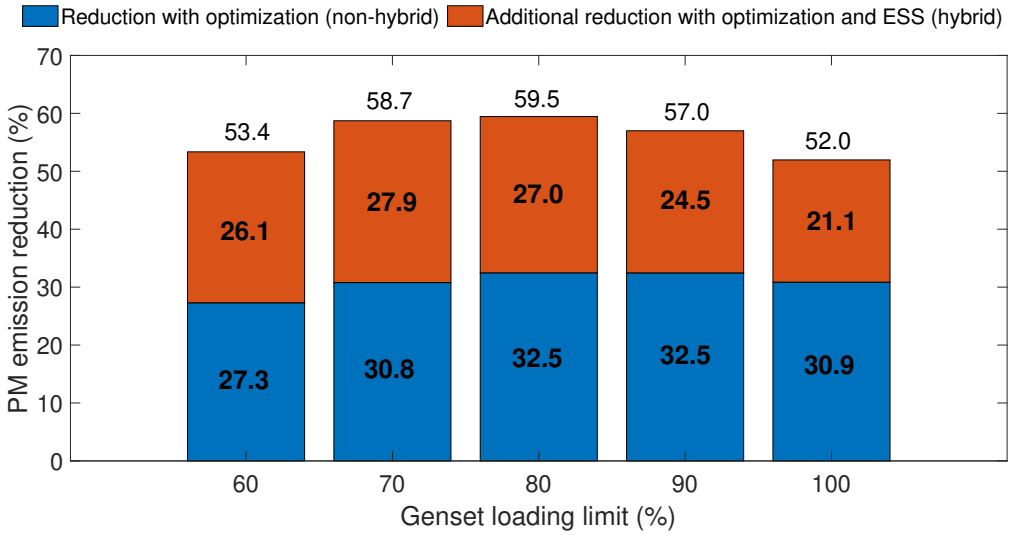

Figure 72 – PM emission reductions for the hybrid case with genset loading limits and DP constraints, including the additional reductions provided by the battery (ESS) and system optimization compared to the genset optimization in the non-hybrid configuration.

80% limit. The reductions increase with the load, reaching the maximum at the load of 80% and then decrease for higher loads. The battery system enabled additional reductions that went from approximately 21% to 28%, with a peak at the 70% limit, closely followed by the reduction at 80%. Also, the battery enabled an operational mode that almost doubled reductions in PM emissions compared to the DPO case.

In sequence, we have the NO_x emissions divided into the first month(month 1), Fig. 73, and the rest (months 2-5), Fig. 74, given the significant differences. The general behavior of the NO_x emissions is similar, considering the hybrid and non-hybrid cases in both charts. At lower loads, mainly at 60%, the NO_x emissions can be reduced. However, at loads such as 80% to 90%, where the vessel operation would be more energy-efficient, the NO_x emissions tend to increase. At loads of 60% and 70%, the hybrid system performed better than the original configuration, achieving emission reductions of 6.1%-14.4% for month 1 and 9.6% to 20.7% for months 2-5. The additional reductions enabled by the battery use are considerable for the 60% to 70%, almost doubling the reductions for months 2-5, and bringing decrements of NO_x emissions from 8% to 11% for month 1. From the 80% limit on, the NO_x generally increases for both cases, hybrid and non-hybrid, with battery performing worst, except on the punctual 80% load condition for month 1. For the hybrid, the NO_x can achieve up to 16%, considering month 1 and months 2-5, at a viable operating load of 90%. As in section 6.1.1, the after-treatment system was not included in the modeling.

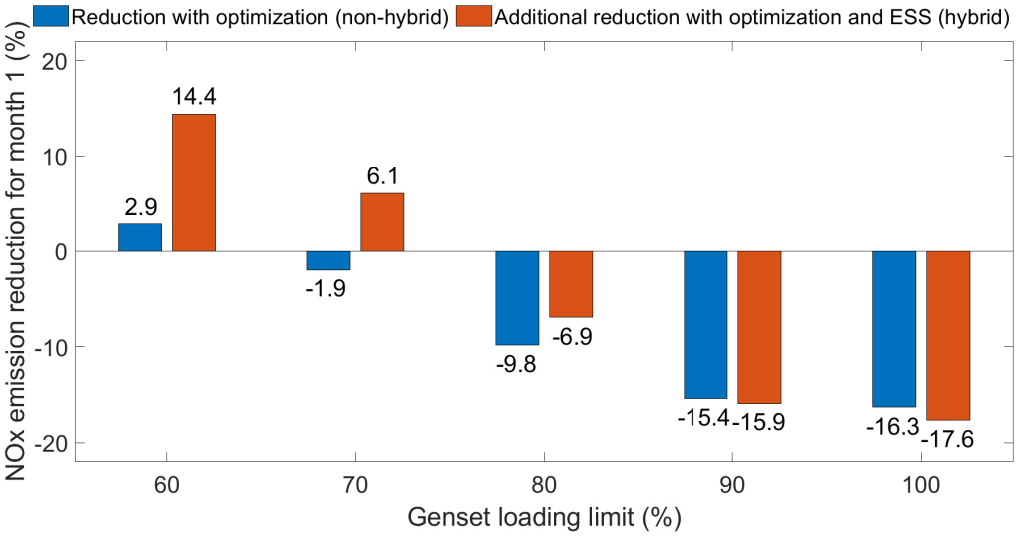

Figure 73 – NO_x emission reductions considering the hybrid case with genset loading limits and DP constraints for month 1, including the additional reductions provided by the battery (ESS) and system optimization compared to the genset optimization in the non-hybrid configuration.

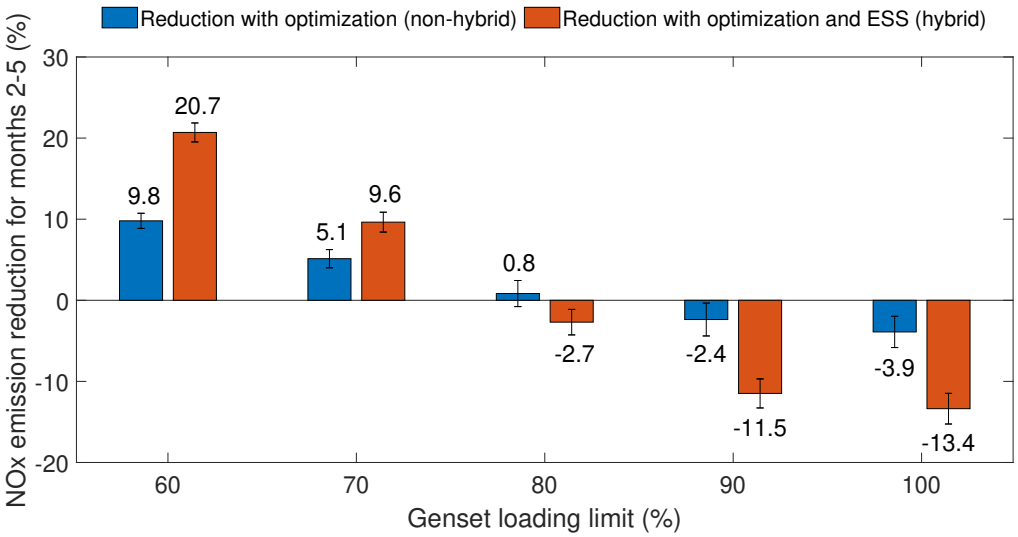

Figure 74 – NO_x emission reductions considering the hybrid case with genset loading limits and DP constraints for months 2-5, including the additional reductions provided by the battery (ESS) and system optimization compared to the genset optimization in the non-hybrid configuration.

The results in this section show that, in general, additional reductions in fuel consumption, genset running hours, and emissions of CO_2, PM and NO_x can be achieved through strategic loading with the use of a battery system, in comparison with both the original and the optimized operations with non-hybrid configurations in different genset loading limits. As in the non-hybrid system results, in the last section, increasing the genset loads enabled benefits for the hybrid case, with the best results near 80% and 90% loads, which are reasonable limits for the hybrid power system operation. The NO_x emissions had the best results for loads near 60% to 70%. In the most energy-efficient regions, the NO_x emissions have increased for the hybrid powertrain. The power system could operate more efficiently and cleaner with an after-treatment system and the right parameter trade-off.

In the 90% genset loading limit, fuel savings of 14.3% and 5.9% were achieved in comparison with the original and optimized power dispatch strategies, respectively. The CO_2 was reduced in 13.8% and 5.3% compared to the original and optimized operations. The fuel consumption and CO_2 emission reductions vary in the literature for hybrid power systems using batteries. A recent technical report from the European Maritime Safety Agency mentions the fuel savings potential for OSVs (which includes PSVs) is expected to be between 5-20% [16]. In the work of [20], the authors have reported a 7.4% reduction in CO_2 emissions, considering the addition of a 1000 kW/1000 kWh battery to a PSV power system, which comprised initially four gensets with 1850 kW each unit. Based on the mentioned literature, the results obtained in this work are within an acceptable range of what has been expected for fuel savings and CO_2 emission reductions for a PSV.

For the hybrid power system, the NO_x emissions varied depeding on the genset loading limit and month of analysis, being reduced in almost 21% (60% load) and increased in 16% (90% load). In [13], which compared a hybrid and a non-hybrid plant, NOx reductions up to 85% were observed for the hybrid plant. Of course, this depends on the case, not only on the hybrid system's performance but also on the original topology and control. In [6], the authors suggest, considering their studies for tugs and literature results for engines, that a trade-off between fuel consumption minimization and NOx emissions have to be established to reduce both fuel and NOx emissions. In their work, the fuel consumption minimization using ECMS also leads to an increase of NOx emissions considering higher loads.

The particulate matter and genset running hours dropped considerably for the hybrid power system, almost doubling the reductions compared to the non-hybrid system with dispatch

Table 12 – Compilation of percentage reductions comparing the hybrid case with strategic loading and original operation with mean and standard deviation

Reductions hybrid case (%)					
Quantity	Genset loading (%)				
	60	70	80	90	100
Fuel consumption	10.15 ± 0.36	12.23 ± 0.48	13.61 ± 0.55	14.31 ± 0.51	13.56 ± 0.47
Genset running hours	45.92 ± 1.2	52.69 ± 1.34	56.83 ± 1.49	59.84 ± 1.42	62.04 ± 1.35
CO_2 emission	11.82 ± 0.84	13.02 ± 0.98	13.77 ± 1.03	13.86 ± 0.97	13.54 ± 0.97
PM emission	53.35 ± 1.54	58.72 ± 1.84	59.45 ± 2.06	56.99 ± 2.19	51.96 ± 2.35
NO_x emission month1	14.39	6.06	-6.87	-15.94	-17.63
NO_x emission months 2-5	20.7 ± 1.17	9.64 ± 1.22	-2.7 ± 1.57	-11.48 ± 1.79	-13.37 ± 1.89

optimization. At 90% of load limit, the PM decreased in 57% and 24.5%, compared to the original and optimized dispatch strategies, respectively. The reduction in PM is essential for improving air quality. At 90% load, the operating time was reduced by almost 60% compared to the original operation and 27% considering the non-hybrid case with strategic loading. A lower number of running hours reduces maintenance and expenses for spare parts.

6.2 RESPONSE SURFACE METHODOLOGY (RSM) APPLIED TO HYBRID POWER SYSTEM DESIGN

There are several parameters to be considered when designing a hybrid solution, given the objectives. Deciding how to size an optimal ESS, including battery and converter settings, as well as determining the best genset loading limit for operation can be a challenge. As seen in the previous sections, power system settings as the genset load significantly impact several interest quantities, such as fuel consumption and emissions. A multi-response optimization can be even more challenging, considering the number of parameters that affect the vessel's performance.

To produce information about the sensitivity of the hybrid power system performance to the variation of different parameters and give us a tool for optimal sizing and operation, we will consider the Response Surface Methodology (RSM) methodology. The RSM comprehends statistical and mathematical techniques that are useful for developing, improving and optimizing processes, design and development of products. With this methodology, we can select input variables over a particular region of interest, design experiments and measure one or more responses. Then, we produce models that can be used for mapping a response surface, optimization, and selection of operating conditions to achieve desired objectives [87].

The input variables selected for the following analysis are battery DOD, genset loading limits, battery converter efficiency, battery energy, and power, described by the symbols x_1, x_2, x_3,

x_4, and x_5, respectively. The simulation experiments were planned using the Central Composite Design (CCD) approach to produce a second-order hypersurface with fuel savings as the response. The input variables were defined using five levels equally spaced. The ranges considered were: 10%-60% for DOD, 60%-100% for the genset loading limits, 95%-98% for the battery converter efficiency, 800 kW-2000 kW for the battery rated power, and 800 kWh-2000 kWh for the battery rated energy. The design of experiments (DOE) with the input variable values and the fuel consumption reductions are shown in Tab. 13.

It is worth mentioning that with the CCD, the number of simulation experiments was 36, which is small compared to the full factorial that would require 3125 experiments, but also would allow higher-order regressions. The simulations were carried out for one month of vessel operation, using the input values in Tab. 13 and using an $ECMS_{const}$ (constant equivalence factor) strategy and static models. With the battery enabling strategic loading on non-DP operations and being used as a spinning reserve in DP with an open bus-tie, the same methodology was used in section 6.1.2, but with changes in the five mentioned parameters. The fuel savings described in this section consider the original topology and operation of the vessel for comparison.

The values of the first five columns in Tab. 13 were standardized following equation

$$\text{standardized value} = \frac{\text{(value - mean value)}}{\text{value step}}, \tag{115}$$

where the quantities are reduced by the mean within the region in analysis and the delta in each level. Considering the genset loading limit, for example, we would have a mean value of 80% and value step of 10%.

A second-order regression was performed using the rsm package of the R software, whose output is shown in Fig. 75. This regression is complete, including linear, interaction, and quadratic terms. Some results are highlighted in different colors. In the first lines of the output table, the R software gives us the significance of each term used to build the regression. To define which are and which are not important, we can use the probability value (p-value) in the column Pr(>|t|).

The most significant terms are indicated in the green boxes, considering a p-value of 1%, with the significant codes underlined in orange. The variables with the strongest influence in the fuel consumption reductions are the genset loading limit (x_2), with a significant linear and quadratic term, the battery DOD, rated power, and converter efficiency (x_1, x_5, and x_3), with a linear effect on the outcome. The battery rated energy (x_4) had a p-value close to 5%, which is still large considering the other input variables.

Table 13 – Design of experiments (DOE) following a Central Composite Design (CCD) used for simulations with the fuel consumption reductions. The symbols x_1, x_2, x_3, x_4, and x_5, stand for battery DOD, genset loading limits, battery converter efficiency, battery energy and power, respectively.

x_1 (%)	x_2 (%)	x_3 (%)	x_4 (kW)	x_5 (kWh)	Fuel red.(%)
22.5	70	95.8	1100	1700	12.4
22.5	70	95.8	1700	1100	12.8
22.5	70	97.2	1100	1100	13.3
22.5	70	97.2	1700	1700	13.5
22.5	90	95.8	1100	1100	15.4
22.5	90	95.8	1700	1700	14.9
22.5	90	97.2	1100	1700	16
22.5	90	97.2	1700	1100	16.7
47.5	70	95.8	1100	1100	13.6
47.5	70	95.8	1700	1700	13.3
47.5	70	97.2	1100	1700	14.2
47.5	70	97.2	1700	1100	14.2
47.5	90	95.8	1100	1700	15.7
47.5	90	95.8	1700	1100	16.9
47.5	90	97.2	1100	1100	17.2
47.5	90	97.2	1700	1700	17.1
10	80	96.5	1400	1400	13.6
60	80	96.5	1400	1400	17.1
35	60	96.5	1400	1400	10.6
35	100	96.5	1400	1400	15.8
35	80	95	1400	1400	14.6
35	80	98	1400	1400	16.3
35	80	96.5	800	1400	14.9
35	80	96.5	2000	1400	15.5
35	80	96.5	1400	800	16.1
35	80	96.5	1400	2000	15
35	80	96.5	1400	1400	15.4
35	80	96.5	1400	1400	15.7
35	80	96.5	1400	1400	15.5
35	80	96.5	1400	1400	15.4
35	80	96.5	1400	1400	15.7
35	80	96.5	1400	1400	15.5
35	80	96.5	1400	1400	15.4
35	80	96.5	1400	1400	15.7
35	80	96.5	1400	1400	15.5
35	80	96.5	1400	1400	15.4

In this analysis, the battery energy does not directly impact fuel consumption reduction. However, it must be noted that ESS energy plays an essential role in battery sizing. To assure the battery will work appropriately for strategic loading and spinning reserve, the designer has to select an energy setting that provides, for example, operation autonomy to supply power for certain amounts of time. Also, battery energy correlates with its chemical degradation. The battery SOH is inversely proportional to the number of cycles, as defined in Eq. (75); therefore, a high-energy battery will have fewer cycles for the same battery use and, hence, a smaller degradation.

As the independent variables are standardized, the estimate coefficients give us a sense of the importance of each input, with x_2, x_1 and x_3 having the most considerable effects on fuel consumption reduction. No interaction term was significant; this means the inputs combined in pairs do not have a more substantial impact on the outcome than the sum of the individual effects alone.

We can see a high R-squared value (98%) in the blue box, which indicates a good fit. The analysis of variance table is shown in the black box, with the green boxes highlighting that the first-order (FO) and second-order (SO) terms have significance, contrary to the interactions (TWI). Nevertheless, the lack of fit, which measures how good the regression model is, has a very small p-value, indicating the model is not as good as expected. The lack of fit may be small due to the poor choice of variables, for example.

Rewriting the model using only the significant terms, in Fig. 76, we can see that all terms are significant in the green boxes and the p-value for the lack of fit is around 7.7%. Then, with a significance level of 5%, we can say that the model represents the data well. The R-squared still is high, being approximately 97%. The final model is described in Eq. (116), as bellow

$$\text{fuel red.}(\%) = 15.4353 - 0.5823x_2^2 + 0.5882x_1 + 1.3727x_2 + 0.4415x_3 - 0.2122x_5. \quad (116)$$

We executed nine more simulations with random input values to check the model accuracy within the region being analyzed and for the same month. The fuel consumption errors were below 0.5% comparing the model fit and the results generated directly by the system simulation.

The purple line highlights the stationary point in the original units. The optimization has shown a maximum fuel consumption reduction value for a 35% DOD, 91.78% of genset loading limit, 96.5% converter efficiency, and 1400 1400 kW of battery rated power. However, this result has to be treated carefully because a near-stationary-ridge situation was observed. The ridge systems occur when an approximate maximum is found on a region instead of a point. This

```
rsm(formula = fuel ~ SO(x1, x2, x3, x4, x5), data = CR)

             Estimate Std. Error  t value  Pr(>|t|)
(Intercept) 15.5113934  0.0927865 167.1729 < 2.2e-16 ***
x1           0.5882132  0.0607430   9.6836 7.615e-08 ***
x2           1.3727425  0.0607430  22.5992 5.336e-13 ***
x3           0.4415539  0.0607430   7.2692 2.744e-06 ***
x4           0.1166724  0.0607430   1.9208  0.073979 .
x5          -0.2122016  0.0607430  -3.4934  0.003267 **
x1:x2        0.0370755  0.0743947   0.4984  0.625457
x1:x3       -0.0505839  0.0743947  -0.6799  0.506902
x1:x4       -0.0037044  0.0743947  -0.0498  0.960944
x1:x5       -0.0124331  0.0743947  -0.1671  0.869505
x2:x3        0.0590101  0.0743947   0.7932  0.440027
x2:x4        0.0568752  0.0743947   0.7645  0.456425
x2:x5       -0.1245000  0.0743947  -1.6735  0.114948
x3:x4        0.0062044  0.0743947   0.0834  0.934638
x3:x5        0.1087627  0.0743947   1.4620  0.164384
x4:x5       -0.0393803  0.0743947  -0.5293  0.604315
x1^2        -0.0450061  0.0526050  -0.8555  0.405707
x2^2        -0.5823733  0.0526050 -11.0707 1.290e-08 ***
x3^2        -0.0092882  0.0526050  -0.1766  0.862213
x4^2        -0.0660098  0.0526050  -1.2548  0.228744
x5^2         0.0061383  0.0526050   0.1167  0.908656
---
Signif. codes:  0 ‘***’ 0.001 ‘**’ 0.01 ‘*’ 0.05 ‘.’ 0.1 ‘ ’ 1

Multiple R-squared:  0.9817,    Adjusted R-squared:  0.9573
F-statistic: 40.27 on 20 and 15 DF,  p-value: 1.343e-09

Analysis of Variance Table

Response: fuel
                         Df Sum Sq Mean Sq  F value    Pr(>F)
FO(x1, x2, x3, x4, x5)    5 59.617 11.9233 134.6461 6.516e-12
TWI(x1, x2, x3, x4, x5) 10  0.636  0.0636   0.7180  0.697122
PQ(x1, x2, x3, x4, x5)    5 11.061  2.2123  24.9823 8.933e-07
Residuals                15  1.328  0.0886
Lack of fit               6  1.128  0.1881   8.4714  0.002732
Pure error                9  0.200  0.0222
```

Figure 75 – Response surface analysis for the fuel consumption reduction including linear, interactions, and quadratic terms.

provides an interesting opportunity to optimize the response, giving more freedom to select the input values and having a near maximum performance.

Figure 77 shows fuel consumption contour plots representing the hypersurface fit slices. Figures 77(a), 77(d), and 77(e) show contour plots of the genset loading limit by the battery DOD, converter efficiency (η_{rec}), and battery rated power. The largest fuel savings occur near 90% load, as observed in previous sections, with the maximum DOD and η_{rec}, but with the smaller battery rated power. Differences up to 7% can be observed, varying mainly the generator limits, with the other variables slightly impacting the fuel response. Even with minor effects, some trade-offs can be made. We could, for example, reduce the genset loading from 90% to 80% and increase the η_{rec} from 96% to 97.5%, keeping the fuel savings at 16%.

In Fig. 77(b), the converter efficiency and DOD are on the same plot. Varying the DOD and the efficiency would allow changes of approximately 3% in fuel consumption, with the

```
rsm(formula = fuel ~ PQ(x2) + FO(x1, x2, x3, x5), data = CR)

             Estimate Std. Error  t value  Pr(>|t|)
(Intercept) 15.435283   0.058914 261.9971 < 2.2e-16 ***
x2^2        -0.582373   0.051021 -11.4144 1.927e-12 ***
x1           0.588213   0.058914   9.9843 4.746e-11 ***
x2           1.372743   0.058914  23.3008 < 2.2e-16 ***
x3           0.441554   0.058914   7.4949 2.355e-08 ***
x5          -0.212202   0.058914  -3.6019  0.001125 **
---
Signif. codes:  0 ‘***’ 0.001 ‘**’ 0.01 ‘*’ 0.05 ‘.’ 0.1 ‘ ’ 1

Multiple R-squared:  0.9656,    Adjusted R-squared:  0.9599
F-statistic: 168.4 on 5 and 30 DF,  p-value: < 2.2e-16

Analysis of Variance Table

Response: fuel
                  Df Sum Sq Mean Sq  F value    Pr(>F)
PQ(x2)             1 10.853 10.8531 130.2884 1.927e-12
FO(x1, x2, x3, x5)  4 59.290 14.8225 177.9402 < 2.2e-16
Residuals          30  2.499  0.0833
Lack of fit        19  2.001  0.1053   2.3246   0.07688
Pure error         11  0.498  0.0453

Stationary point of response surface:
      x1       x2       x3       x5
0.000000 1.178576 0.000000 0.000000

Stationary point in original units:
       x1       x2       x3       x5
  35.00000   91.78576   96.50000 1400.00000
```

Figure 76 – Response surface analysis for the fuel consumption reduction including only significant terms.

highest reductions for the maximum DOD and η_{rec}. The lines show that we could increase the converter efficiency and reduce the DOD or vice versa, maintaining almost the same fuel savings. For example, we could size the system to have a 95% converter efficiency operating with a 50% DOD, and that would be equal to using a converter of 97% efficiency with a 23% DOD, giving the designer the option to choose between configurations considering other constraints such as component price.

Figure 77(c) shows the rated battery power by the DOD. Fuel consumption changes of around 2% can be achieved by changing the parameters inside the experiment region. The highest savings can be found using the maximum DOD and the minimum power, and a balance between power and DOD can also be made. For the same DOD, the power dispatch did not present significant differences considering the dispatch optimization. However, it makes quite a difference in the DP part because the battery acts as a spinning reserve. Then, an 800 kW battery probably would not be enough to switch off the two gensets as we are currently doing due to safety constraints. We could, however, size the battery for high power but set a dispatch limit to run the battery with an 800 kW during the power dispatch in non-DP operations.

In Fig. 77(f), changing the battery power and converter efficiency did not significantly impact the fuel savings within the region of analysis. Finally, the contour plots and regression coefficients gave us a general perspective of how the input variables or the system parameters affect fuel reductions. Besides evaluating one outcome, balancing multiple responses would also be possible. Having a tool as this model fit would allow the designer to rapidly try several configurations to achieve the best performance given the selected objectives and budget.

6.3 ENERGY MANAGEMENT STRATEGIES FOR HYBRID POWER SYSTEMS CONSIDERING DYNAMICAL MODELS FOR THE ELECTRICAL POWER SYSTEM

In this section, we will discuss higher frequency simulations, running on a time step of 0.1 s, so the dynamical models explained in chapter 4 can be explored. The following results will consider a modeling approach similar to that presented in the previous sections, but the use of dynamical models will enable new analyses, such as battery aging evaluation. We will compare the fuel consumption, emissions, genset running hours, overall power system efficiency, and battery aspects, considering the non-hybrid and hybrid cases with different EMS approaches. The presented results do not imply that one EMS strategy is necessarily better than the other, they only compare the performances of the implementations for this specific case based on the quantities of interest.

For a more complete perspective, besides analyzing the genset responses such as fuel savings, it is essential to look at the battery capacity fading or chemical degradation. The battery degradation depends on factors such as current and temperature, and there is also a correlation with how much the battery is used, charged, and discharged, quantified as the number of cycles [20, 66]. The battery can improve the power system's fuel efficiency and provide other benefits, but a fast energy storage degradation is generally undesirable.

The power and energy management follow the structure presented in Fig. 46 and Fig. 47, modeling the electrical power system, i.e., the power sources (generators and battery), electrical network, converter, and the EMS/PMS, of the Ulstein PSV topologies in Fig. 19 and Fig. 20. The genset and battery models used in the high frequency simulations were defined in sections 4.1 and 4.4, respectively.

For the original topology (non-hybrid), we considered the dispatch optimization presented in section 5.3 with the DPO configuration, i. e., operating with an open bus tie in DP at 80% of genset load limit. For the hybrid configuration, we applied different power and energy

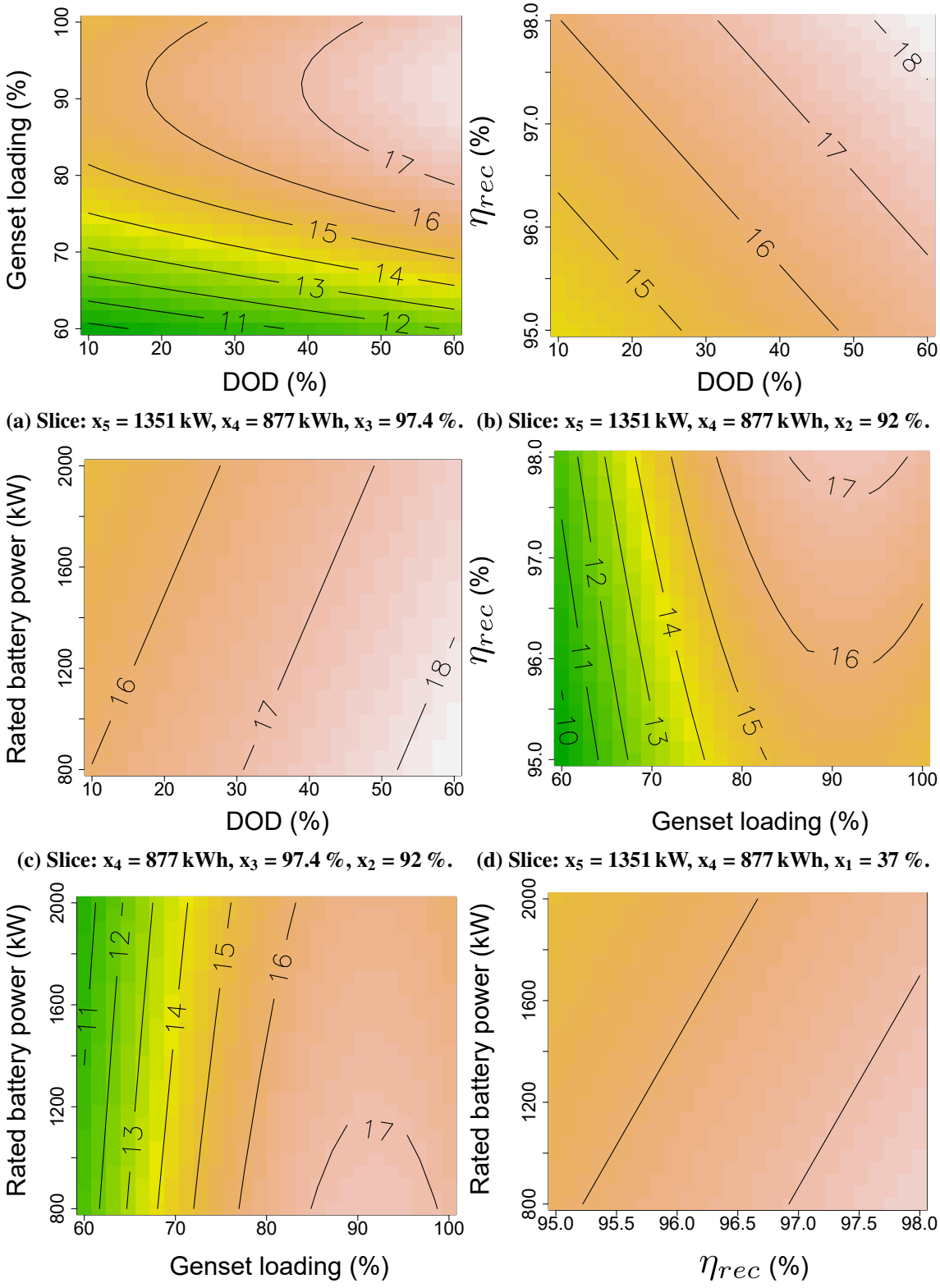

(a) Slice: x_5 = 1351 kW, x_4 = 877 kWh, x_3 = 97.4 %. **(b) Slice: x_5 = 1351 kW, x_4 = 877 kWh, x_2 = 92 %.**

(c) Slice: x_4 = 877 kWh, x_3 = 97.4 %, x_2 = 92 %. **(d) Slice: x_5 = 1351 kW, x_4 = 877 kWh, x_1 = 37 %.**

(e) Slice: x_4 = 877 kWh, x_1 = 37 %, x_3 = 97.4 %. **(f) Slice: x_4 = 877 kWh, x_1 = 37 %, x_2 = 92 %.**

Figure 77 – Fuel consumption reduction contour plots representing slices of the hyper surface fit.

Table 14 – Parameters used for the electrical power system simulation considering dynamical models

Parameter	Symbol	Value	Unit
Genset loading limit for the non-hybrid case	$P_{G,max}$	80%	-
Genset loading limit for the hybrid case	$P_{G,max}$	90%	-
Lower genset power limit for the RB case	$P_{G,on}$	700	kW
Fraction power to cut peaks	f_{peak}	95%	-
Max discharging power	P_{dmax}	1700	kW
Max charging power	P_{cmax}	-1700	kW
Min state of charge	SOC_{min}	20%	-
Max state of charge	SOC_{max}	80%	-
Battery DOD	DOD	60%	-
Number of cells in parallel	NP	703	-
Number of cells in series	NS	333	-
Battery converter efficiency	η_{rec}	97%	-
Reference SOC for the AECMS	SOC_{ref}	50%	-
Proportional gain for the AECMS	k_{ps}	0.8	-
Equivalence factor	s	2.43	-
Min cell current	I_{min}	-2.2 (1C)	A
Max cell current	I_{max}	2.2 (1C)	A
Min equivalence factor	s_{min}	2.22	-
Max equivalence factor	s_{max}	2.25	-
Capacity of each cell	C_{bat}	1.129	Ah
Battery rated energy	E	0.87	MWh
Battery rated power	P	1.7	MW
Time step	Δt	0.1	s

management strategies with an open bus tie operation in DP, two gensets off, and the battery used as a spinning reserve, able to supply power to each side of the main bus tie-breaker, as considered in section 6.1.2, and illustrated in Fig. 68. The battery used for the simulations used the settings from section 6.1.2, with rated power and energy of 1.7 MW and 0.87 MWh, respectively, and a C-rate of 1 C, operating between the SOC range of 20%-80% (60% DOD).

The parameters employed in the simulations are given in Tab. 14. Using the knowledge provided by the response surface analysis in section 6.2, we set the genset loading limit to 90%, the battery converter efficiency to 97% (the maximum found in commercial applications), and the DOD to 60%. The energy was kept low at 0.87 MWh, but this is enough to supply rated power for at least 15 minutes in case of a fault. The power was defined as 1700 kW to allow the use of the battery as a spinning reserve.

Four energy management strategies for the hybrid power system will be discussed: the rule-based (RB) strategy, which follows the method described in section 5.4, and three ECMS approaches mentioned in section 5.5. The first approach ($\text{ECMS}_{\text{const}}$) refers to an ECMS that uses a constant equivalence factor, while ECMS_{opt} is associated with optimizing the equivalence factor within some predefined range. Finally, we consider an adaptative ECMS (AECMS), which uses a proportional controller for optimization.

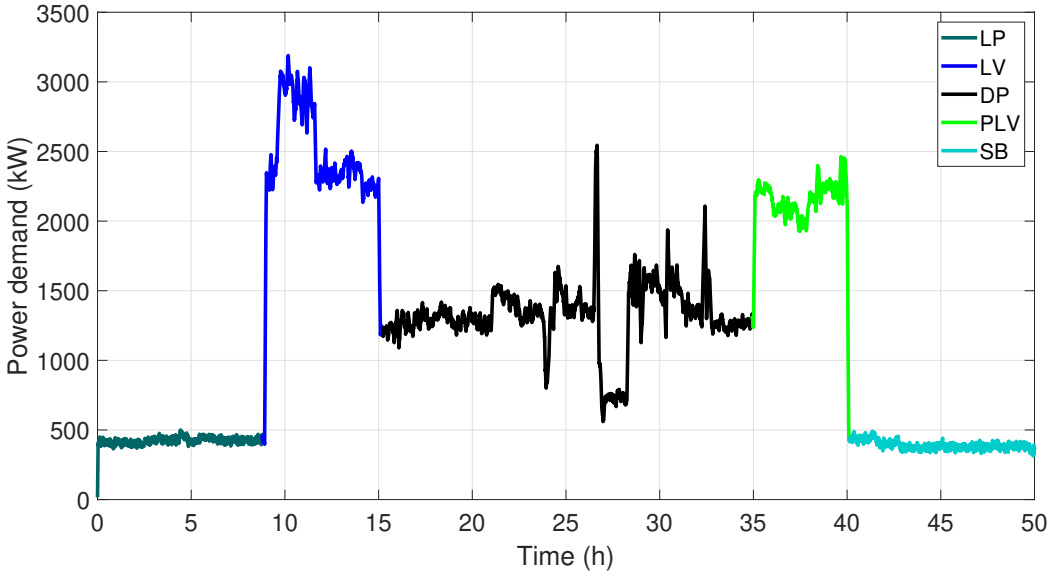

Figure 78 – Power demand profile in the simulations: Mission 1.

Table 15 – Statistics of the power demand profile used in the dynamical simulations

Operating profile statistics					
Mission part	LP	LV	DP	PLV	SB
Time (%)	18	13	39	10	20
Average power demand (kW)	423±21	2429±477	1320±237	2122±243	390±28

The power demand profile considered for the simulations in this section, in Fig. 78, follows the same operation modes of the mission profile described in Fig. 57, with five parts: loading in port (LP), laden voyage (LV), dynamical positioning (DP), partial load voyage (PLV), and standby (SB), and the same time percentage in each part of the mission. However, the time was reduced to 50 hours to decrease the computational cost of dynamical models in high-frequency simulations.

The mission in Fig. 78 was built considering data from real operations, extracting power demands from the data used in section 6.1, and interpolating over time, with the addition of white noise to represent fast oscillations of the load demand. The operating profile statistics are described in Tab. 15.

The turn on and off procedures will not be considered for the gensets, as well as loading ramps. Instead, we assume that the engine speed set-point is constant and that it can supply power at any time. When the genset power references are zero, they are disconnected from the grid, hence the fuel consumption and any emissions are null. When the gensets are switched on, the simulation follows the model described in section 4.1. Besides, the batteries can supply immediate power at any time.

Table 16 – Compilation of results generated through dynamical simulations for comparison between the non-hybrid case and hybrid case with different EMS strategies.

Integral results: comparing the non-hybrid case and hybrid cases							
Case			Non-hybrid	RB	$ECMS_{const}$	$ECMS_{opt}$	AECMS
Quantity		Unit					
Fuel	m_f	(kg)	15207.0	13736.0	13825.0	13916.0	13857.0
	red.	(%)	-	9.7	9.1	8.5	8.9
CO_2	m_{CO_2}	(kg)	46490.0	42145.0	42381.0	42645.0	42480.0
	red.	(%)	-	9.3	8.8	8.3	8.6
NO_x	m_{NO_x}	(kg)	437.3	400.6	391.4	390.5	393.0
	red.	(%)	-	8.4	10.5	10.7	10.1
PM	m_{PM}	(kg)	10.1	5.3	5.5	5.5	5.5
	red.	(%)	-	47.7	45.6	45.6	45.6
SOC		(% / %)	-	80 / 45.7	80 / 22.8	80 / 54.3	50 / 36.2
ΔSOH		(%)	-	0.070	0.075	0.082	0.078
η_{ps}		(%)	33.3	36.8	36.6	36.4	36.5
Number of battery cycles		(-)	-	22.1	24.5	27.3	25.7
Genset running hours	time	(h)	122.3	62.1	65.0	65.5	65.1
	red.	(%)	-	49.2	46.8	46.4	46.7

6.3.1 Integral analysis

Table 16 lists the genset running hours and reductions, the masses of fuel consumed, CO_2, NOx, and particulate matter emissions, as well as the mass reductions between the non-hybrid and the hybrid cases. Also, the table comprehends the initial and final states of charge (separated by a slash "/"), a variation in the state of health (SOH), and the number of battery cycles for the hybrid cases. Finally, the global efficiency index, defined in section 4.7, is also considered. Results of power dispatch for all configurations are shown in Figs. 79–82.

All EMS strategies have presented fuel savings for the hybrid topologies compared to the non-hybrid. The most significant reduction was achieved for the RB case, with fuel savings of 9.7%, closely followed by the $ECMS_{const}$ with 9.1% of fuel reduction. The AECMS presented 8.9% of fuel savings. The lowest fuel reductions were obtained using the optimization of the equivalence factor in the $ECMS_{opt}$, with 8.5%. Nonetheless, the performance differences among the hybrid strategies were relatively low.

For the ECMS strategies, we noted higher variations in the power dispatch, with the gensets being switched on and off more frequently (Figs. 80, 81, and 82), which happened less for the RB case, probably due to the hysteresis settings (Fig. 79). These power variations can help to explain why the ECMS results were better for the low-frequency simulations in section 6.1.2 and are worse in the dynamic case. Finally, the power profiles and equivalence factors are different between this section and section 6.1.2, and this probably contributed to the difference in the results.

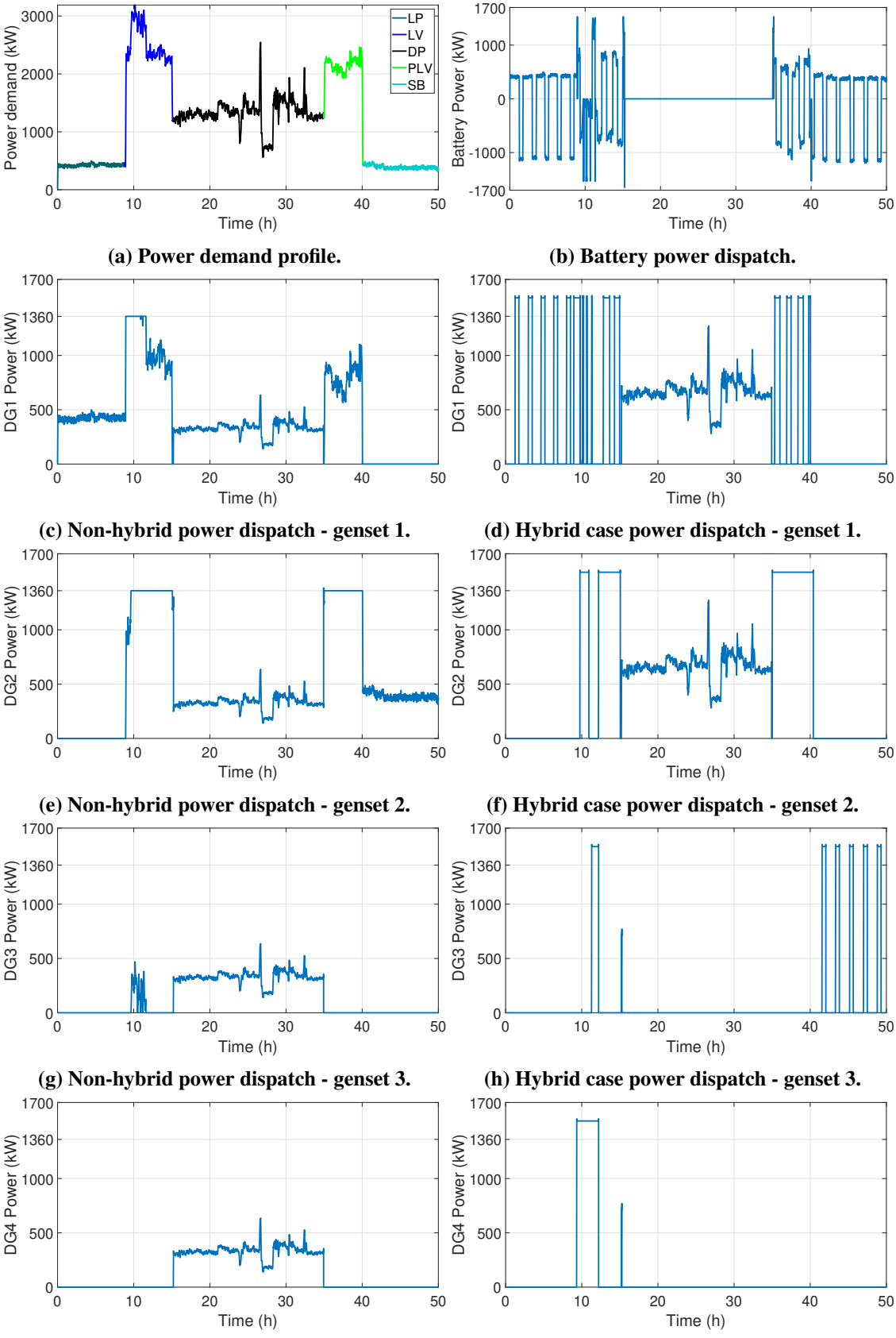

(a) Power demand profile.

(b) Battery power dispatch.

(c) Non-hybrid power dispatch - genset 1.

(d) Hybrid case power dispatch - genset 1.

(e) Non-hybrid power dispatch - genset 2.

(f) Hybrid case power dispatch - genset 2.

(g) Non-hybrid power dispatch - genset 3.

(h) Hybrid case power dispatch - genset 3.

(i) Non-hybrid power dispatch - genset 4.

(j) Hybrid case power dispatch - genset 4.

Figure 79 – Power demand, and power dispatch of the base case (non-hybrid) and the hybrid power system with rule-based (RB) EMS.

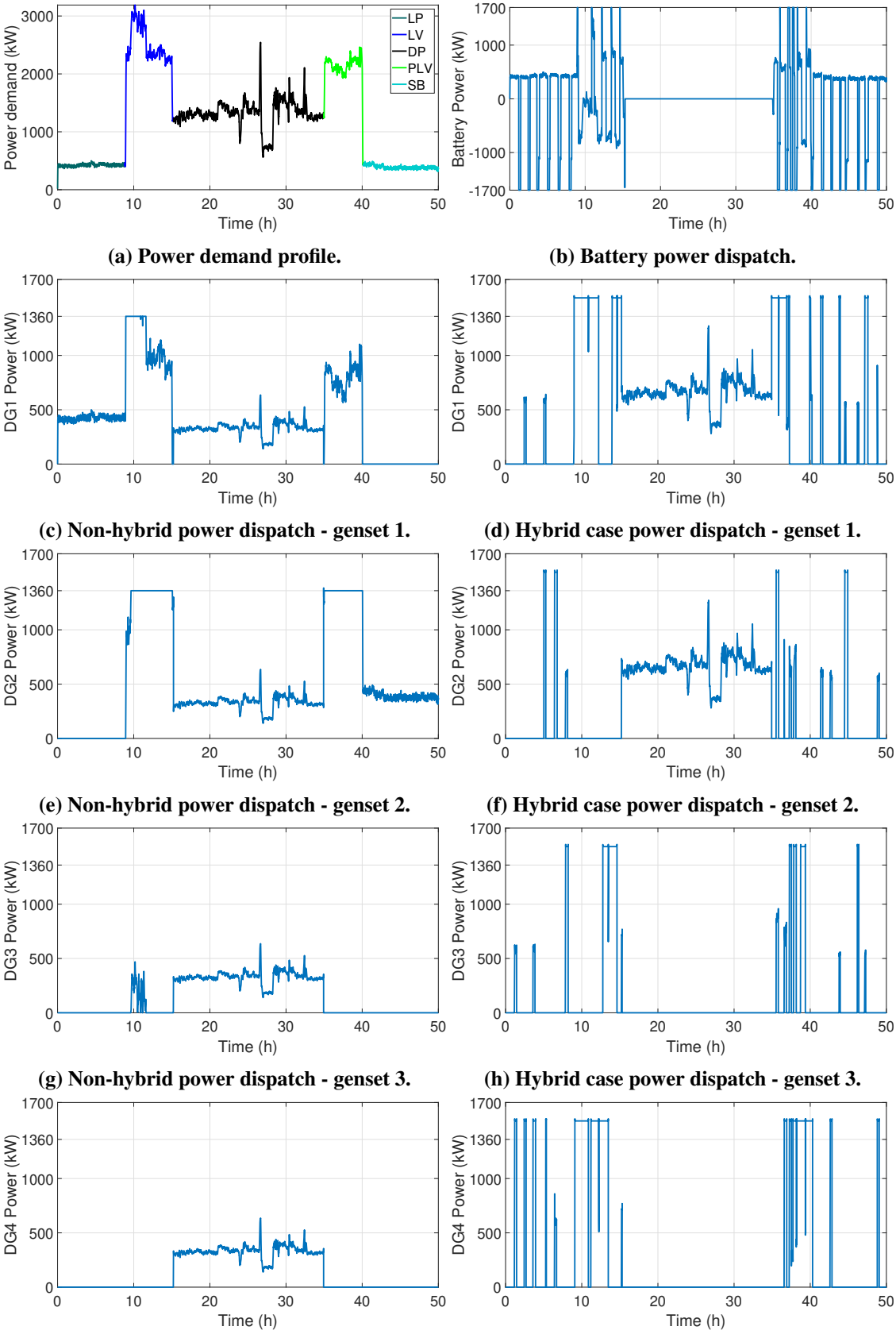

(a) Power demand profile. **(b) Battery power dispatch.**

(c) Non-hybrid power dispatch - genset 1. **(d) Hybrid case power dispatch - genset 1.**

(e) Non-hybrid power dispatch - genset 2. **(f) Hybrid case power dispatch - genset 2.**

(g) Non-hybrid power dispatch - genset 3. **(h) Hybrid case power dispatch - genset 3.**

(i) Non-hybrid power dispatch - genset 4. **(j) Hybrid case power dispatch - genset 4.**

Figure 80 – Power demand, and power dispatch of the base case (non-hybrid) and the hybrid power system using the ECMS with a constant equivalence factor ($ECMS_{const}$).

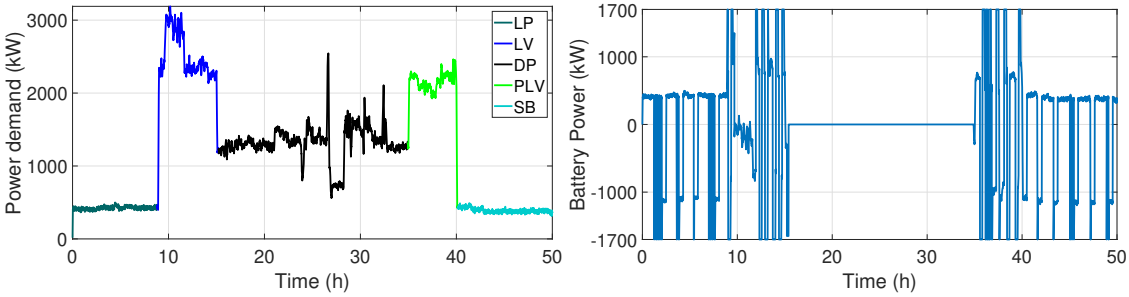

(a) Power demand profile.

(b) Battery power dispatch.

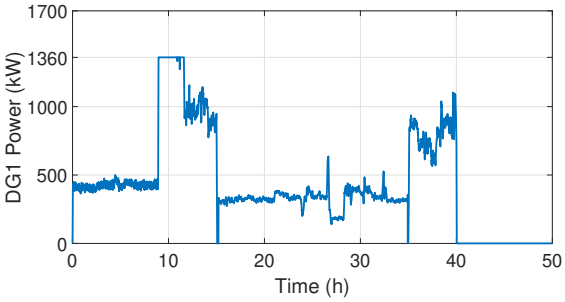

(c) Non-hybrid power dispatch - genset 1.

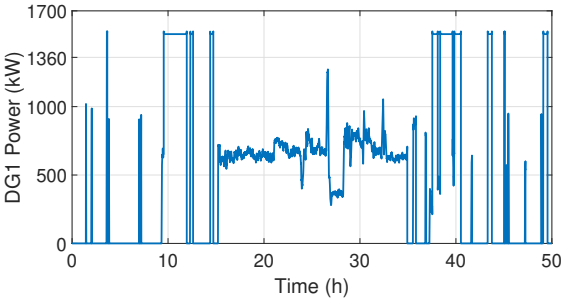

(d) Hybrid case power dispatch - genset 1.

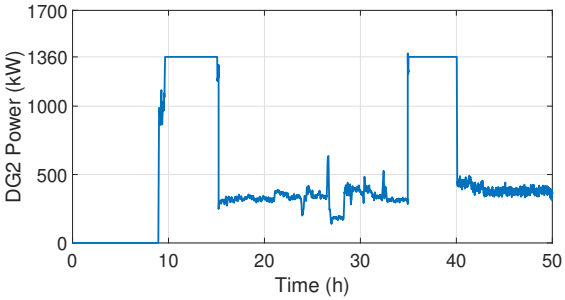

(e) Non-hybrid power dispatch - genset 2.

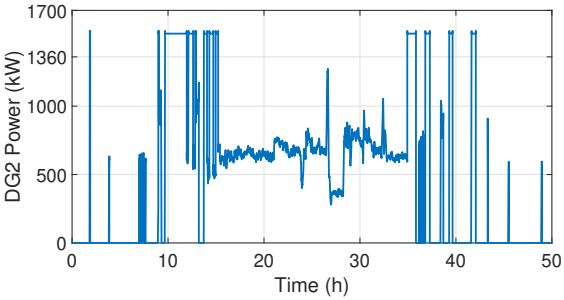

(f) Hybrid case power dispatch - genset 2.

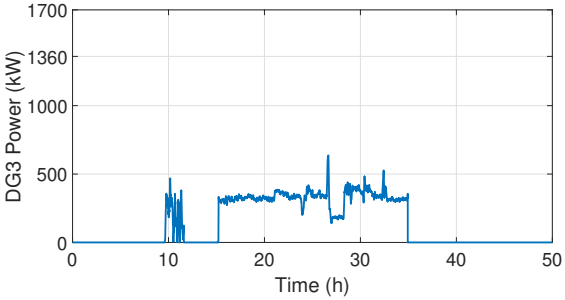

(g) Non-hybrid power dispatch - genset 3.

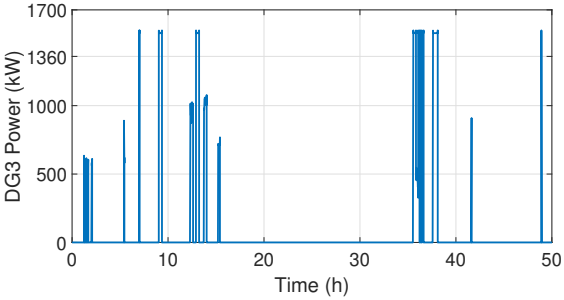

(h) Hybrid case power dispatch - genset 3.

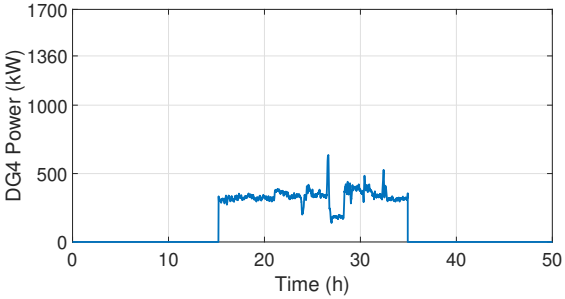

(i) Non-hybrid power dispatch - genset 4.

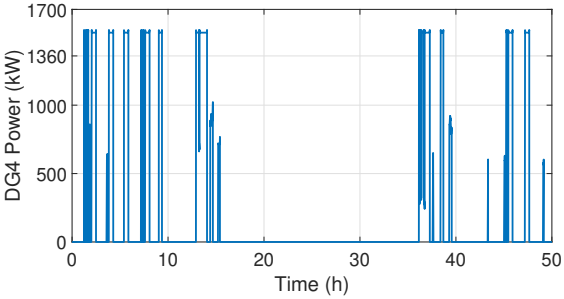

(j) Hybrid case power dispatch - genset 4.

Figure 81 – Power demand, and power dispatch of the base case (non-hybrid) and the hybrid power system using the ECMS and optimizing the equivalence factor ($ECMS_{opt}$).

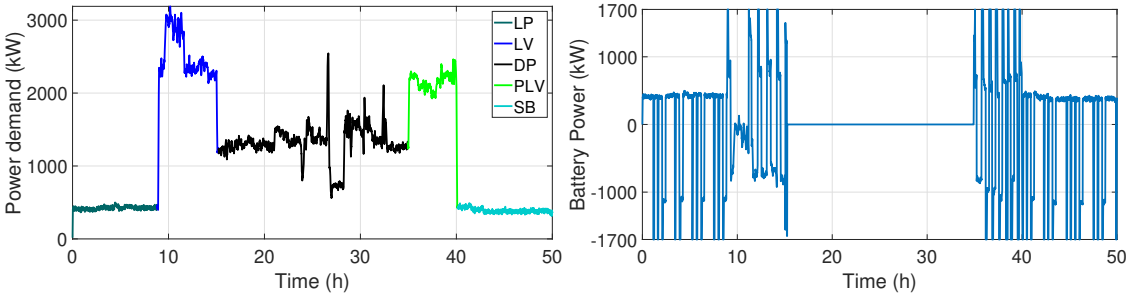

(a) Power demand profile.

(b) Battery power dispatch.

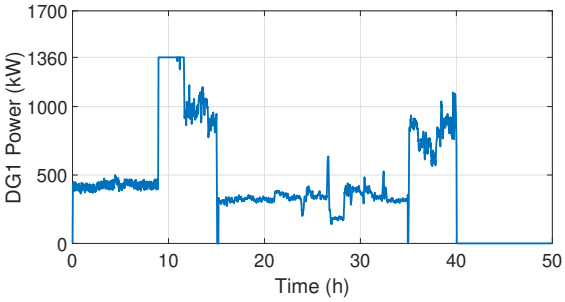

(c) Non-hybrid power dispatch - genset 1.

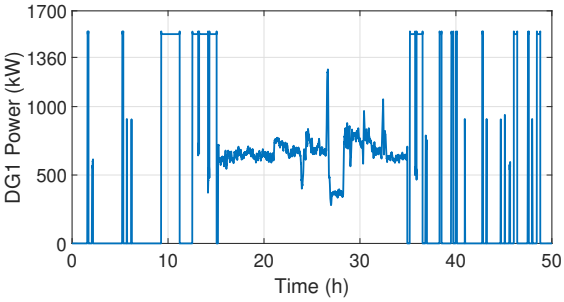

(d) Hybrid case power dispatch - genset 1.

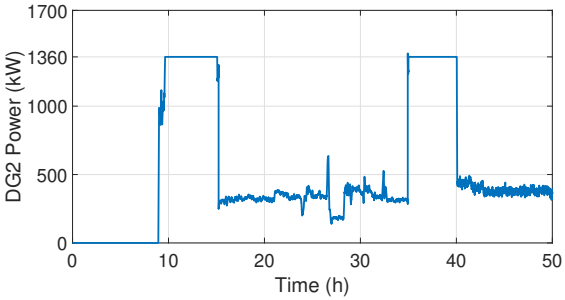

(e) Non-hybrid power dispatch - genset 2.

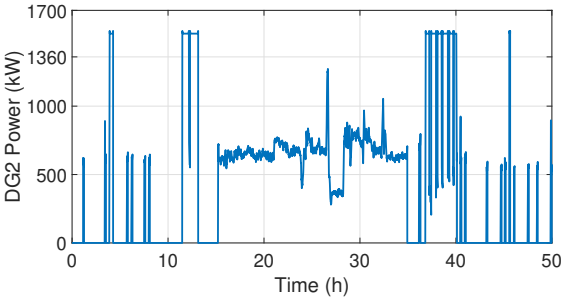

(f) Hybrid case power dispatch - genset 2.

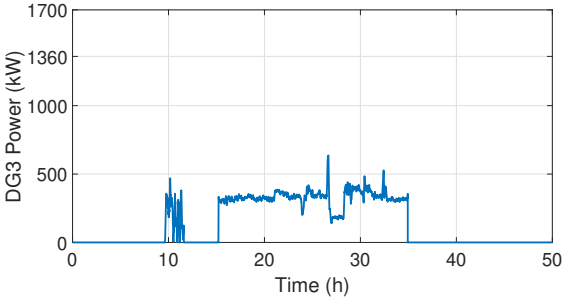

(g) Non-hybrid power dispatch - genset 3.

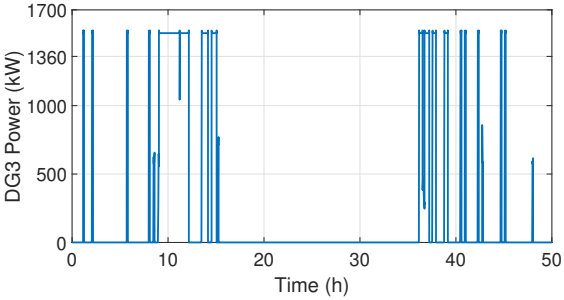

(h) Hybrid case power dispatch - genset 3.

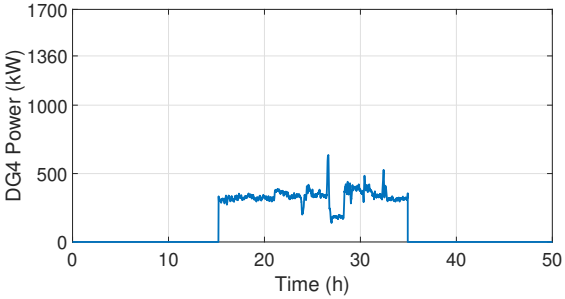

(i) Non-hybrid power dispatch - genset 4.

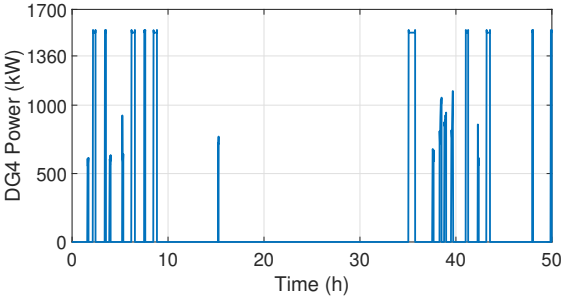

(j) Hybrid case power dispatch - genset 4.

Figure 82 – Power demand, and power dispatch of the base case (non-hybrid) and the hybrid power system using adaptative ECMS (AECMS).

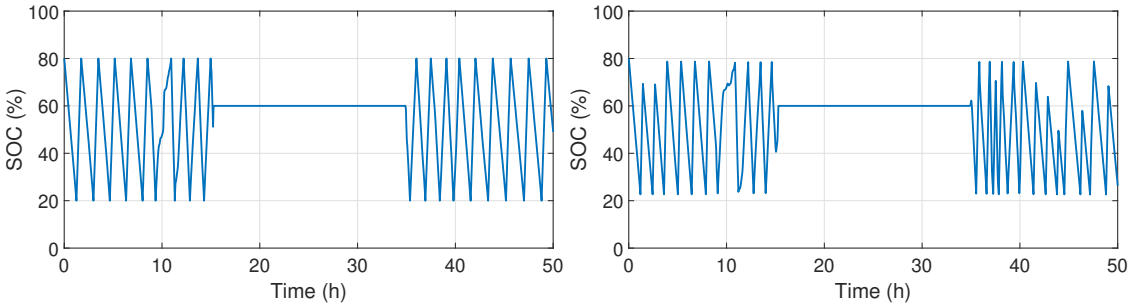

(a) SOC for the RB strategy. **(b) SOC for the ECMS$_{const}$ strategy.**

Figure 83 – State of charge for the hybrid case using the ECMS$_{const}$ and RB strategies.

The power system efficiency rose above 3% for all hybrid cases. The best results were achieved by the RB and ECMS$_{const}$ cases, with increases of 3.5% and 3.3%, respectively. The CO_2 emissions are proportional to the fuel consumption, showing the same reduction pattern; however, with slightly smaller values. The maximum CO_2 reductions were of 9.3% and 8.8% for the RB and ECMS$_{const}$, respectively. Based on the discussion presented in section 6.1.2, we can say the results for fuel consumption and CO_2 emissions are within expected ranges for a PSV.

The NO_x emissions were reduced for all hybrid cases, varying from 8.4% (RB) to 10.7% (ECMS$_{opt}$), with the worst result for the most efficient case, which is also a tendency observed in sections 6.1.1 and 6.1.2. The particulate matter dropped considerably for all hybrid cases, with the most significant reduction for the RB case with 47.7%, followed closely by the ECMS strategies, which produced the same PM reductions of 45.6%. Finally, the decrease in genset operating time was significant, with the highest decrement for the RB (49.2%), followed by around 46% for the ECMS cases.

The final SOC was smaller than the initial SOC for all cases. As shown in Fig. 79, Fig. 80, Fig. 81, and Fig. 82, the battery was not depleted or charged in the DP part of the mission. The implemented control made sure, through a conditional, to recharge the battery to at least 60% near DP to enable the spinning reserve function for the battery, as it can be seen in the SOC of for the ECMS$_{const}$ and RB, in Fig. 83.

The number of cycles directly impacted the ΔSOH of the battery. A higher number of cycles caused higher battery capacity fading. The RB case achieved the smallest degradation, only 0.070%, followed by the ECMS$_{constant}$. The worst case was observed by the ECMS$_{opt}$ with a 0.082% of ΔSOH. The mission being considered has 50 hours, so if we linearly extrapolate the loss of capacity by the time, we would have over eight years of battery operation for the RB case and seven years for the worst case ECMS$_{opt}$. Clearly, the battery calendar life would have to

Table 17 – NOx emission reduction percentages by mission part

NOx emission reduction					
Mission part	LP	LV	DP	PLV	SB
Reduction(%)	-14	-70	252	-63	-5

be considered, and somehow, it is already embedded into the aging model in the Ah throughput calculation, which is directly proportional to time [66].

Switching off two generators at DP and using the battery as a spinning reserve has substantial benefits for the vessel's power system. While in section 6.1 we found around 6% of additional gains by comparing the hybrid power system with a non-hybrid both with power dispatch optimization, in this section, we observed savings of around 10%, and the NO_x emissions were reduced. The mission considered here spends 40% of the time in DP, instead of 20% as that described in section 6.1.

In Fig. 84, we can see the percentage reductions of quantities of interest by each part of the mission. The charts clearly show that the hybrid system had a massive impact on the DP operation. Around 60% of the fuel saved, CO_2 emission, and operating time reductions are associated with the new operating mode enabled in DP. Over 70% of the PM reductions occurred in DP. The battery was used as a spinning reserve in DP, not being requested as we did not consider a fault condition.

Between 23%-26% of the fuel savings, CO_2 emission, and genset running hour reductions are assigned to both the LP and SB parts of the mission, with each having a similar impact. In loading and standby, the ESS was most requested with a total capacity loss of 59%. However, it enabled the generators to run at higher efficiency regions or to be disconnected from the grid, as it can be seen in Figs. 79–82.

The smallest battery benefits were observed in the transit part of the mission (LV and PLV). The vessel requires higher loads in these operational modes and does not work with highly dynamic power demands or redundancy as in DP. Around 41% of the battery degradation was attributed the vessel transit, with the highest capacity fading for the LV, closely followed by the PLV part.

The NO_x emissions are displayed in Tab. 17. It can be seen that enabling a more efficient operation in LP, LV, PLV, and SB increased the NO_x emissions. However, the reductions in DP were so expressive due to switching off two generators that, in general, the yield of this pollutant was reduced as shown in Tab. 16. Again, the after-treatment system was not considered in the analysis.

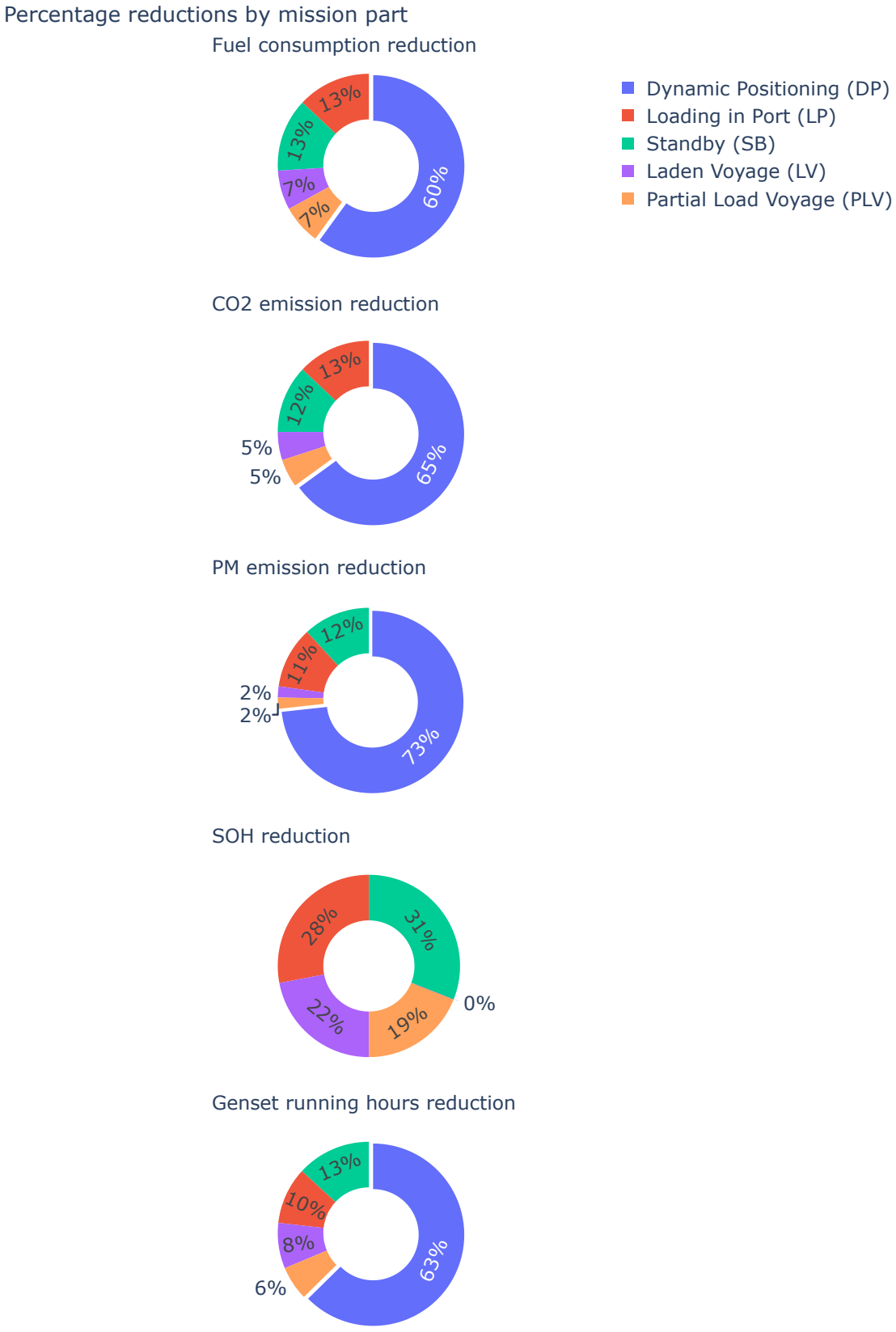

Figure 84 – Percentage reductions of fuel consumption, CO_2 and PM emissions, SOH and genset running hours by mission part.

In general, the addition of the battery allowed the reduction of fuel consumption, emissions, genset operating time, as well as an increase in the overall energy efficiency of the vessel's power system. With the capacity fading extrapolation, we observed that the battery could be used for 7 to 8 years, enabling more energy-efficient and cleaner operations. The most significant battery benefits were observed for the DP part of the mission, followed by the loading in port and standby. The latter mission parts had the highest impact on battery degradation. The smallest benefits were observed in the transit part (laden and partial load voyages). The NO_x reduction in DP was so expressive that the overall emissions were reduced.

6.3.2 Power dispatch analysis

Figures 79, 80, 81, and 82 show the total power demand and power dispatch of the hybrid and non-hybrid power systems for the different energy management strategies considered, and whose results were discussed in section 6.3.1. The non-hybrid power dispatch, with gensets only, is represented in the first column (results on the left), with the load demand above, for the visualization of the mission profile. The power dispatch of the hybrid case, including the battery and gensets, can be seen in the second column (on the right).

When the vessel is being loaded in port (LP) and when the vessel is in standby (SB), it is possible to see that the load is smaller than the power capacity of one genset, which is 1700 kW. Therefore, the load is sustained by only one generator in the non-hybrid case. However, in the hybrid case, the battery is heavily used, being charged and discharged in all EMS strategies since the load is often smaller than 700 kW. Moreover, the gensets work in higher and more efficient power regions for the hybrid topology and are, many times, disconnected compared to the non-hybrid case. The hybrid system can also reduce the total genset operation time and reduce CO_2 emissions near the port, except for NO_x, which increased 14% in LP and 5% in SB but could probably be reduced or eliminated by using an after-treatment system.

In LV the vessel is fully loaded and in transit, so this part of the mission is characterized by high power demands. In the non-hybrid system, the first two gensets operate in the nominal condition almost all the time, with genset 3 balancing the higher load variations. Regarding the hybrid power system, the genset use varies, but the system tends to run in more efficient regions, not having gensets with small loads such as genset 3.

Evaluating the DP part, we can see that the four gensets share equal loads in the non-hybrid case. However, the hybrid power system enables switching off two generators using only

two gensets which share equal loads. Therefore, the two gensets run at higher loads bringing numerous benefits as mentioned in section 6.3.1. The battery is neither depleted nor charged.

The partial load voyage (PLV) and standby (SB) had similar power dispatch behaviors to the LV and LP mission parts. Looking at the power dispatch, it is clear that the ECMS showed more power variations, switching the gensets on and off more frequently, which is undesirable. Also, in some situations, such as in Fig. 80, loading in port, the ECMS decided to operate gensets in smaller loads compared to the RB strategy, indicating that the optimization procedure still has space for improvement in the dynamical simulations.

6.3.3 Vessel acceleration simulation using the complete electric propulsion system

Until now, we have been modeling mainly the electrical power system. With the comprehensive model set developed in this work, different power system modeling approaches are available, and it is possible to choose how to perform the simulations based on the premises and the variables of interest. This section extends the number of models, including the electrical propulsion system, which comprises the three-phase electrical motors, the drivetrain, and the simplified vessel physics.

The following simulations consider the dynamical models used in section 6.3.1 with the RB strategy and the same parameters integrated with the propulsion system presented in section 4.3. We will evaluate the vessel acceleration until reaching the rated velocity, as in Fig. 35. Figure 85 shows the power demand profile and the power dispatch of the gensets for the non-hybrid case on the left hand side. On the right hand side, we see the power dispatch of the battery and gensets for the hybrid case.

The hybrid power system allows the gensets to operate at higher loads from 80% to 90% of the rated power, while the non-hybrid topology is limited to 80%. Also, the genset 4 runs at loads below 700 kW, which are within an inefficient region. Using the efficiency index developed in section 4.7, we calculated an increase in efficiency of 10%, going from 38% to 48% on the vessel departure using a hybrid power system. This efficiency increase impacts on fuel consumption and emissions. Another benefit that can be explored is the vessel response time, once the battery supplies almost instant power. In an actual vessel rapid acceleration, the gensets would require more time to be connected and disconnected from the grid, which would probably make the battery an even better solution.

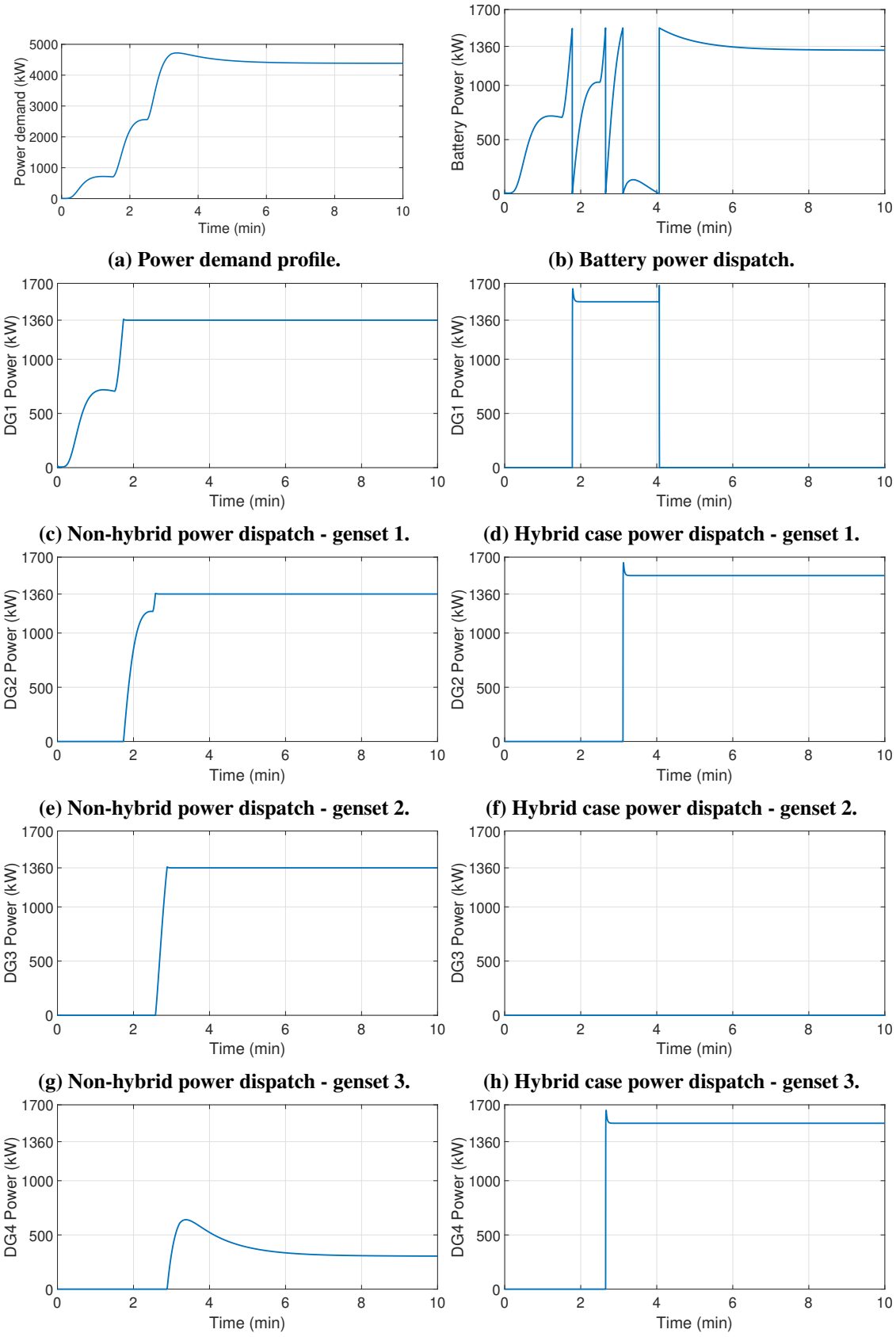

(a) Power demand profile.

(b) Battery power dispatch.

(c) Non-hybrid power dispatch - genset 1.

(d) Hybrid case power dispatch - genset 1.

(e) Non-hybrid power dispatch - genset 2.

(f) Hybrid case power dispatch - genset 2.

(g) Non-hybrid power dispatch - genset 3.

(h) Hybrid case power dispatch - genset 3.

(i) Non-hybrid power dispatch - genset 4.

(j) Hybrid case power dispatch - genset 4.

Figure 85 – Power demand, and power dispatch of the base case (non-hybrid) and the hybrid power system using the RB strategy and simulating the complete electric propulsion system, which includes the electrical power system, the electrical motors, drivetrain and a simplified vessel physics.

7 CONCLUSION

Vessels are essential for human society, performing a variety of tasks. Due to the different operating profiles and regulations, marine propulsion systems have to meet many performance criteria, including fuel consumption reduction to reduce operational costs and reduce emissions for climate change action and meet international regulations.

The hybridization of power systems can be a feasible solution for the mentioned challenges, allowing the flexibility to combine different power modes to meet operational demands based on different performance indices. However, the increase in power sources increases the number of system components and control complexity. Designing optimal energy management strategies can be challenging considering different situations, vessel types, objectives, and operational profiles. Given the challenges, it is essential to analyze the proposed hybrid solutions to justify the increase in cost and complexity. In this context, model-based simulations are extremely valuable for research, decision-making, and project design.

In this work, we focused on the development of power system simulators, including the development of individual models for the system components and their integration towards more comprehensive simulations, especially hybrid ones, to predict the behavior and propose control strategies to improve the performance of such systems. Next, we performed simulations to provide valuable information for the understanding of powertrain solutions and vessel hybridization.

To understand the vessel's power system, different architectures, hybrid power supply, batteries, and control strategies, we started with a literature review and studied models previously developed in Project 7 in chapters 2 and 3. Subsequently, chapter 4 described the modeling process, showing the results for the models developed for the main components of a diesel-electric propulsion system with a hybrid power supply for a PSV. In chapter 5, a multilevel power management structure was presented, and we developed reduced-order models and energy management strategies. The results that integrated all the models for the electric power system part and the energy management strategies were shown in chapter 6. We also analyzed different cases and variables, including energy efficiency, fuel consumption, emissions, genset running hours, and battery capacity fading, varying operational parameters and using data based on real operational profiles.

The methodology adopted in this work has shown promising results in the development of vessel powertrain models that are capable to produce information about different powertrain

aspects. Depending on the analysis, different models can be more appropriate, so a model set as that being built in Project 7 is essential for a comprehensive understanding of powertrains used in vessels. With model integration and the development of multilevel control strategies, we could perform simulations for the electric propulsion system and present several results. The models were either validated with data measured in real operations or compared with the scientific literature, as well as compared with well validated computational tools such as MATLAB/Simulink. We used a causal approach because it enables the representation of real-time systems.

The main contributions of this work include:

- The development of a generator set (genset) model and its validation with errors below 2% for fuel consumption, considering measured data from a project partner from the shipping industry. Using the measured data, we could also see that the engine velocity was kept within the expected limits. The system model has also shown a dynamic performance between acceptable limits regarding speed and power output for the different performed simulations.

- Through parameter identification, it was possible to increase the DC motor efficiency by up to 10%, considering the previous model implemented in Project 7 power system simulator.

- The development of a three-phase induction motor model, which has been compared with the asynchronous squirrel-cage model from MATLAB/Simulink library and showed small differences. Moreover, the results have shown excellent tracking performance for the rotor speed and flux control using the Sliding Mode Control (SMC), with the induction motor model combined with the drivetrain models and simplified vessel physics.

- The development of a battery system model. When comparing the battery cell model with results from the literature, the results have shown errors below 1% for comparisons of various battery states such as voltage, temperature, state of charge and state of health.

- Model reduction for genset and battery to allow faster optimization. When the genset is in operation supplying power to the grid, we could see that the model fit is accurate, with differences below 4% considering the transient behavior and below 2.5% for steady-state. Regarding the battery model reduction, the results show small differences when the current

is constant, with errors smaller than 2%. However, when there are fast load variations, the difference can increase to 8%.

- A multilevel power management control framework oriented for fuel consumption and emissions analysis was proposed based on the literature, including the implementation of strategies to control non-hybrid and hybrid power systems.

- We have shown that it was possible to reduce fuel consumption, emissions of CO_2 and PM, as well as genset running hours through strategic loading in a non-hybrid PSV configuration using data real operating profiles and considering different operational parameters. In general, increasing the genset loading ranges near the maximum 80%-100% brought the most significant benefits, except for the NO_x emissions which increased, thus requiring the consideration of an after-treatment system. In comparison with a base case, for a viable genset loading limit of 60%-80%, we observed reductions of: 5%-8% for fuel, 7%-8% for CO_2, 23%-30% for genset operating time, and 27%-32% for PM. The NO_x emissions decreased in small loads, up to 10%, and increased by 10% in higher loads. The genset redundancy had a negative and significant impact on all quantities of interest.

- We have shown that the hybridization through the introduction of a battery can bring additional benefits to the vessel's power system compared to the non-hybrid topology, except for the NO_x which increased and requires the after-treatment consideration. In comparison with the optimized non-hybrid operation, for a viable genset loading limit (60%-90%), we observed additional reductions of: 5%-6% for fuel, 5% for CO_2, 23%-27% for genset operating time, and 26%-27% for PM. The NO_x emissions decreased in small loads, up to 11% and increased by 9% in higher loads.

- The development of a representative response surface to model fuel consumption reductions based on genset loading limit, battery energy, power, DOD, and converter efficiency to help in the hybrid power system design and selection of operation parameters.

- Development of a 50 h power demand profile for a PSV to run high-frequency simulations with dynamical models based on actual vessel operations and the scientific literature.

- Through high-frequency simulations, the 50 h power profile, and different energy management strategies for the hybrid configurations, we have shown more battery benefits: fuel consumption, CO_2 and NO_x emission reductions around 10%, around 47% reduction

on PM emission and a 49% decrease on genset operating time. Furthermore, the power system efficiency rose above 3% for all hybrid cases. With a capacity fading extrapolation, we found that the battery could be used for around eight years if the mission profile was continuously repeated. The most significant benefits were observed for the DP part of the mission, followed by the loading in port and standby. In this case, the DP operation represented a large part of the mission, around 40% of the operation time;

- Simulating the vessel acceleration until the rated speed, we calculated an increase in efficiency of 10% comparing the non-hybrid and hybrid configurations with the complete electric propulsion system.

- Last, we published an article in the International Congress of Mechanical Engineering (COBEM) named simulation of hybrid power systems for vessels, showing the benefits of PSV hybridization with addition of Li-ion batteries. In addition, our group is working on another paper about the benefits of strategic loading and hybridization on vessel power systems that conveys results included in this dissertation to be submitted to an international journal.

7.1 RECOMMENDED FUTURE WORK

We intend to integrate the complete electric propulsion system described in this work into the TPN simulator and perform comprehensive high-frequency simulations. These calculations will test the flexibility of the models and robustness of the control strategies and conclusions we have drawn so far.

It is also worth looking into different power and energy management strategies, fuel cells, and power generation with alternative fuels in future works. These strategies can bring additional decrements in the environmental impacts of vessels, and the modeling framework established in this research can serve as a convenient, fast and inexpensive way of testing them and comparing with other solutions.

Finally, some additions to the models can make them more realistic and sophisticated. For example, the power dynamics could be added to the control strategies, spinning reserve constraints could be added to the optimization, and the models could consider the power ramps of generators and the start/stop time required by the gensets. This will allow deeper analyses and

would cover shorter time scale details of the behaviour of the systems, which are particularly relevant for highly transient operation stages, like DP.

REFERENCES

[1] UNFCCC, United Nations Framework Convention on Climate Change. The Paris Agreement. 2016. Disponível em: https://unfccc.int/process-and-meetings/the-paris-agreement/the-paris-agreement. Acesso em: 22 Fev. 2020.

[2] ALLEN, Myles et al. **Chapter 1 framing and context**. In: MASSON-DELMOTTE, Valery, ed., et al. Global warming of 1.5 °C. An IPCC special report on the impacts of global warming of 1.5 °C. 2018. Disponível em: https://www.ccardesa.org/knowledge-products/ipcc-special-report-global-warming-15-%C2%BAc-chapter-1-framing-and-context. Acesso em: 28 Jun. 2022.

[3] KALIKATZARAKIS, M. et al. R.R. Ship energy management for hybrid propulsion and power supply with shore charging. **Control Engineering Practice**, v. 76, p. 133–154, July, 2018.

[4] CRIPPA, M. et al. Fossil CO2 and GHG emissions of all world countries: report. 2019. Disponível em: http://publications.europa.eu/publication/manifestation_identifier/PUB_KJNA29849ENN. Acesso em: 22 Fev. 2020.

[5] IMO. International Maritime Organization. 3rd IMO GHG study. 2014. Disponível em: https://www.imo.org/en/OurWork/Environment/Pages/Greenhouse-Gas-Studies-2014.aspx: Acesso em : 23 Fev. 2020.

[6] CHUA, Liza Wan Yuan. A strategy for power management of electric hybrid marine power systems. 2019. Tese (Doutorado) — Nanyang Technological University, 2019. Disponível em: http://hdl.handle.net/10220/48078. Acesso em: 23 Fev. 2020.

[7] IMO. International Maritime Organization. Prevention of Air Pollution from Ships. 2021. Disponível em: https://www.imo.org/en/OurWork/Environment/Pages/Air-Pollution.aspx. Acesso em: 08 Out. 2020.

[8] IMO. International Maritime Organization. Greenhouse Gas Emissions. 2020. Disponível em: http://www.imo.org/en/OurWork/Environment/PollutionPrevention/AirPollution/Pages/GHG-Emissions.aspx. Acesso em: 23 Fev. 2020.

[9] RAENG, Royal academy of engineering. Future ship powering options Exploring alternative methods of ship propulsion. 2013. Disponível em: https://www.raeng.org.uk/publications/reports/future-ship-powering-options. Acesso em: 23 Fev. 2020.

[10] KELLY, S; EATON, C. Rising prices show tighter supplies of cleaner fuel for global shipping. 2020. Disponível em: https://www.reuters.com/article/us-shipping-imo-fuel/rising-prices-show-tighter-supplies-of-cleaner-fuel-for-global-shipping-idUSKBN1Z82G4. Acesso em: 23 Fev. 2020.

[11] CHUA, Liza W. Y. et al. Implementation of optimization-based power management for all-electric hybrid vessels. **IEEE**, v. 6, p. 74339–74354, 2018.

[12] BLOMGREN, George E. The development and future of lithium ion batteries. **Journal of The Electrochemical Society**, v. 164, n. 1, p. A5019–A5025, 2017.

[13] MIYAZAKI, Michel R . et al. Reduction of fuel consumption on hybrid marine power plants by strategic loading with energy storage devices. **IEEE Transactions on Power Systems**, v. 3, p. 207–217, Dec., 2016.

[14] GEERTSMA, R.D. et al. Design and control of hybrid power and propulsion systems for smart ships: a review of developments. **Applied Energy**, v. 194, p. 30–54, May 2017.

[15] VALERA-GARCIA, Juan Jose; ATUTXA-LEKUE, Inigo. On the optimal design of hybrid-electric power systems for offshore vessels. **IEEE Transactions on Transportation Electrification**, v. 5, n. 1, p. 324–334, Mar. 2019.

[16] EMSA. Electrical energy storage for ships. 2020.

[17] CBO. Wärtsilä and CBO to partner in Latin America's first hybrid vessel upgrade project. 2020. Disponível em: https://www.grupocbo.com.br/en/blog/wartsila-and-cbo-will-partner-latin-americas-first-hybrid-vessel-upgrade-project. Acesso em: 23 Ago. 2022.

[18] YUAN, Liza Chua Wan. Et al. Optimizing fuel savings and power system reliability for all-electric hybrid vessels using model predictive control. In: IEEE INTERNATIONAL CONFERENCE ON ADVANCED INTELLIGENT MECHATRONICS (AIM). **IEEE**, 2017. p.

1532–1537. Disponível em: http://ieeexplore.ieee.org/document/8014236/. Acesso em: 29 Jun. 2022.

[19] WU, Peng; PARTRIDGE, Julius; BUCKNAL L, Richard. Cost-effective reinforcement learning energy management for plug-in hybrid fuel cell and battery ships. **Applied Energy**, v. 275, p. 115258, Oct., 2020.

[20] PERALTA P., César. et al. Evaluation of the CO2 emissions reduction potential of li-ion batteries in ship power systems. **Energies**, v. 12, n. 3, p. 375, Jan. 2019.

[21] GUZZELLA, Lino; SCIARRETTA, Antonio. **Vehicle propulsion systems**. Heidelberg: Springer, 2013. Disponível em: http://link.springer.com/10.1007/978-3-642-35913-2. Acesso em: 27 Jun. 2022.

[22] HOU, Jun; SUN, Jing; HOFMANN, Heath F. Mitigating power fluctuations in electric ship propulsion with hybrid energy storage system: design and analysis. **IEEE Journal of Oceanic Engineering**, v. 43, n. 1, p. 93–107, Jan. 2018.

[23] MIYAZAKI, Michel R. et al. Hybrid modeling of strategic loading of a marine hybrid power plant with experimental validation. **IEEE Access**, v. 4, p. 8793–8804, 2016.

[24] PURACA, Rodolfo Curci; CARMO, Bruno Souza. **Hybrid power system dynamical model developed by Project 7**: activity report. Sao Paulo, RCGI, 2019.

[25] ESFANDIARI, Ramin S. **Numerical methods for engineers and scientists using MATLAB.** 2.ed..: CRC Press, 2017.

[26] SCIARRETTA, A. et. al. Control benchmark on the energy management of a plug-in hybrid electric vehicle. **Control Engineering Practice**, v. 29, p. 287–298, Aug.. 2014.

[27] VASQUEZ, Cristian Andres Morales. A methodology to select the electric propulsion system for Platform Supply Vessels (PSV). 2014. Tese (Doutorado) — Universidade de Sao Paulo, 2014. Disponível em: http://www.teses.usp.br/teses/disponiveis/3/3135/tde-26122014-164655/. Acesso em: 28 Jun. 2022.

[28] INTERREG. Fact sheet N ° 2: Diesel-electric propulsion. 2019. Disponível em: https://www.interreg-danube.eu/uploads/media/approved_project_public/0001/29/915654de0400ca6d1a605b5c18abf6bd186ef916.pdf. Acesso em: 25 Ago. 2022.

[29] NIU, Hai-chun; ZHAO, Mei-lian; QIN, Fu-zhen. Study on the Ship Electric Propulsion System and its Development. In: 7th International Conference on Applied Science, Engineering and Technology (ICASET 2017). **Atlantis press**, 2017. volume 112. Disponível em: https://www.atlantis-press.com/article/25876778.pdf. Acesso em: 25 Ago. 2022.

[30] ADNANES, A. K. Maritime Electrical Installations and Diesel Electric Propulsion. **ABB AS Marine and Turbocharging Tutorial Report**, 2003. Disponível em: http://citeseerx.ist.psu.edu/viewdoc/download?doi=10.1.1.372.301&rep=rep1&type=pdf. Acesso em: 25 Ago. 2022.

[31] AL-FALAHI, Monaaf, et. al . Ac ship microgrids: control and power management optimization. **Energies**, v. 11, n. 6, p. 1458, June, 2018.

[32] RADAN, Damir. **Integrared control of marine electrical power systems**. 2008. 231 p. Tese (Doutorado) — Norwegian University of Science and Technology, Norway, 2008.

[33] DIAMANTIS, G. Simulation of a ship propulsion system with DTC driving scheme. In: INTERNATIONAL CONFERENCE ON POWER ELECTRONICS, MACHINES AND DRIVES. 2., Edinburgh, UK, 2004. **PEND 2004**. London: Institution of Electrical Engineers, 2004. v. 2, p. 562-567. Disponível em: https://digital-library.theiet.org/content/conferences/10.1049/cp_20040349. Acesso em: 30 Jun. 2022.

[34] HEIDE, Brandstädter. **Sliding mode control of electromechanical systems**. 2008. 140 p. Tese (Doutorado) - Technische Universität München, München, DE, 2008.

[35] INAL, Omer Berkehan; CHARPENTIER, Jean-Frederic; DENIZ, Cengiz. Hybrid power and propulsion systems for ships: current status and future challenges. **Renewable and Sustainable Energy Reviews**, v. 156, p. 1-15, Mar. 2022.

[36] MAURO, Francesco et al. Design of hybrid-electric megayachts: the impact of operative profile and smart berthing infrastructures. **Journal of Marine Science and Engineering**, v. 9, n. 2, p. 186, Feb. 2021.

[37] ABELLEIRA, Maria Teresa Troncoso. Batteries for marine applications. Norwegian University of Science and Technology (NTNU). 2013. p. 66. Disponível em: https://ntnuopen.ntnu.no/ntnu-xmlui/bitstream/handle/11250/238654/649652_FULLTEXT01.pdf?sequence=1. Acesso em 30 Jun. 2022.

[38] LINDTJØRN, John Olav et al. Demonstrating the benefits of advanced power systems and energy storage for DP vessels. In: DYNAMIC POSITIONING CONFERENCE, Houston. **Proceedings**. 2014. Disponível em: https://dynamic-positioning.com/proceedings/dp2014/Green_initiatives_Lindtjorn.pdf. Acesso em: 30 Jun. 2022. p. 24.

[39] SKJONG, Espen, et al. Past, present, and future challenges of the marine vessel's electrical power system. **IEEE Transactions on Transportation Electrification**, v. 2, n. 4, p. 522–537, Dec. 2016.

[40] ALI, Ahmed; SOFFKER, Dirk. Towards optimal power management of hybrid electric vehicles in real-time: a review on methods, challenges, and state-of-the-art solutions. **Energies**, v. 11, n. 3, p. 476, Feb. 2018.

[41] ZHANG, Zehui; GUAN, Cong; LIU, Zhiyong. Real-time optimization energy management strategy for fuel cell hybrid ships considering power sources degradation. **IEEE Access**, v. 8, p. 1-14, Apr. 2020.

[42] DIJU, Gao et al. Control strategy of hybrid electric ship based on improved fuzzy logic threshold. In: 29th CHINESE CONTROL AND DECISION CONFERENCE (CDDC). Chongqing, China. **IEEE**. 2017. p. 6995–7000.

[43] NATSHEH, Emad M; ALBARBAR, Alhussein. Hybrid power systems energy controller based on neural network and fuzzy logic. **Smart Grid and Renewable Energy**, v. 4, n. 2, p.187–197, 2013.

[44] BØ, Torstein Ingebrigtsen; JOHANSEN, Tor Arne. Battery power smoothing control in a marine electric power plant using nonlinear model predictive control. **IEEE Transactions on Control Systems Technology**, v. 25, n. 4, p. 1449–1456, July, 2017.

[45] PARK, Hyeongjun et al. Real-time model predictive control for shipboard power management using the IPA-SQP approach. **IEEE Transactions on Control Systems Technology**, v. 23, n. 6, p. 2129–2143, Nov. 2015.

[46] GAO, Diju et al. An energy optimization strategy for hybrid power ships under load uncertainty based on load power prediction and improved NSGA-II algorithm. **Energies**, v. 11, n. 7, p. 1699, July, 2018.

[47] THANH LONG, Vu. Power management for electric tugboats through operating load estimation. **IEEE Transactions on Control Systems Technology**, v. 23, n. 6, p. 2375–2382, Nov. 2015.

[48] YING, Bai; DALI, Wang. Fundamentals of fuzzy logic control: fuzzy sets, fuzzy rules and defuzzifications. In: **Advanced Fuzzy Logic Technologies in Industrial Applications**. London: Springer, 2006. (Advances in Industrial Control), p. 17–36. Disponível em: http://link.springer.com/10.1007/978-1-84628-469-4_2. Acesso em: 29 Jun. 2022.

[49] SERRAO, L. et al. Open issues in supervisory control of hybrid electric vehicles: a unified approach using optimal control methods. **Oil & Gas Science and Technology - Revue d'IFP Energies Nouvelles**, v. 68, n. 1, p. 23–33, Jan. 2013.

[50] GEERING, H. P. **Optimal control with engineering applications**. Berlin: Springer, 2007.

[51] NÜESCH, Tobias et al. Equivalent consumption minimization strategy for the control of real driving NOx emissions of a Diesel hybrid electric vehicle. **Energies**, v. 7, n. 5, p. 3148–3178, May 2014.

[52] CAMPOS, Roberto Dacio de Arruda; JUNIOR, Silvio de Oliveira. **Modelagem e simulação de um Sistema híbrido de potência aplicado a um navio de suporte a plataformas**. São Paulo: EPUSP, 2017. (Partial report of the course PME 2600-integrated Project III).

[53] BELL, Ian H. et al. Pure and pseudo-pure fluid thermophysical property evaluation and the open-source thermophysical property library coolprop. **Industrial & Engineering Chemistry Research**, v. 53, n. 6, p. 2498–2508, 2014. Disponível em: http://pubs.acs.org/doi/abs/10.1021/ie4033999. Acesso em: 30 Jun. 2022.

[54] MARTIN, Chris. HOT Thermodynamic tools for MATLAB: MATLAB central file exchange. 2017. Disponível em: https://www.mathworks.com/matlabcentral/fileexchange/26430-hot-thermodynamic-tools-for-matlab. Acesso em: 30 Jun. 2022.

[55] TUFFAHA, Mutaz; GRAVDAHL, Jan T. Control-oriented model of a generating set comprising a diesel engine and a synchronous generator. **Modeling, Identification and Control**: A Norwegian Research Bulletin, v. 36, n. 4, p. 199–214, 2015.

[56] SYVERUD, Tron Hansen. Modeling and control of a DC-grid hybrid power system with battery and variable speed diesel generators. Norwegian University of Science Technology (NTNU), 2016. p. 94. Disponível em: https://ntnuopen.ntnu.no/ntnu-xmlui/handle/11250/2404021. Acesso em: 30 jun. 2022.

[57] QI, Fang, et al. Motor handbook: iSEA power electronics and electrical drives, 2019. 110 p.

[58] BASSHAM, Bobby A. **An evaluation of electric motors for ship propulsion**. 2003. Tese (Doutorado) - Naval Postgraduate School, Monterey, California, 2003.

[59] KIRTLEY, James L.; BANERJEE, Arijit; ENGLEBRETSON, Steven. Motors for ship propulsion. **Proceedings of the IEEE**, v. 103, n. 12, p. 2320–2332, Dec. 2015.

[60] WEG Industries. Características e especificações de motores de corrente continua e conversores CA/CC. 2020 (Technical specifications and selection of motors and converters).

[61] SEVINC, A. Model parameters of electric motors for desired operating conditions. **Advances in Electrical and Computer Engineering**, v. 19, n. 2, p. 29–36, 2019.

[62] IMO. International Maritime Organization. Module 4: Ship Board Energy. In: IMO Train the Trainer (TTT) Course on Energy Efficient Ship Operation Trainers' Manual. London: IMO, 2016.

[63] VADIM, Utkin; JURGEN, Guldner; JINGXIN, Shi. **Sliding mode control in electromehcanical systems**. London, UK: Taylor & Francis, 1999. 325 p.

[64] RIGATOS, Gerasimos; SIANO, Pierluigi; ABBASZADEH, Masoud. Nonlinear optimal control for ship propulsion systems comprising an induction motor and a drivetrain. **Proceedings**

of the Institution of Mechanical Engineers: Journal of Engineering for the Maritime Environment, v. 234, n. 2, part. M. p. 409–425, May, 2020.

[65] PLETT, Gregory L. **Battery management systems: battery Modeling**. Norwood: Artech House, 2015. v. 1.

[66] PEREZ, Hector Eduardo et al. Optimal charging of li-ion batteries with coupled electro-thermal-aging dynamics. **IEEE Transactions on Vehicular Technology**, v. 66, n. 9, p. 7761–7770, Sept. 2017.

[67] MOUSAVI, G. S. M.; NIKDEL, M. Various battery models for various simulation studies and applications. **Renewable and Sustainable Energy Reviews**, v. 32, p. 477–485, Apr. 2014.

[68] TREMBLAY, Olivier; DESSAINT, Louis-A.; DEKKICHE, Abdel-Illah. A generic battery model for the dynamic simulation of hybrid electric vehicles. In: IEEE VEHICLE POWER AND PROPULSION CONFERENCE, 2017. **Proceedings IEEE**. 2007. p. 284–289. Disponível em: http://ieeexplore.ieee.org/document/4544139/. Acesso em: 30 Jun. 2022.

[69] BØ, Torstein Ingebrigtsen. Dynamic Model Predictive Control for Load Sharing in Electric Power Plants for Ships. 2012. Tese (Doutorado) — Norwegian University of Science and Technology (NTNU), Trondheim, Norway, 2012.

[70] YE, Baoyu. A four-quadrant thrust estimation scheme based on chebyshev fit and experiment of ship model. **The Open Mechanical Engineering Journal**, v. 6, n. 1, p. 148–154, Dec. 2012.

[71] ULSTEIN. Giving a second life to laid-up platform supply vessels. 2022. Disponível em: https://ulstein.com/giving-a-second-life-to-laid-up-platform-supply-vessels. Acesso em: 25 Ago. 2022.

[72] HEYWOOD, J.; HEYWOOD, P.J. **Internal combustion engine fundamentals**. Singapore: Mc Graw Hill International, 1988. (Automative technology series).

[73] GUERRERO, Josep M. et al. Shipboard microgrids: maritime islanded power systems technologies. In: INTERNATIONAL EXHIBITION AND CONFERENCE FOR POWER ELECTRONICS, INTELLIGENT MOTION, RENEWABLE ENERGY AND ENERGY MANAGEMENT, Shanghai, China, 2016. **PCIM Asia 2016**. Berlin, Germany: VDE, 2016.

[74] WÄRTSILÄ. **Wärtsilä 34DF product guide**. 2015. Marine engine performance maps. Disponível em: https://www.wartsila.com/marine/build/marine-brochures-pardot-redirects/engines/dual-fuel-engines/wartsila-34df-product-guide. Acesso em: 27 Jun. 21.

[75] GE. Technical description: container genset JGC 620 GS-S.L. 2009.

[76] KIM, Sang-Hoon. Alternating current motors. **Electric Motor Control**. Amsterdam, Netherlands: Elsevier, 2017. p. 95–152.

[77] IITH. Indian Institute of Technology Hyderabad. 2.5 MW doubly fed induction generator. 2020. Disponível em: https://www.iith.ac.in/~seshadri/Data/2p5-DFIG-Data.pdf. Acesso em: 22 Out. 2020.

[78] LIN, Xinfan, et al. A lumped-parameter electro-thermal model for cylindrical batteries. **Journal of Power Sources**, v. 257, p. 1–11, July, 2014.

[79] WANG, John, et al. Cycle-life model for graphite-LiFePO4 cells. **Journal of Power Sources**, v. 196, n. 8, p. 3942–3948, Apr. 2011.

[80] LIU, Kailong et al. Charging pattern optimization for Lithium-ion batteries with an electrothermal-aging model. **IEEE Transactions on Industrial Informatics**, v. 14, n. 12, p. 5463–5474, Dec. 2018.

[81] CHRISTEN, Thomas. Ragone plots and discharge efficiency-power relations of electric and thermal energy storage devices. **Journal of Energy Storage**, v. 27, p. 1-7, Feb., 2020.

[82] ARORA, Jasbir. **Introduction to optimum design**. 4. ed. London, UK: Academic Press, 2016.

[83] HANSEN, Jan Fredrik. Modelling and control of marine power systems. 2000. 119 p. Tese (Doutorado) - Norwegian University of Science and Technology (NTNU), Trondheim, Norway, 2000.

[84] AMERICAN BUREAU OF SHIPPING (ABS). Guide for dynamic positioning systems. 2021. Disponível em: https://ww2.eagle.org/content/dam/eagle/rules-and-guides/current/other/191_dynamic_positioning_systems/dps-guide-oct21.pdf. Acesso em: 22 Out. 2020.

[85] GARG, Kamal; SHAH, Saurabh. Dynamic positioning power plant system reliability and design. In: PETROLEUM AND CHEMICAL INDUSTRY CONFERENCE EUROPE CONFERENCE PROCEEDINGS, Italy, 2011. PCIC EUROPE 2011. Piscataway, NJ IEEE 2011. p. 11. Disponível em: https://cmscdn.selinc.com/assets/Literature/Publications/Technical%20Papers/6472_DynamicPositioning_KG_20110317_Web.pdf?v=20180604-22562. Acesso em: 30 Jun. 2022.

[86] ZHU, Yuanqing, et al. Application and development of selective catalytic reduction technology for marine low-speed diesel engine: trade-off among high sulfur fuel, high thermal efficiency, and low pollution emission. Atmosphere, v. 13, n. 5, p. 731, May, 2022.

[87] MYERS, Raymond H. **Response Surface Methodology**. Hoboken: Wiley, 2016. 855 p.

[88] SLOTINE, J. J. E.; LI, Weiping. **Applied nonlinear control**. Englewood Cliffs, N.J: Prentice Hall, 1991.

[89] FOSSEN, Thor I.; FOSS, Bjarne A. Sliding control of MIMO nonlinear systems. **Modeling, Identification and Control**: a Norwegian Research Bulletin, v. 12, n. 3, p. 129–138, 1991.

APPENDIX A – SMC APPLIED TO THE THREE-PHASE INDUCTION MOTOR

In this appendix, we will briefly describe the sliding mode control (SMC) theory applied to control the three-phase induction motor model in chapter 4.3. The SMC control technique allows the development of a control law that enforces all system trajectories to converge on a surface, the sliding surface, defined by an intermediate variable s, contained in the state space. Nonlinear n^{th}-order dynamics are replaced by simpler equivalent 1^{st}-order ones, and controlling the transformed problem implies controlling the original one. Excellent performance can be achieved in the presence of bounded uncertainties at the price of high control activity [88].

In the powertrain simulations, the rotor angular speed ω_m is controlled, but flux control is also required to allow operational profiles in the constant torque and weakening field regions. Before deriving the control law, the system will be rewritten as a square system, in terms of the controlled variables $\mathbf{y} = [\omega_m, \lambda]^T$, where $\lambda = \lambda_\alpha^2 + \lambda_\beta^2$ is the square flux:

$$\ddot{\mathbf{y}} = \mathbf{f}^*(\mathbf{x}) + \mathbf{g}^*(\mathbf{x})\mathbf{u}. \tag{117}$$

The functions $\mathbf{f}^*(\mathbf{x})$ and $\mathbf{g}^*(\mathbf{x})$ are defined as

$$\mathbf{f}^*(\mathbf{x}) = \begin{bmatrix} \frac{\mu}{J_{eq}}(f_2 x_3 + x_2 f_3 - f_1 x_4 - x_1 f_4) - \frac{B_{eq}}{J_{eq}} f_5 - \frac{1}{J_{eq}} \frac{\dot{T}_{prop}}{red} \\ 2\{f_3^2 + f_4^2 + x_3[\eta f_3 - N_r(f_5 x_4 + x_5 f_4) + \eta L_h f_1] + x_4[-\eta f_4 + \\ + N_r(f_5 x_3 + x_5 f_3) + \eta L_h f_2]\} \end{bmatrix} \tag{118}$$

and

$$\mathbf{g}^*(\mathbf{x}) = \begin{bmatrix} -\frac{\mu x_4}{J_{eq}\sigma L_s} & \frac{\mu x_3}{J_{eq}\sigma L_s} \\ \frac{2x_3\eta L_h}{\sigma L_s} & \frac{2x_4\eta L_h}{\sigma L_s} \end{bmatrix}. \tag{119}$$

The sliding surface is defined below through the s variable. Two variables are controlled, ω_m and λ, with relative degree of two for each one, so $j = 1, 2$:

$$s_j = \frac{de_j}{dt} + \tau_j e_j, \tag{120}$$

$$e_j = y_j - y_{j,d}. \tag{121}$$

The symbol e is the error, y_j is the controlled variable and $y_{j,d}$ is the desired trajectory. The parameter τ_j specifies the control bandwidth. Taking the derivative of s_j, and defining a virtual reference vector α_d, the first-order equivalent systems are obtained as

$$\dot{s}_j = y_j^{(r_j)} - \alpha_{d,j}. \tag{122}$$

The complete control law for the multiple-input-multiple-output (MIMO) system containing equivalent (discontinuous) terms is presented below, as described in [89],

$$\mathbf{u} = (\hat{\mathbf{g}}^*(\mathbf{x}))^{-1}[\boldsymbol{\alpha}_d - \hat{\mathbf{f}}^*(\mathbf{x}) - \mathbf{K}sat(\mathbf{z})], \tag{123}$$

where $z_j = s_j/\phi_j$, with ϕ_j representing the boundary layer thickness on the sliding surface. The symbol $\mathbf{K}$ represents a diagonal matrix with control gains k_j and sat defines the saturation function. The functions $\hat{\mathbf{g}}^*(\mathbf{x})$ and $\hat{\mathbf{f}}^*(\mathbf{x})$ are approximations of the functions defined in (118) and (119), which help to define upper bounds for parametric deviations and disturbances in the system.

The term $sat(\mathbf{z})$ is a continuous approximation of the switching control law to attenuate chattering, which is a high-frequency switching control signal sent to the actuators as input [88]. Controlled chattering should not be a serious problem for the IM, as the inverters, commonly used in the electric drive system, work with high-frequency pulse generation.

Besides the fluxes, the other terms in $\mathbf{g}^*$ represent the construction parameters of the IM, considered here as known with accuracy. Considering full state estimation with accuracy, the function $\mathbf{g}^*$ does not present considerable deviations to be taken into account. However, $\mathbf{f}^*$ contains terms such as the load torque (propeller torque reduced by the gearbox) and its derivative. The load torque can be hard to estimate with accuracy due to the complex physics of the sea environment, therefore gain margins can be studied in variations of $\mathbf{f}^*$.

Considering only deviations in $\mathbf{f}^*$, the sliding condition is satisfied, leading the error to zero if the gains $k_j \geq k'_j$, $\forall_j$, where $\mathbf{k}'$ satisfies

$$\mathbf{k}' = \boldsymbol{\delta} + \boldsymbol{\nu}, \tag{124}$$

in which $\boldsymbol{\nu}$ represents strictly positive constants ν_j associated with the control effort to achieve the boundary layer, and $\boldsymbol{\delta}$ expresses the difference between the approximate $\hat{\mathbf{f}}^*$ and the true $\mathbf{f}^*$, for each j as

$$\left|\hat{\mathbf{f}}^*(\mathbf{x}) - \mathbf{f}^*(\mathbf{x})\right| \leq \boldsymbol{\delta}. \tag{125}$$

APPENDIX B – PUBLICATION IN CONFERENCE PROCEEDINGS

The following paper was presented in the mechatronics and automation control session at the 26th International Congress of Mechanical Engineering and was published in the conference proceedings.

COBEM 2021 26th International Congress of Mechanical Engineering
November 22-26, 2021, Virtual Congress, Brazil
ABCM Associação Brasileira de Engenharia e Ciências Mecânicas

COB-2021-0365
SIMULATION OF HYBRID POWER SYSTEMS FOR VESSELS

Crisley de Souza Peixoto
Bruno Souza Carmo
Department of Mechanical Engineering, Escola Politécnica, University of São Paulo. Av. Prof. Mello Moraes, 2231, Cidade Universitária, São Paulo-SP, Brazil. 05508-030
crisley.peixoto@usp.br
bruno.carmo@usp.br

Abstract. *Climate concerns, regulations, and fuel costs are driving higher efficiency designs in the shipping industry. Research works suggest that hybrid power systems can be a viable option to reduce fuel consumption and emissions. However, more studies are required to analyze its net gains in different applications. In this work, numerical simulations of power systems are performed in a causal approach, including a non-hybrid or base case and a hybrid case, for a diesel-electric Platform Supply Vessel (PSV). Dynamical and static models are considered for the power sources, namely, diesel generator sets (gensets) and a lithium-ion battery pack connected through an AC electrical network. For the Energy Management System (EMS) of the base case, an optimization of gensets is performed, and for the hybrid case, a rule-based control combined with an optimization of the generators is considered. The analysis shows, for the case study, that the greatest potential for battery usage is achieved in near port operations. Cleaner operations were allowed in these regions due to the increase in energy efficiency and the disconnection of generators. A fuel consumption reduction of 6.35% and CO_2 emission reductions of 5.81% were achieved for the complete mission. Also, an increase of 1.73% in the overall energy efficiency was accomplished.*

Keywords: *hybrid power systems, marine vessels, energy efficiency, emission reductions, lithium-ion batteries*

1. INTRODUCTION

The shipping industry represents the carriage of 90% of the world trade, with projected growth in the following years (Kalikatzarakis *et al.*, 2018). However, the ship operation is responsible for 1.8% of the total 37.9 Gt of CO_2 emissions worldwide, comparable to the 8th nation on the ranking of top-emitting countries (Crippa *et al.*, 2019). Due to climate concerns, the International Maritime Organization (IMO) strategy is to reduce GHG emissions from vessels, requiring more efficient designs, and cutting CO_2 emissions by at least 40% by 2030, compared to 2008. Fuel costs are another driver for change in the shipping industry, accounting for as much as 50% to 60% of all operational costs (RAENG, 2020).

Hybrid technology can be a viable option to adapt vessels and for new designs. The automotive industry is already employing hybrid technologies successfully. For the shipping industry, it also looks promising. Research works suggest that reductions could achieve up to 10%–35% in fuel consumption and emissions (Geertsma *et al.*, 2017). In this context, Platform Supply Vessels (PSVs), a category of Offshore Support Vessels (OSVs) used in oil and gas platforms, are among the viable options to receive hybrid power supply due to their operational profile (Garcia *et al.*, 2019).

Some studies have been showing the potential for fuel savings, reduction of CO_2, GHG gases, and other components. Miyazaki *et al.* (2016) proposed a power system model to calculate the fuel savings and emission reduction potential of a ship hybrid powertrain with a battery module. A fuel consumption reduction of approximately 45% and a NOx emission reduction of 85.6% were achieved. However, neither the load demand nor the CO_2 was described.

Peralta *et al.* (2019) analyzed the reduction of CO_2 emissions using a hybrid power system for a PSV and performed a sensitivity analysis. The energy dispatch was optimized, considering the cost of the energy sources. Reductions in CO_2 emissions of up to 8.7% were obtained with the addition of auxiliary diesel engines and batteries. For a combination of generators and a battery, a reduction in emissions of 7.4% was achieved. The optimization methodology and the models were not discussed in detail. Besides, the optimization is global, requiring the complete load profile, which is interesting for setting benchmarks. However, in a real situation, a causal approach is necessary.

Improving the energy management of a power system is very important to increase energy efficiency. Approaches for control strategies in energy management systems (EMS) include heuristic, based on rules or fuzzy logic, optimal and predictive (Geertsma *et al.*, 2017). In the works of Kalikatzarakis *et al.* (2018) and Chua *et al.* (2018), the formulations of EMS are described, and different options are compared for hybrid tugs. However, non-hybrid cases are not considered. In addition, the authors did not study the combination of rule-based strategies and the optimization of generators. Such a study can provide a more conservative perspective of the gains of hybrid solutions.

The hybridization of power systems allows the flexibility to combine different power modes; however, increasing power sources increases the number of systems and control complexity. The majority of works found in the literature define EMS to improve the power dispatch of Tugs and Ferries (Kalikatzarakis *et al.*, 2018; Chua *et al.*, 2018; Chua Wan Yuan *et al.*, 2017; Zhang *et al.*, 2020). In general, PSVs have more power sources and demand more power than Tugs and ferries, increasing the EMS design complexity for this class of vessels.

The objective of this work is to compare hybrid and non-hybrid power systems for a diesel-electric PSV. With this, we intend to contribute to the understanding of vessel hybridization, including the behavior of the powertrain and improvements in energy efficiency, which can lead to fuel economy and emission reduction. We will follow a causal approach for the numerical simulations, considering dynamical models and EMS that enable strategic power dispatch.

2. SYSTEM DESCRIPTION AND MODELING

In this study, we consider two power system topologies for a PSV: a base case, which is a non-hybrid design, and a hybrid power system, which considers the addition of a Li-ion battery to the base case. The base case power system comprises four equal diesel generator sets (gensets) with 1700 kW of electrical power each, resulting in 6800 kW. For the hybrid case, the same number of gensets was considered and we included a battery pack of Lithium Iron Phosphate ($LiFePO_4$/LFP) of nominal capacity and power of 1000 kWh and 1000 kW, respectively, resulting in 7800 kW.

The models presented here combine static and dynamic formulations, described by algebraic (AE) and ordinary differential equations (ODEs), respectively. The ODEs are solved using Runge-Kutta methods. The models and energy management strategies were implemented and simulated in MATLAB following the causal approach. The optimization of the generators was performed using Casadi, through the interior point method. The gensets and batteries are connected through a static electrical network, which accounts only for power balance, considering the conservation of energy. The battery converter model considers only a constant efficiency, whose symbol is η_c.

2.1 Mission profile

The mission profile in Fig. 1 is an adaptation of results found in the literature. To obtain this curve, the power demand in Peralta *et al.* (2019) was normalized by the nominal installed power of the four equal gensets (total of 7400 kW) and then multiplied by the nominal power installed of the four gensets studied in this work (total of 6800 kW). Then, white noise with small amplitude was added to represent fast oscillations of the load demand. Also, the mission time has been reduced by approximately 100 times, to enable faster simulations.

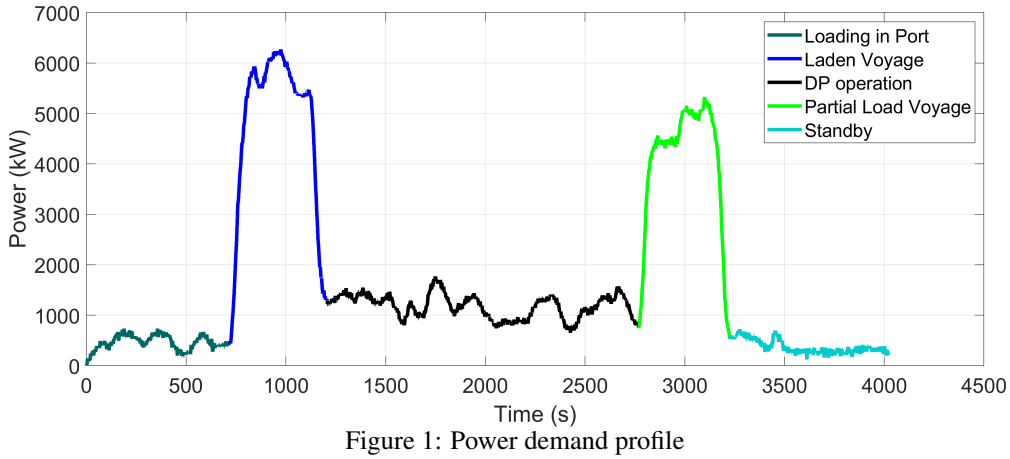

Figure 1: Power demand profile

The power demand in the mission is divided into five parts, starting with the loading in port, where the ship is loaded with goods. In the Laden Voyage, the ship travels fully loaded heading to the platform. When it stops, given appropriate conditions, the ship starts the Dynamical Positioning (DP), in which the forces acting on the vessel are counterbalanced by the thrusters to keep the ship at a defined position. After the DP, the ship travels back to the port with only part of the load, defining the partial load voyage. When the ship arrives near the port area, it can wait for a docking space to be available (standby).

2.2 Engine-generator set

A diesel engine-generator set model has been developed adapting the methodology presented in the work of Kalikatzarakis *et al.* (2018). A steady-state electrical model, based on a simplified per-phase circuit was considered for the

synchronous generator, omitting the Automatic Voltage Generator (AVR). The generator per-phase voltage u_g was defined as proportional to the engine speed ω_{dg},

$$u_g(t) = u_{g,nom}\frac{\omega_{dg}(t)}{\omega_{dg,nom}(t)}, \tag{1}$$

where its rate of change is determined by the nominal per-phase voltage $u_{g,nom}$ and engine speed $\omega_{dg,nom}$. The electrical frequency f is determined through the engine speed and the number of poles of the electrical motor P_p,

$$f = \omega_{dg}\frac{Pp}{4\pi}. \tag{2}$$

The electrical power demand $P_{g,el}$ is translated in a current demand in the terminals of the generator i_g. The active power is defined as:

$$P_{g,el} = 3u_g(t)i_g(t)\cos(f_p) \tag{3}$$

in which $\cos(f_p)$ is the power factor. Considering only friction and copper losses, the generator losses can be written as

$$P_{g,loss}(t) = P_{g,nom}c_f + i_g(t)^2 r_g, \tag{4}$$

where c_f is the friction rate and r_g is the resistance of the electrical motor per-phase. The mechanical load P_g due to the electrical demand can be defined as

$$P_g(t) = P_{g,el}(t) + P_{g,loss}(t), \tag{5}$$

while the torque load is determined through the power and rotational speed of the engine, as in

$$Mg(t) = \frac{P_g(t)}{\omega_{dg}(t)}. \tag{6}$$

A governor is required for the generator to regulate the fuel injection and control its angular speed. The rotation dynamics is described by

$$\frac{d\omega_{dg}}{dt} = \frac{M_{dg} - M_g}{J_{dg}}. \tag{7}$$

The variable M_{dg} is the engine torque obtained through the fuel combustion, and J_{dg} represents the generator moment of inertia. A polynomial fit was produced to represent the relation between the fuel consumption of the generator and the torque,

$$M_{dg} = a_0 + a_1\dot{m}_{f,dg} + a_2\dot{m}_{f,dg}^2 + a_3\dot{m}_{f,dg}^3 + a_4\dot{m}_{f,dg}^4, \tag{8}$$

in which the values a_i, with $i = 1, .., 4$, are polynomial coefficients. To control the engine speed an anti-windup PI control was implemented. The fuel to be injected was determined through

$$\dot{m}_{f,dg} = k_p(\omega_{dg,ref} - \omega_{dg}(t)) + k_i\int_0^t(\omega_{dg,ref} - \omega_{dg}(t))dt, \tag{9}$$

where the proportional and integral gains of the controller are k_p, and k_i, respectively, and $\omega_{dg,ref}$ is the velocity reference.

The genset model considers that the power demand can be supplied by the generator as fast as it is required and the EMS must determine the proper power references. The dynamics are handled by the engine speed. To account for the CO_2 emissions, a static model was developed through a polynomial fit,

$$\dot{m}_{\mathrm{CO_2}} = c_0 + c_1 P_{g,el}. \tag{10}$$

The model receives the electrical power output of the generator $P_{g,el}$ as input and gives as output the mass flow rate of carbon dioxide, $\dot{m}_{\mathrm{CO_2}}$.

Since it is necessary to maintain the grid frequency in 60 Hz, the speed reference is set to be 1800 rpm and the engine speed will be regulated through the governor to seek this value. Therefore, a constant engine speed is a reasonable assumption.

2.3 Energy storage system – battery

The battery model considered in this work is based on a second-order Thevenin equivalent circuit for a lithium-iron-phosphate ($LiFePO_4$/LFP) cell. The structure of the model was mainly based on the work of Perez *et al.* (2017). Particularly, the LFP electrical and thermal performances have led to its use in maritime applications as mentioned in Kalikatzarakis *et al.* (2018).

2.3.1 Electrical Model

The circuit model comprises an open circuit voltage V_{OC}, function of the state of charge (SOC), a series ohmic resistor R_0, and two RC pairs R_1, C_1, R_2, C_2, which are functions of the SOC and the cell temperature. The cell temperature was considered constant and equal to 298.15 K. The variable $I(t)$ defines the current running through the battery (positive for discharging and negative for charging) and C_{bat} is the nominal capacity. The voltages across the two RC pairs are V_1 and V_2. The set of differential equations below evaluates the voltage and SOC dynamics,

$$\frac{dSOC(t)}{dt} = -\frac{I(t)}{C_{bat}}, \tag{11}$$

$$\frac{dV_1(t)}{dt} = \frac{-V_1(t)}{R_1C_1} + \frac{I(t)}{C_1}, \tag{12}$$

$$\frac{dV_2(t)}{dt} = \frac{-V_2(t)}{R_2C_2} + \frac{I(t)}{C_2}, \tag{13}$$

while the voltage in the terminals of the cell is given by

$$V_t(t) = V_{oc}(SOC) - V_1(t) - V_2(t) - R_0I(t). \tag{14}$$

2.3.2 Battery Pack

The parametric data used to implement the model was taken from Perez *et al.* (2017). The battery pack model considers a combination of cells in series and in parallel with a uniform behavior. This means that the states are considered to be equal for all cells. With the mentioned hypothesis, the total capacity C_{pack}, resultant voltage V_{pack}, current I_{pack} and power in the terminals P_{pack} of the battery become:

$$C_{pack} = NP \times C_{bat}, \tag{15}$$

$$V_{pack} = NS \times V_t, \tag{16}$$

$$I_{pack} = NP \times I, \tag{17}$$

$$P_{pack} = V_{pack} \times I_{pack}. \tag{18}$$

The number of cells in parallel and in series are NP and NS, respectively. The values of NP and NS were determined considering the capacity and nominal power of the battery, 1000 kWh and 1000 kW. The nominal current of the battery is $2C$, following the values considered for an LFP battery pack with the same power and capacity in (Peralta *et al.*, 2019).

2.4 Genset optimization

As mentioned in Kalikatzarakis *et al.* (2018), quasi-static efficiency maps of the power modes suffice for fuel economy estimation in an optimization process. This allows fast computational optimization. The complete and transient model runs to provide global powertrain information, and an inner quasi-static loop runs with the reduced models for optimization. A quadratic relation between the fuel consumption $\dot{m}_{f,dg}$ and the electrical power output $P_{g,el}$ is established,

$$\dot{m}_{f,dg} = b_0 + b_1P_{g,el} + b_2P_{g,el}^2. \tag{19}$$

In this work, the generators will be optimized to reduce fuel consumption. Then, a cost function is assigned to the system considering the total fuel consumption for the four generators $\dot{m}_{f,opt}$,

$$\dot{m}_{f,opt}(t) = \sum_{i}^{4} w_i\dot{m}_{f,dgi}(t). \tag{20}$$

The index i represents each of the four generators, and their instantaneous fuel consumption rate are $\dot{m}_{f,dgi}(t)$. The variable w_i is a weight, defined for each generator to customize the cost function with rules. Some constraints are

imposed to the optimization formulation, such as the power balance equality,

$$\sum_{i}^{4} P_i = P_L. \tag{21}$$

In this constraint, the load assigned to the gensets P_L must be supplied, considering each power output of the generators, P_i. Moreover, the power balance limits must be satisfied as well,

$$0 \leq P_i \leq P_{nom}, \tag{22}$$

where P_{nom} is the nominal power of the generators (equal for all gensets). The resulting optimization problem consists of finding the power allocation vector $\mathbf{u}^0$ that minimizes the fuel consumption of the gensets and satisfies the mentioned constraints. That is,

$$\mathbf{u}^0(t) = \arg\min_{\mathbf{u}} \dot{m}_{f,opt}(P_i, P_L). \tag{23}$$

To force the system to work with fewer generators, a weight is assigned to the generators based on Tab. 1.

Table 1: Genset weights used for the simulations.

Power intervals	genset 1	genset 2	genset 3	genset 4
$0 \leq$ PL $\leq$ P_{nom}	1	5	5	5
$P_{nom} <$ PL ≤ 2 P_{nom}	1	1	5	5
2 $P_{nom} <$ PL ≤ 3 P_{nom}	1	1	1	5
3 $P_{nom} <$ PL ≤ 4 P_{nom}	1	1	1	1

2.5 Hybrid management strategy

In this work, the hybrid EMS is characterized by a combination of rule-based strategies that define the power split between the gensets and the battery, and an optimization process for power dispatch of the generators. The set of rules are based on the work of Chua *et al.* (2018), where a rule-based strategy was presented for two generators and a battery. Table 2 describes the heuristic control considered for managing the power modes. The SOC of the battery and the load demand P_{Load} are taken as inputs and, through the decision table, the power references for the set of generators and battery are determined. Then, the optimization occurs to assign the power dispatch of each generator.

Table 2: Rule-Based strategy for an all-electric hybrid power system with four gensets and a battery.

SOC / Power	SOC $\leq$ SOC_{min}	$SOC_{min} <$ SOC $< SOC_{max}$	SOC $\geq$ SOC_{max}
$P_{Load} \leq P_{G,on}$	$P_{GT} = P_{opt}$ $P_{bat} = P_{Load}$-P_{GT} if($P_{bat} < P_{cmax}$) $P_{bat} = P_{cmax}$ $P_{GT} = P_{Load}$-P_{bat} end	$P_{GT} = 0$ $P_{bat} = P_{Load}$ if($P_{bat} > P_{dmax}$) $P_{bat} = P_{dmax}$ $P_{GT} = P_{Load}$-P_{bat} end	$P_{GT} = 0$ $P_{bat} = P_{Load}$ if($P_{bat} > P_{dmax}$) $P_{bat} = P_{dmax}$ $P_{GT} = P_{Load}$-P_{bat} end
$P_{G,on} < P_{Load} \leq 4$ $P_{opt} \times f_{peak}$	$P_{GT} = n_g \times P_{opt}$ $P_{bat} = P_{Load}$-P_{GT} if($P_{bat} < P_{cmax}$) $P_{bat} = P_{cmax}$ $P_{GT} = P_{Load}$-P_{bat} end	$P_{GT} = n_g \times P_{opt}$ $P_{bat} = P_{Load}$-P_{GT} if($P_{bat} < P_{cmax}$) $P_{bat} = P_{cmax}$ $P_{GT} = P_{Load}$-P_{bat} end	$P_{GT} = P_{Load}$ $P_{bat} = 0$
$P_{Load} > 4$ $P_{opt} \times f_{peak}$	$P_{GT} = 4$ P_{opt} $P_{bat} = 0$	$P_{GT} = 4$ $P_{opt} \times f_{peak}$ $P_{bat} = P_{Load}$-P_{GT} if($P_{bat} > P_{dmax}$) $P_{bat} = P_{dmax}$ $P_{GT} = P_{Load}$-P_{bat} $P_{GT} = \min(P_{GT}, 4$ $P_{nom})$ end	$P_{GT} = 4$ $P_{opt} \times f_{peak}$ $P_{bat} = P_{Load}$-P_{GT} if($P_{bat} > P_{dmax}$) $P_{bat} = P_{dmax}$ $P_{GT} = P_{Load}$-P_{bat} $P_{GT} = \min(P_{GT}, 4$ $P_{nom})$ end

Table 3: Parameters used for rule-based EMS.

Parameter	Symbol	Value	Unit
Lower genset power limit	$P_{G,on}$	700	kW
Fraction power to cut peaks	f_{peak}	0.9	-
Max discharging power	P_{dmax}	1000	kW
Max charging power	P_{cmax}	-1000	kW
Min state of charge	SOC_{min}	20%	-
Intermediate state of charge	SOC_m	40%	-
Max state of charge	SOC_{max}	80%	-

It is important to avoid the use of the generators in the less efficient regions, which are, in general, when the generators are working with low loads. The first line of Tab. 2 considers the low load demands of the mission. If the SOC is below the limit, one generator is switched on with the optimal power $P_{GT} = P_{opt}$. The excess of power is used to charge the battery, given the maximum charging power of the battery P_{cmax}. If necessary, the generator power reference can be readjusted in a way that only the demand is supplied. If the battery SOC is above the lower limit, the battery will supply the power, limited its maximum discharging power P_{dmax}, while the generator is kept off.

In the second line of Tab. 2, the load demand is above a lower limit to switch at least one generator on and below an upper bound. The value of f_{peak}, which is between 0 and 1, can be used to customize the mentioned upper power bound. In this regime, if the SOC is less than the maximum, the power set to the generators is optimal, given the range of power, and the least number of generators n_g that need to be switched on to balance the load. The excess of power assigned to the generators is used to charge the battery. If necessary, the power of the gensets can be readjusted to supply the required power. When the battery reaches the maximum SOC, the load is delivered to the set of generators, where an optimization takes place. If, after the optimization, loads less than or equal to $P_{G,on}$ are identified for at least one generator, the battery is allowed to supply power until an intermediate $\mathrm{SOC_m}$ limit, avoiding generator operation on low loads.

In the third line of Tab. 2, there is a condition to shave high load peaks using the battery. If necessary, the function min is applied to the power of the generators to limit the operation within the nominal bounds of operation. The load set to the generators is optimized.

2.6 The base and hybrid cases

In this work, there will be a comparison between two power systems. The non-hybrid power system or the base case will only use (four) gensets to supply the power demand. The power split between the generators will be determined through optimization. However, the power dispatch of the hybrid power system will be set through the ruled-based EMS and the optimization. The values of the parameters used for the EMS can be found below, in Tab. 3.

The parameters used for the simulations, shown in Tab. 4, were found in the literature, estimated based on the literature results, or were estimated using data obtained through communication with the naval industry (for the gensets).

2.7 Efficiency index for the power system

A global efficiency index η_{ps} is proposed in this work to study how the hybrid power system can increase the overall efficiency of the vessel. In addition, it can help in comparisons to avoid false interpretations of results. In some situations, mainly when the mission simulation time is small, a fuel consumption reduction can be achieved along with a decrease in the SOC. Looking only at the fuel savings, the energy spent by the battery is not considered.

To consider the power modes in the same base, the methodology is based on the total energy input and output. In the base case, the input energy is given by the energy stored in the fuel, $E_{in} = m_f Q_{lhv}$, where m_f considers all the mass of fuel consumed during the mission and Q_{lhv} is the low heat value of the diesel. Since a power balance is achieved, the output energy along the mission is determined as, $E_{out} = \int_0^{t_f} P_d \, dt$, where P_d is the power demand. For the base case, the efficiency is given by

$$\eta_{ps} = \frac{\int_0^{t_f} P_d \, dt}{m_f Q_{lhv}}. \tag{24}$$

For the hybrid case, the energy input of the gensets is defined as before. However, it is necessary to consider the energy flow associated with the battery SOC. In general, the final state of charge of the battery can be different than the initial. Therefore, we consider the amount of energy that would be required to restore the initial SOC, defined as $E_{bat} = \int_{t_f}^{t_b} V_{pack} I_{pack} \, dt$. The integration goes from the final time t_f until the time t_b, in which the battery restores its $\mathrm{SOC_i}$. If the $\mathrm{SOC_f}$ is greater than the initial, the excess of energy could be used to supply some demand of the ship. Thus,

Table 4: Parameters used for the simulations

Parameter	Symbol	Value	Unit	Reference
Number of poles	P_p	4	-	D
Nominal frequency	f	60	hz	D
Power factor	$cos(f_p)$	0.9	-	E
Nominal electrical power	P_{nom}	1700	kW	D
Friction rate	c_f	0.005	-	E
Generator internal resistance	r_g	0.0324	Ω	E
Moment of inertia	J_g	69.21	kgm^2	(GE, 2009)
Coefficients for engine torque fit	a_0	1.74×10^{-3}	kNm	E
	a_1	7.95×10	kNm/kg	E
	a_2	-5.16×10^2	kNms^2/kg^2	E
	a_3	1.64×10^4	kNms^3/kg^3	E
	a_4	-9.78×10^4	kNms^4/kg^4	E
Coefficients for fuel power relation	b_0	4×10^{-3}	kg/s	E
	b_1	6.4×10^{-5}	kg/(skW)	E
	b_2	5.1×10^{-9}	kg/(skW^2)	E
Coefficients for CO2 power fit	c_0	0.022	kg/s	E
	c_1	0.00017	kg/(skW)	E
Nominal grid voltage	$u_{g,nom}$	690	V	D
Diesel low heat value	Q_{lhv}	42780	kJ/kg	D
Number of cells in parallel	NP	1136	-	E
Number of cells in series	NS	63	-	E
Battery converter efficiency	η_c	97.5%	-	(Kalikatzarakis *et al.*, 2018)

E - estimated
D - directly obtained

the efficiency is:

$$\eta_{ps} = \frac{\int_0^{t_f} P_d \, dt + |\int_{t_f}^{t_b} V_{pack} I_{pack} \, dt|}{m_f Q_{lhv}}. \tag{25}$$

When the SOC_f is smaller than SOC_i, it means that energy would be required for recharging the battery to its initial state. Then, an input of energy would be necessary. Therefore, in this case, the efficiency becomes:

$$\eta_{ps} = \frac{\int_0^{t_f} P_d \, dt}{m_f Q_{lhv} + |\int_{t_f}^{t_b} V_{pack} I_{pack} \, dt|}. \tag{26}$$

3. RESULTS AND DISCUSSION

A strategy to increase the energy efficiency of a vessel's power system is to improve the power dispatch. For a better dispatch, options include optimizing the energy management system with the same power system topology or adding components such as a battery. Figure 2 shows the complete power demand and power dispatch of both the hybrid and non-hybrid power systems. The base case power dispatch, with gensets only, is represented in the first column of the results, in Fig. 2c, 2e, 2g and 2i with the load demand above, shown in Fig. 2a, for the visualization of the mission profile. The power dispatch of the hybrid case, including the battery and gensets, can be seen in the second column, Fig. 2b, 2d, 2f, 2h and 2j.

When the vessel is being loaded in port, part 1 of the mission, and when the vessel is in standby, part 5, it is possible to see that the load is smaller than the power capacity of one genset, which is 1700 kW. Therefore, the load is sustained by only one generator in the base case. However, in the hybrid case, the battery is heavily used in those parts of the mission, since the load is often smaller than 700 kW, which is the lower power limit for the genset to be switched on. Moreover, the gensets work in higher and more efficient power regions for the hybrid topology, in comparison with the base case. The hybrid system can also reduce the total genset operation time and reduce CO_2 emissions near the port.

In 2, the ship is on a laden voyage. Since the ship is fully loaded and traveling at the nominal speed, this part of the mission is characterized by high power demands. In the non-hybrid system, the first three gensets operate in the nominal condition almost all the time, with genset 4 balancing the higher load variations. Regarding the hybrid power system, a considerable difference appears in the use of genset 4, which operates in a steady-state and in a more efficient region, while the load variations are handled by the battery.

Evaluating the DP part, corresponding to range 3, genset 1 was set to deliver practically all demand, for the base case, with a small peak handled by genset 2. The hybrid system operated with only genset 1 switched on and the battery dealt mainly with lower and higher peaks, in short times. At the beginning of the DP, the battery was charged, allowing genset 1 to operate in nominal condition for some time, which did not happen in the base case in the same part of the mission. In both cases, no spinning reserve nor backup power were considered, and the generators were allowed to work at nominal power. As the power load is within the envelope of one genset, and above the lower power limit of 700 kW, almost all the time, the battery usage was limited in the DP part of the mission in this simulation.

Regarding the partial load voyage, part 4, gensets 1 and 2 operated at nominal power for the base case, while genset 3 handled the rest of the load with a small contribution of genset 4. Considering the hybrid case, the low load delivered by genset 4 was replaced by the battery power supply. This can improve the energy efficiency since genset 4 was operating below 500 kW in the base case for this part of the mission.

When analyzing the power dispatch of the hybrid and base cases, it can be noted that adding the battery allowed gensets to be disconnected in some conditions, mainly near the port. Also, a more efficient operation was observed, with the gensets running with higher loads. In Peralta *et al.* (2019), the hybrid power system simulation has shown the higher potential of CO_2 reductions for batteries near the port, in loading and standby operations, for a PSV, even allowing the disconnection of generators. Considering the relation between CO_2 emissions, fuel consumption, and the power system increase in efficiency, it can be said that the mentioned literature results are in accordance with the results obtained in this work. As it can be seen in Fig. (2), for laden and partial load voyage, the battery is quite used, something that does not happen in Peralta *et al.* (2019). The dispatch will depend on several factors such as load demand, the topology of the vessel's power system, and EMS. Therefore, differences are expected to occur.

Different aspects can be used to evaluate the gains of the hybridization of a vessel in its power supply system. For achieving a more cost-effective and cleaner operation, it is essential to analyze fuel consumption savings and CO_2 emissions. However, for a better perspective, it is also important to take into consideration the final state of charge SOC_f and evaluate the increase in vessel efficiency. Table 5 lists the masses of fuel consumed and CO_2 emissions, as well as mass reductions between the base case and the hybrid case. For the hybrid case, the initial and final states of charge are considered. Also, the global efficiency index is considered in the last column of the table for all cases. A fuel consumption reduction of 6.35% and CO_2 emission reductions of 5.81% were achieved. Although the SOC_f is smaller than the SOC_i, the power system efficiency increased by 1.73%. The addition of the battery allowed the reduction of fuel consumption, emissions, and an increase in the overall energy efficiency of the vessel's power system.

Table 5: Compilation of results for comparison between the base and hybrid cases

Case	Fuel		CO_2 emissions		SOC		η_{ps}
	m_f	reduction	m_{CO_2}	reduction	SOC_i	SOC_f	
	[kg]	[%]	[kg]	[%]	[%]	[%]	[%]
Base	414.59	-	1287.6	-	-	-	37.51
Hybrid	388.28	6.35	1212.8	5.81	80	62.39	39.24

The fuel consumption and CO_2 emission reductions vary in the literature for hybrid power systems using batteries, depending on the case of study. Fuel savings of up to 45% have been found in some works, for special cases (Miyazaki *et al.*, 2016). However, in a recent technical report from the European Maritime Safety Agency, the fuel savings potential for OSVs is expected to be between 5-20% (EMSA, 2020). The work of Peralta *et al.* (2019) was found to be the closer study to this work. The authors have reported a 7.4% reduction in CO_2 emissions, considering the addition of a 1000 kW/1000 kWh battery to a PSV power system, which comprised initially, four gensets with 1850 kW each unit. Based on the mentioned literature, the results obtained in this work are within an acceptable range of what has been expected for fuel savings and CO_2 emission reductions for a PSV.

4. CONCLUSIONS

The methodology presented in this work has shown promising results. We used a causal because it enables the representation of real-time systems. Fuel savings, emission reductions, and an increase in energy efficiency were observed. The addition of the battery, with a consistent EMS control for power dispatch, allowed benefits for the PSV's power system. Understanding how hybrid solutions work, and their benefits, is essential for increasing the adoption of such technologies to achieve more cost-effective and cleaner vessel operations, as well as other improvements in performance. Based on the case study considered, the results suggest that:

- The battery shows great usage potential when the ship is being loaded in port or on standby. In these parts of the mission, the generators operated in higher efficiency regions, and some were even disconnected. With this, the battery can enable cleaner operations near the port;

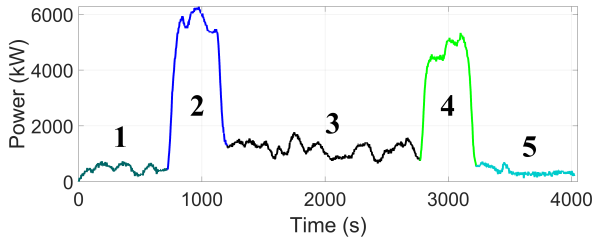

(a) Power demand profile

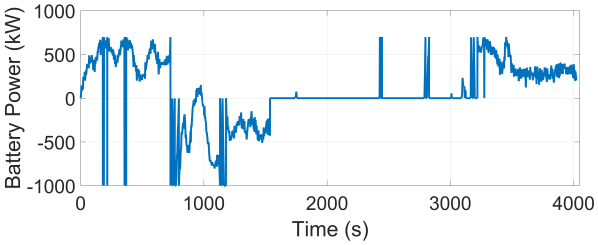

(b) Battery power dispatch

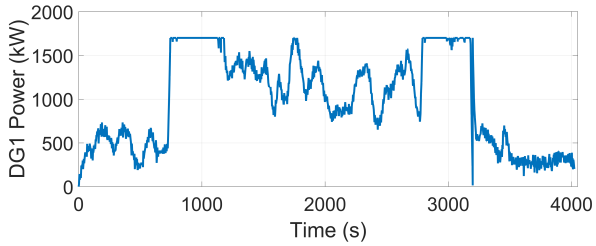

(c) Base case power dispatch - genset 1

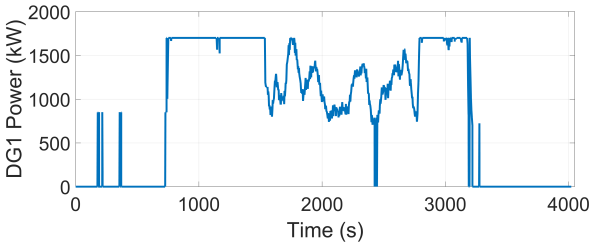

(d) Hybrid case power dispatch - genset 1

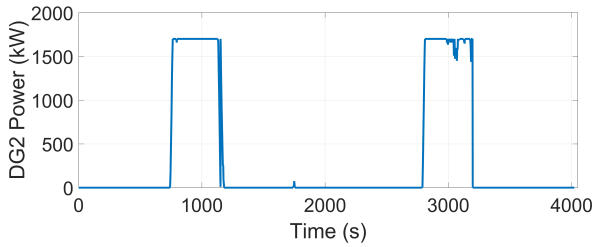

(e) Base case power dispatch - genset 2

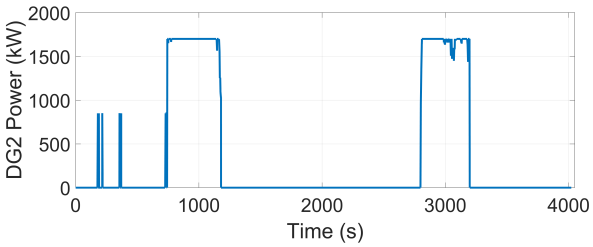

(f) Hybrid case power dispatch - genset 2

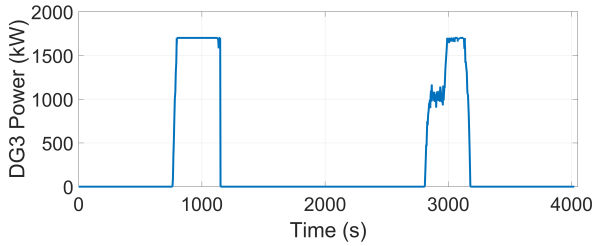

(g) Base case power dispatch - genset 3

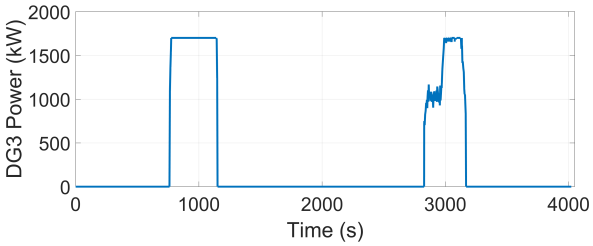

(h) Hybrid case power dispatch - genset 3

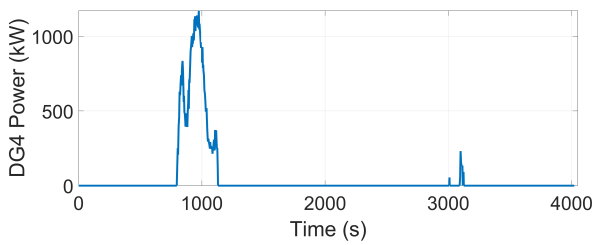

(i) Base case power dispatch - genset 4

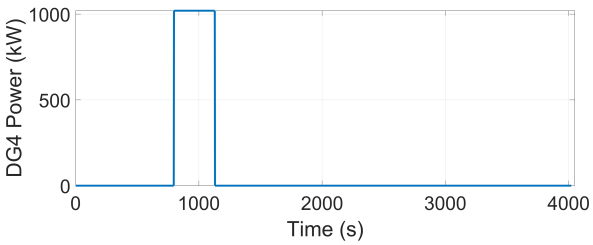

(j) Hybrid case power dispatch - genset 4

Figure 2: Power demand, and power dispatch of the base case (non-hybrid) and the hybrid power system

- For the laden and partial load voyages, the battery can also enable the generators to run at higher efficiencies;

- The battery was not much used in DP, probably due to the load profile, general assumptions, and EMS. In a real operation, due to the safety requirements and redundancy of gensets in DP, the battery could be used more effectively. Our group has been studying such conditions for further analysis and publications;

- The hybridization of the power system can enable an increase in energy efficiency and, therefore, reductions in fuel consumption and CO_2 emissions. An increase in the energy efficiency of 1.73%, fuel savings of 6.35%, and CO_2 emission reductions of 5.81% have been achieved by the hybrid solution.

Future work may look into designing specific energy management solutions for the DP part of the mission, and developing optimal strategies to improve the performance of the hybrid solutions, evaluating fuel consumption, emissions, as well as battery capacity fading. In addition, it would be interesting to test the power systems in different missions to analyze the robustness of the power dispatch strategies and the effects of the power profile on the behavior of the hybrid systems.

5. ACKNOWLEDGEMENTS

We gratefully acknowledge support of the RCGI – Research Centre for Gas Innovation, hosted by the University of São Paulo (USP) and sponsored by FAPESP – São Paulo Research Foundation (2014/50279-4) and Shell Brasil, and the strategic importance of the support given by ANP (Brazil's National Oil, Natural Gas and Biofuels Agency) through the R&D levy regulation. The authors would like to thank the Brazilian National Council for Scientific and Technological Development (CNPq) for financial support in the form of a scholarship, number 133627/2020-9, granted to the graduate student, Crisley S. Peixoto. In addition, B. S. Carmo thanks the Brazilian National Council for Scientific and Technological Development (CNPq) for financial support in the form of a productivity grant, number 312951/2018-3.

6. REFERENCES

Chua, L.W.Y., Tjahjowidodo, T., Seet, G.G.L. and Chan, R., 2018. "Implementation of optimization-based power management for all-electric hybrid vessels". *IEEE Access*, Vol. 6, p. 74339–74354. ISSN 2169-3536. doi: 10.1109/ACCESS.2018.2883324.

Chua Wan Yuan, L., Tjahjowidodo, T., Lee, G.S.G. and Chan, R., 2017. "Optimizing fuel savings and power system reliability for all-electric hybrid vessels using model predictive control". In *2017 IEEE International Conference on Advanced Intelligent Mechatronics (AIM)*. IEEE, p. 1532–1537. ISBN 978-1-5090-5998-0. doi: 10.1109/AIM.2017.8014236. URL `http://ieeexplore.ieee.org/document/8014236/`.

Crippa, M., Oreggioni, G., Guizzardi, D., Muntean, M., Schaaf, E., Lo Vullo, E., Solazzo, E., Monforti-Ferrario, F., Olivier, J., Vignati, E. and et al., 2019. *Fossil CO2 and GHG emissions of all world countries: 2019 report.* Publications Office of the European Union. ISBN 978-92-76-11100-9. URL `http://publications.europa.eu/publication/manifestation_identifier/PUB_KJNA29849ENN`.

EMSA, 2020. "Electrical energy storage for ships". Technical report, EMSA.

Garcia, V., Jose, J. and Inigo, I.A.L., 2019. "On the optimal design of hybrid-electric power systems for offshore vessels". *IEEE Transactions on Transportation Electrification*, Vol. 5, No. 1, p. 324–334. ISSN 2332-7782, 2372-2088. doi: 10.1109/TTE.2018.2883870.

GE, 2009. "Technical description: container genset jgc 620 gs-s.l". Technical report, GE.

Geertsma, R., Negenborn, R., Visser, K. and Hopman, J., 2017. "Design and control of hybrid power and propulsion systems for smart ships: A review of developments". *Applied Energy*, Vol. 194, p. 30–54. ISSN 03062619. doi: 10.1016/j.apenergy.2017.02.060.

Kalikatzarakis, M., Geertsma, R., Boonen, E., Visser, K. and Negenborn, R., 2018. "Ship energy management for hybrid propulsion and power supply with shore charging". *Control Engineering Practice*, Vol. 76, p. 133–154. ISSN 09670661. doi:10.1016/j.conengprac.2018.04.009.

Miyazaki, M.R., Sorensen, A.J. and Vartdal, B.J., 2016. "reduction of fuel consumption on hybrid marine power plants by strategic loading with energy storage devices". *IEEE Transactions on Power Systems*, Vol. 3, p. 207–217. ISSN 2332-7707. doi:10.1109/JPETS.2016.2621117.

Peralta, C.O., Vieira, G., Meunier, S., Vale, R., Salles, M. and Carmo, B., 2019. "Evaluation of the co2 emissions reduction potential of li-ion batteries in ship power systems". *Energies*, Vol. 12, No. 3, p. 375. ISSN 1996-1073. doi:10.3390/en12030375.

Perez, H.E., Hu, X., Dey, S. and Moura, S.J., 2017. "Optimal charging of li-ion batteries with coupled electro-thermal-aging dynamics". *IEEE Transactions on Vehicular Technology*, Vol. 66, No. 9, p. 7761–7770. ISSN 0018-9545, 1939-9359. doi:10.1109/TVT.2017.2676044.

RAENG, 2020. "Future ship powering options exploring alternative methods of ship propulsion". Technical report, Royal academy of engineering. URL `https://www.raeng.org.uk/publications/reports/future-ship-powering-options`.

Zhang, Z., Guan, C. and Liu, Z., 2020. "Real-time optimization energy management strategy for fuel cell hybrid ships considering power sources degradation". *IEEE Access*, Vol. 8, p. 87046–87059. ISSN 2169-3536. doi: 10.1109/ACCESS.2020.2991519.

7. RESPONSIBILITY NOTICE

The authors are solely responsible for the printed material included in this paper.